CASE FILE
COPY

Copy
RM L57D19

NACA RM L57D19

NACA

RESEARCH MEMORANDUM

AERODYNAMIC CHARACTERISTICS OF MISSILE CONFIGURATIONS WITH WINGS OF LOW ASPECT RATIO FOR VARIOUS COMBINATIONS OF FOREBODIES, AFTERBODIES, AND NOSE SHAPES FOR COMBINED ANGLES OF ATTACK AND SIDESLIP AT A MACH NUMBER OF 2.01

By Ross B. Robinson

Langley Aeronautical Laboratory
Langley Field, Va.

NATIONAL ADVISORY COMMITTEE
FOR AERONAUTICS

WASHINGTON
June 25, 1957
Declassified January 12, 1961

NATIONAL ADVISORY COMMITTEE FOR AERONAUTICS

RESEARCH MEMORANDUM

AERODYNAMIC CHARACTERISTICS OF MISSILE CONFIGURATIONS WITH WINGS OF LOW ASPECT RATIO FOR VARIOUS COMBINATIONS OF FOREBODIES, AFTERBODIES, AND NOSE SHAPES FOR COMBINED ANGLES OF ATTACK AND SIDESLIP AT A MACH NUMBER OF 2.01

By Ross B. Robinson

SUMMARY

An investigation has been made in the Langley 4- by 4-foot supersonic pressure tunnel to determine the aerodynamic characteristics of a series of missile configurations having low-aspect-ratio wings at a Mach number of 2.01. The effects of wing plan form and size, length-diameter ratio, forebody and afterbody length, boattailed and flared afterbodies, and various nose shapes were determined. Six-component force and moment data are presented for combined angles of attack and sideslip to about 28°. No analysis of the data has been made in this report.

INTRODUCTION

A problem of increasing importance in missile design is the efficient utilization of internal stowage space in aircraft. The use of low-aspect-ratio lifting surfaces with small span-diameter ratios would result in more compact missiles occupying materially less volume than the same number of configurations with large-span lifting surfaces.

Another problem of missile design is the maneuverability required by the limited scanning angles of the missile seeking equipment. The missile should be capable of large attitude changes with minimum control deflections. A configuration with nonlinear lift and pitching-moment variations such that the values of static margin and lift-curve slope are low near zero angle of attack would satisfy this requirement.

Some previous investigations have presented a limited amount of information on missiles having low-span wings. The results of an investigation of monowing strips of span-diameter ratios from 1.19 to 2.01 on a body of revolution at a Mach number of 1.41 are presented in reference 1. The aerodynamic characteristics in pitch for Mach numbers from 1.97 to 3.33 of a series of missile configurations having low-aspect-ratio monowings and various types of controls are given in references 2 and 3.

This report contains the results of an investigation of a series of missile configurations having various length-diameter ratios, wing plan forms, nose shapes, and forebody and afterbody arrangements at a Mach number of 2.01 in the Langley 4- by 4-foot supersonic pressure tunnel. Six-component force and moment data were obtained for combined angles of attack and sideslip to about 28°. No analysis of the data has been made in this report.

SYMBOLS

The data are presented as coefficients of forces and moments with the center of moments at the leading edge of the exposed root chord of the wing. All the data are referred to the body-axis system (fig. 1).

C_N normal-force coefficient, $\frac{N}{qS}$

C_A axial-force coefficient, $\frac{A}{qS}$

C_m pitching-moment coefficient, $\frac{M_Y}{qS\bar{d}}$

C_l rolling-moment coefficient, $\frac{M_X}{qSd}$

C_n yawing-moment coefficient, $\frac{M_Z}{qSd}$

C_Y side-force coefficient, $\frac{Y}{qS}$

N normal force

A axial force

Y	side force
M_Y	pitching moment
M_X	rolling moment
M_Z	yawing moment
d	diameter of cylindrical section of body, 3.00 in.
S	cross-sectional area of cylindrical portion of body, 0.0491 sq ft
q	dynamic pressure
α	angle of attack of model center line, deg
β	angle of sideslip of model center line, deg
δ_s	deflection angle of spoiler, perpendicular to hinge line, positive when trailing edge deflected upward, deg
x	longitudinal distance of moment center rearward of nose of body
l	length of body
x/l	position of moment center rearward of nose
l/d	length-diameter ratio of body

Model components (see fig. 2):

Forebodies (figs. 2(b) and 2(c)):

F_1, F_7, F_8, F_9	ogive-cylinders with varying lengths of cylindrical portion (fig. 2(b))
F_2	flat-face cylinder with tripod tip
F_3	F_2 with wire mesh on tripod
F_5	modified ogive-cylinder with hemispherical nose
F_4	F_5 with 3-inch spike
F_6	F_5 with slotted cone fairing

Afterbodies (fig. 2(d)):

A_0	no afterbody
A_1, A_2	cylindrical afterbodies
A_3, A_4, A_5	boattailed afterbodies
A_6, A_7, A_8	flared afterbodies

Wings (fig. 2(f)):

W_0	wing off
W_1, W_2, W_3	delta wings
W_4, W_5, W_6	rectangular wings

MODEL AND APPARATUS

Sketches of a typical complete model and of the model components are shown in figure 2. The geometric characteristics of the various components and combinations of forebodies, wings, and afterbodies are given in table I. Values of x/l and l/d for all the bodies are also given in table I. The models used in this investigation are shown in figure 3.

The various configurations were obtained by attaching combinations of forebodies, afterbodies, and wings to a cylindrical section W_0 having a diameter of 3.00 inches (this diameter is hereinafter referred to as 1 caliber in calculating body lengths) housing the internal strain-gage balance (fig. 2(f)).

The basic forebodies investigated were a series of 3.5-caliber ogive-cylinders with varying lengths of cylindrical section (fig. 2(b)). In addition, a 3.5-caliber ogive with a rounded nose (F_5, fig. 2(c)) to which a slotted cage (F_6, fig. 2(c)) or a 3-inch spike could be attached (F_4, fig. 2(c)), and a flat-face cylinder with a tripod, with and without a wire mesh around the tripod (F_2 and F_3, fig. 2(c)) were tested. The 3-inch spike was selected as a result of tests at a Mach number of 1.61 of a similar configuration (refs. 4 and 5) which indicated this spike length to be optimum for minimum drag at small angles of attack.

The afterbodies, shown in figure 2(d), consisted of the following configurations: A_0, no afterbody; A_1, a 1-caliber cylinder; A_2, a 2-caliber cylinder; A_3, a 1-caliber 6.50° boattail; A_4, a 1-caliber 6.50° boattail attached to a 1-caliber cylinder; A_5, a 2-caliber 3.25° boattail; A_6, a 1-caliber 6.50° flare; A_7, a 1-caliber 6.50° flare attached to a 1-caliber cylinder; and A_8, a 2-caliber 3.25° flare.

Cruciform wings were mounted in slots in the balance housing. Three rectangular-wing and three delta-wing configurations were tested (fig. 2(f) and table 1). The wings were so designed that the exposed areas of the medium and large wings of each series were two and four times, respectively, those of the small wings. Areas of corresponding wings in each series were equal; for example, the exposed area of the large rectangular wing was equal to that of the large delta wing.

Two spoilers, one for each horizontal wing panel, were provided for the large delta wing (fig. 2(g)). Deflections of 45° and 90° were obtained by facing either the oblique or the perpendicular face of the spoiler forward. The length of each spoiler was 3.094 inches and the width of each spoiler was 0.625 inch. The height of each spoiler was 0.625 inch.

The models were mounted on a rotary sting to permit testing through ranges of combined angles of attack and sideslip. Six-component force and moment data were measured by an internal strain-gage balance. Base pressues were measured with a single tube well inside the model. A cylindrical wooden block approximately the same size as the base of the model and 1 inch long was attached to the sting about 1/8 inch behind the model base.

TESTS, CORRECTIONS AND ACCURACY

Test Conditions

The tests were made at a Mach number of 2.01, a stagnation temperature of 100° F, and a stagnation pressure of 1,440 pounds per square foot absolute. The Reynolds number, based on the maximum diameter, was 0.62×10^6 (2.47×10^6 based on a length of 1 foot). Stagnation dewpoints of -25° or below were maintained to eliminate condensation effects. The angle-of-attack range for pitch tests was from -4° to about 28° at zero sideslip, and the angle-of-sideslip range was from -4° to a maximum of about 28° at angles of attack of about 0°, 4.1°, 8.2°, 12.3°, 16.4°, 20.5°, and 24.7° .

Corrections and Accuracy

The angles of attack and sideslip were corrected for the deflection of the balance and sting under load. The Mach number variation was about ±0.015 and the flow-angle variation in the vertical and horizontal planes did not exceed ±0.1°. No corrections have been applied to the data to account for these variations.

The axial-force data were adjusted to a base pressure equal to free-stream static pressure. Since the measured base pressures were about the same as the test-section static pressure for angles of attack to about 8°, the wooden block apparently was effective in producing approximately constant pressures across the base of the model. Base-pressure measurements for several of the configurations were found to be inaccurate because of instrument failure. The axial-force coefficients for these configurations were corrected by using base pressures measured for configurations having the same wing located the same distance from the base.

The probable errors in the force and moment data for small angles of attack and sideslip are considerably larger for the body configurations without wings than for the body-wing configurations because the strain-gage balance was not able to measure very small loads with sufficient accuracy. Small increments of forces and moments could be accurately measured in higher load ranges. Zero shifts and random instrument errors were about the same for all configurations. Comparison of tests made with and without the wooden block for the configuration with large delta wings, no afterbody, and $l/d = 10$ indicated negligible effects of the block on the forces and moments.

Estimated probable errors in the force and moment data based on the repeatability of the results, zero shift, calibration, and random instrument errors are as follows:

C_N	±0.0565
C_A	±0.00583
C_m	±0.0930
C_l	±0.0037
C_n	±0.0923
C_Y	±0.0580

The angles of attack at zero sideslip and sideslip angles at zero angle of attack are estimated to be correct within ±0.1°. For combined angles of attack and sideslip the angles are correct within ±0.2°.

PRESENTATION OF RESULTS

The data are presented in figures 4 to 46. The effects of delta and rectangular wings on the aerodynamic characteristics in pitch and in sideslip at various angles of attack with various cylindrical afterbodies ($l/d = 10$) are found in figures 4 to 21. Figures 22 to 30 present the effects of forebody length on the aerodynamic characteristics in pitch and in sideslip for bodies with various cylindrical afterbodies with and without the large delta wing at various angles of attack (l/d varies). The effects of various boattailed and flared afterbodies with large delta wings on the aerodynamic characteristics in pitch and in sideslip at various angles of attack are presented in figures 31 to 39 ($l/d = 10$). The effects of the various special nose shapes on the aerodynamic characteristics in pitch and in sideslip at various angles of attack with no afterbody and with large delta wings are presented in figures 40 to 45 (l/d varies). The effects of spoiler deflection on a configuration with 1-caliber cylindrical afterbody and large delta wings ($F_7W_1A_1$) on the aerodynamic characteristics in pitch and in sideslip at zero angles of attack are presented in figure 46 ($l/d = 10$).

The axial-force coefficients for the following configurations were corrected for base pressures from similar configurations as described in the preceding section:

Configurations	Figure
$F_1W_1A_0$, $F_7W_1A_0$, $F_9W_1A_0$	22
$F_1W_1A_1$, $F_9W_1A_1$	23
$F_7W_1A_2$, $F_8W_1A_2$, $F_9W_1A_2$	24
$F_2W_1A_0$	40

No axial-force coefficients have been presented for configurations $F_7W_1A_3$ and $F_7W_1A_6$. The measured base pressures were not accurate and no base pressures for similar configurations were available.

CONCLUDING REMARKS

An investigation was made in the Langley 4- by 4-foot supersonic pressure tunnel to determine the aerodynamic characteristics on a configuration with various combinations of forebodies, afterbodies, nose shapes, and wings with low aspect ratio. Six-component force and moment

data were obtained for combined angles of attack and sideslip to about 28°. No analysis of the data has been made in this report.

Langley Aeronautical Laboratory,
National Advisory Committee for Aeronautics,
Langley Field, Va., April 3, 1957.

REFERENCES

1. Spearman, M. Leroy, and Robinson, Ross B.: Aerodynamic Characteristics of a Cruciform-Wing Missile With Canard Control Surfaces and of Some Very Small Span Wing-Body Missiles at a Mach Number of 1.41. NACA RM L54B11, 1954.

2. Katzen, Elliott D., and Jorgensen, Leland H.: Aerodynamics of Missiles Employing Wings of Very Low Aspect Ratio. NACA RM A55L13b, 1956.

3. Jorgensen, Leland H., and Katzen, Elliott D.: Wing-Body Combinations With Wings of Very Low Aspect Ratio at Supersonic Speeds. NACA RM A56G16, 1956.

4. Robins, A. Warner: Preliminary Investigation of the Effects of Several Seeker-Nose Configurations on the Longitudinal Characteristics of a Canard-Type Missile at a Mach Number of 1.60. NACA RM L53I18, 1953.

5. Gapcynski, John P., and Robins, A. Warner: The Effect of Nose Radius and Shape on the Aerodynamic Characteristics of a Fuselage and a Wing-Fuselage Combination at Angles of Attack. NACA RM L53I23a, 1953.

TABLE I.- GEOMETRIC CHARACTERISTICS OF MODELS

(a) Characteristics of model components

Wings:	W_1	W_2	W_3	W_4	W_5	W_6
Area, exposed, sq ft	0.3611	0.1805	0.0903	0.3611	0.1805	0.0903
Span, exposed, in.	8.00	4.00	2.00	4.00	2.00	1.00
Aspect ratio, exposed panel	1.23	0.615	0.308	0.308	0.154	0.077
Taper ratio	0	0	0	1	1	1
Root chord, exposed, in.	13.00	13.00	13.00	13.00	13.00	13.00
Root chord, center line, in.	17.875	22.75	32.50	13.00	13.00	13.00
Leading-edge sweep, deg	72.9	81.3	85.6	0	0	0
Ratio of total span to maximum body diameter	3.667	2.333	1.667	2.333	1.667	1.333
Ratio of exposed wing area to maximum body cross-sectional area	7.35	3.68	1.84	7.35	3.68	1.84

Balance section, W_0:	
Length, in.	13.00
Maximum diameter, in.	3.00
Length-diameter ratio, l/d	4.333
Maximum cross-sectional area, sq ft	0.0491

Forebodies:	F_1	F_7	F_8	F_9
Length, in.	11.00	14.00	17.00	20.00
Maximum diameter, in.	3.00	3.00	3.00	3.00
Length-diameter ratio, l/d	3.667	4.667	5.667	6.667
Maximum cross-sectional area, sq ft	0.0491	0.0491	0.0491	0.0491

Special noses:	F_2	F_3	F_4	F_5	F_6
Length, in.	9.12	9.12	13.36	10.36	13.36
Maximum diameter, in.	3.00	3.00	3.00	3.00	3.00
Maximum cross-sectional area, sq ft	0.0491	0.0491	0.0491	0.0491	0.0491

Afterbodies:	A_1	A_2	A_3	A_4	A_5	A_6	A_7	A_8
Length, in.	3.00	6.00	3.00	6.00	6.00	3.00	6.00	6.00
Forward diameter, in.	3.00	3.00	3.00	3.00	3.00	3.00	3.00	3.00
Ratio of length to forward diameter	1.00	2.00	1.00	2.00	2.00	1.00	2.00	2.00
Half-angle of boattail or flare, deg	0	0	6.50	6.50	3.25	6.50	6.50	3.25
Rear diameter, in.	3.00	3.00	2.32	2.32	2.32	3.68	3.68	3.68

TABLE I.- GEOMETRIC CHARACTERISTICS OF MODELS - Concluded.

(b) Body-component combinations

Component combinations	Length, in.	Length-diameter ratio	Center-of-gravity location from base, calibers	Center-of-gravity location from nose, x/l	Alternate afterbodies used
$F_1W_0A_0$	24.00	8	4.33	0.459	None
$F_7W_0A_0$	27.00	9	4.33	.519	None
$F_1W_0A_1$	27.00	9	5.33	.408	None
$F_8W_0A_0$	30.00	10	4.33	.567	None
$F_7W_0A_1$	30.00	10	5.33	.467	A_3 or A_6
$F_1W_0A_2$	30.00	10	6.33	.367	A_4, A_5, A_7, A_8
$F_9W_0A_0$	33.00	11	4.33	.606	None
$F_8W_0A_1$	33.00	11	5.33	.515	None
$F_7W_0A_2$	33.00	11	6.33	.424	None
$F_9W_0A_1$	36.00	12	5.33	.556	None
$F_8W_0A_2$	36.00	12	6.33	.473	None
$F_9W_0A_2$	39.00	13	6.33	.513	None
$F_5W_0A_0$	23.36	7.78	4.33	.443	None
$F_6W_0A_0$	26.36	8.78	4.33	.507	None
$F_4W_0A_0$	26.36	8.78	4.33	.507	None
$F_3W_0A_0$	22.12	7.37	4.33	.412	None
$F_2W_0A_0$	22.12	7.37	4.33	.412	None

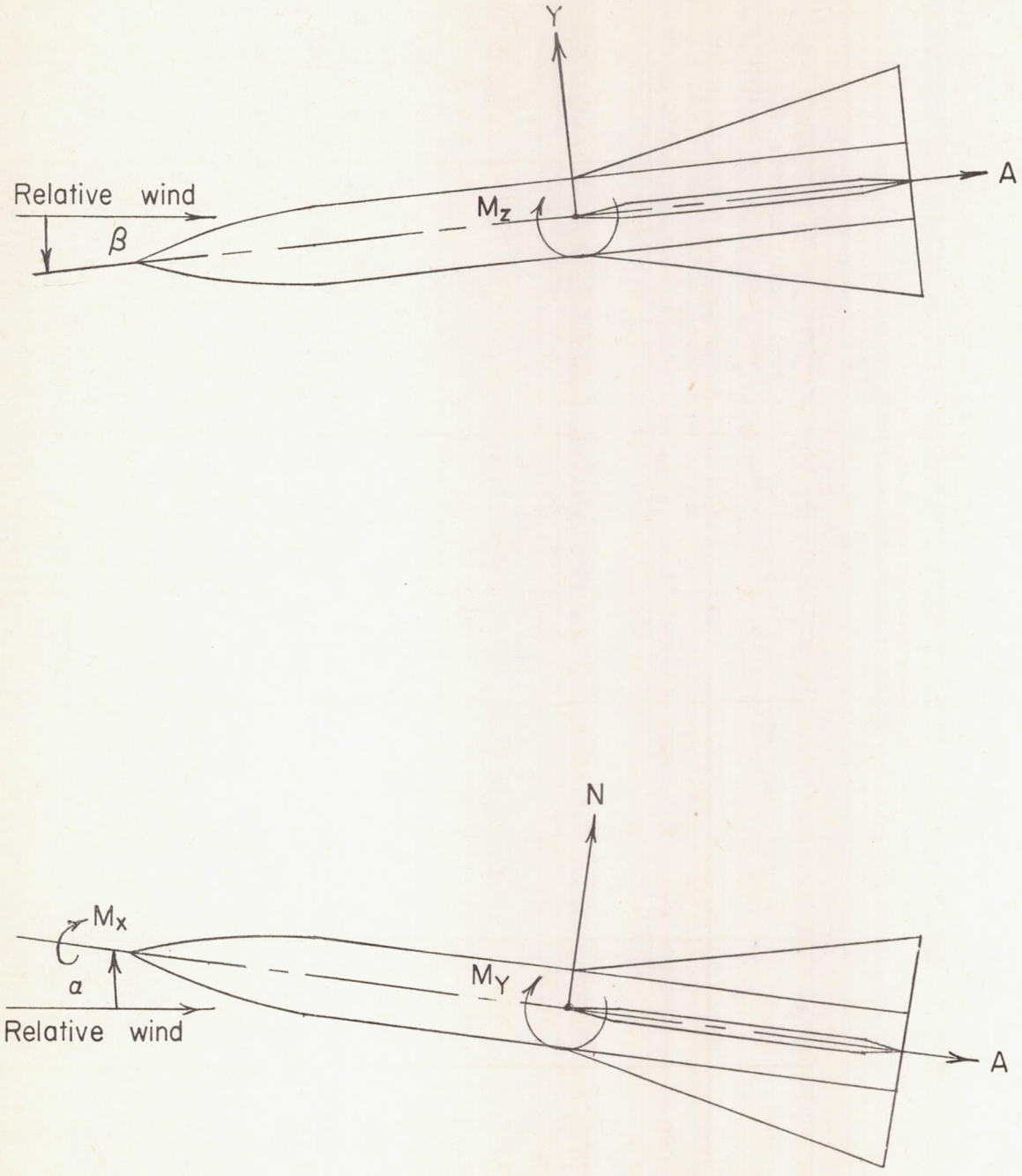
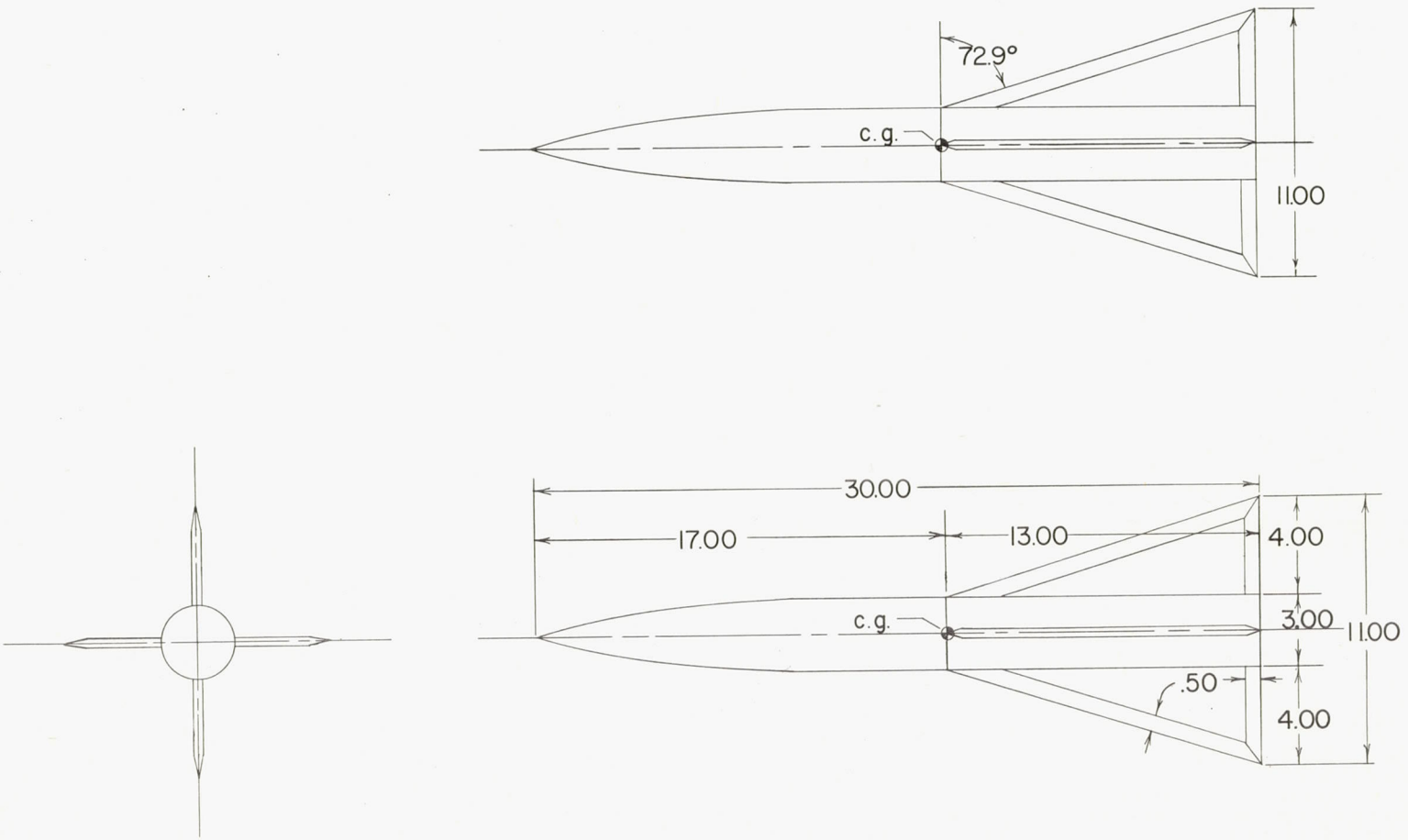
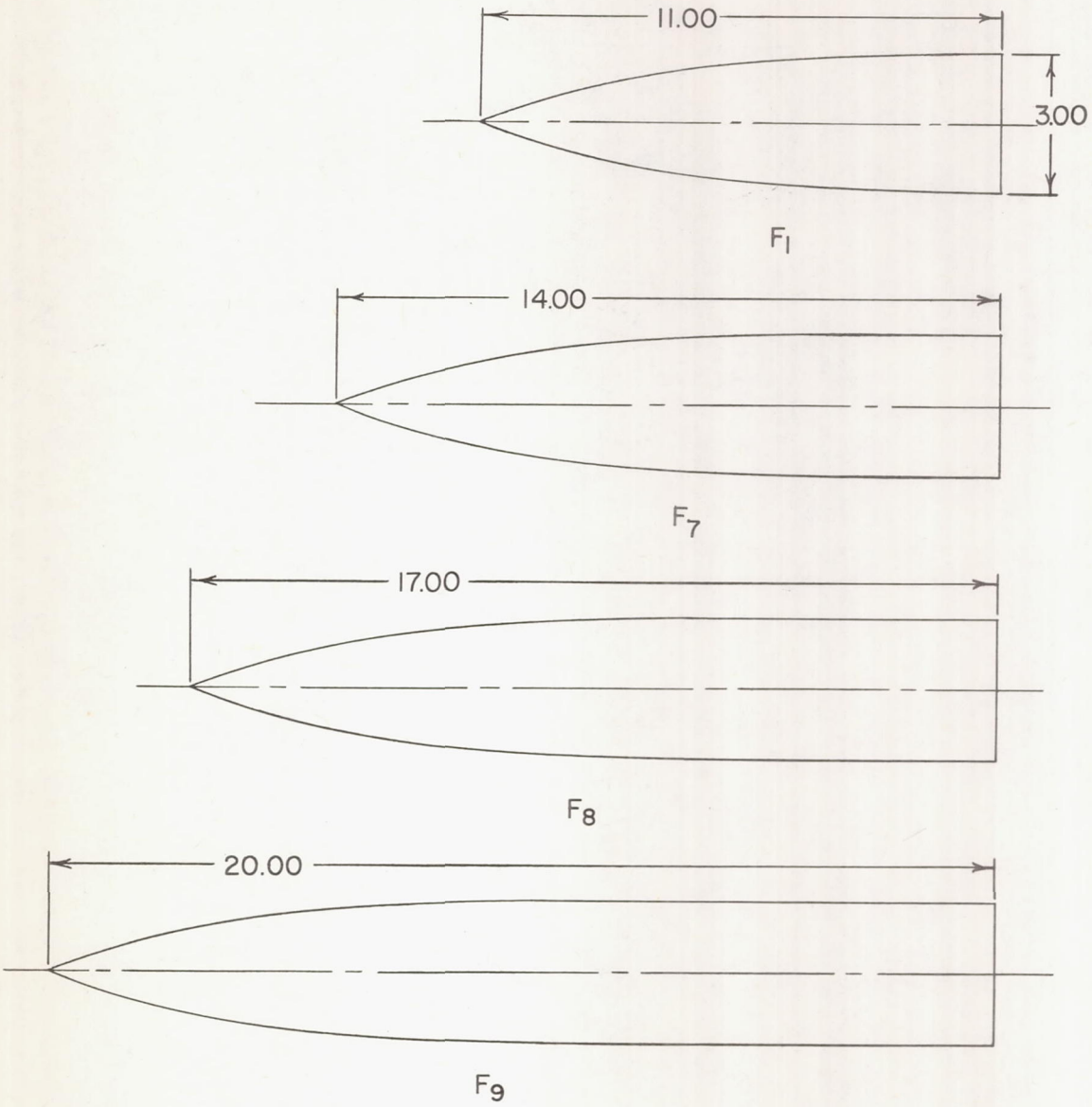


Figure 1.- Axis systems. Arrows indicate positive directions of forces, moments, and angles.



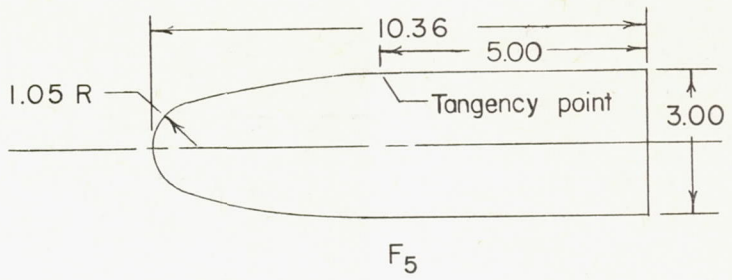
(a) Details of typical configuration, $F_8W_1A_0$.

Figure 2.- Details of models. All dimensions are in inches except as noted.

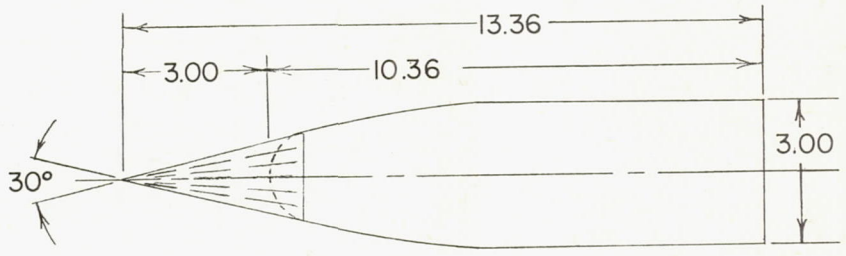


(b) Forebodies with 3.5-caliber-ogive cylinders and with constant rear diameter of 3.00 inches.

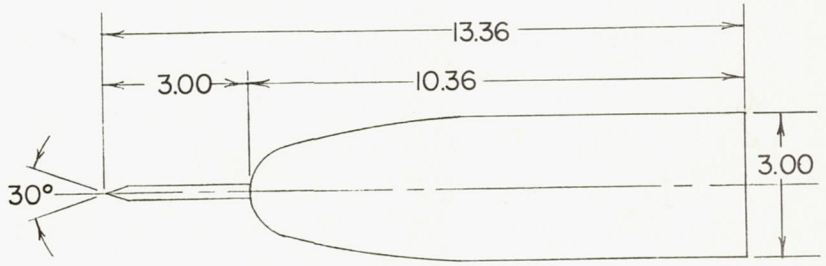
Figure 2.- Continued.



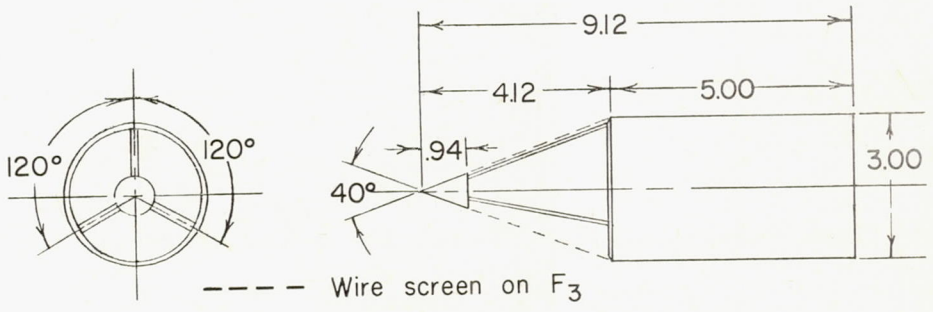
F_5



F_6



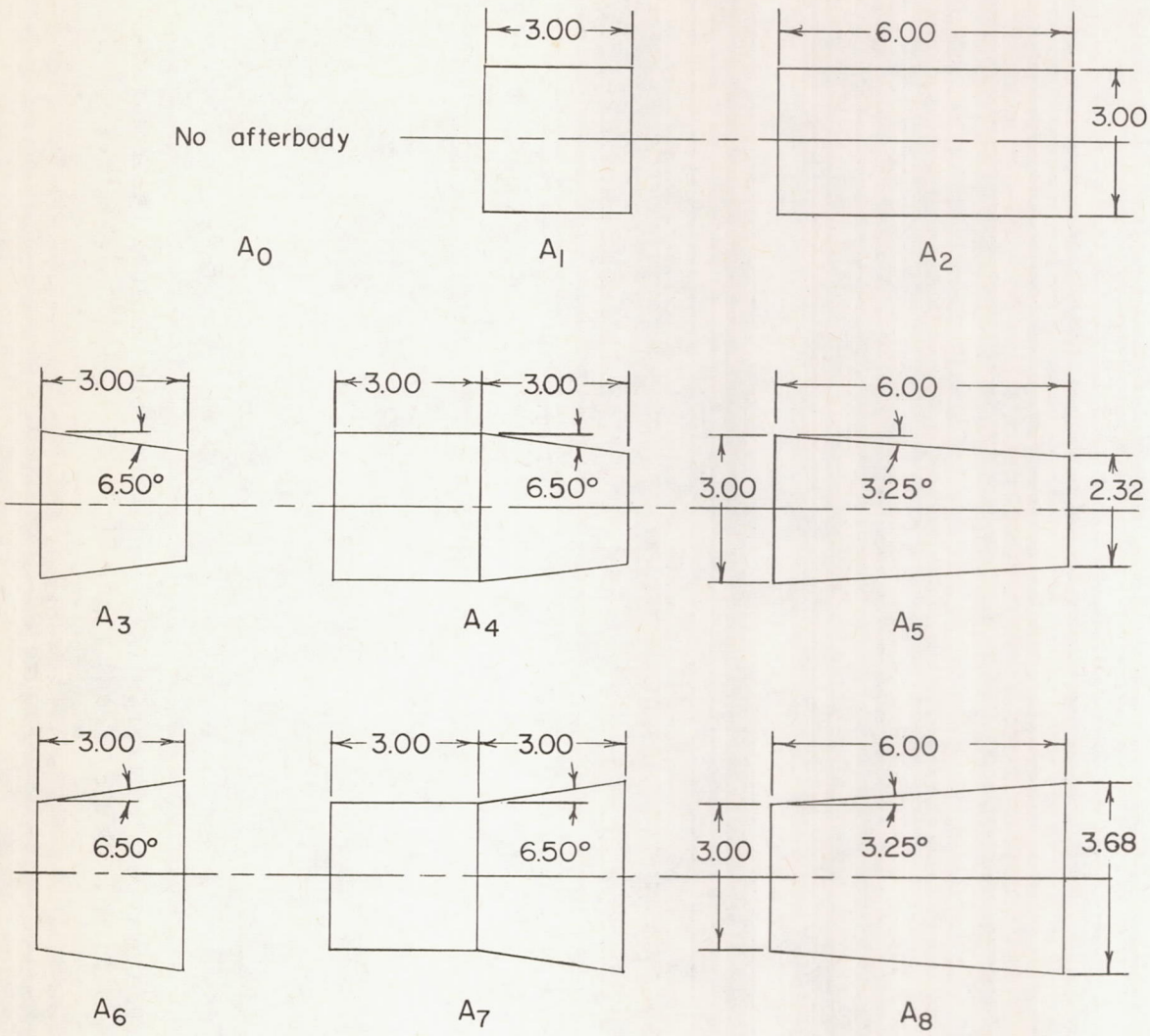
F_4



F_2 and F_3

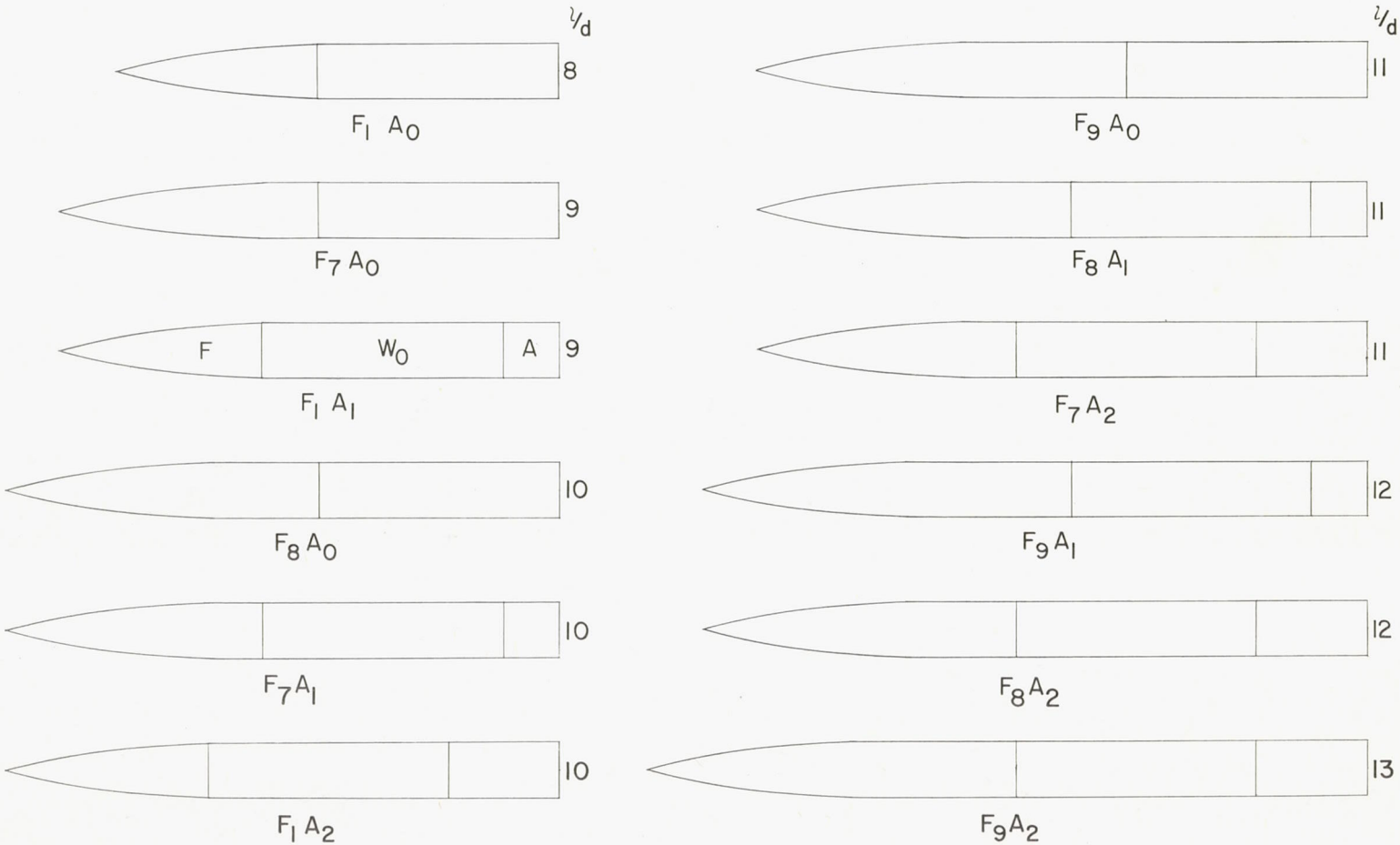
(c) Special nose shapes.

Figure 2.- Continued.



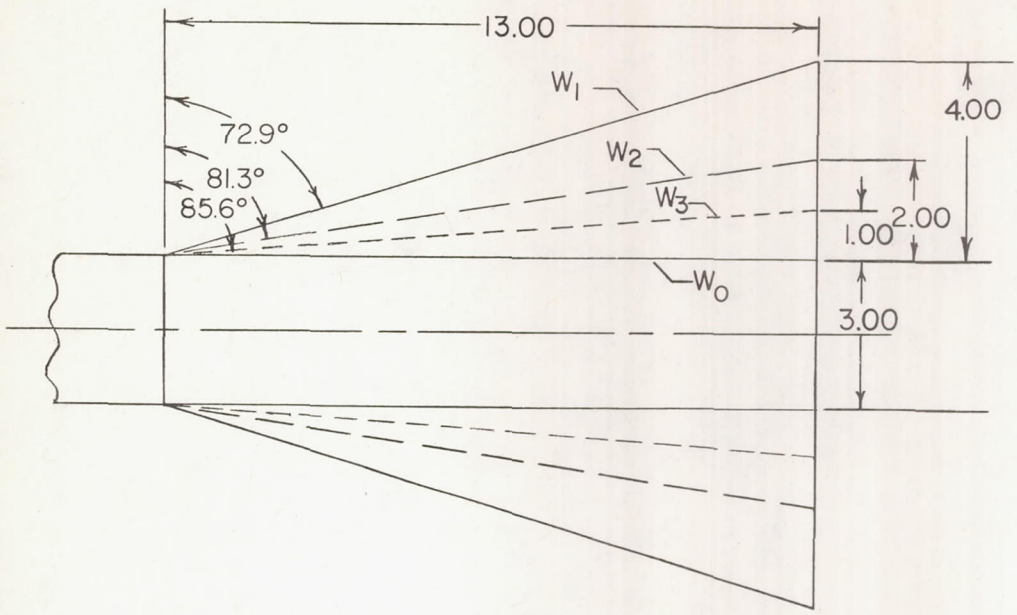
(d) Afterbodies. (All afterbodies are bodies of revolution.)

Figure 2.- Continued.

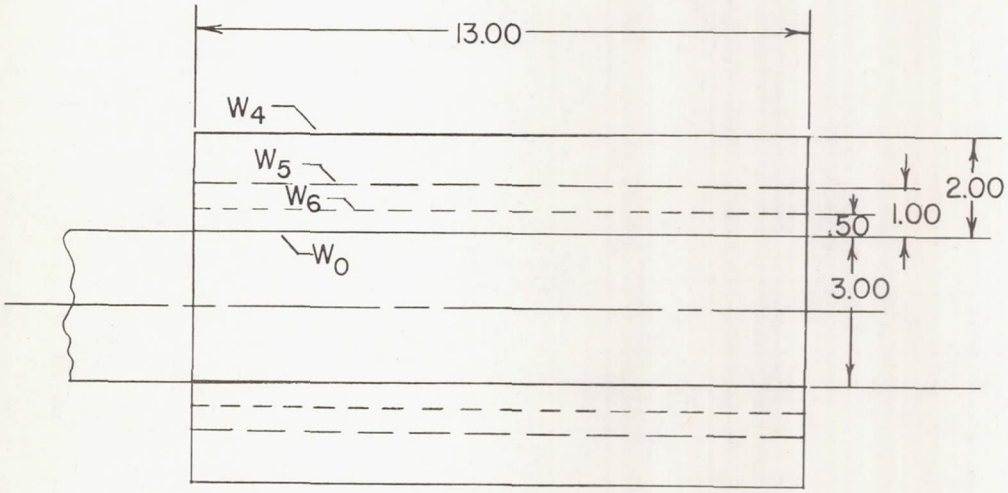


(e) Fuselage combinations. (All configurations include balance section W_0. See F_1A_1 and figs. 2(b) and 2(d) for details.)

Figure 2.- Continued.



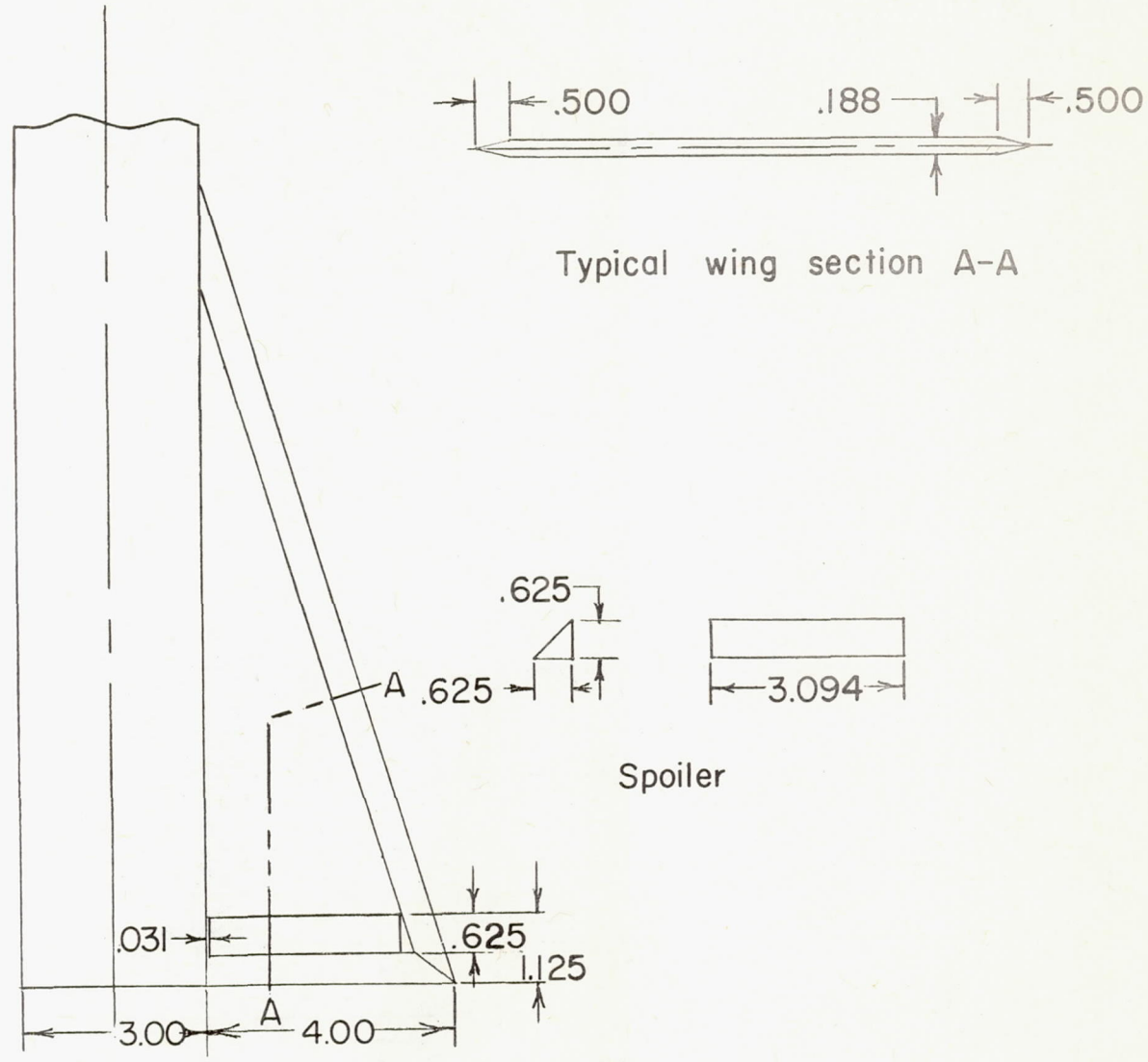
Delta wing series



Rectangular wing series

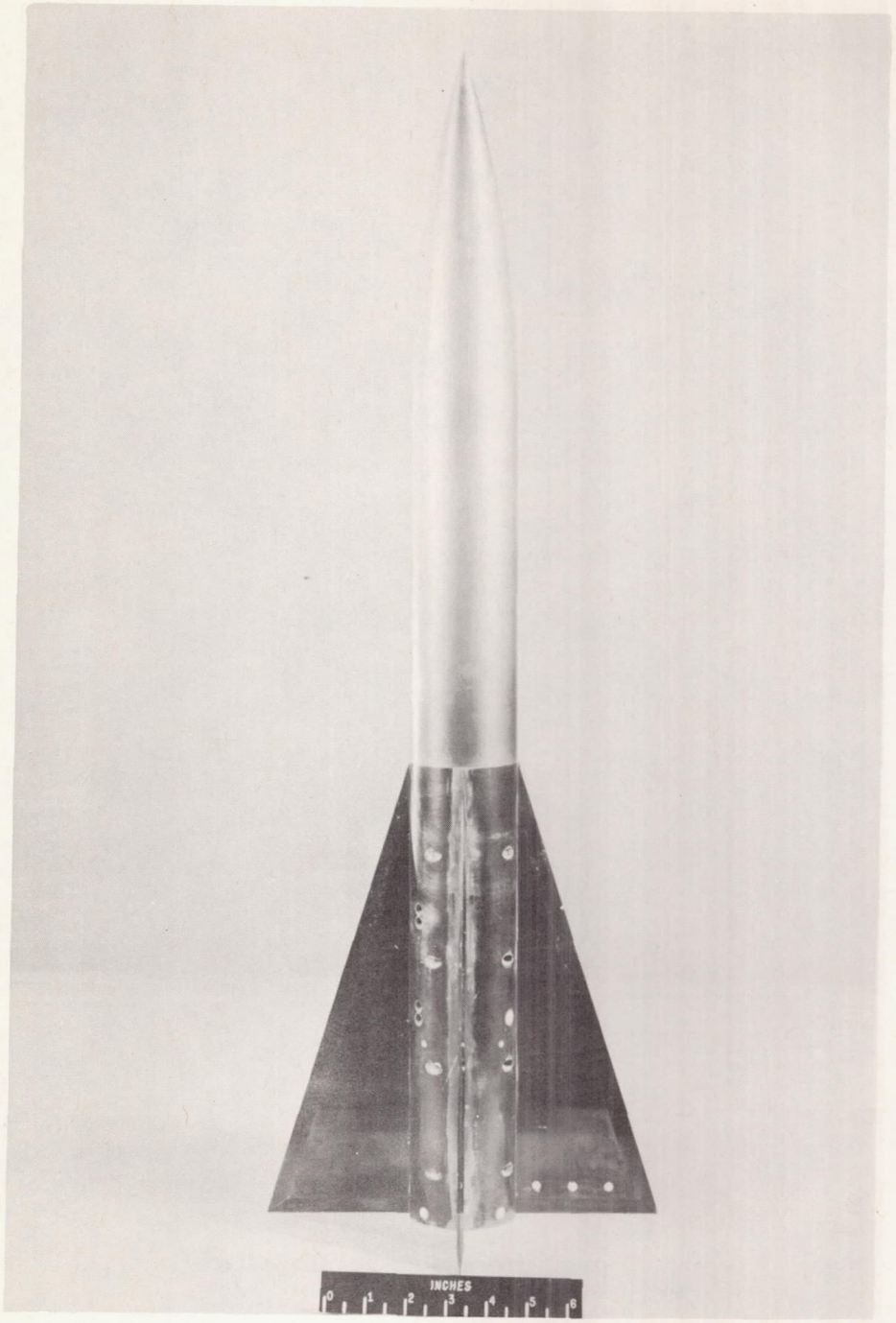
(f) Details of wings.

Figure 2.- Continued.



(g) Details of spoilers.

Figure 2.- Concluded.



(a) Typical delta-wing configuration. L-94318

Figure 3.- Models used in investigation.



(b) Typical rectangular-wing configuration. L-94317

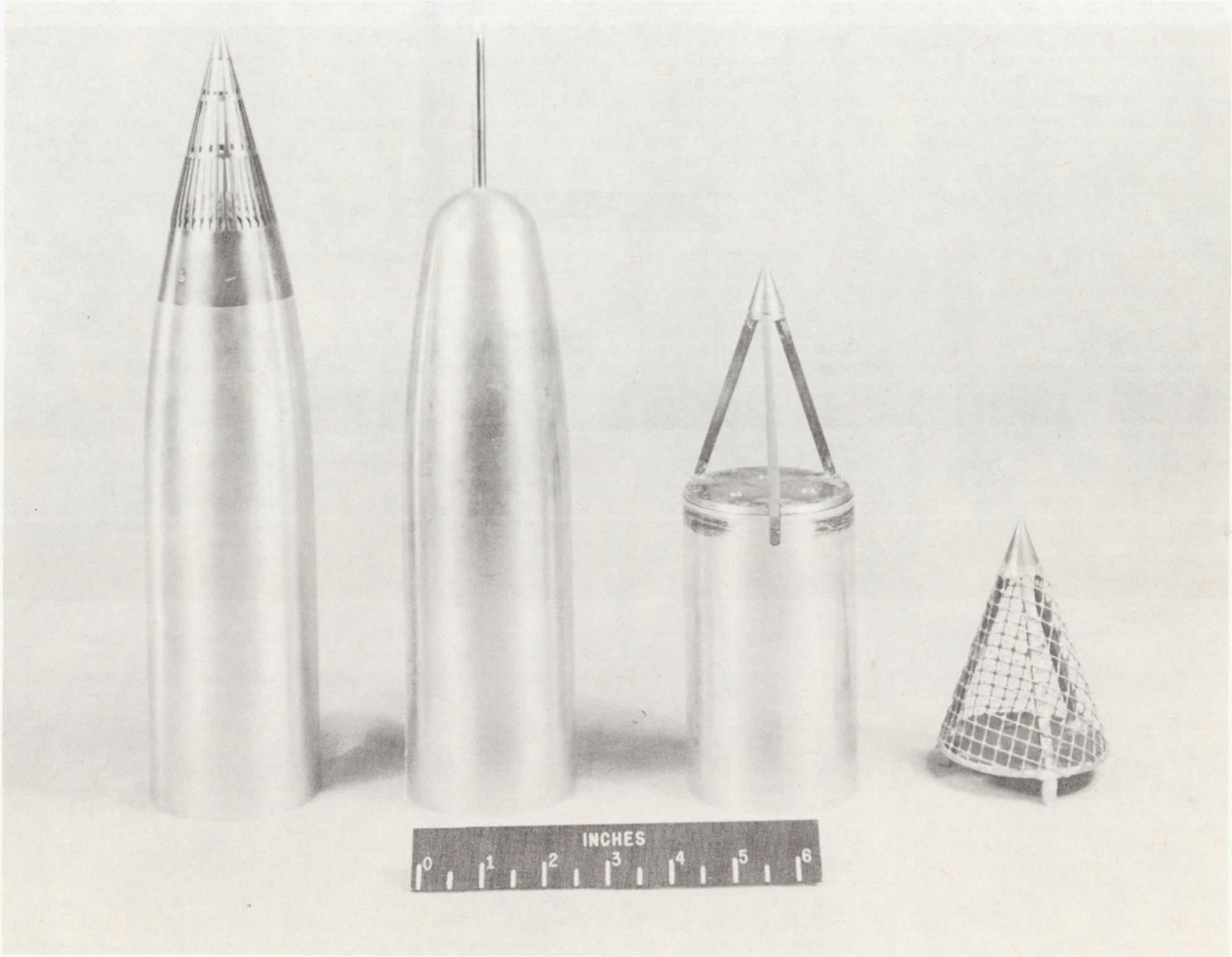
Figure 3.- Continued.



L-94320

(c) Ogive cylinders and 2-caliber boattailed and flared afterbodies.

Figure 3.- Continued.



(d) Rounded ogive and tripod noses. L-94319

Figure 3.- Concluded.

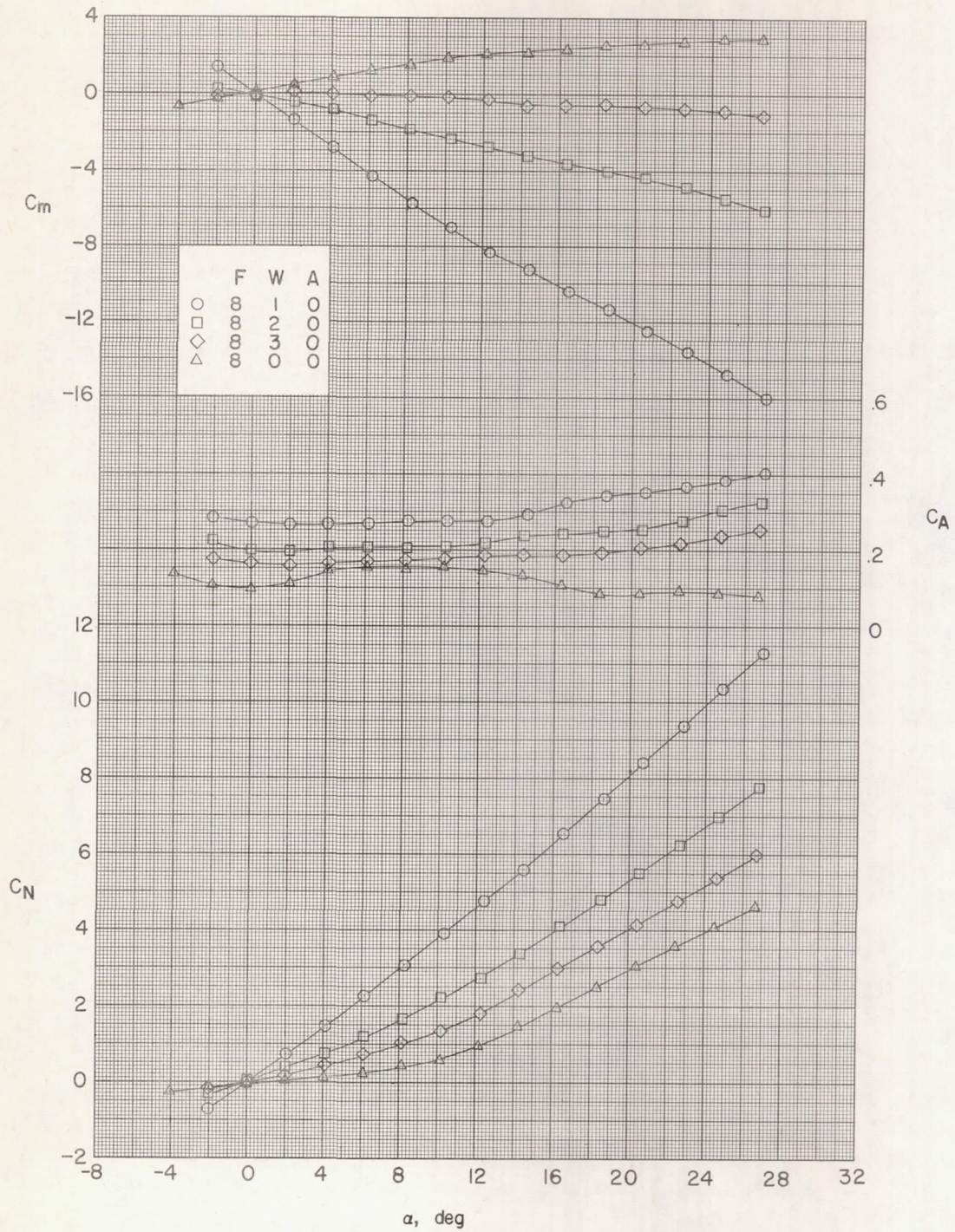


Figure 4.- Effects of delta wings on aerodynamic characteristics in pitch. No afterbody; $l/d = 10$.

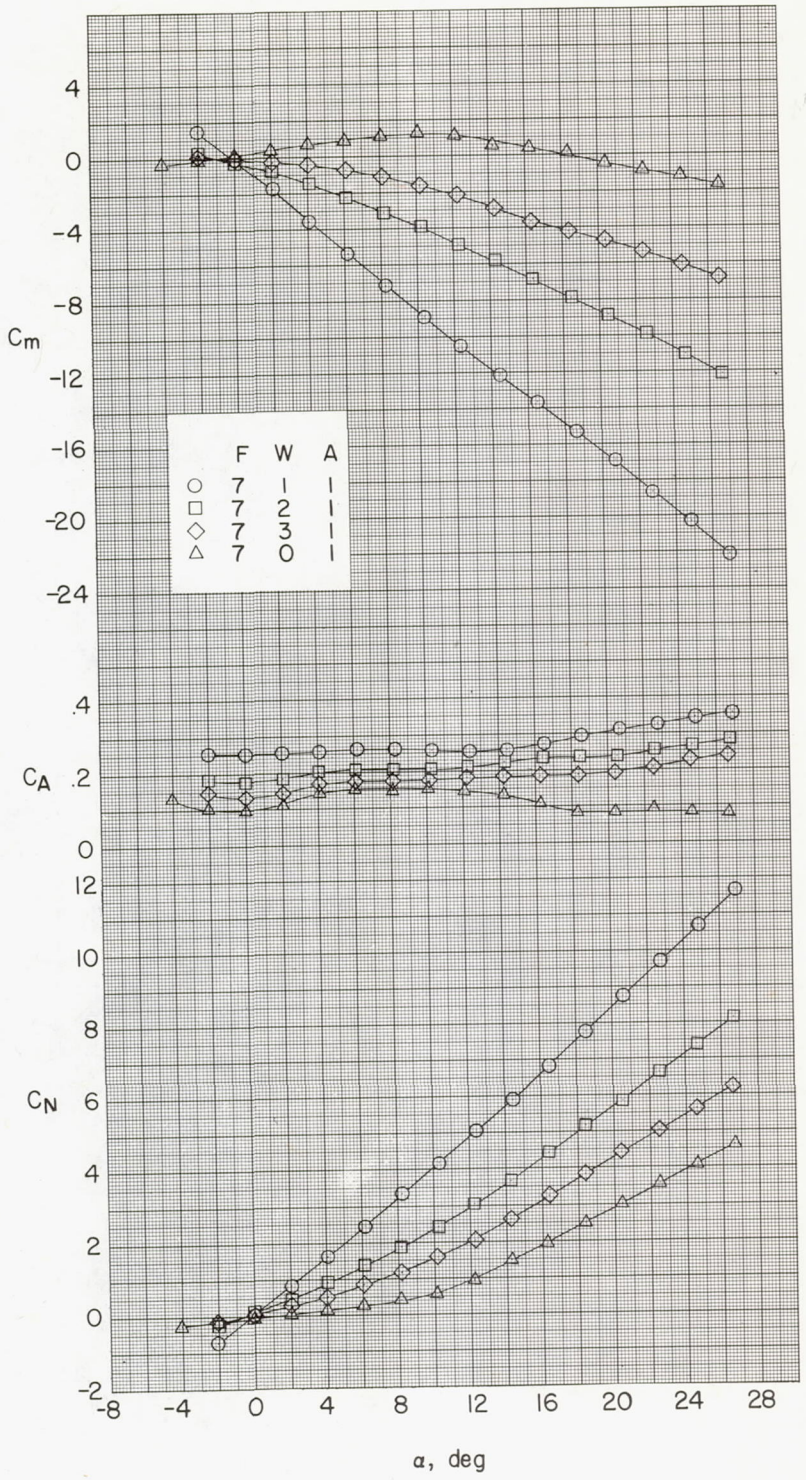


Figure 5.- Effects of delta wings on aerodynamic characteristics in pitch. One-caliber cylindrical afterbody; $l/d = 10$.

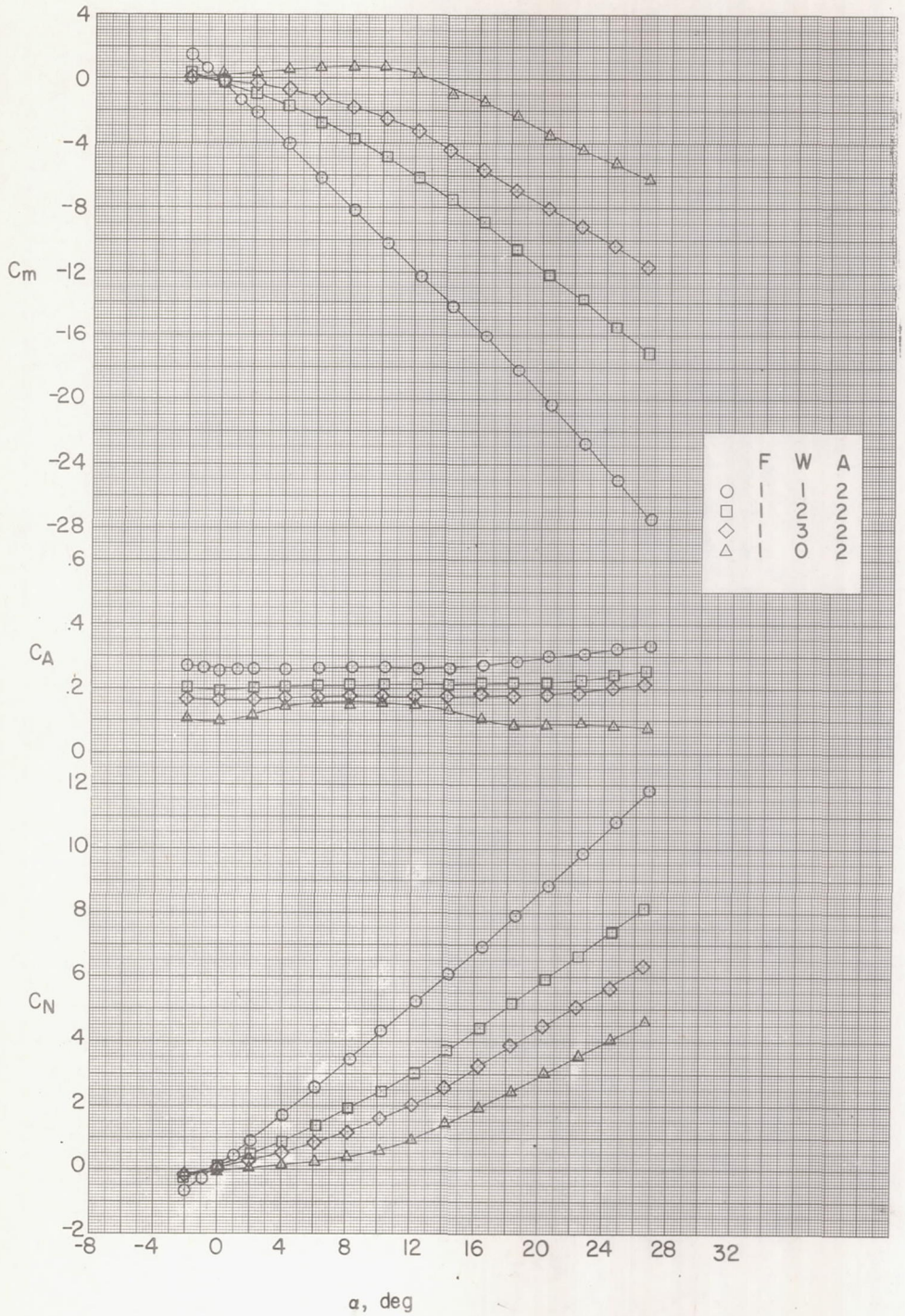
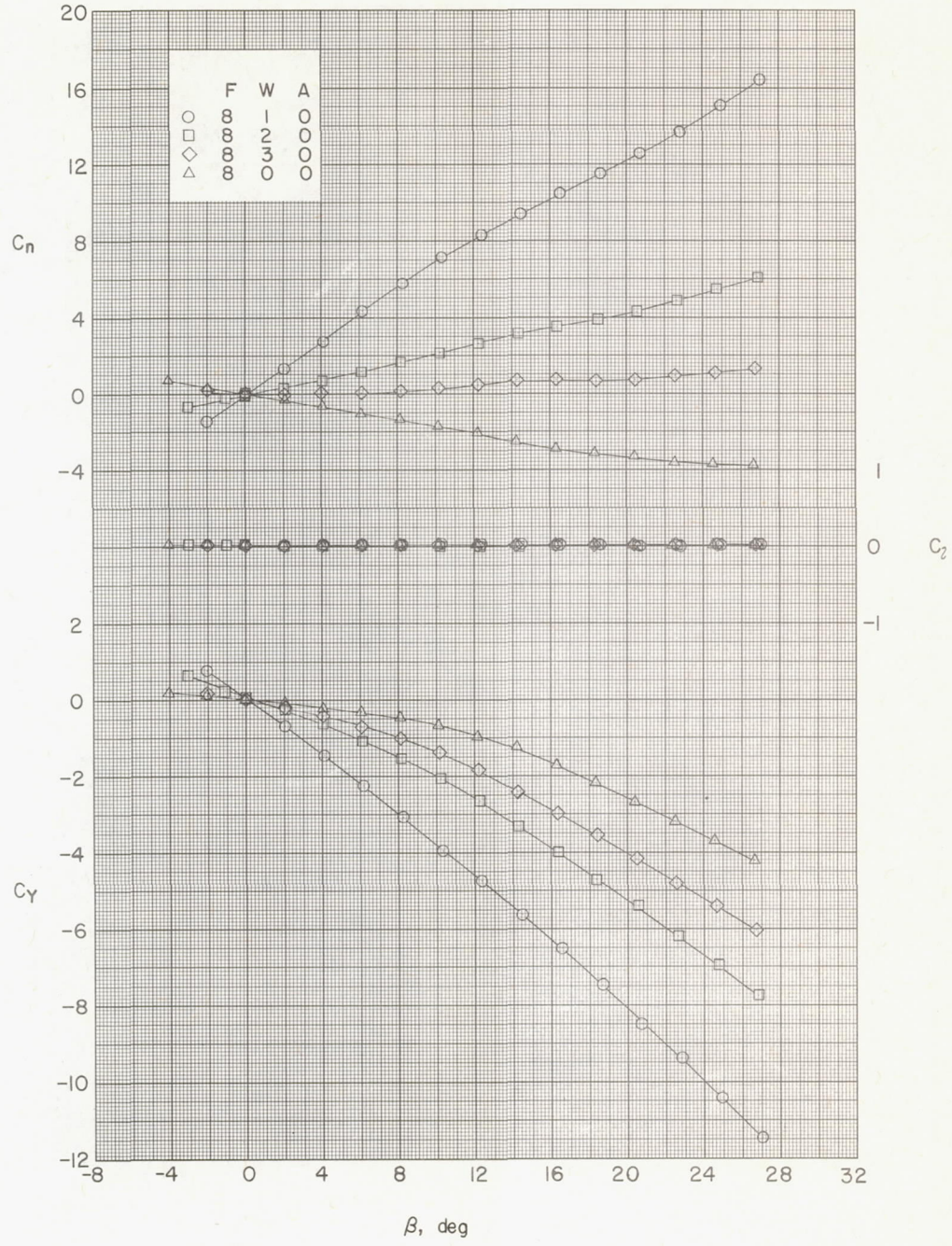
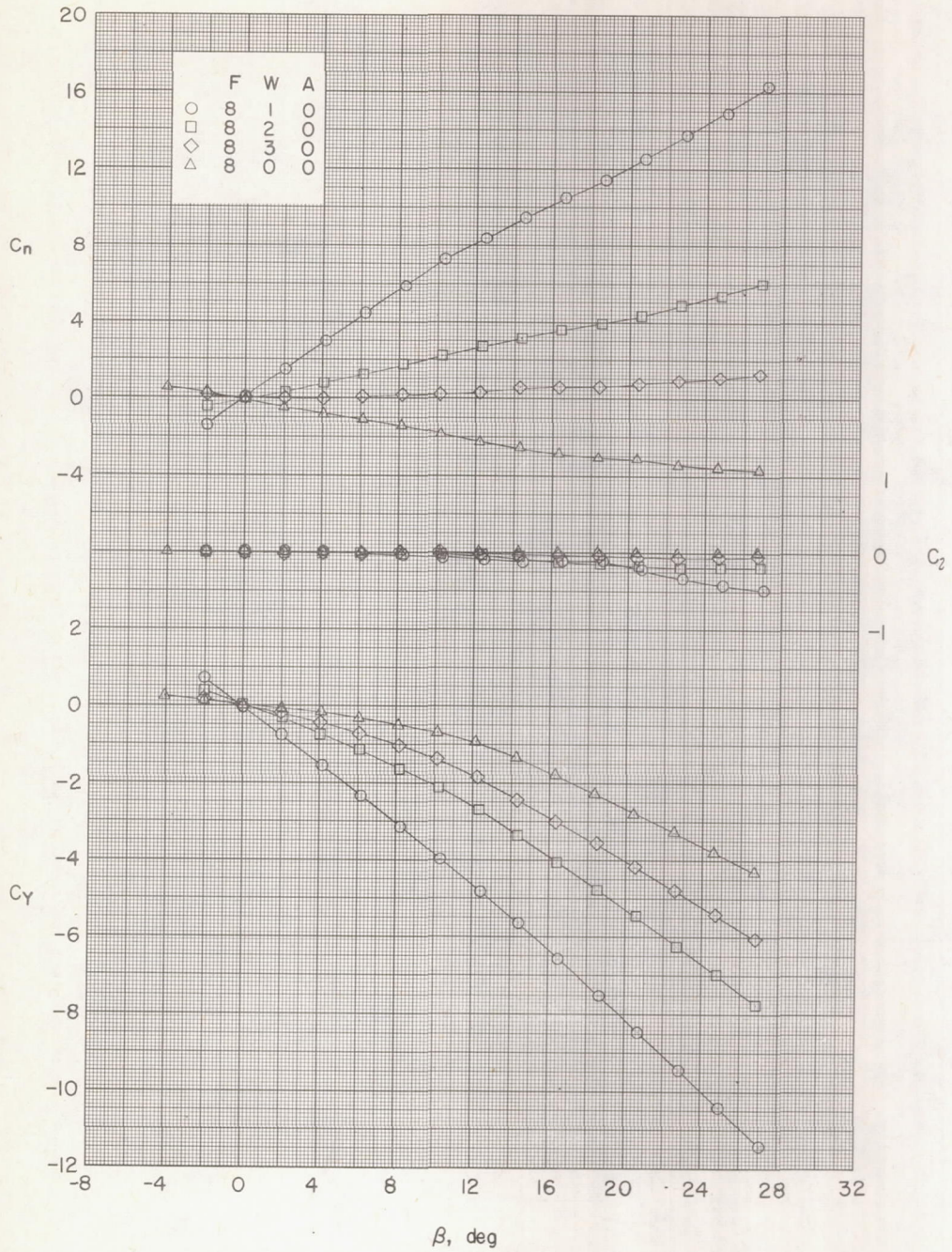


Figure 6.- Effects of delta wings on aerodynamic characteristics in pitch. Two-caliber cylindrical afterbody; $l/d = 10$.



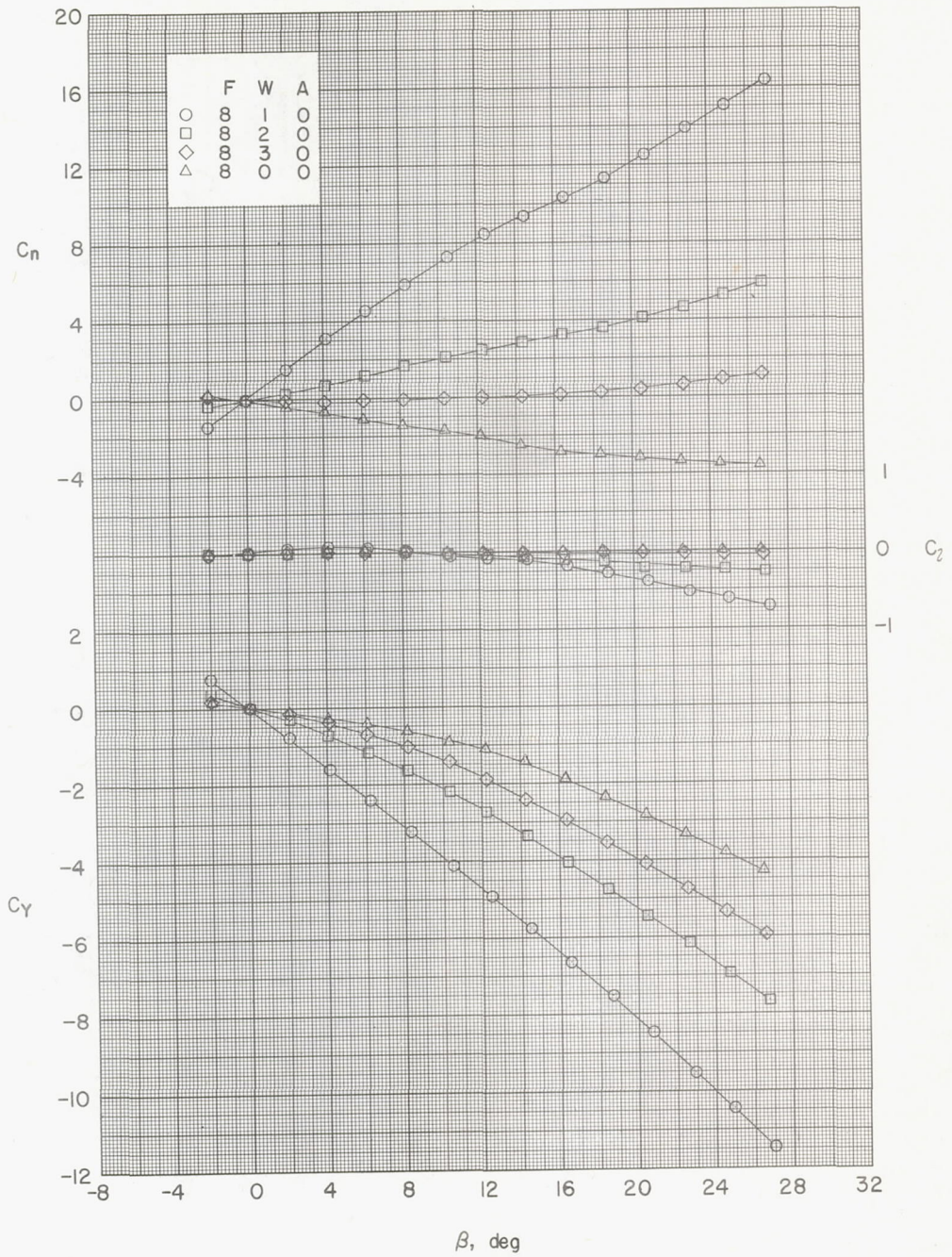
(a) $\alpha = 0^\circ$.

Figure 7.- Effects of delta wings on aerodynamic characteristics in sideslip. No afterbody; $l/d = 10$.



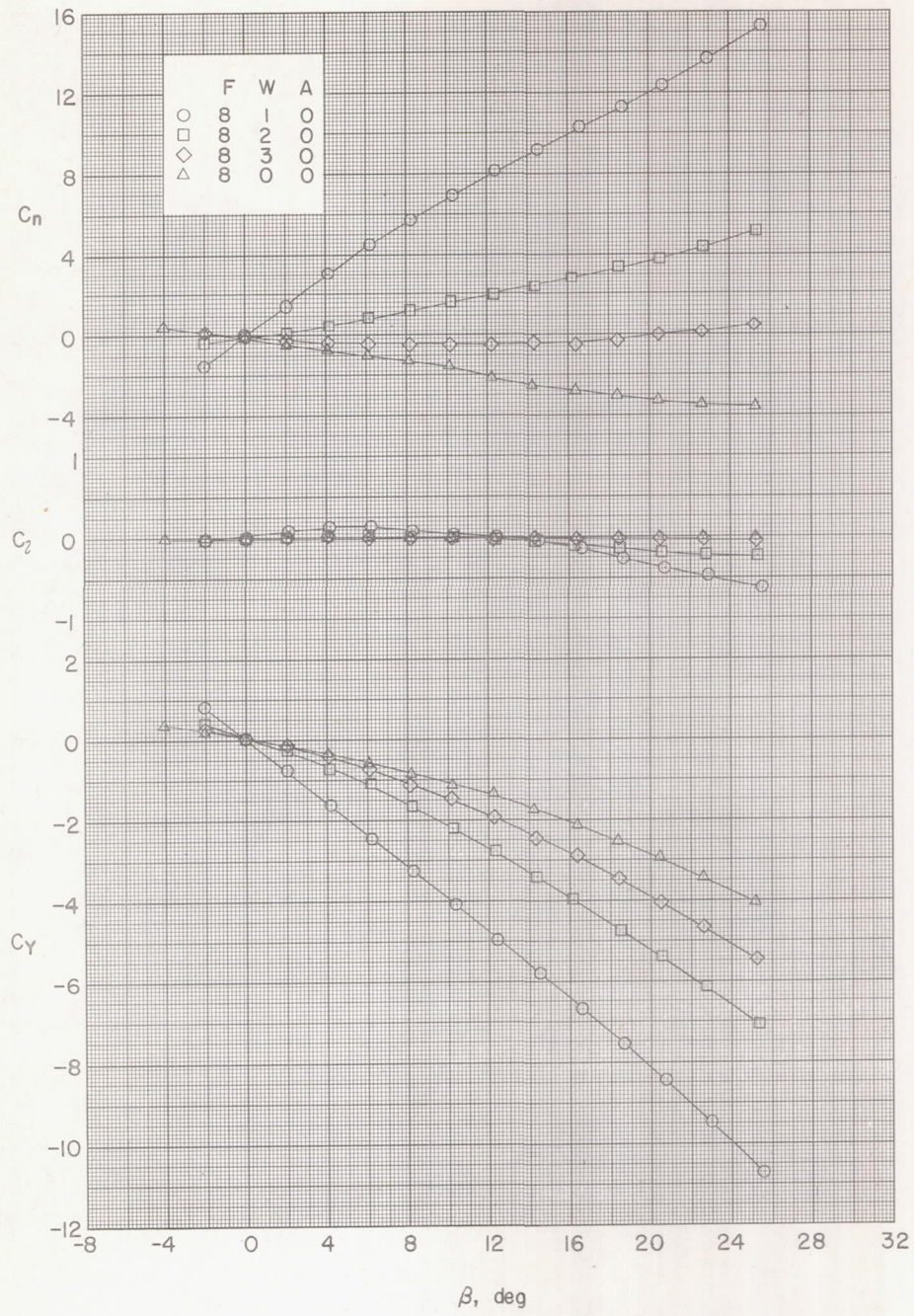
(b) $\alpha \approx 4.1°$.

Figure 7.- Continued.



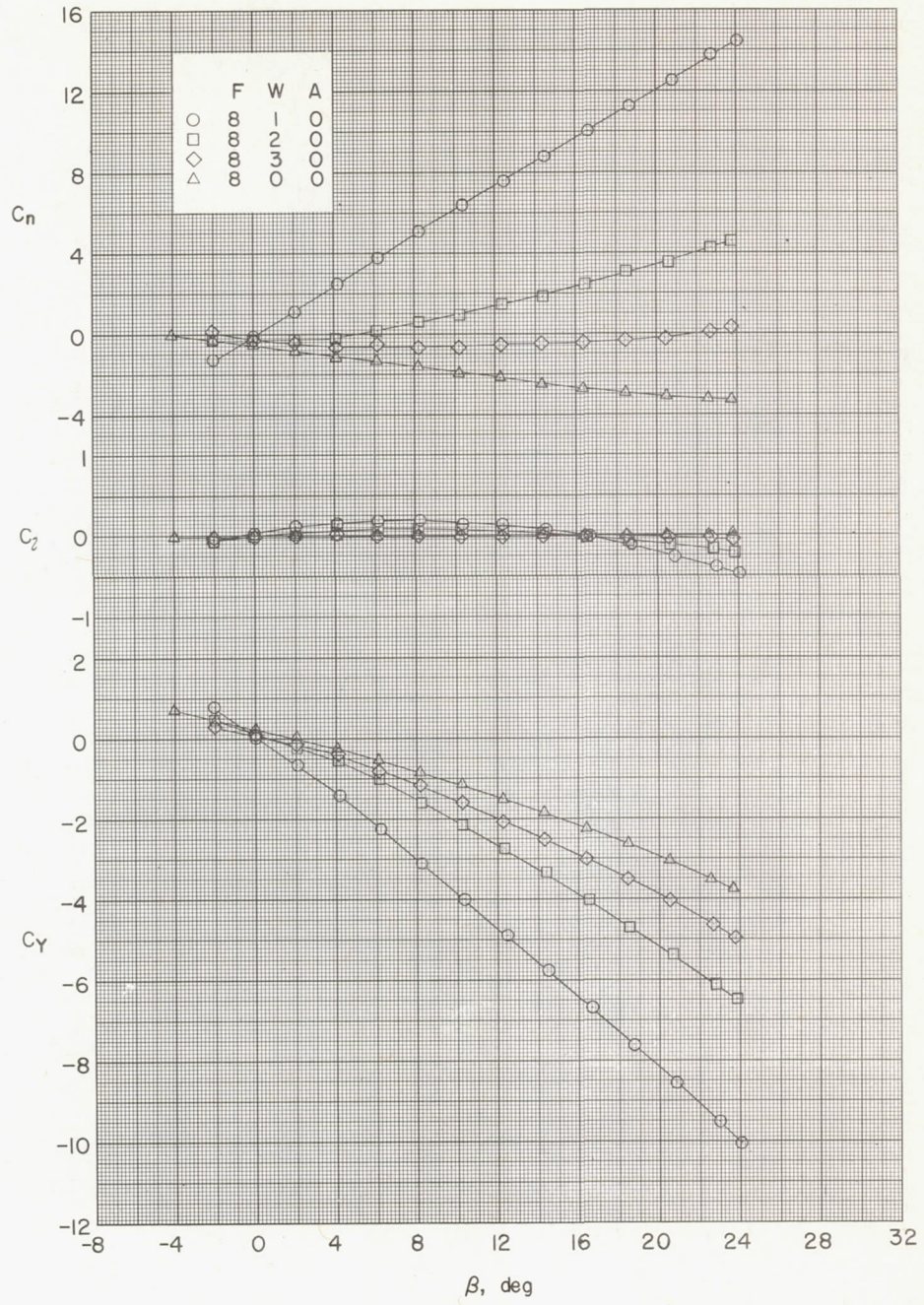
(c) $\alpha \approx 8.2^{\circ}$.

Figure 7.- Continued.



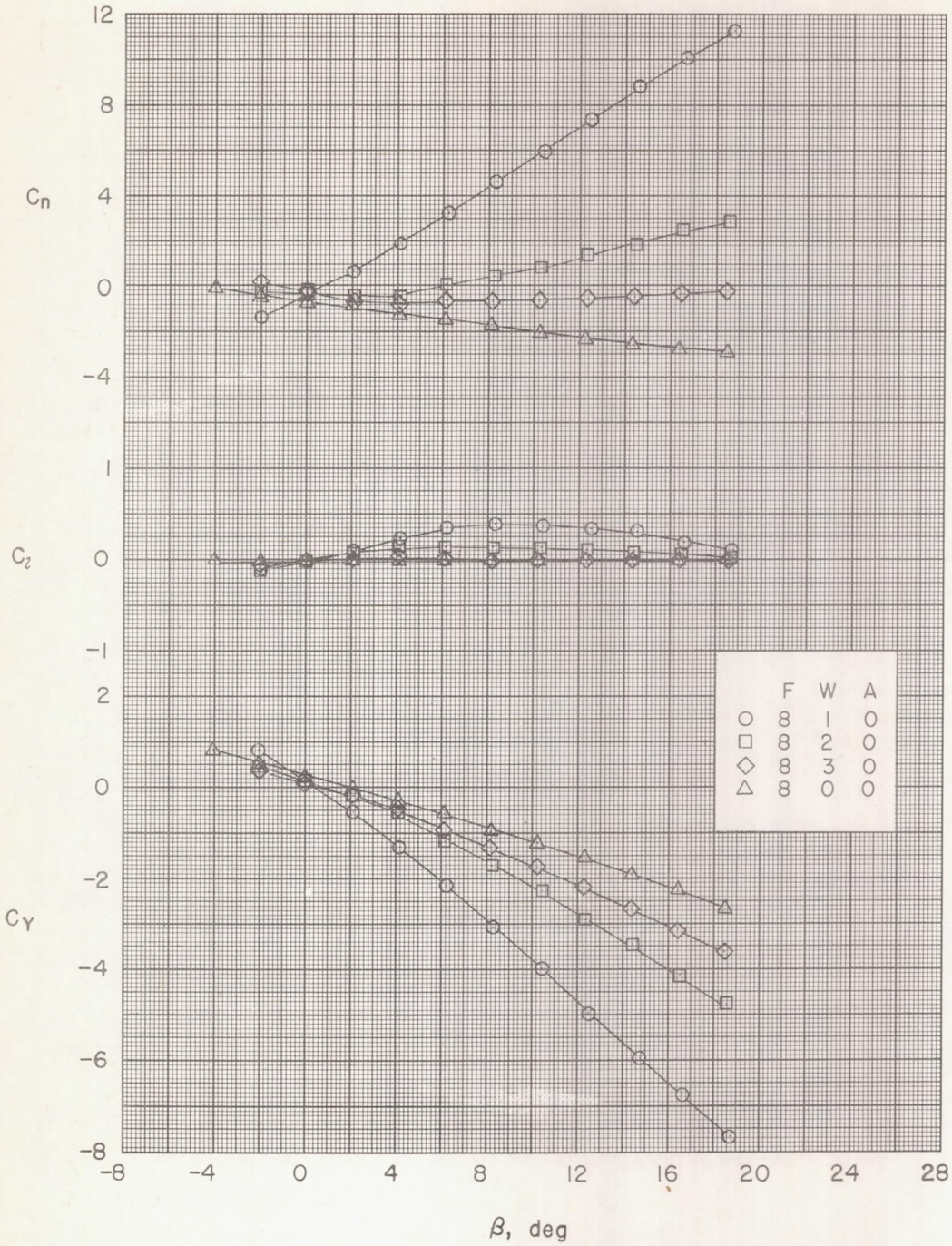
(d) $\alpha \approx 12.3^{\circ}$.

Figure 7.- Continued.



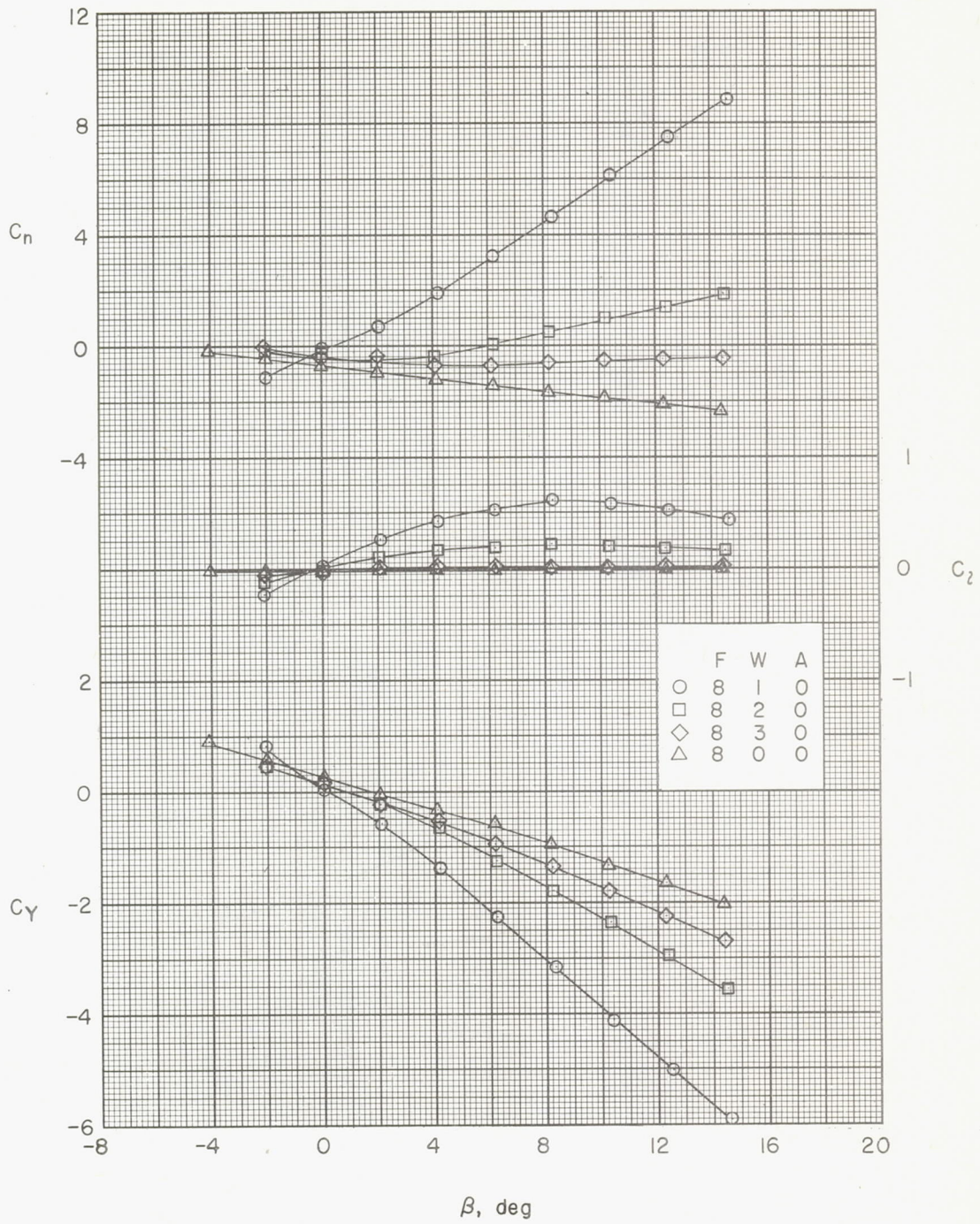
(e) $\alpha \approx 16.4^{\circ}$.

Figure 7.- Continued.



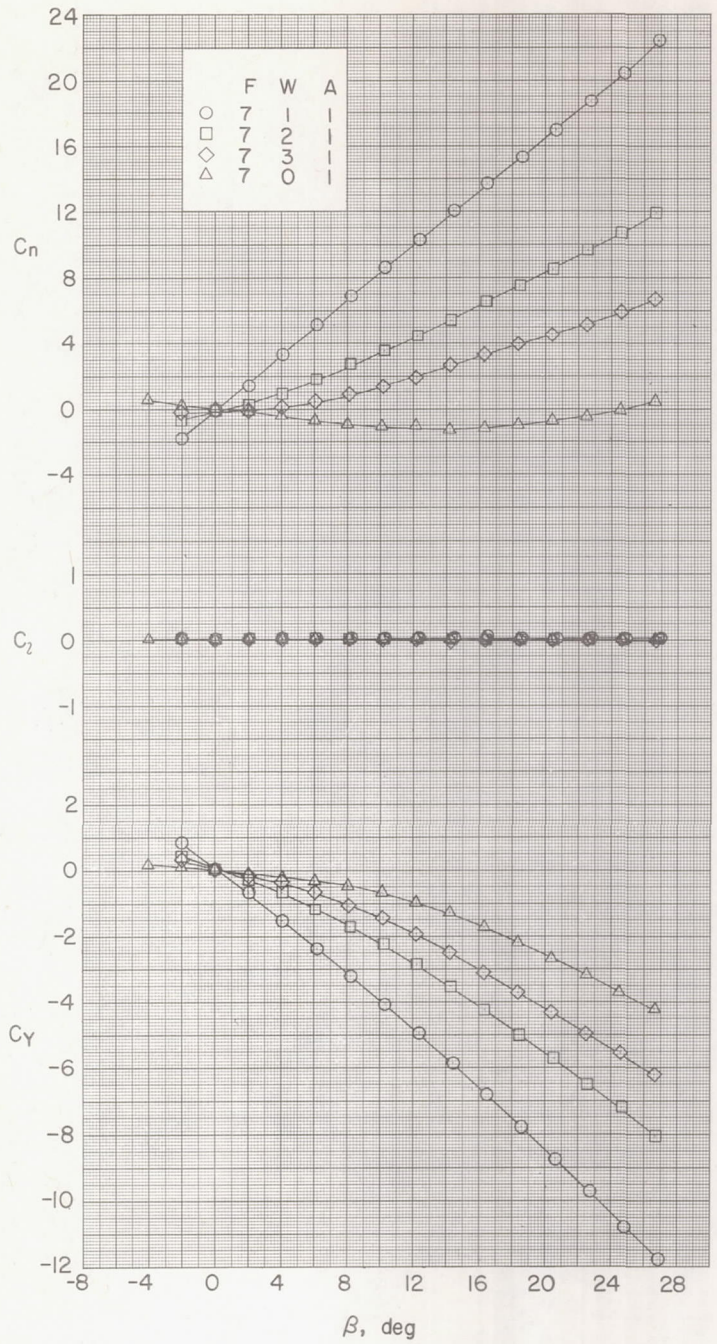
(f) $\alpha \approx 20.5^{\circ}$.

Figure 7.- Continued.



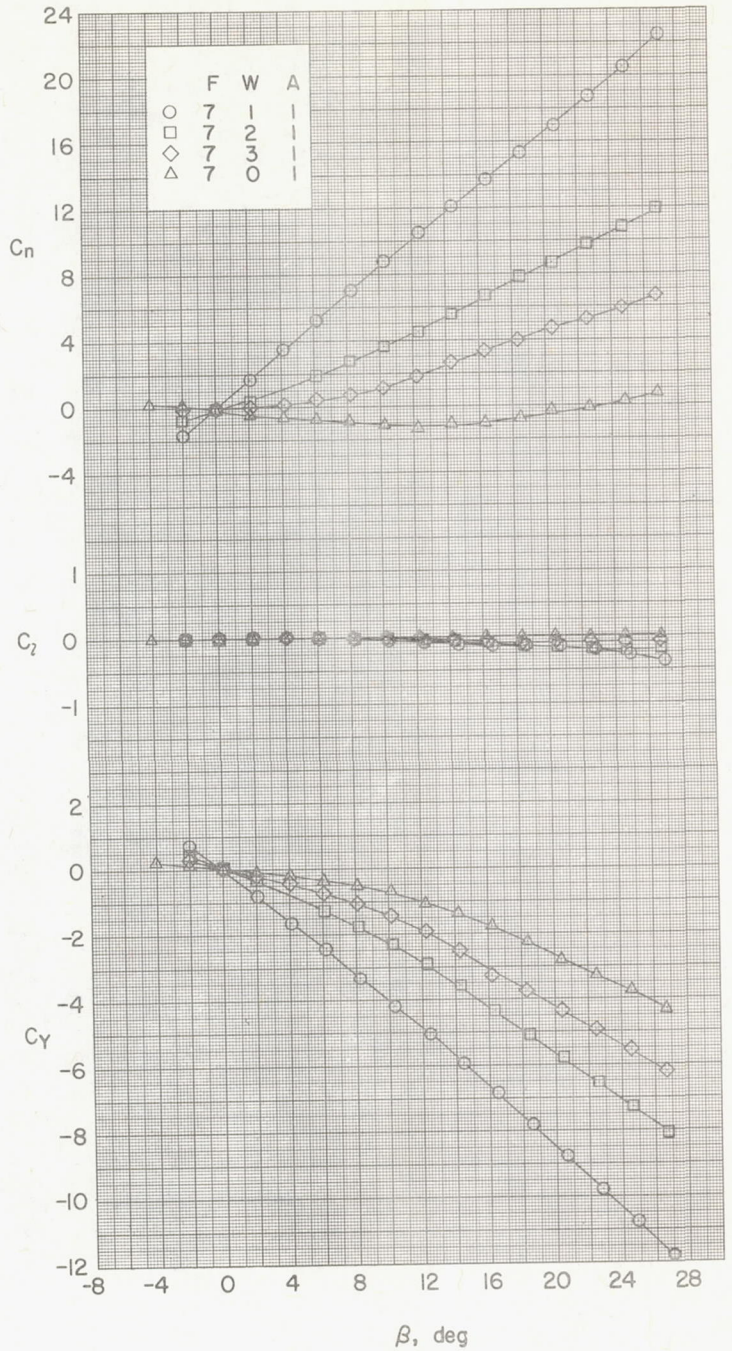
(g) $\alpha \approx 24.7^{\circ}$.

Figure 7.- Concluded.



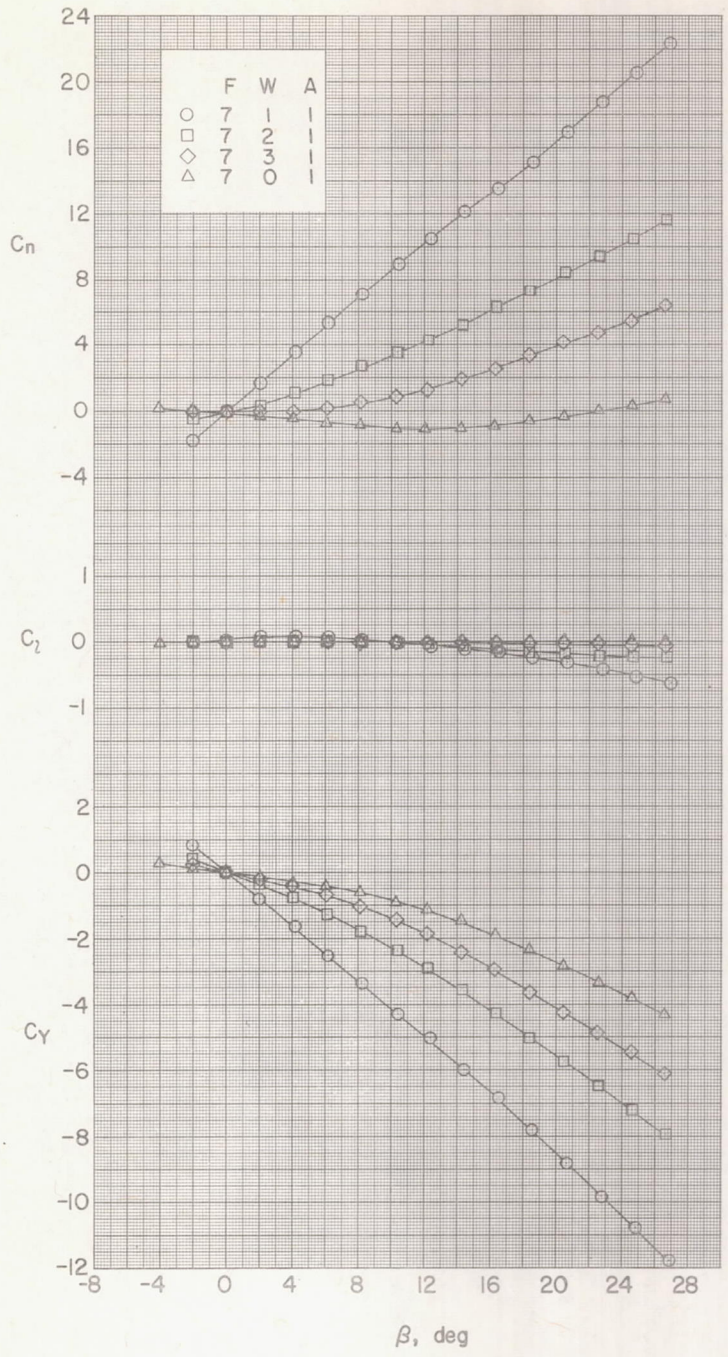
(a) $\alpha = 0^{\circ}$.

Figure 8.- Effects of delta wings on aerodynamic characteristics in sideslip. One-caliber cylindrical afterbody; $l/d = 10$.



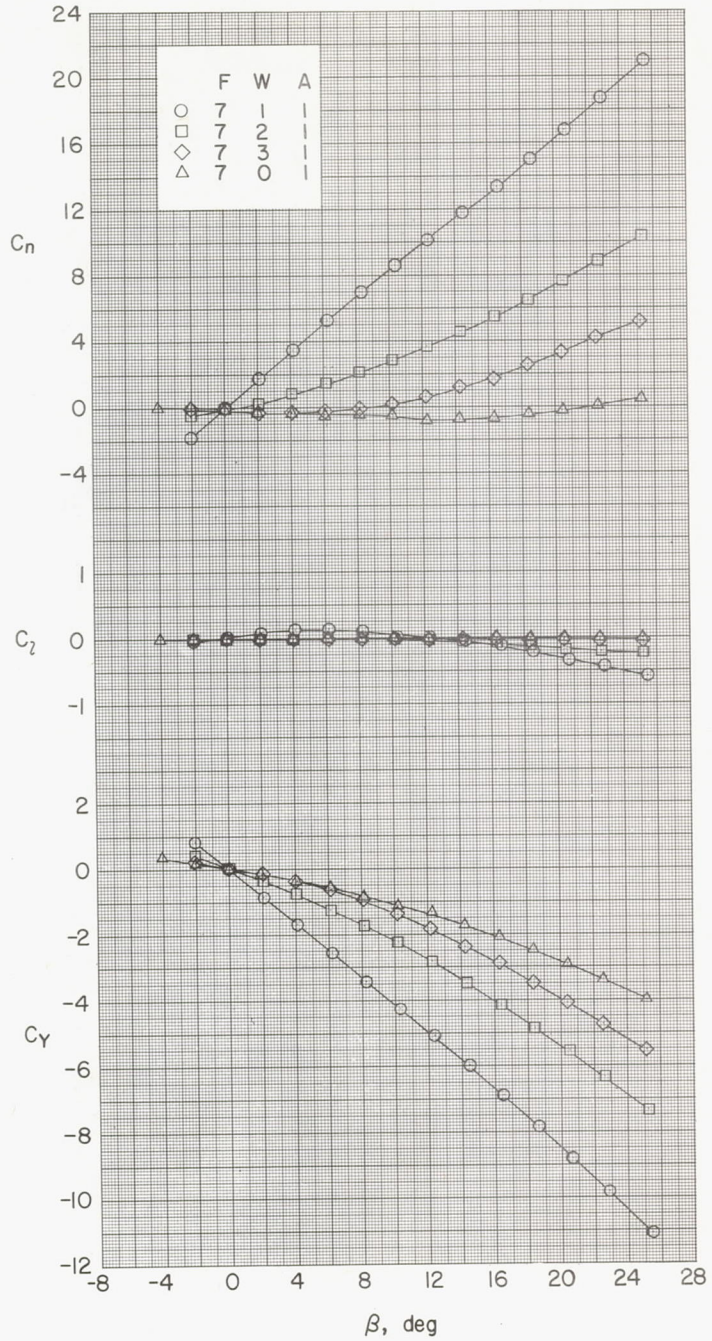
(b) $\alpha \approx 4.1^{\circ}$.

Figure 8.- Continued.



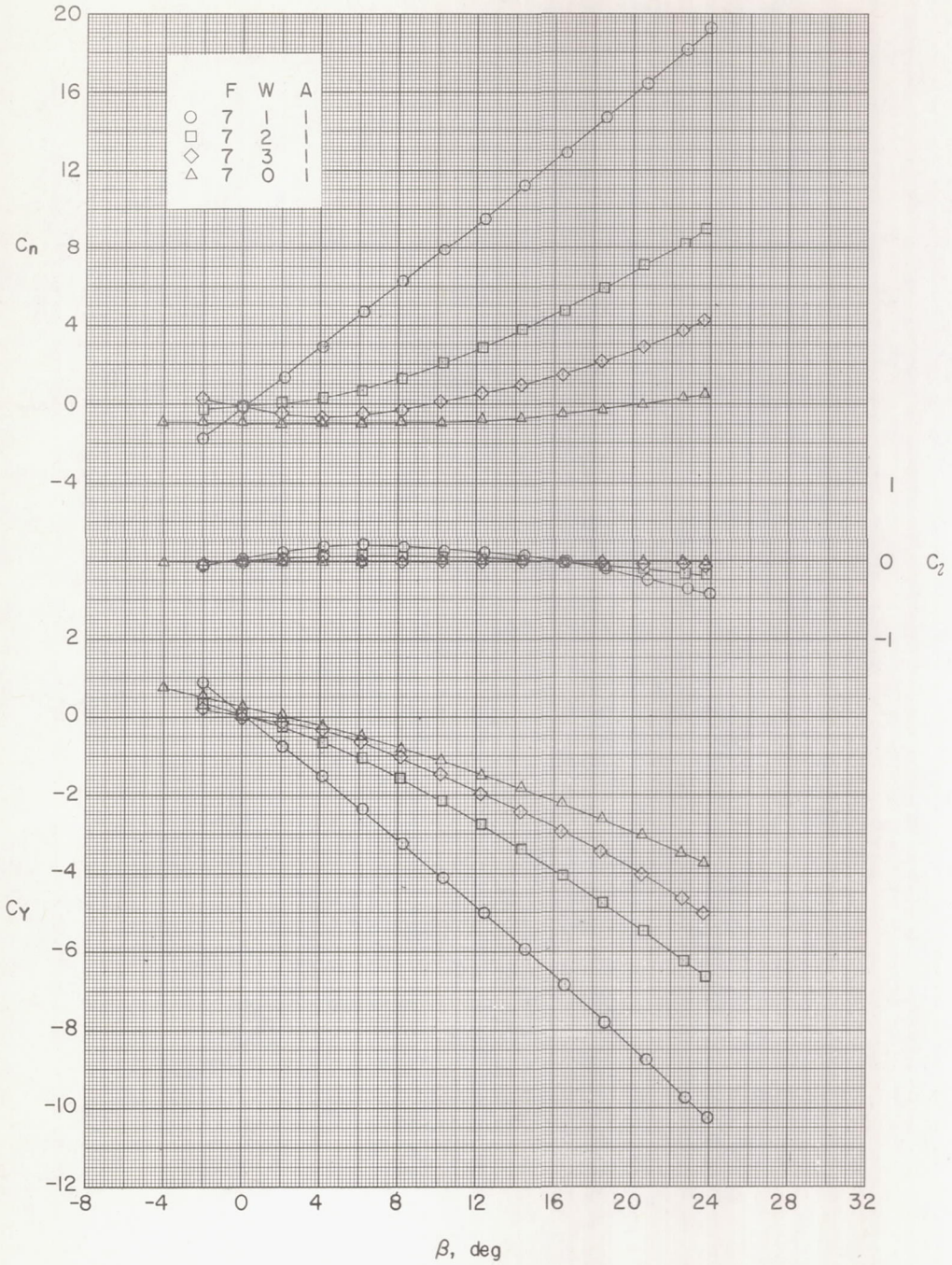
(c) $\alpha \approx 8.2^{\circ}$.

Figure 8.- Continued.



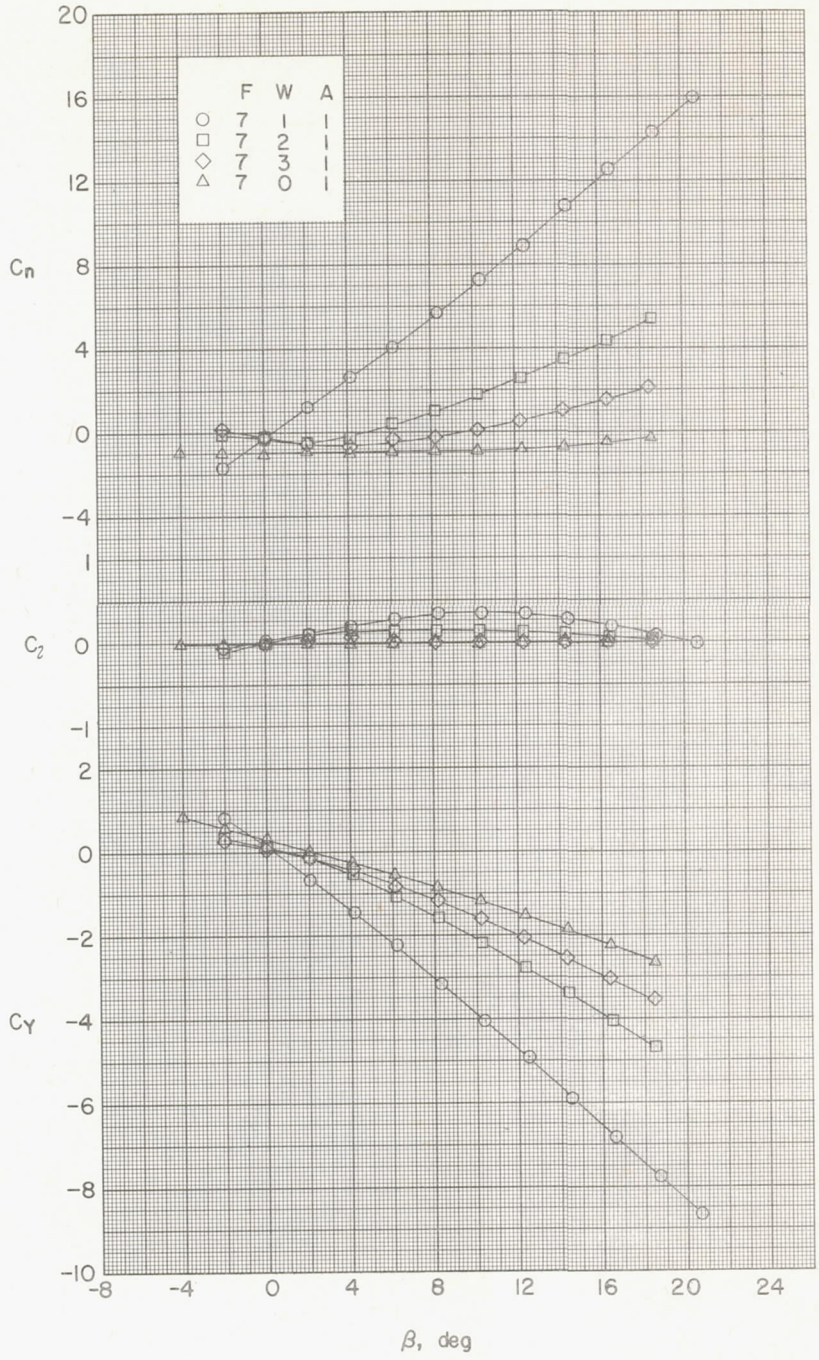
(d) $\alpha \approx 12.3^{\circ}$.

Figure 8.- Continued.



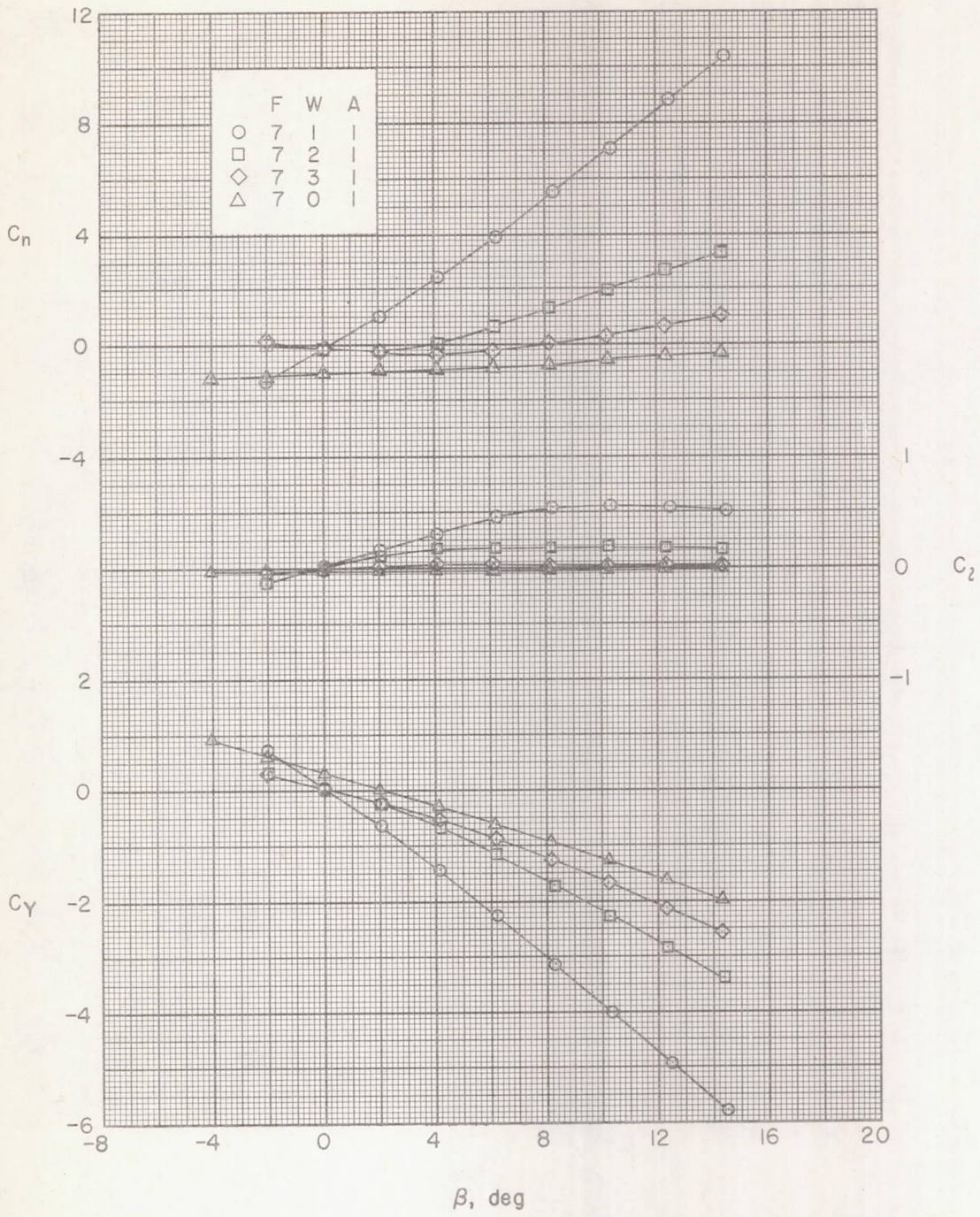
(e) $\alpha \approx 16.4^{\circ}$.

Figure 8.- Continued.



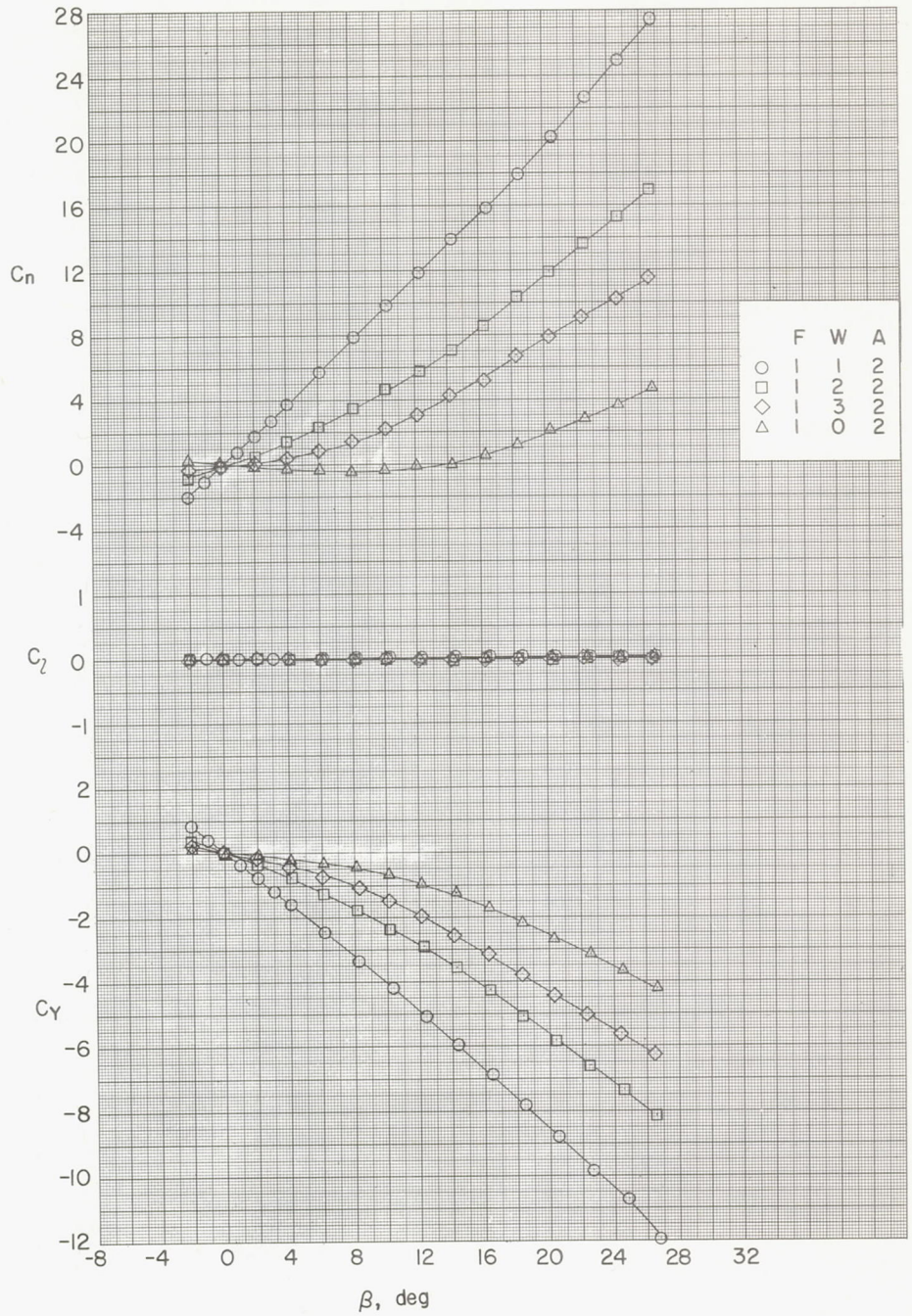
(f) $\alpha \approx 20.5^\circ$.

Figure 8.- Continued.



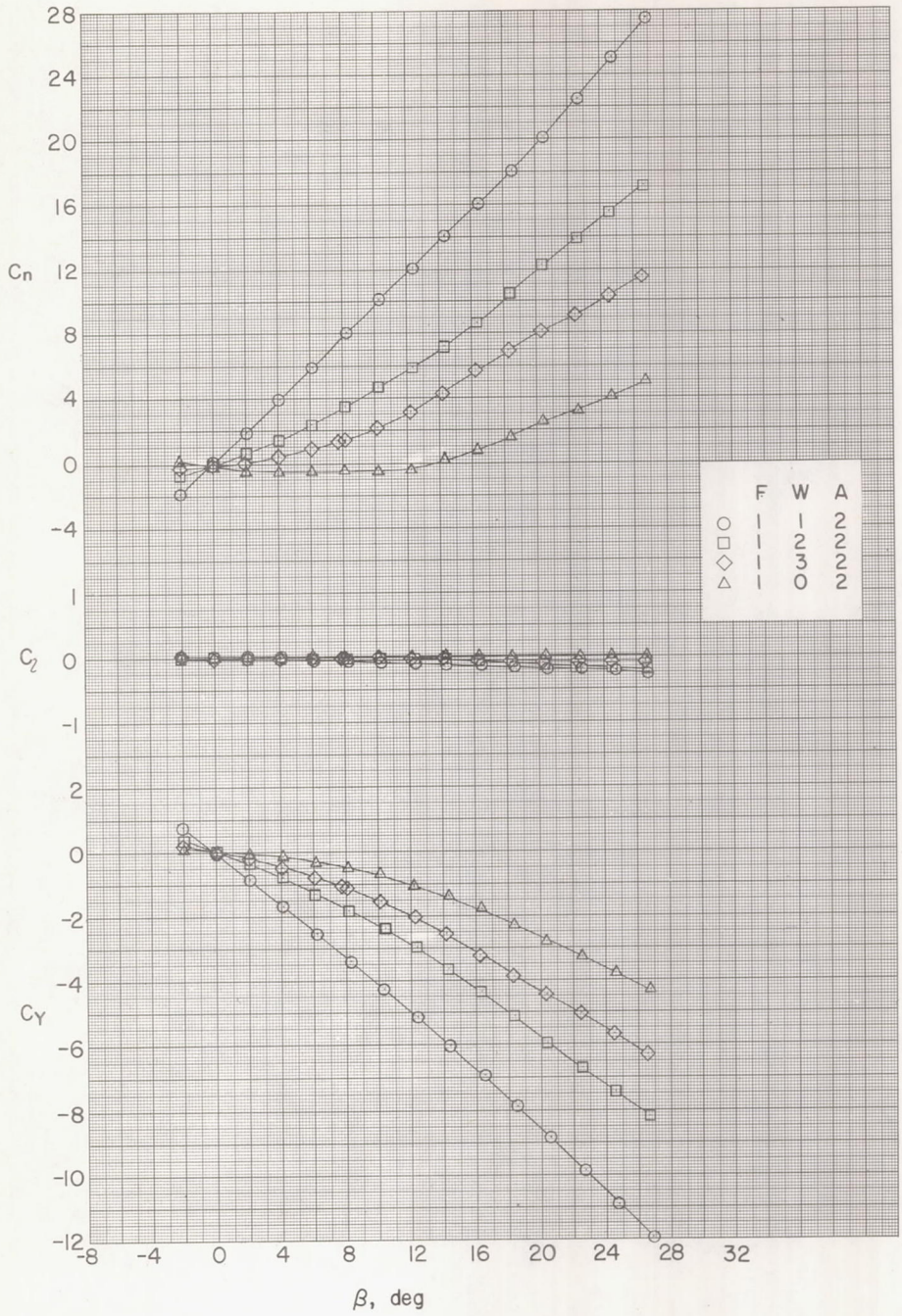
(g) $\alpha \approx 24.7^{\circ}$.

Figure 8.- Concluded.



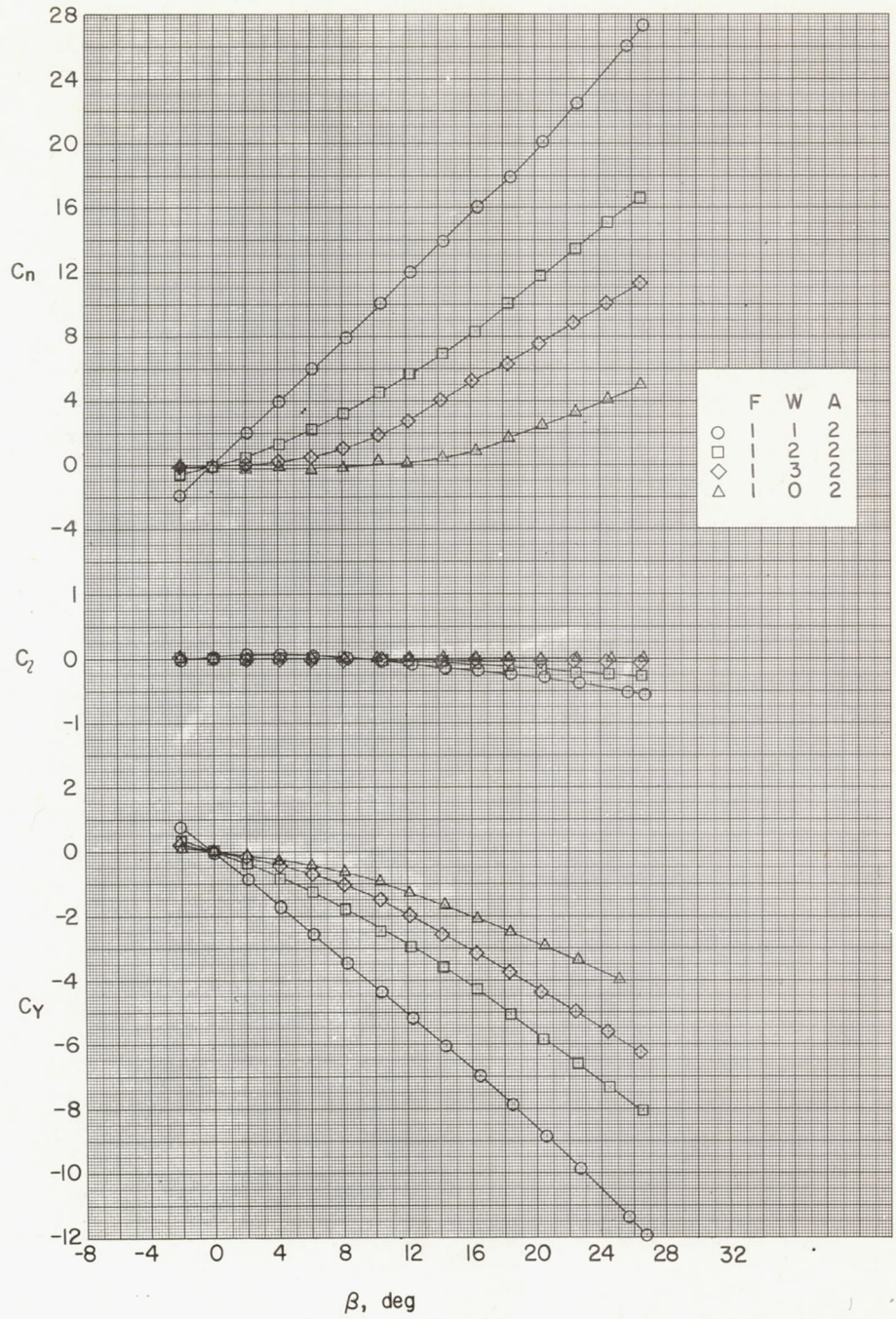
(a) $\alpha \approx 0^\circ$.

Figure 9.- Effects of delta wings on aerodynamic characteristics in sideslip. Two-caliber cylindrical afterbody; $l/d = 10$.



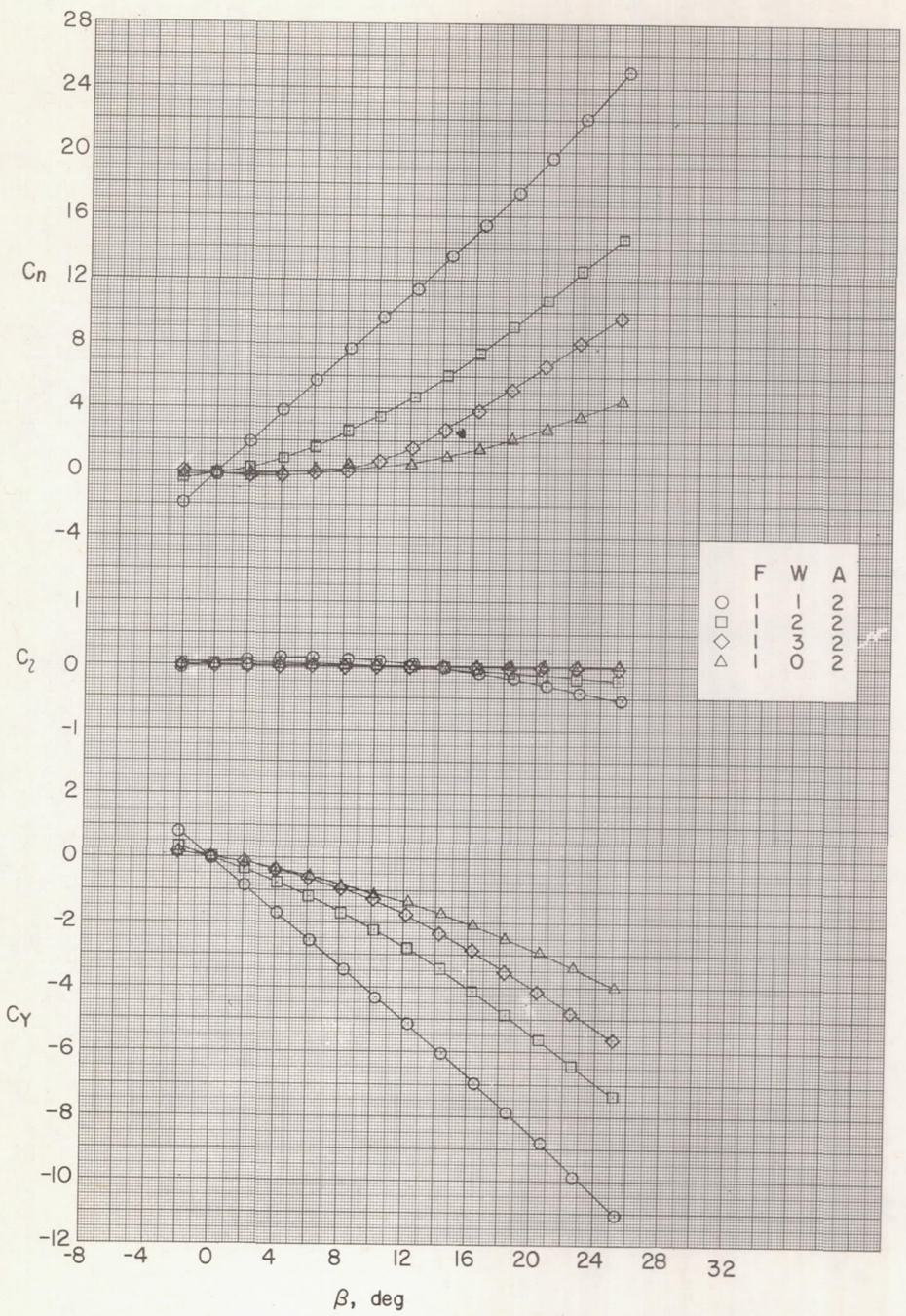
(b) $\alpha \approx 4.1^{\circ}$.

Figure 9.- Continued.



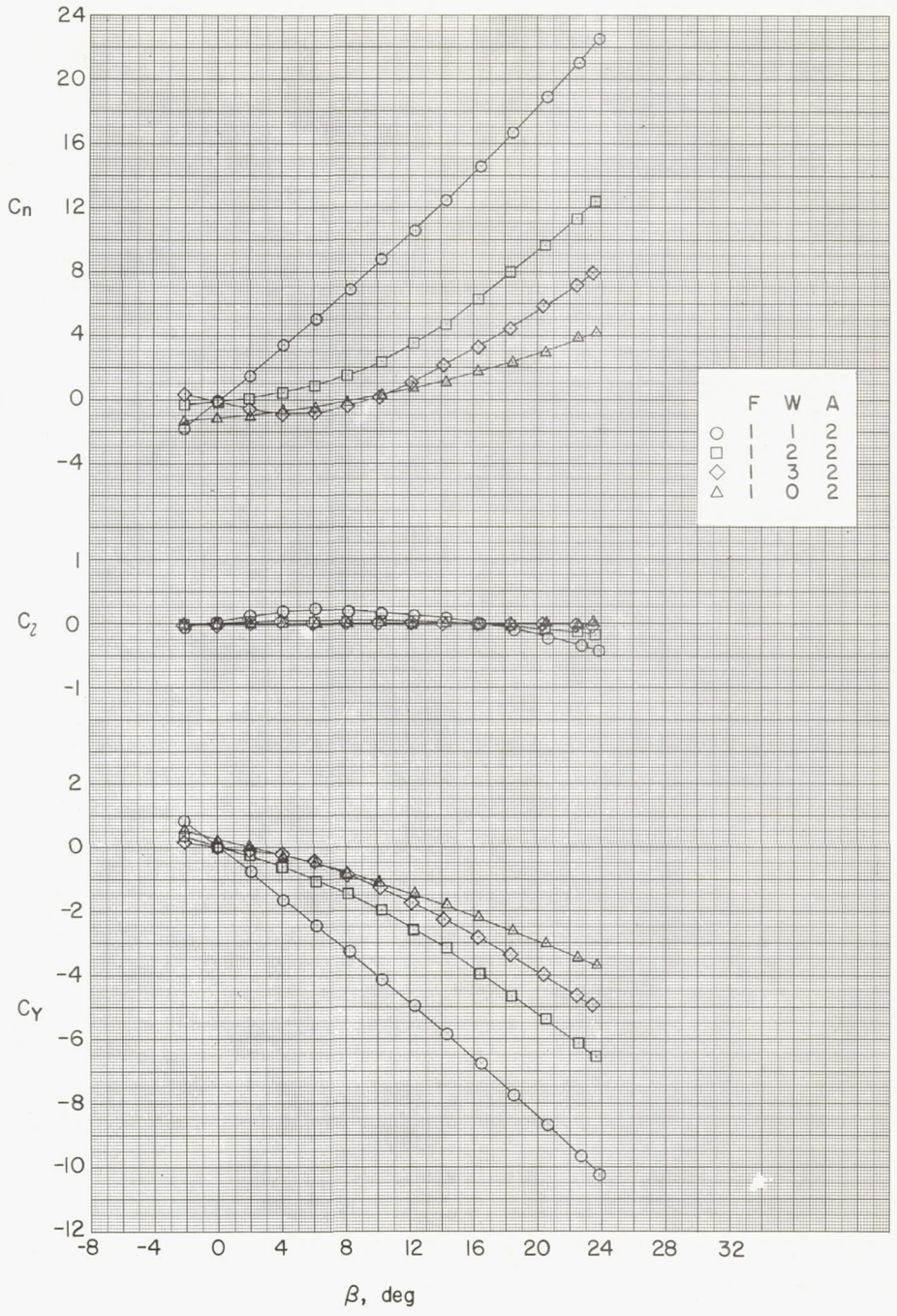
(c) $\alpha \approx 8.2^{\circ}$.

Figure 9.- Continued.



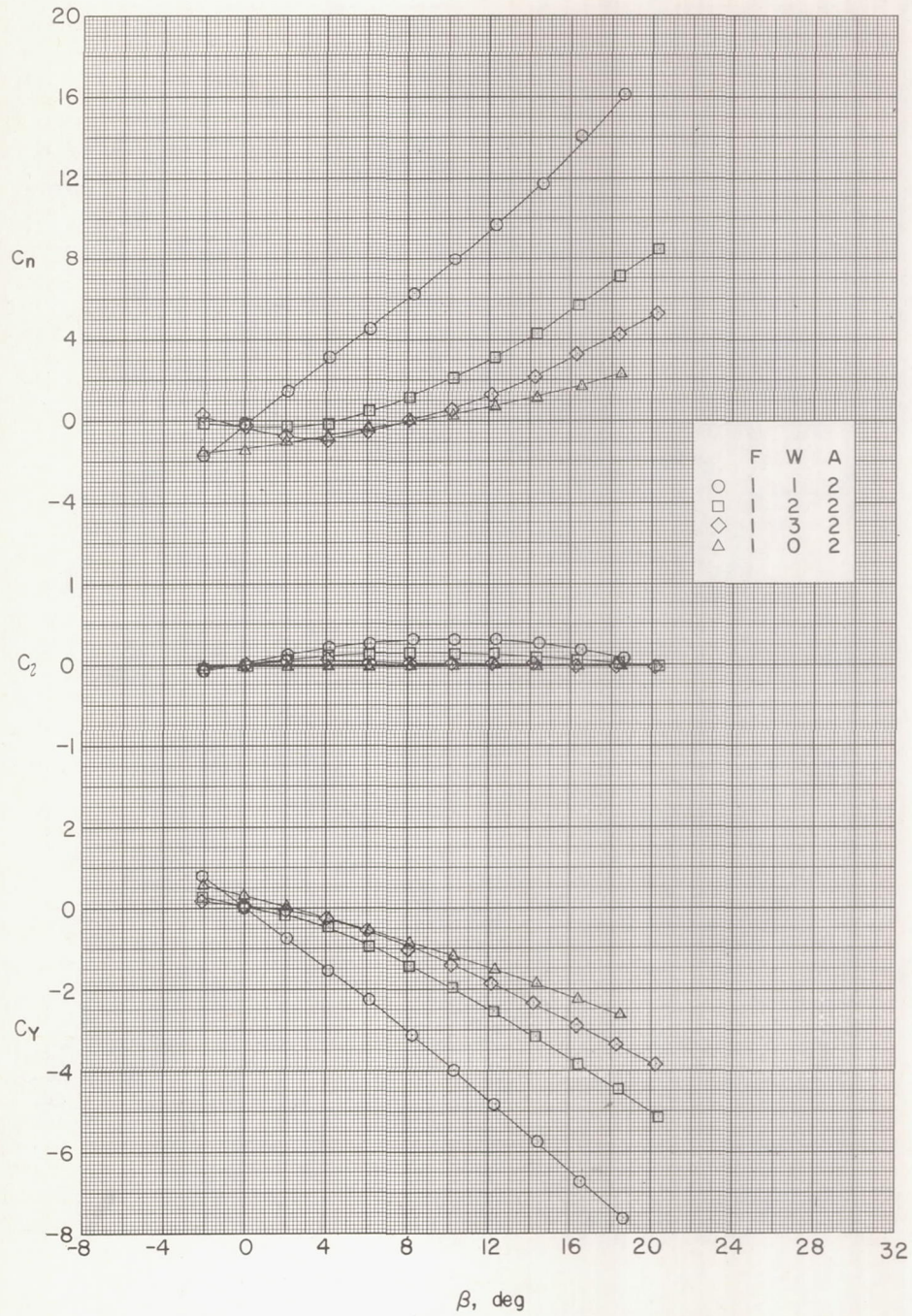
(d) $\alpha \approx 12.3^{\circ}$.

Figure 9.- Continued.



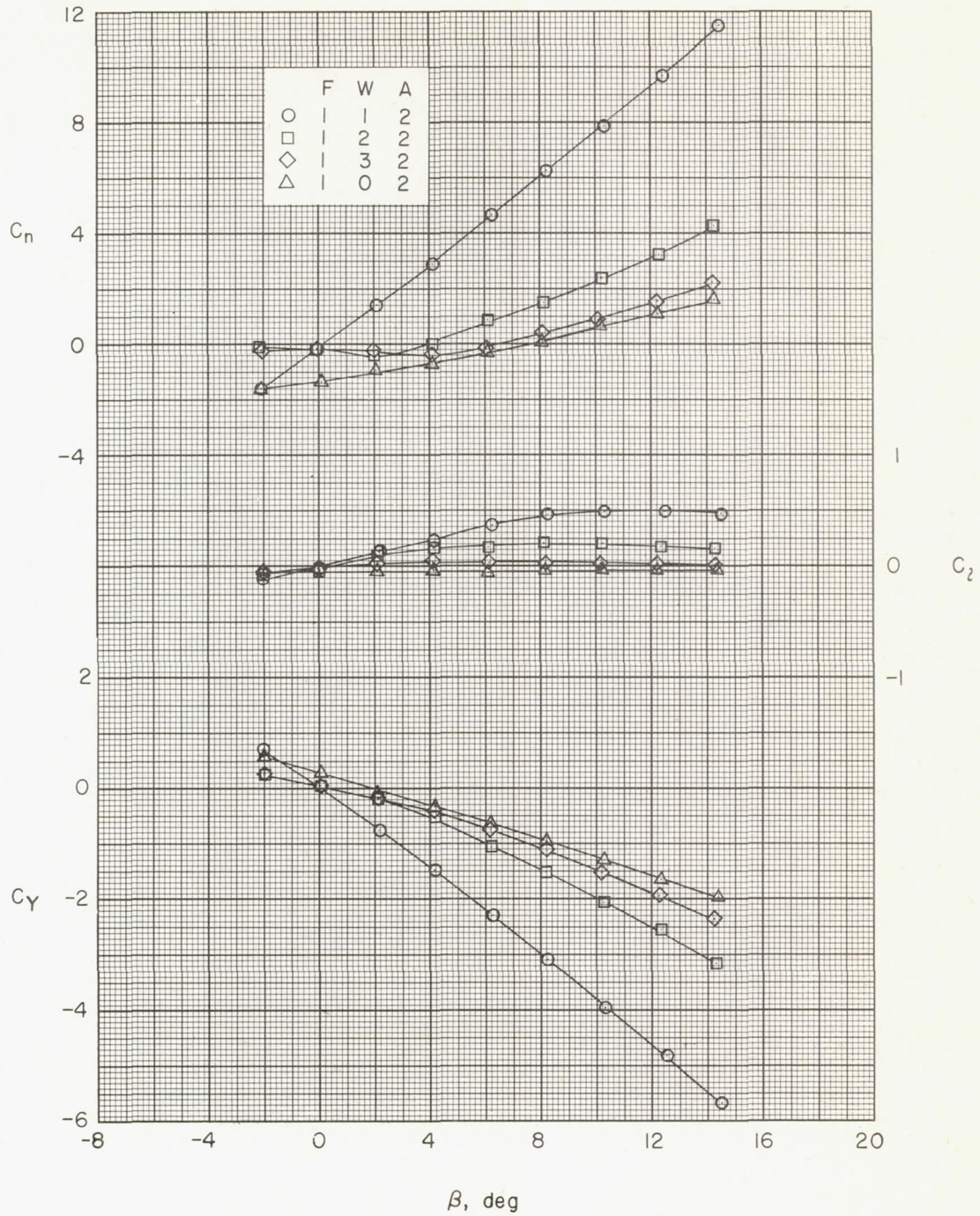
(e) $\alpha \approx 16.4^{\circ}$.

Figure 9.- Continued.



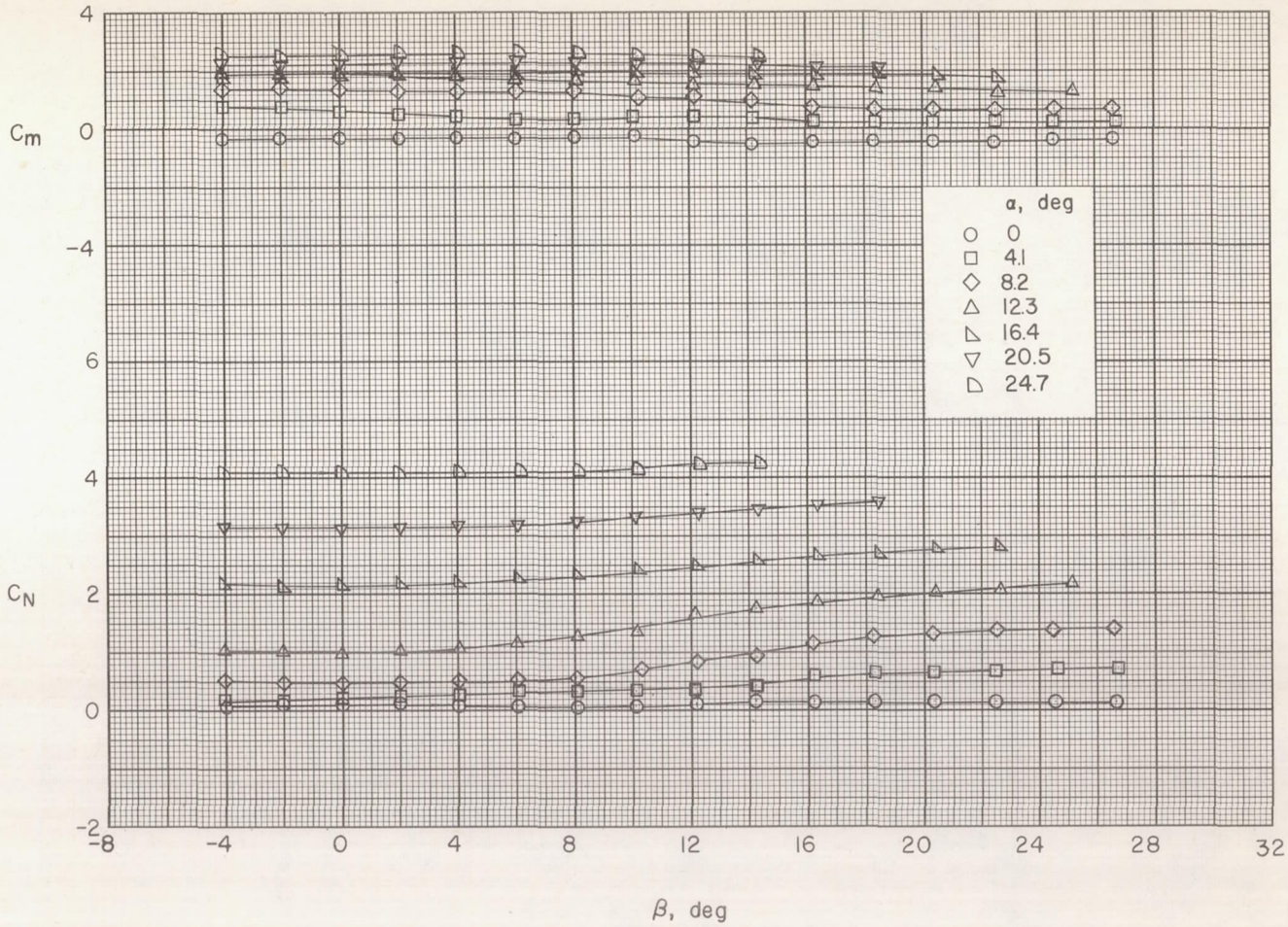
(f) $\alpha \approx 20.5^{\circ}$.

Figure 9.- Continued.



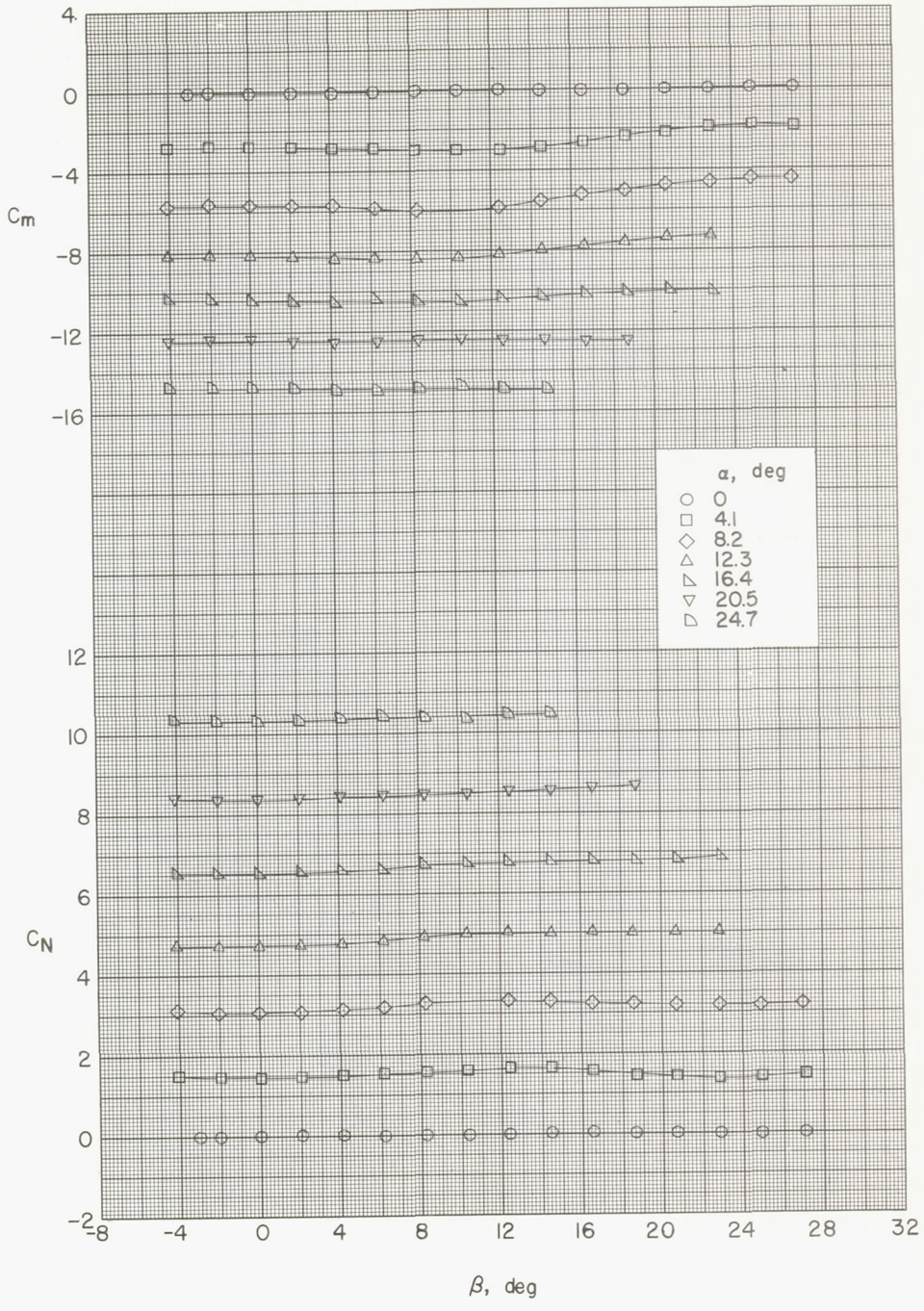
(g) $\alpha \approx 24.7^{\circ}$.

Figure 9.- Concluded.



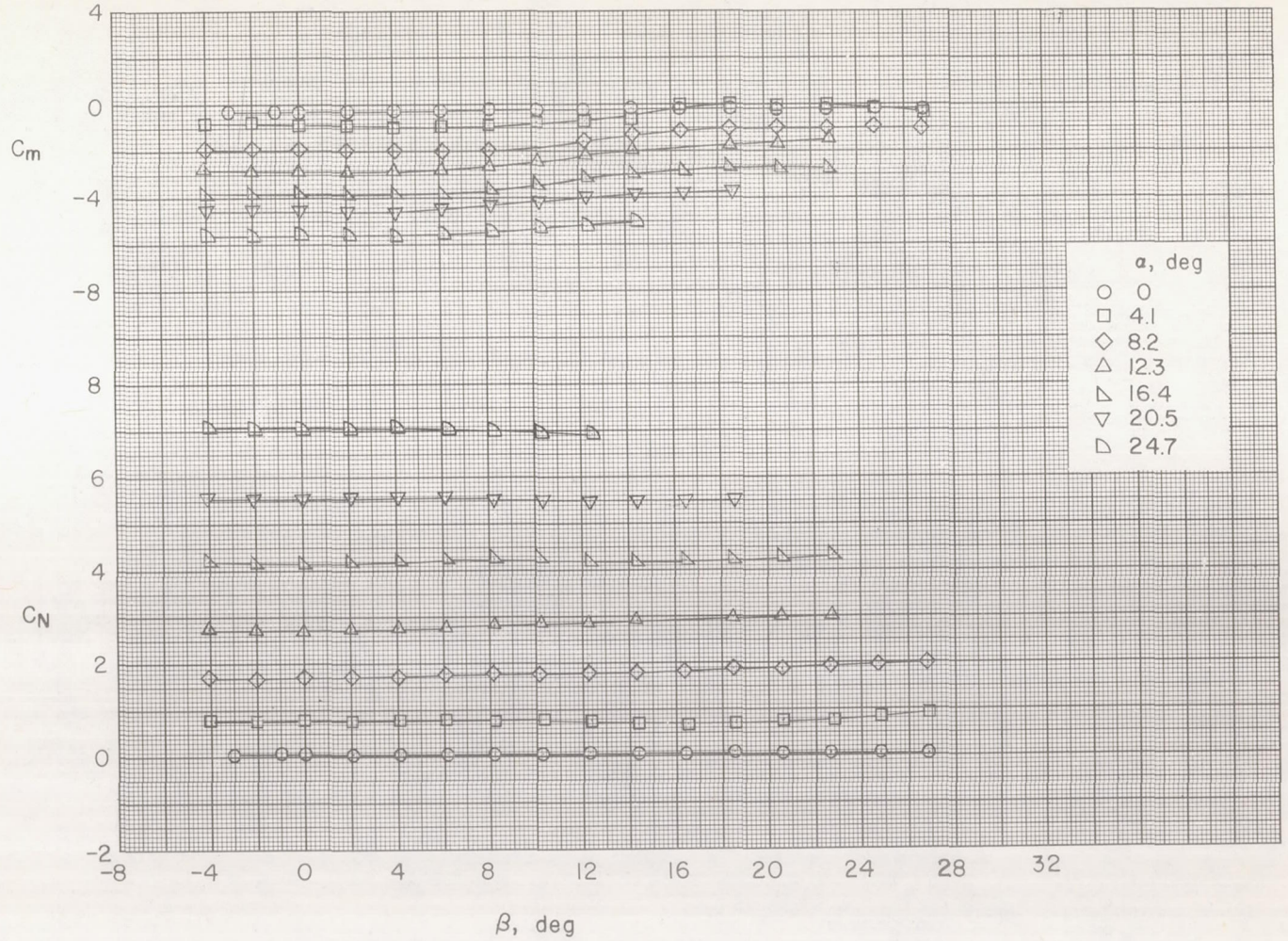
(a) Body alone, $F_8W_0A_0$.

Figure 10.- Variation of C_m and C_N with β for various angles of attack. Delta-wing series; no afterbody; l/d = 10.



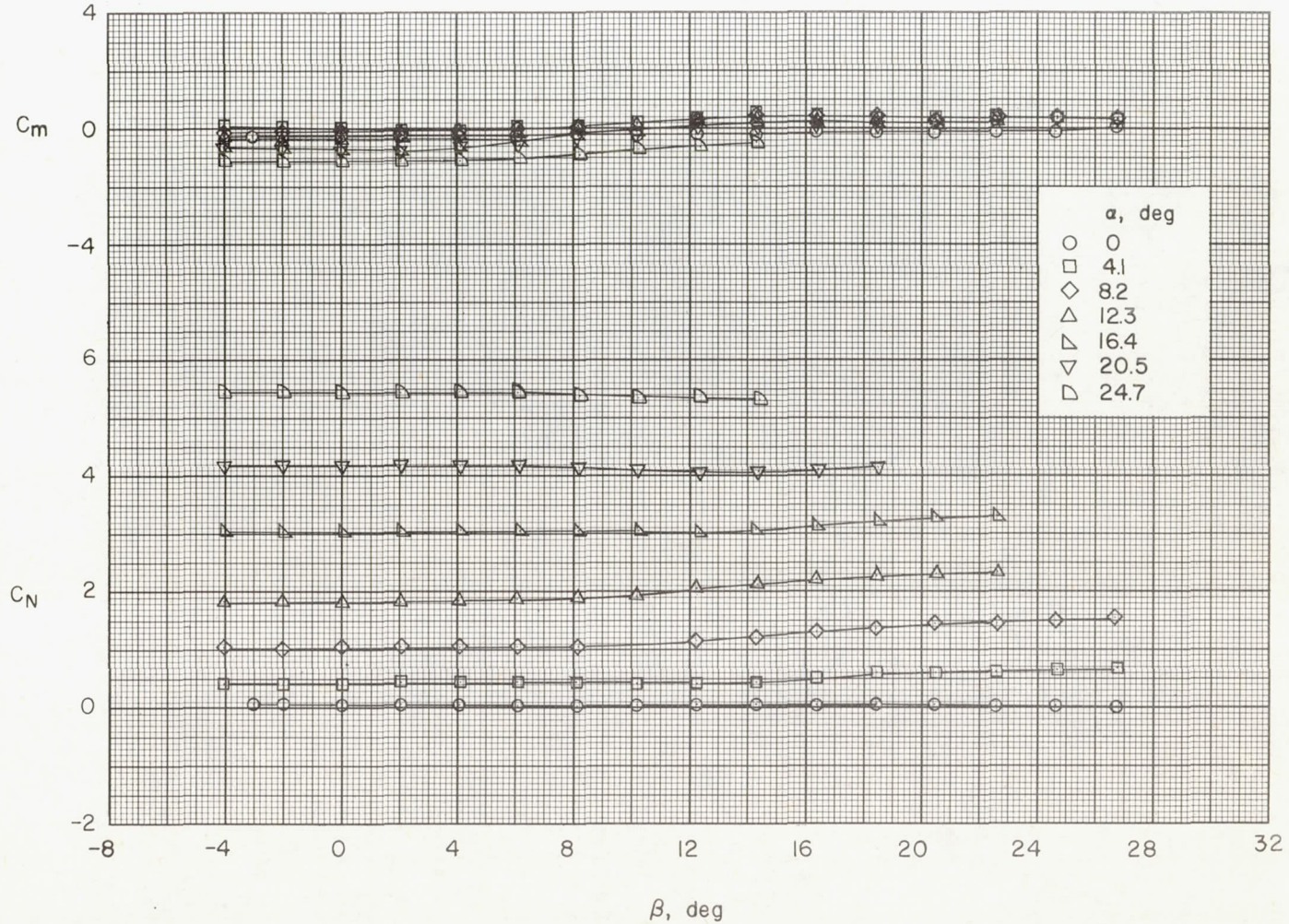
(b) Large delta wing, $F_8W_1A_0$.

Figure 10.- Continued.



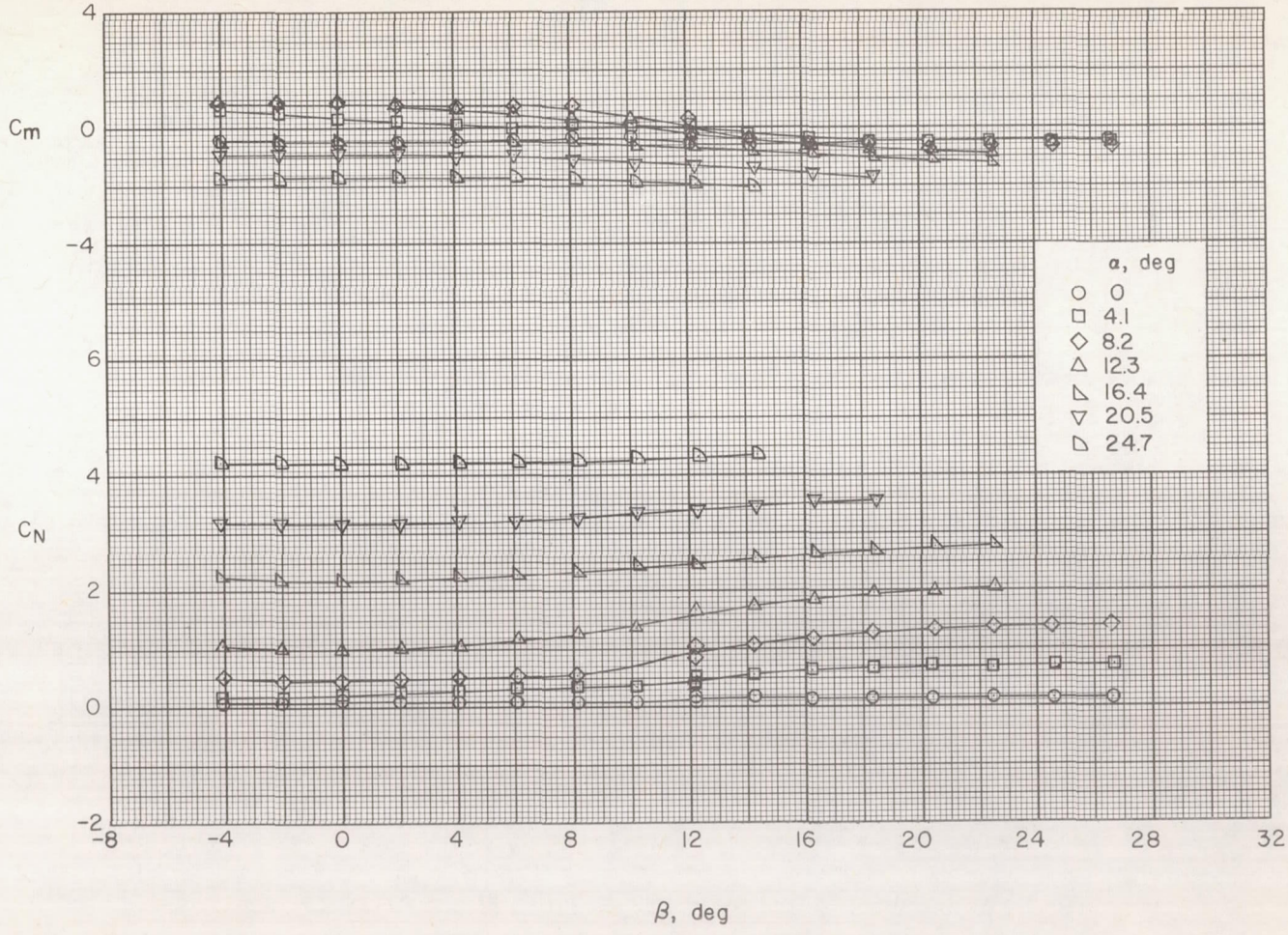
(c) Medium delta wing, $F_8W_2A_0$.

Figure 10.- Continued.



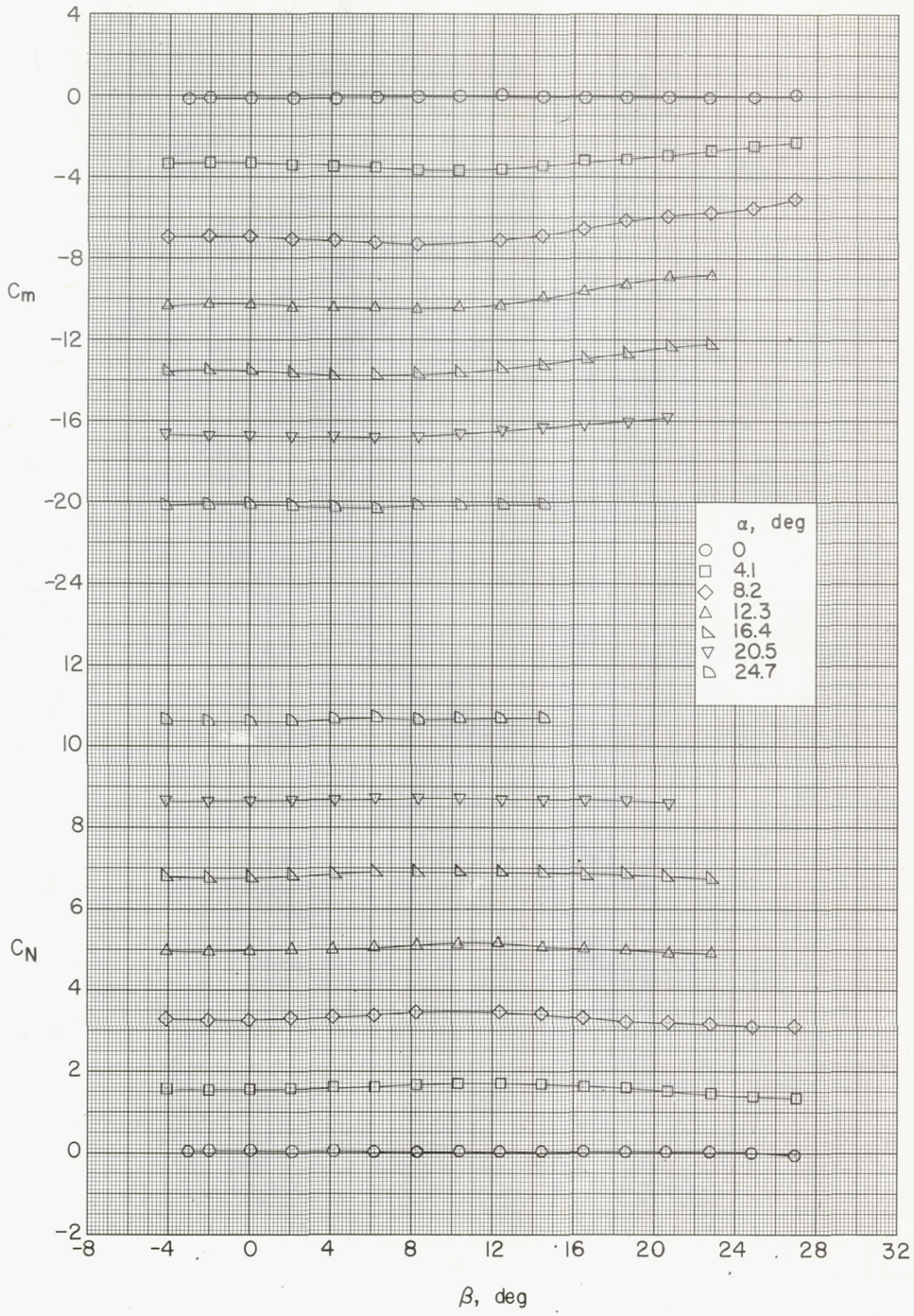
(d) Small delta wing, $F_8W_3A_0$.

Figure 10.- Concluded.



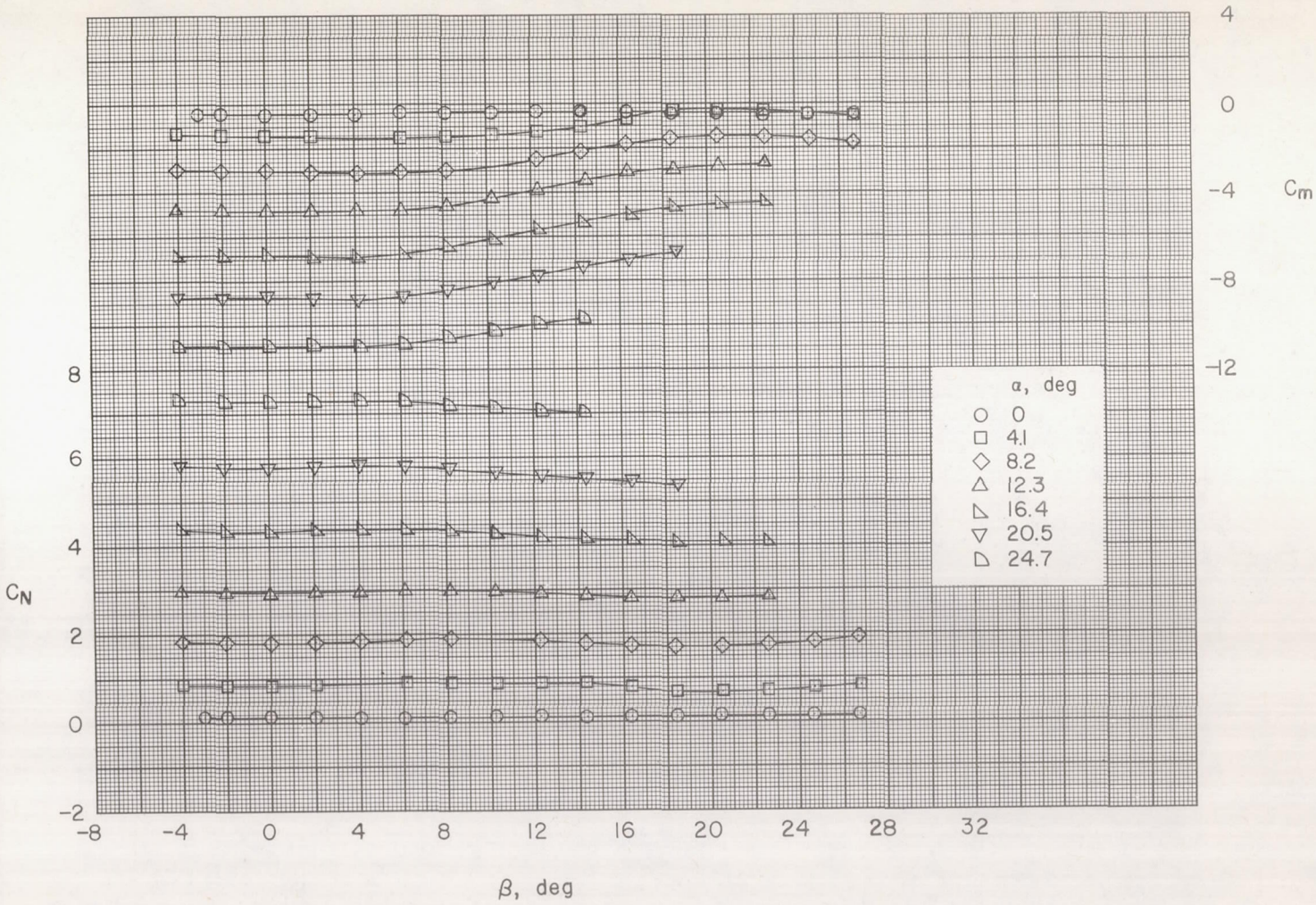
(a) Body alone, $F_7W_0A_1$.

Figure 11.- Variation of C_m and C_N with β for various angles of attack. Delta-wing series; 1-caliber cylindrical afterbody; l/d = 10.



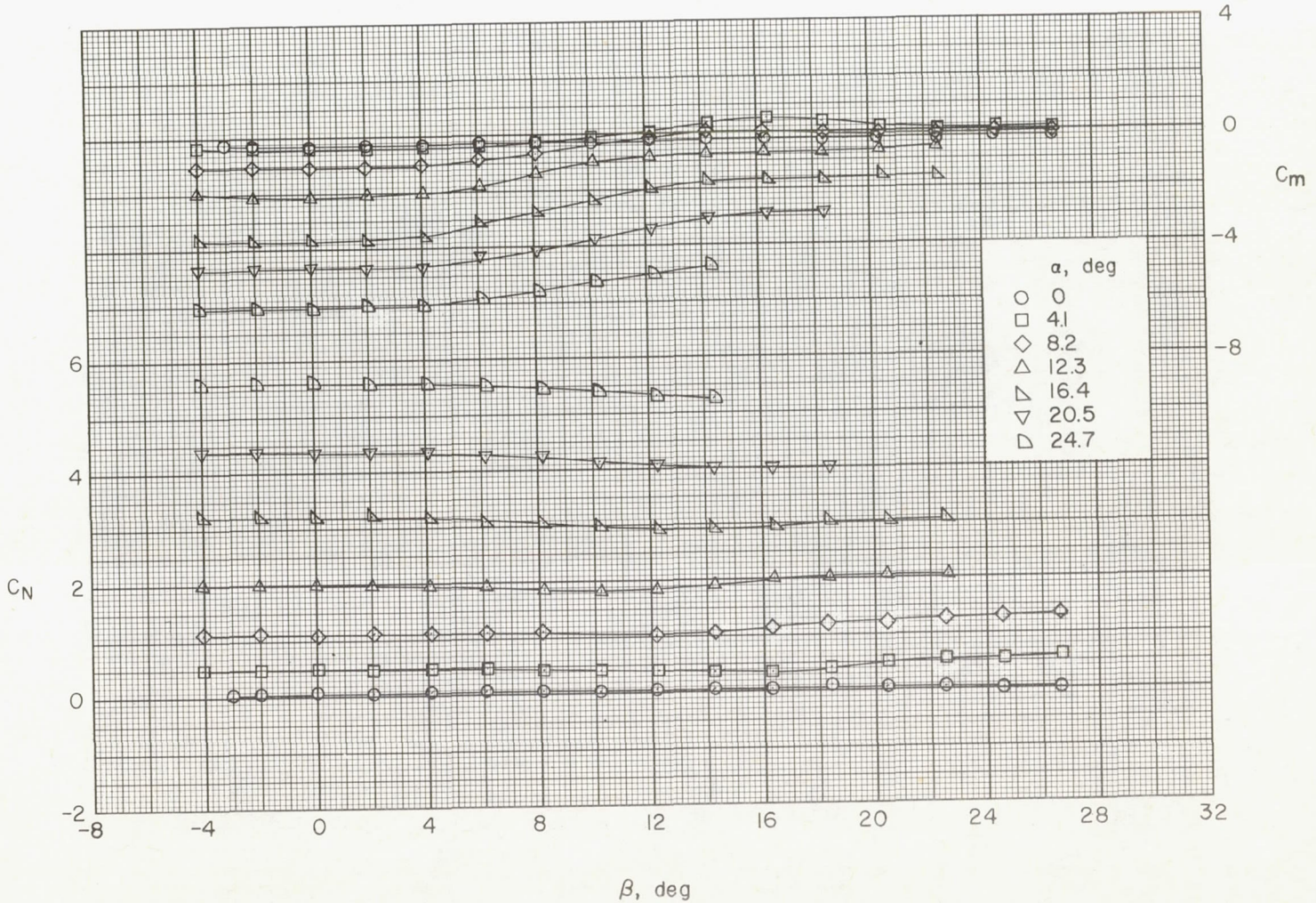
(b) Large delta wing, $F_7W_1A_0$.

Figure 11.- Continued.



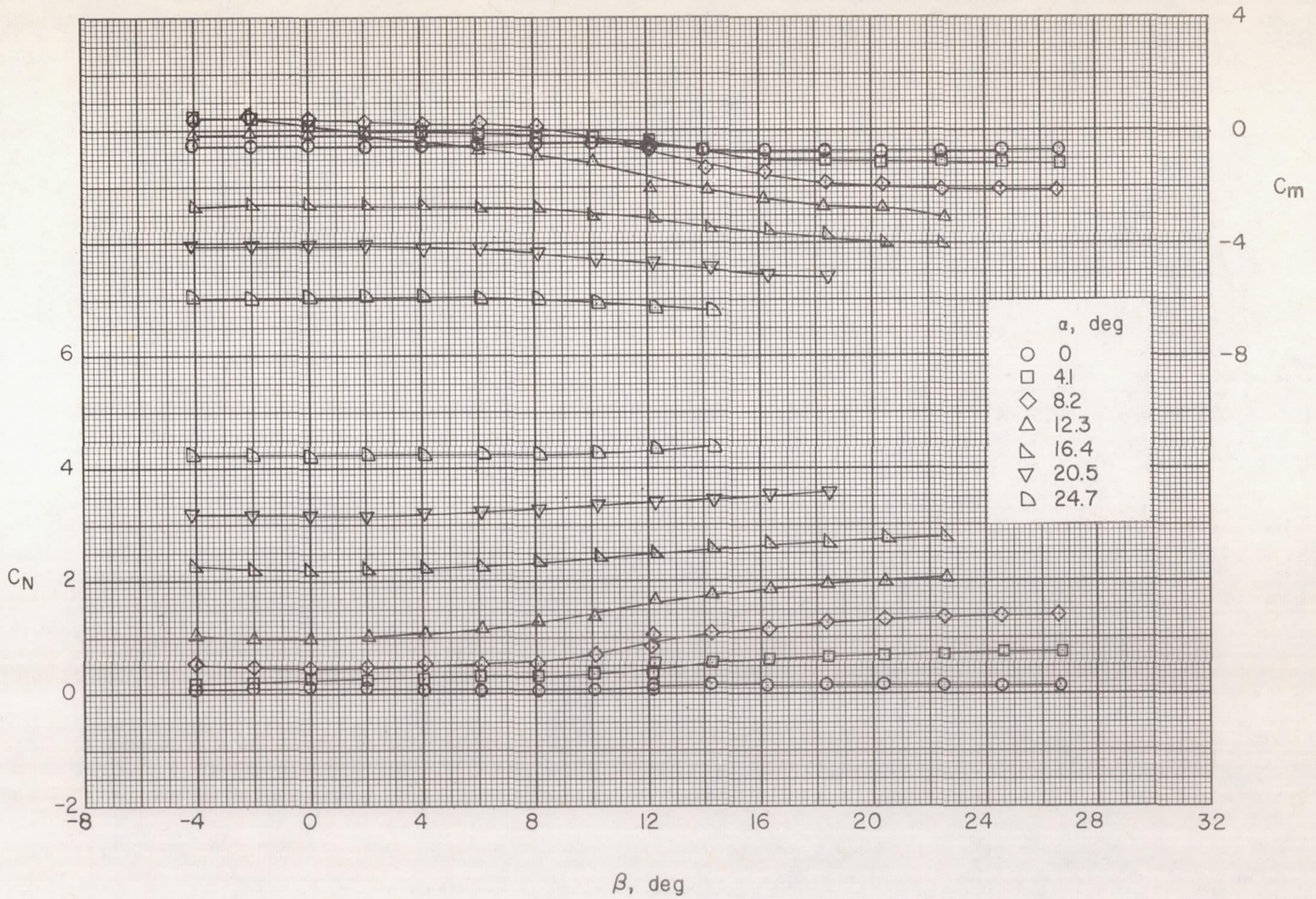
(c) Medium delta wing, $F_7W_2A_1$.

Figure 11.- Continued.



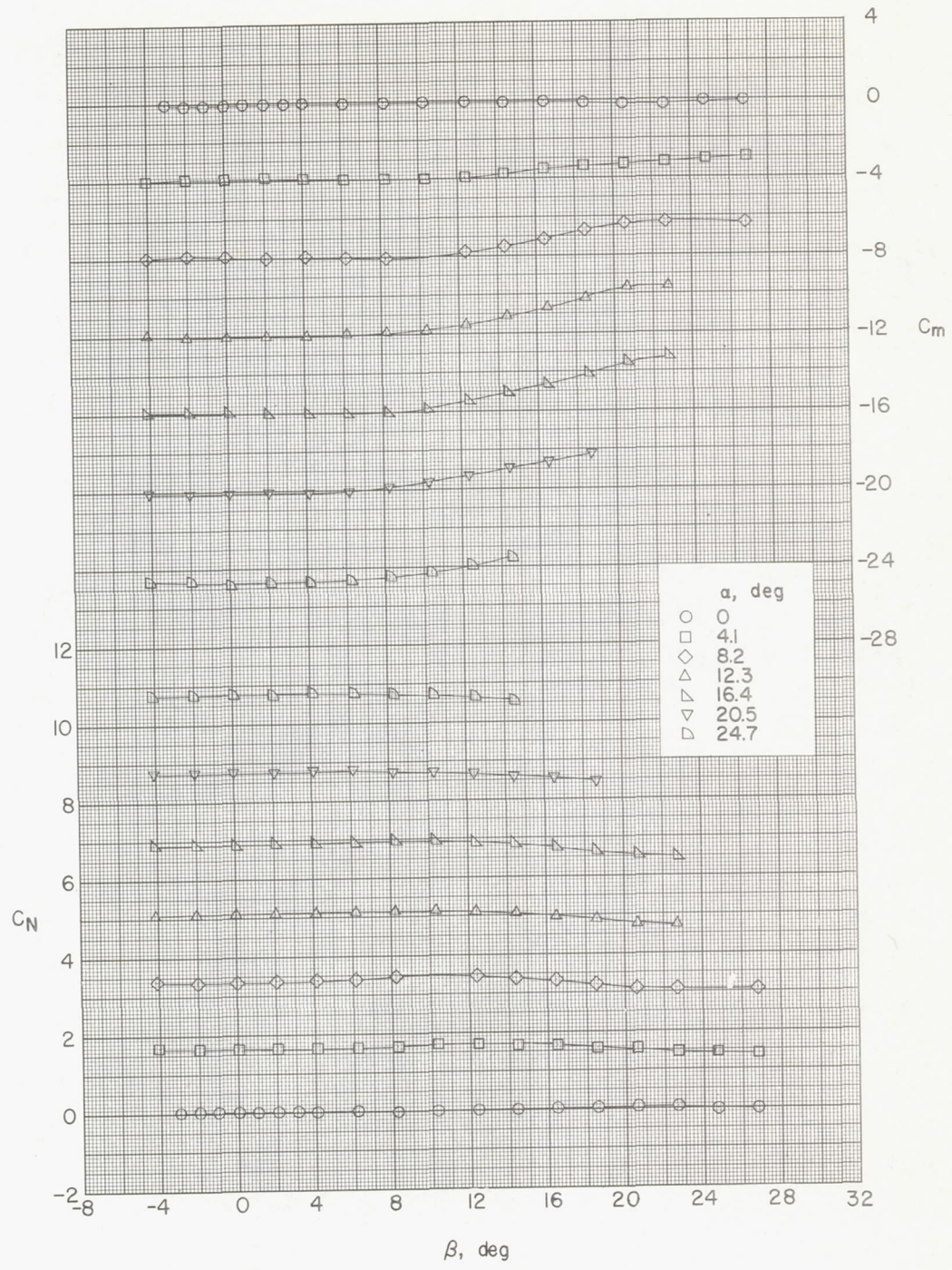
(d) Small delta wing, $F_7W_3A_1$.

Figure 11.- Concluded.



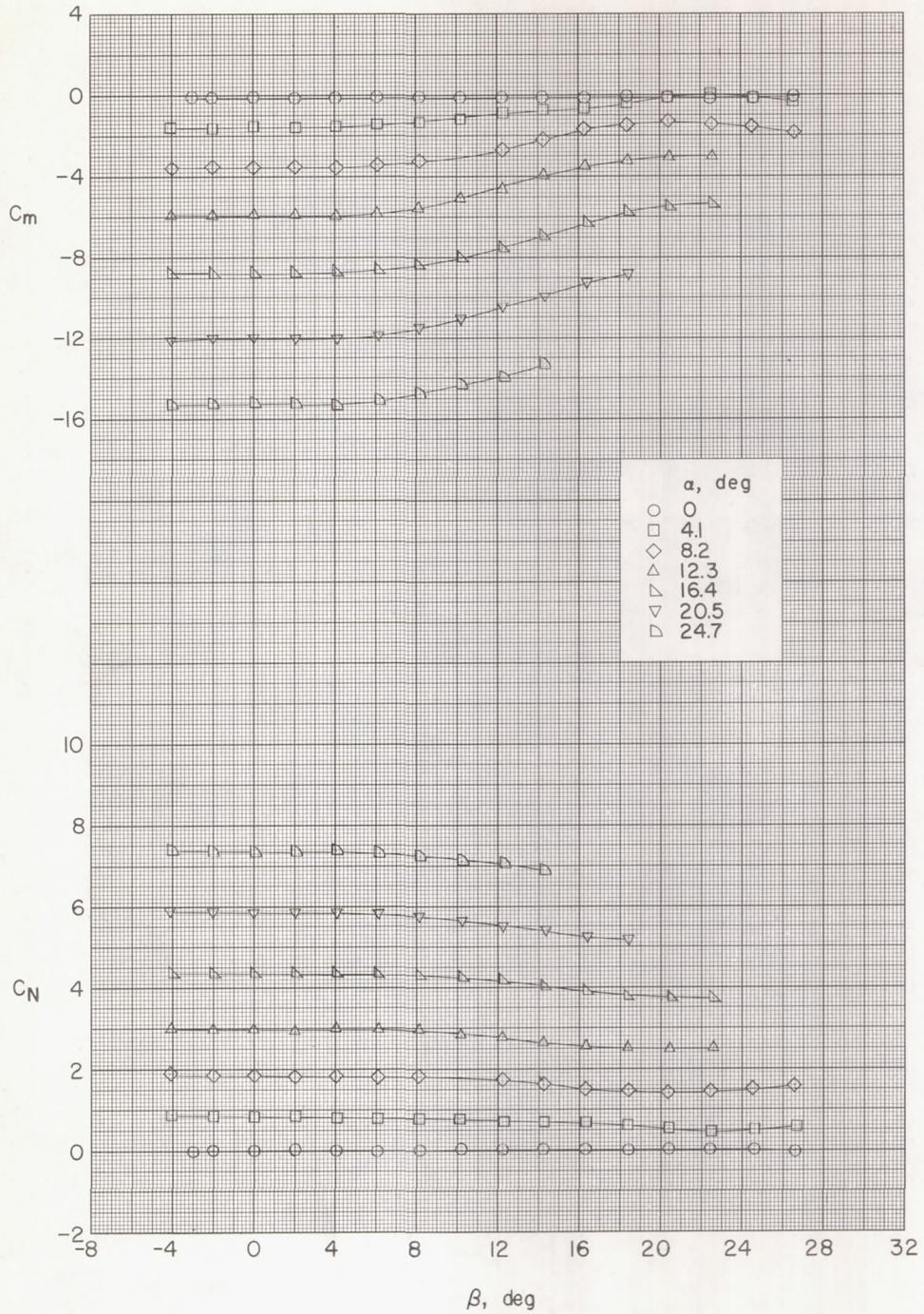
(a) Body alone, $F_1W_0A_2$.

Figure 12.- Variation of C_m and C_N with β for various angles of attack. Delta-wing series; 2-caliber cylindrical afterbody; $l/d = 10$.



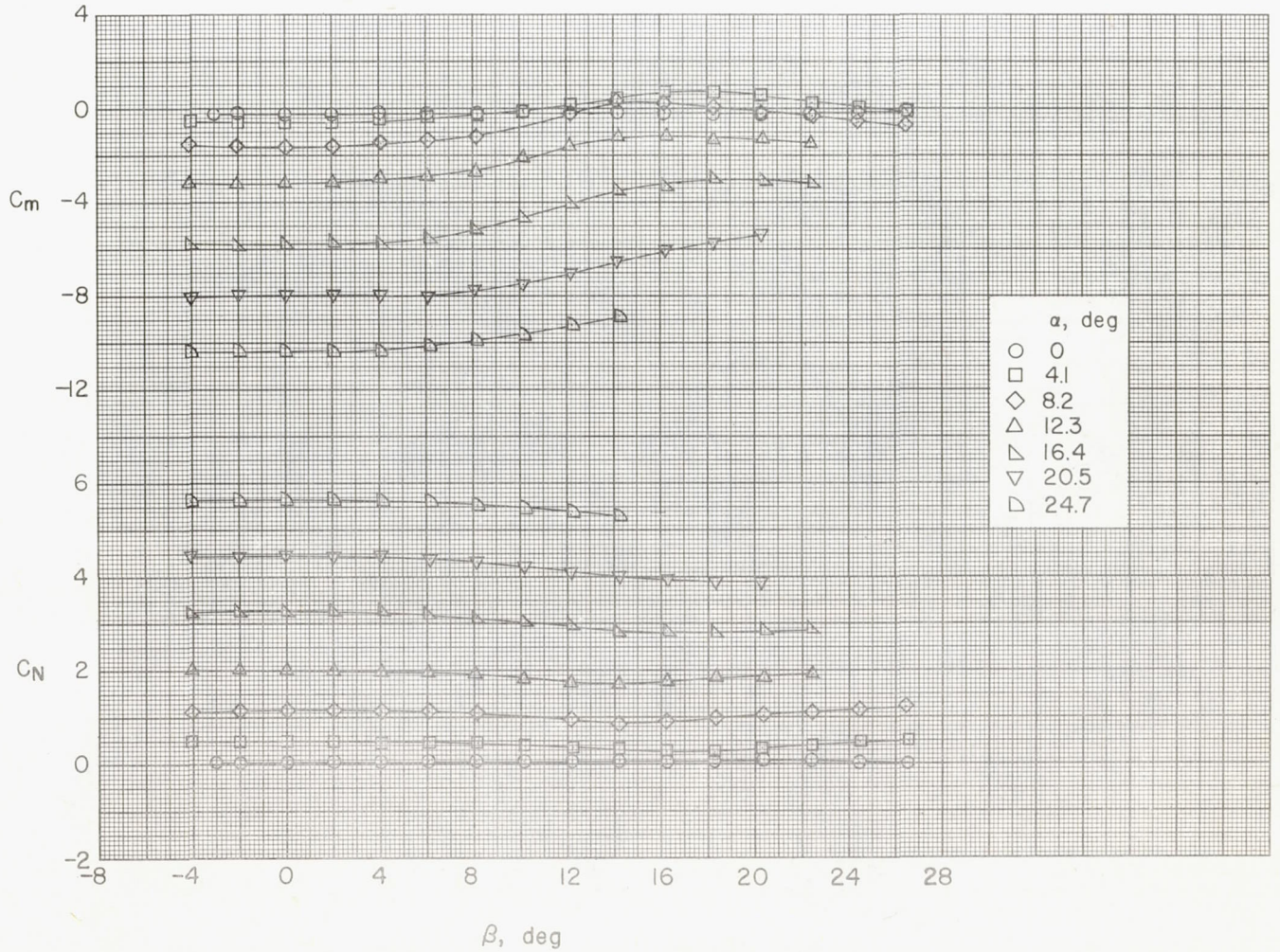
(b) Large delta wing, $F_1W_1A_2$.

Figure 12.- Continued.



(c) Medium delta wing, $F_1W_2A_2$.

Figure 12.- Continued.



(d) Small delta wing, $F_1W_3A_0$.

Figure 12.- Concluded.

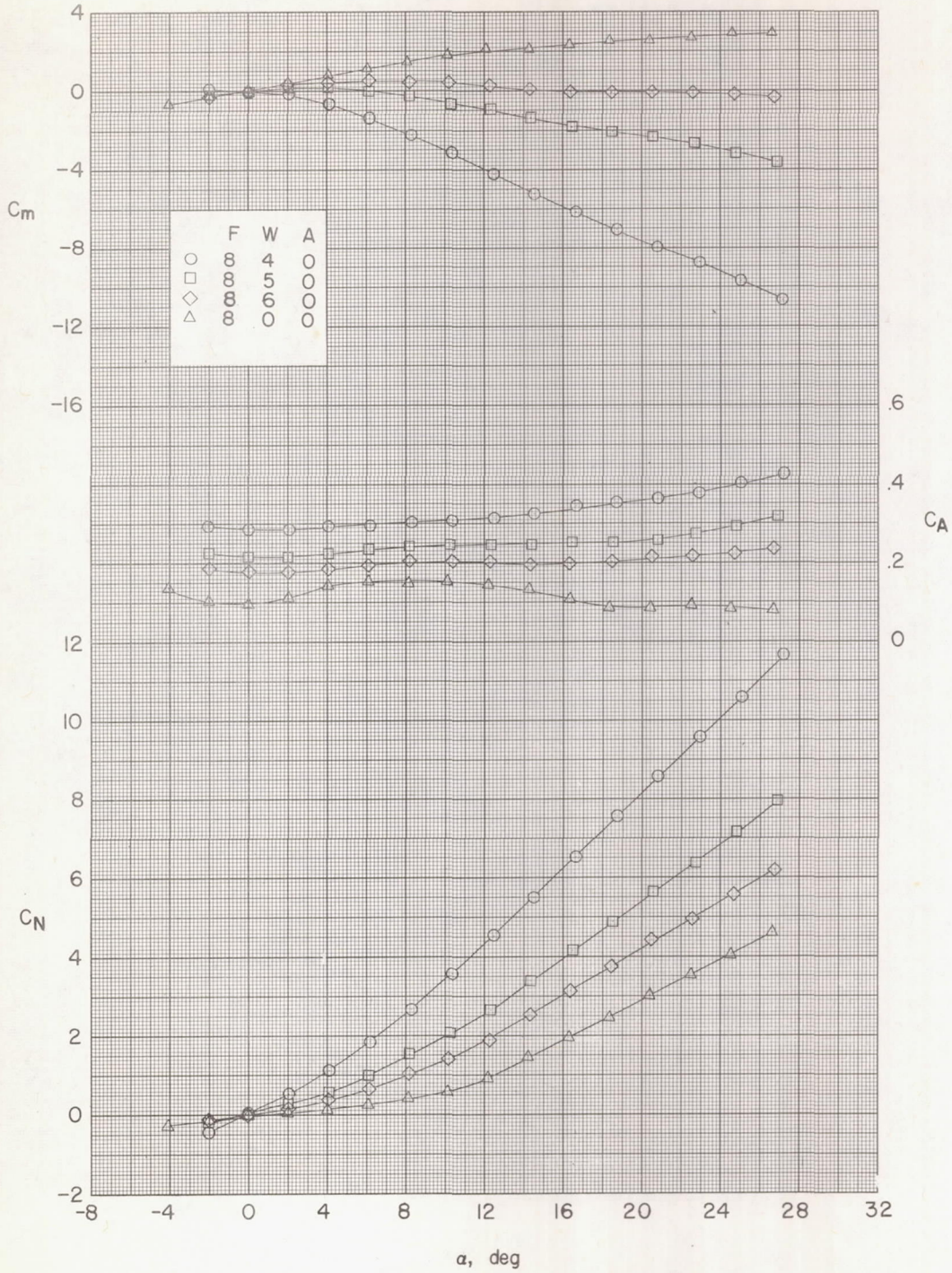


Figure 13.- Effect of rectangular wings on aerodynamic characteristics in pitch. No afterbody; $l/d = 10$.

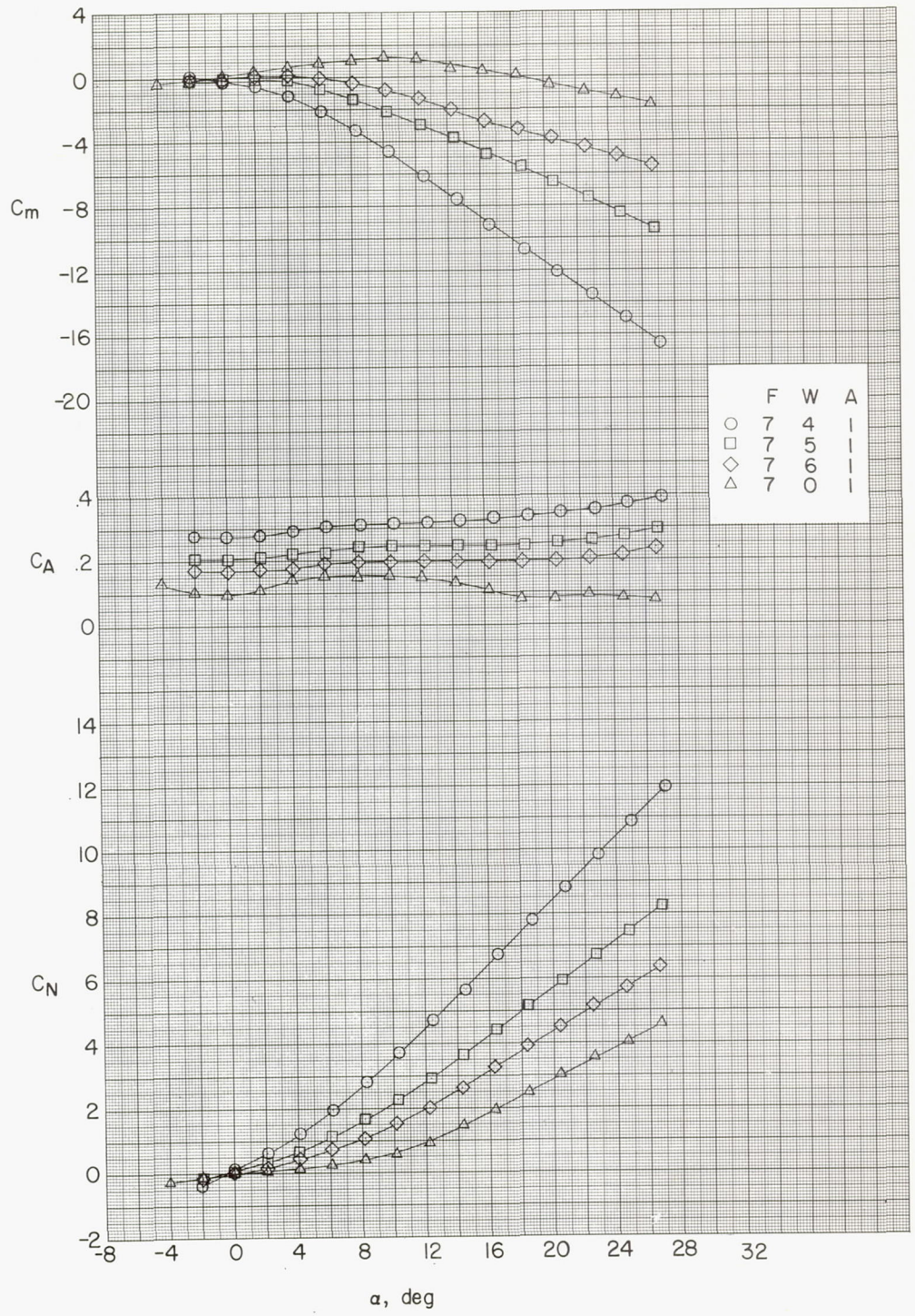


Figure 14.- Effect of rectangular wings on aerodynamic characteristics in pitch. One-caliber cylindrical afterbody; $l/d = 10$.

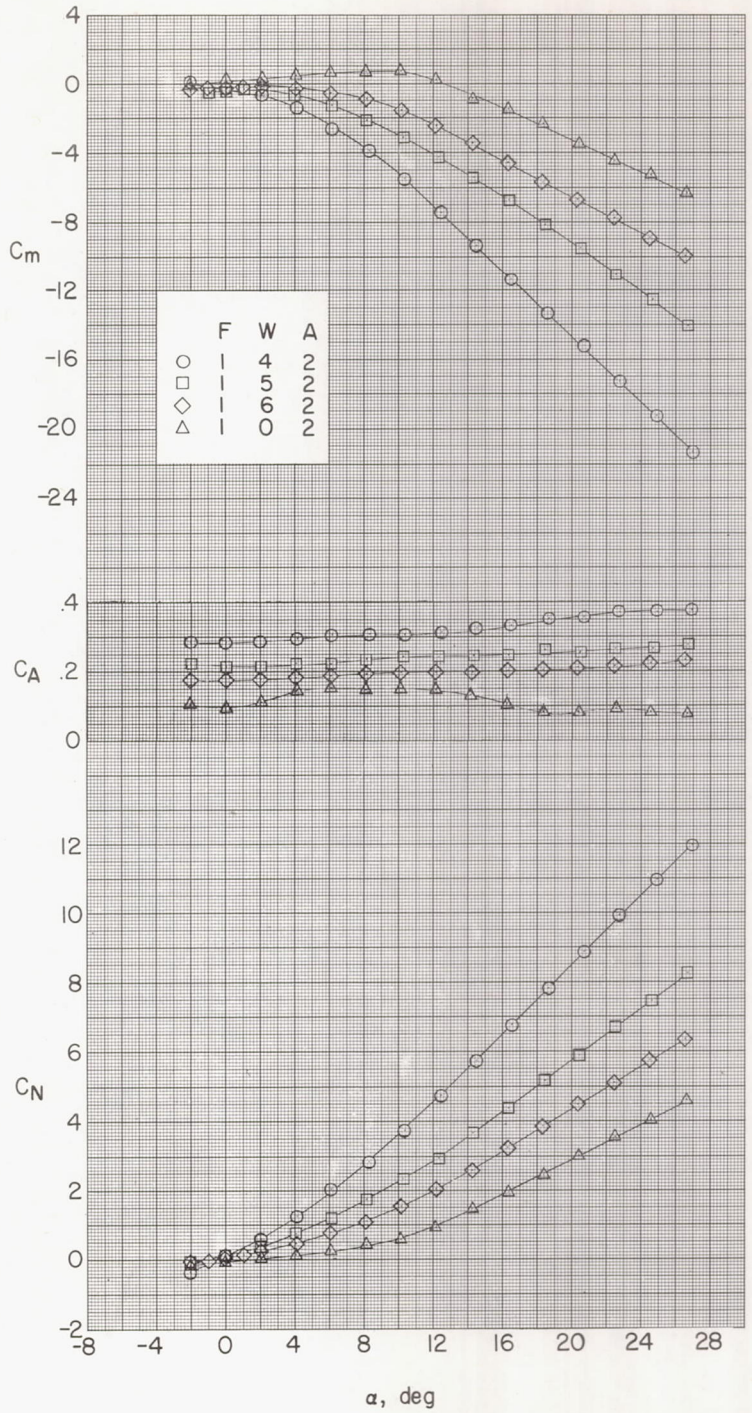
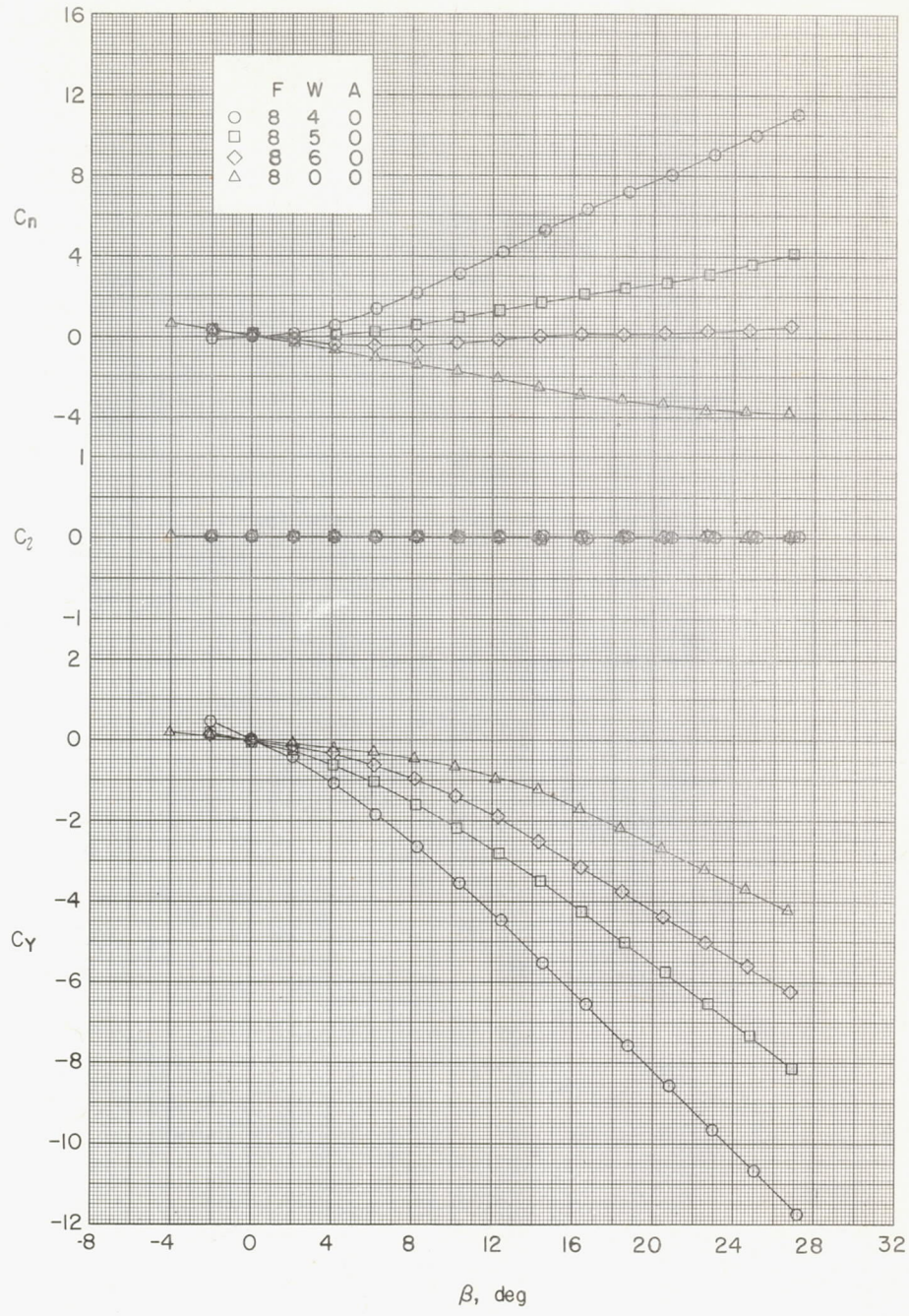
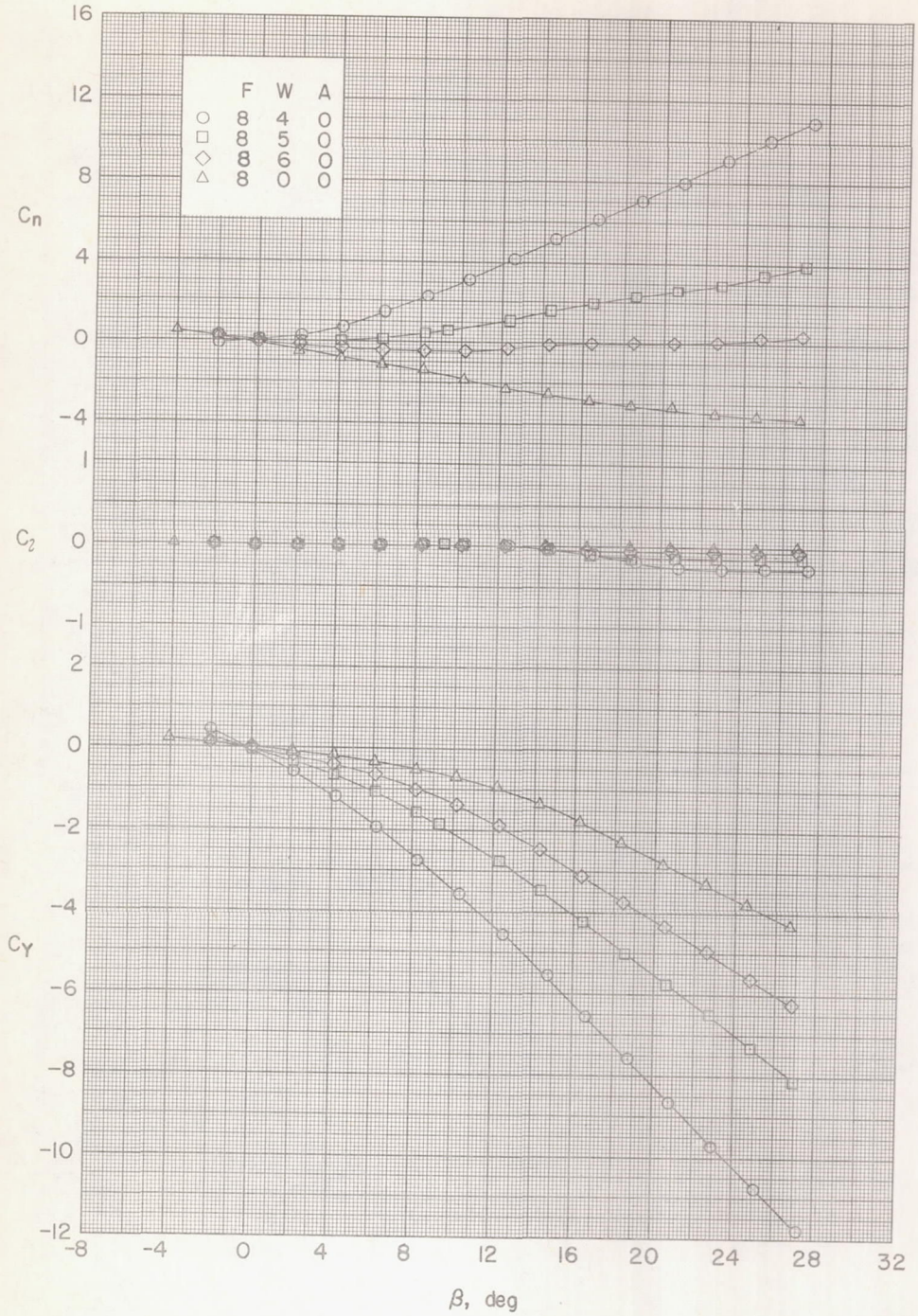


Figure 15.- Effect of rectangular wings on aerodynamic characteristics in pitch. Two-caliber cylindrical afterbody; $l/d = 10$.



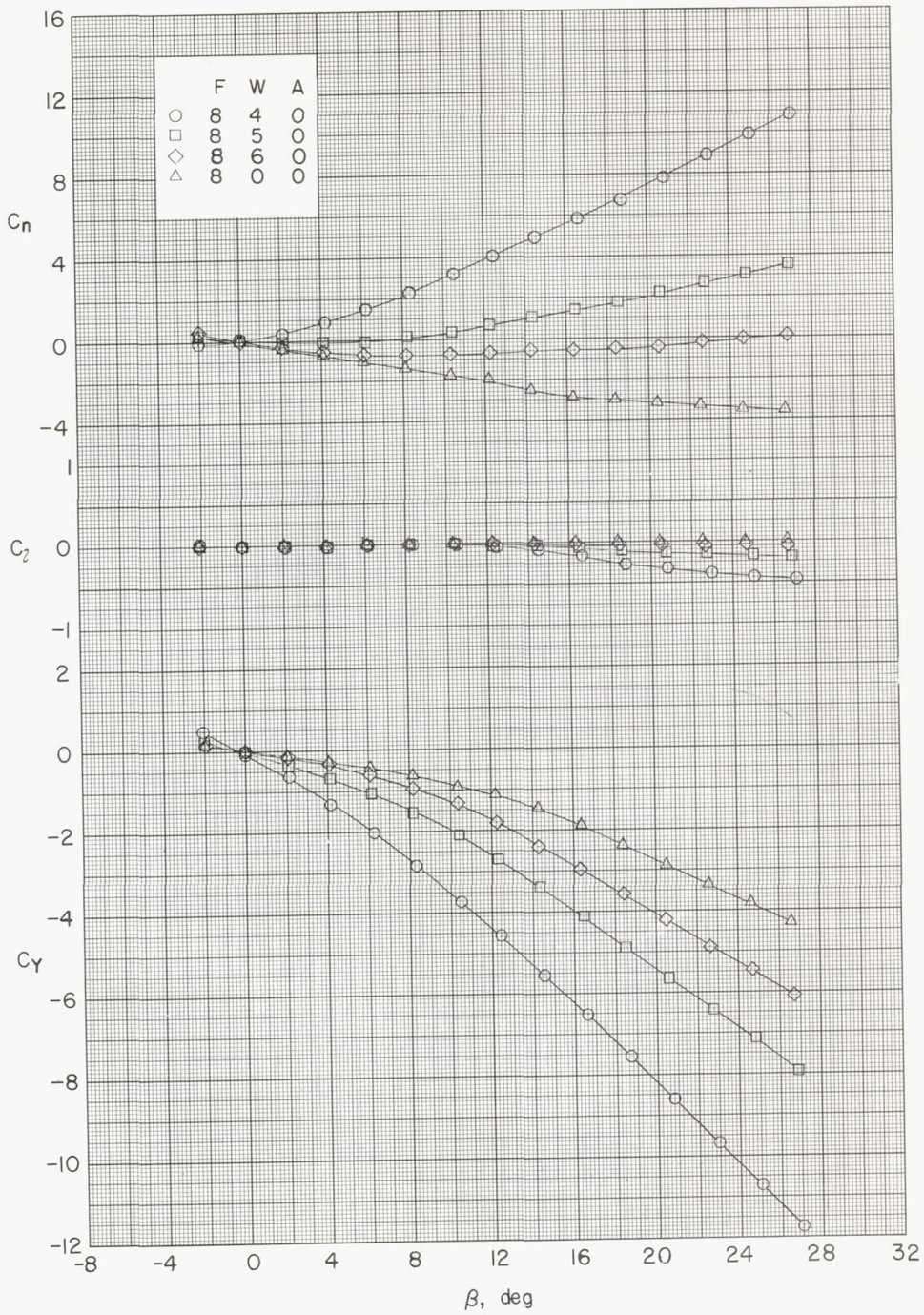
(a) $\alpha \approx 0^\circ$.

Figure 16.- Effect of rectangular wings on aerodynamic characteristics in sideslip. No afterbody; $l/d = 10$.



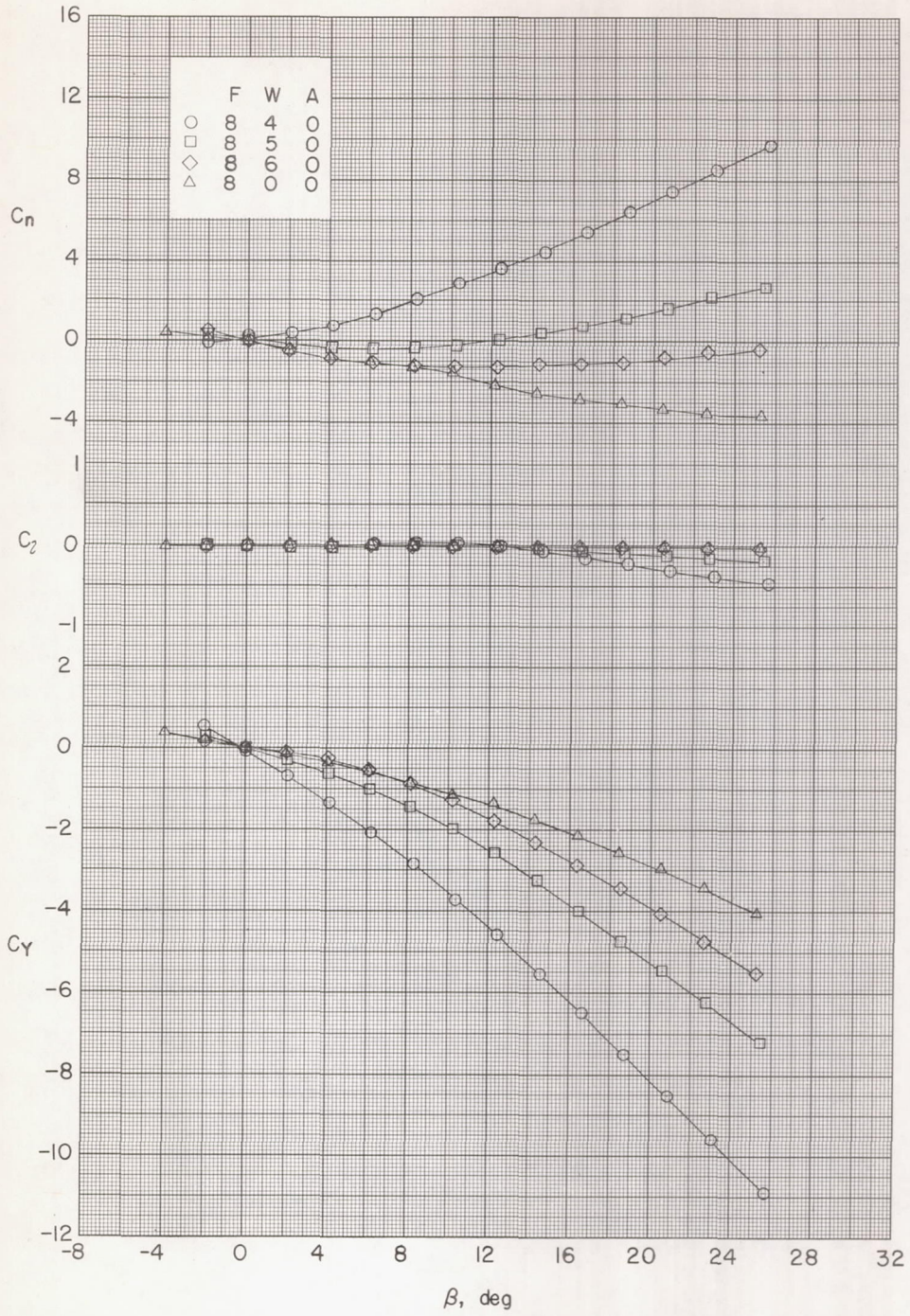
(b) $\alpha \approx 4.1^{\circ}$.

Figure 16.- Continued.



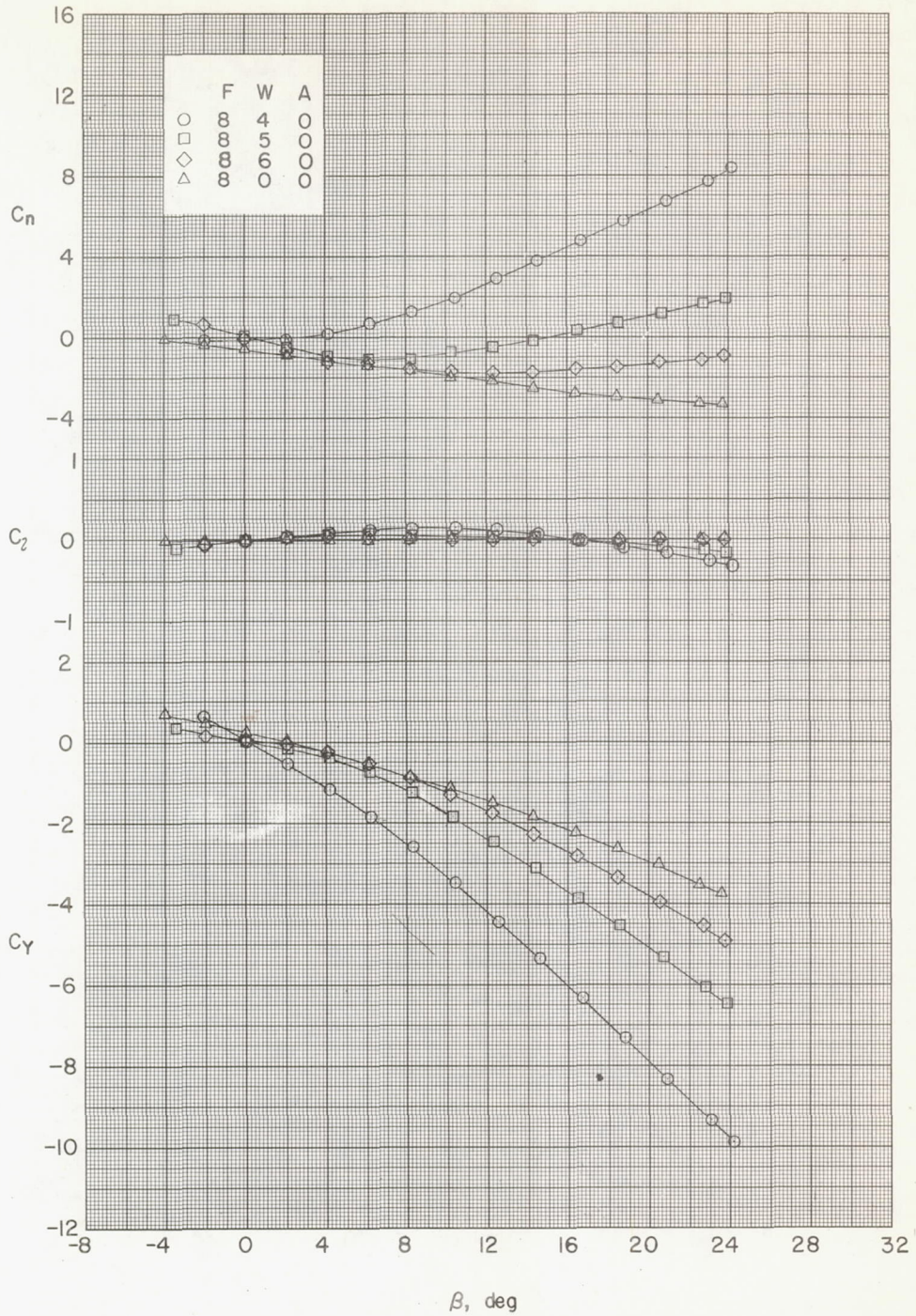
(c) $\alpha \approx 8.2^{\circ}$.

Figure 16.- Continued.



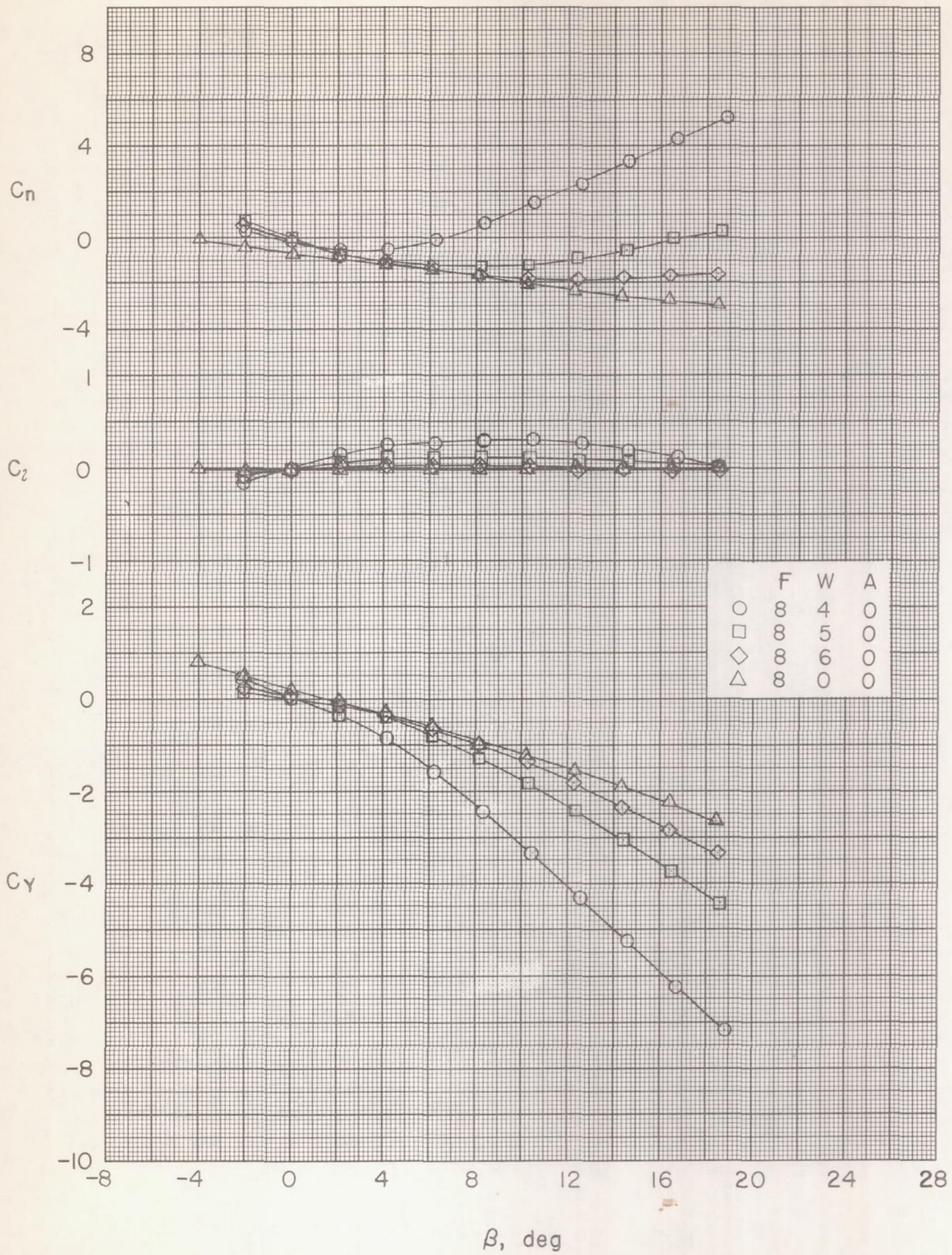
(d) $\alpha \approx 12.3^\circ$.

Figure 16.- Continued.



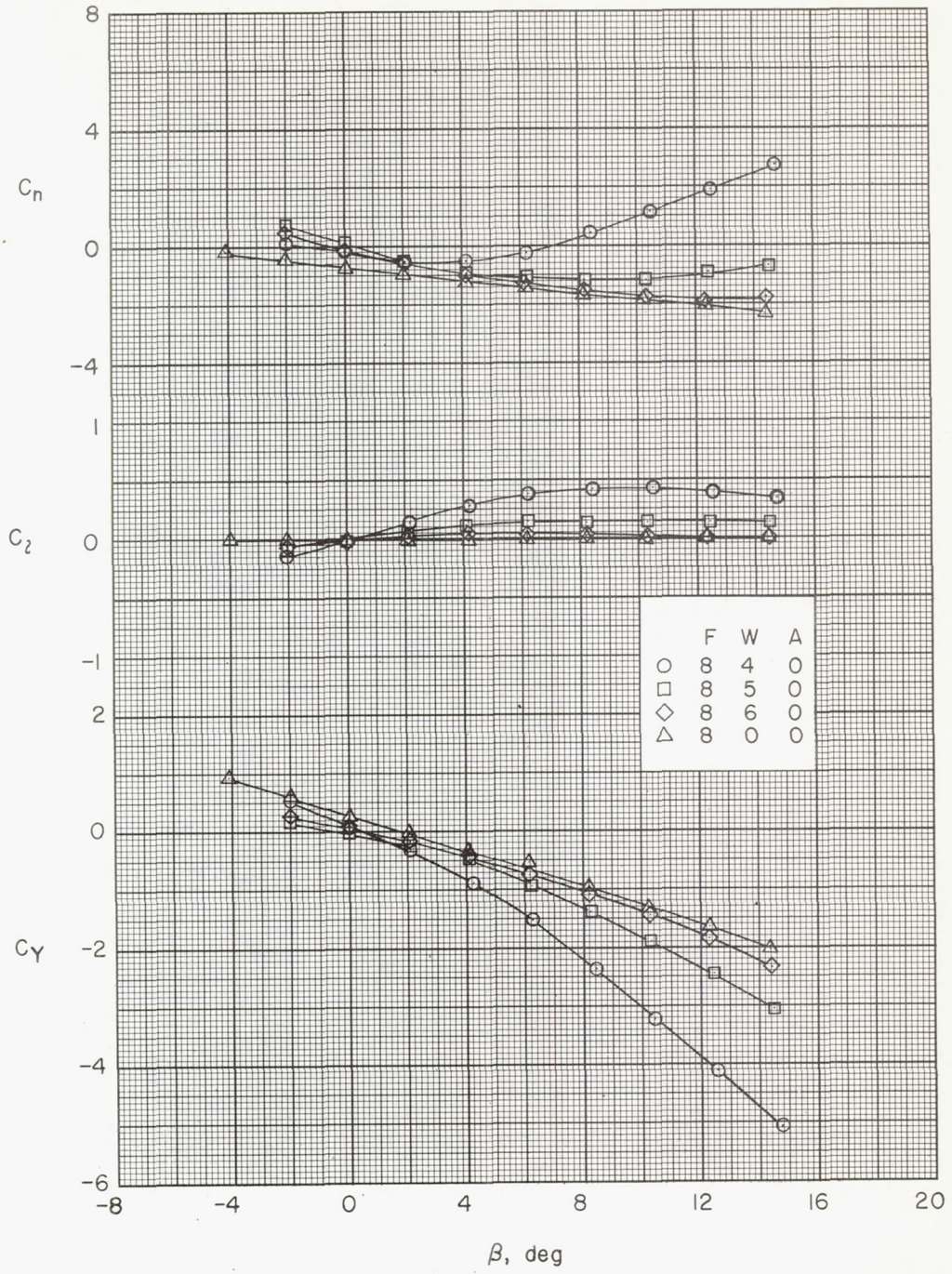
(e) $\alpha \approx 16.4^{\circ}$.

Figure 16.- Continued.



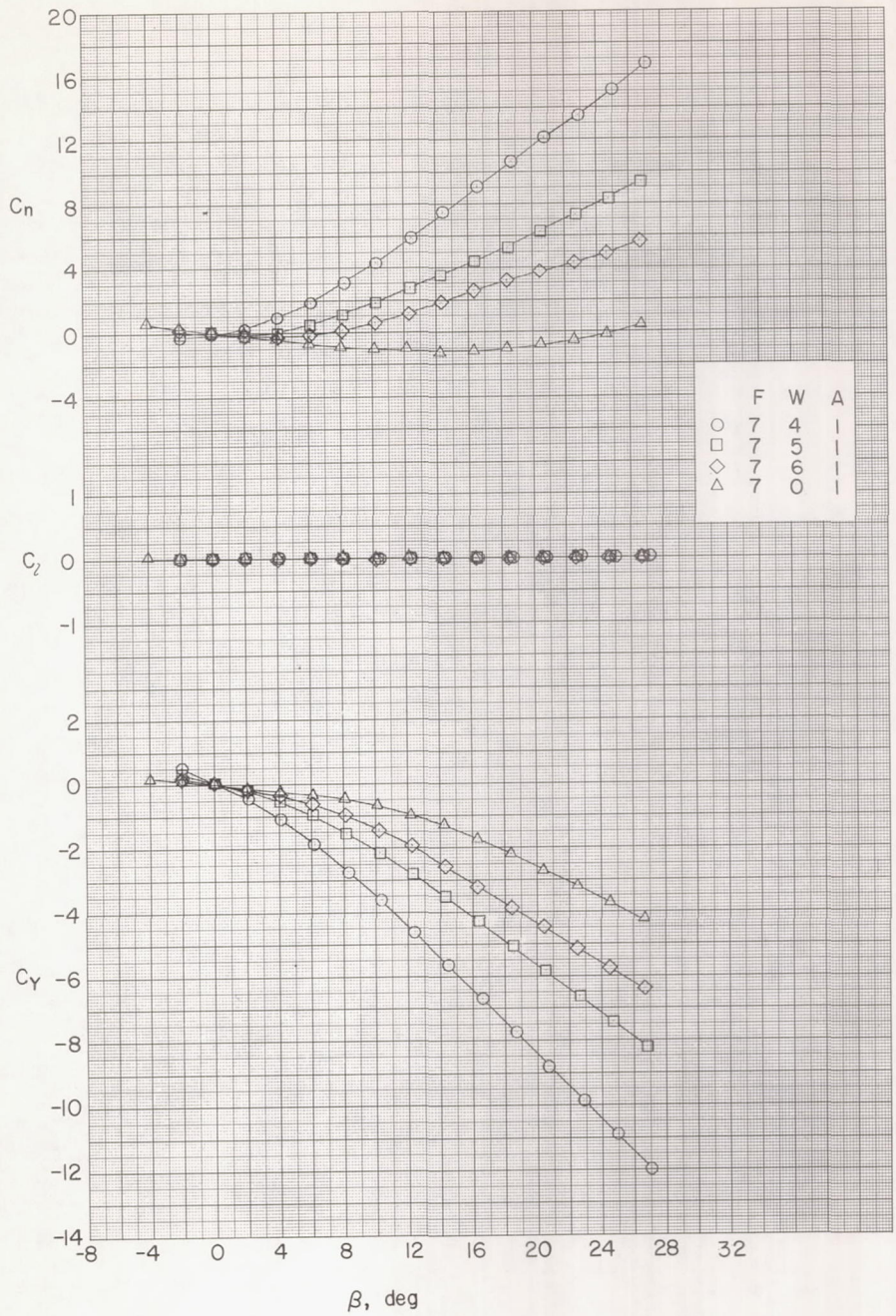
(f) $\alpha \approx 20.5^\circ$.

Figure 16.- Continued.



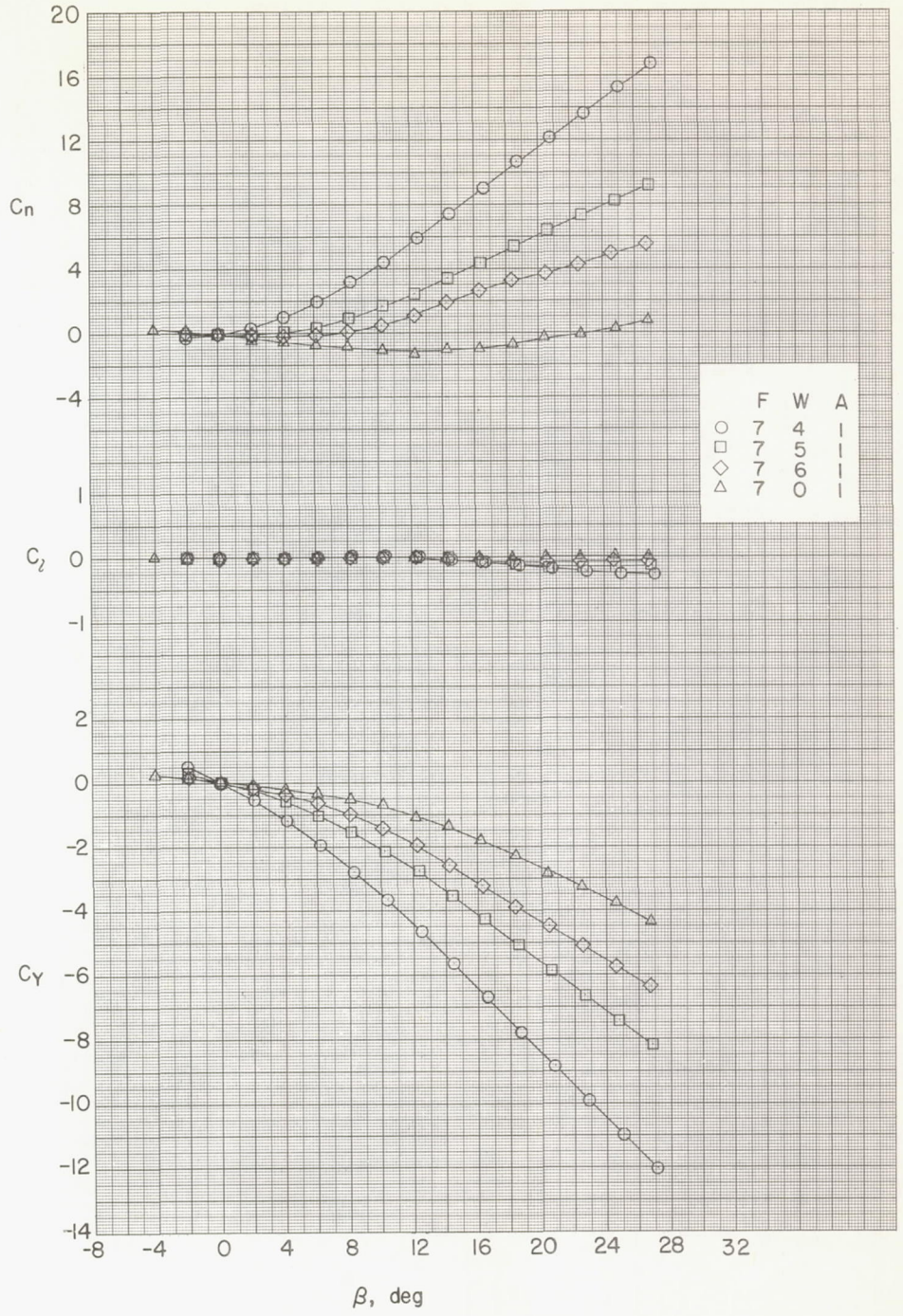
(g) $\alpha \approx 24.7^{\circ}$.

Figure 16.- Concluded.



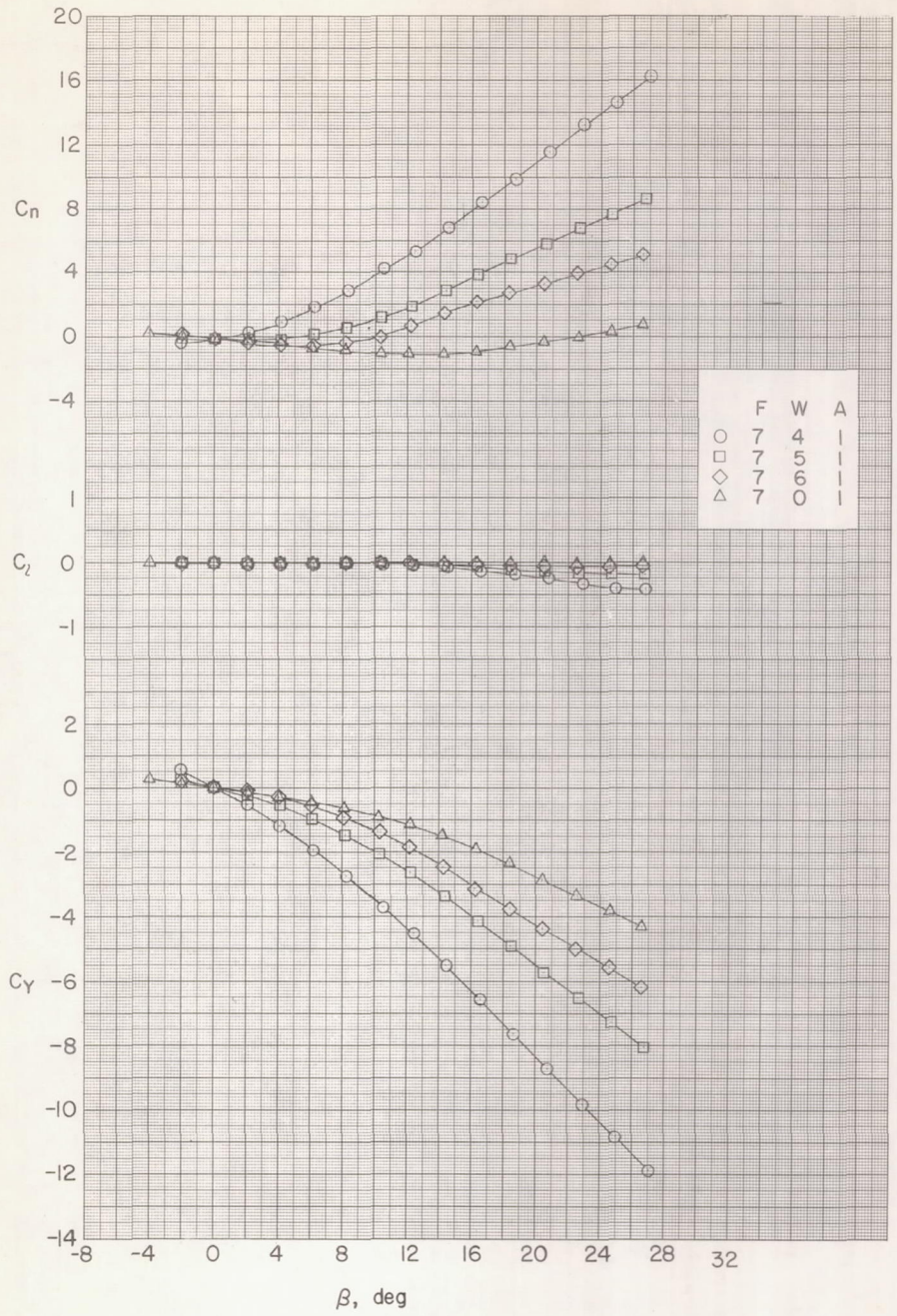
(a) $\alpha \approx 0^\circ$.

Figure 17.- Effects of rectangular wings on aerodynamic characteristics in sideslip. One-caliber cylindrical afterbody; $l/d = 10$.



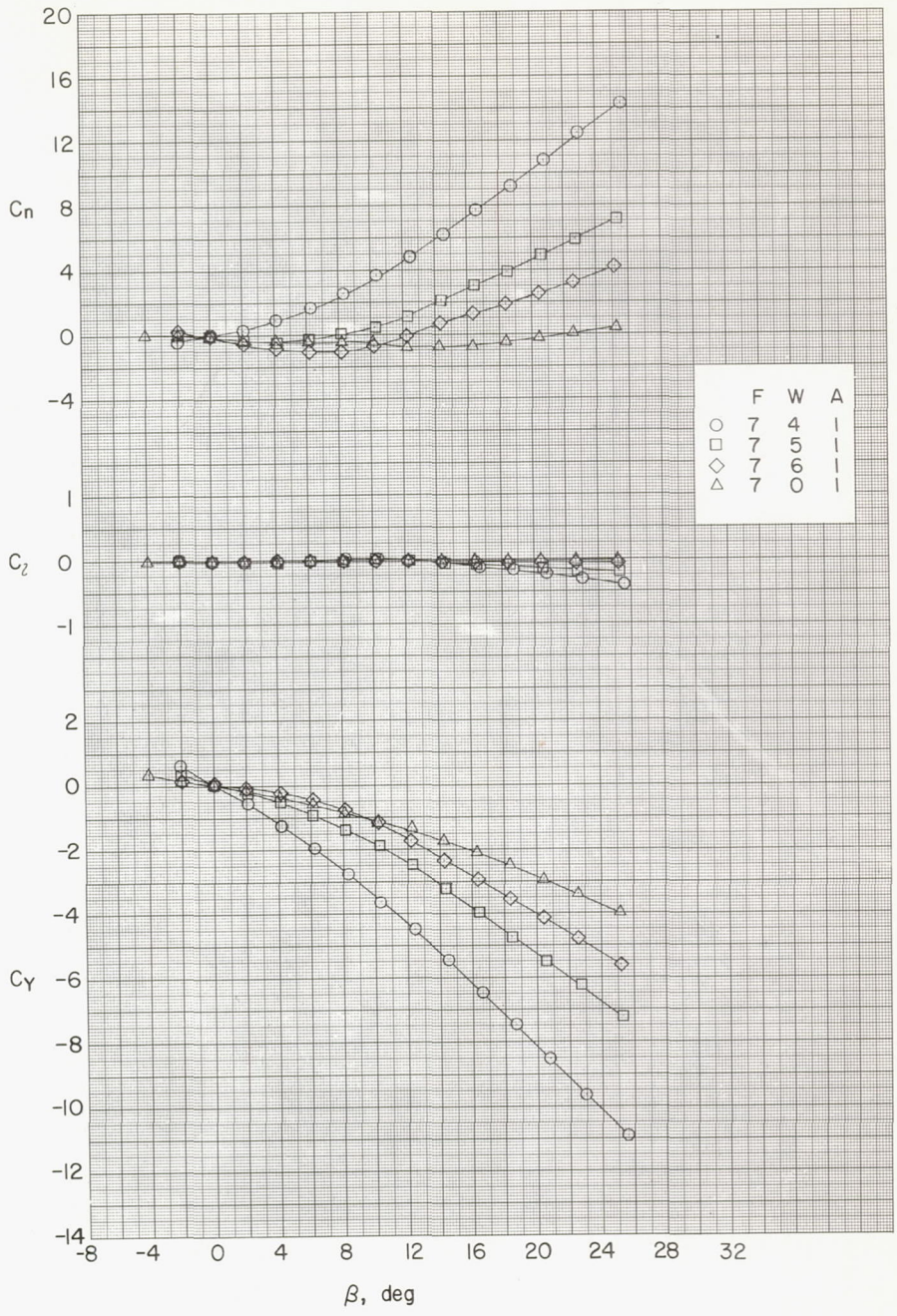
(b) $\alpha \approx 4.1^{\circ}$.

Figure 17.- Continued.



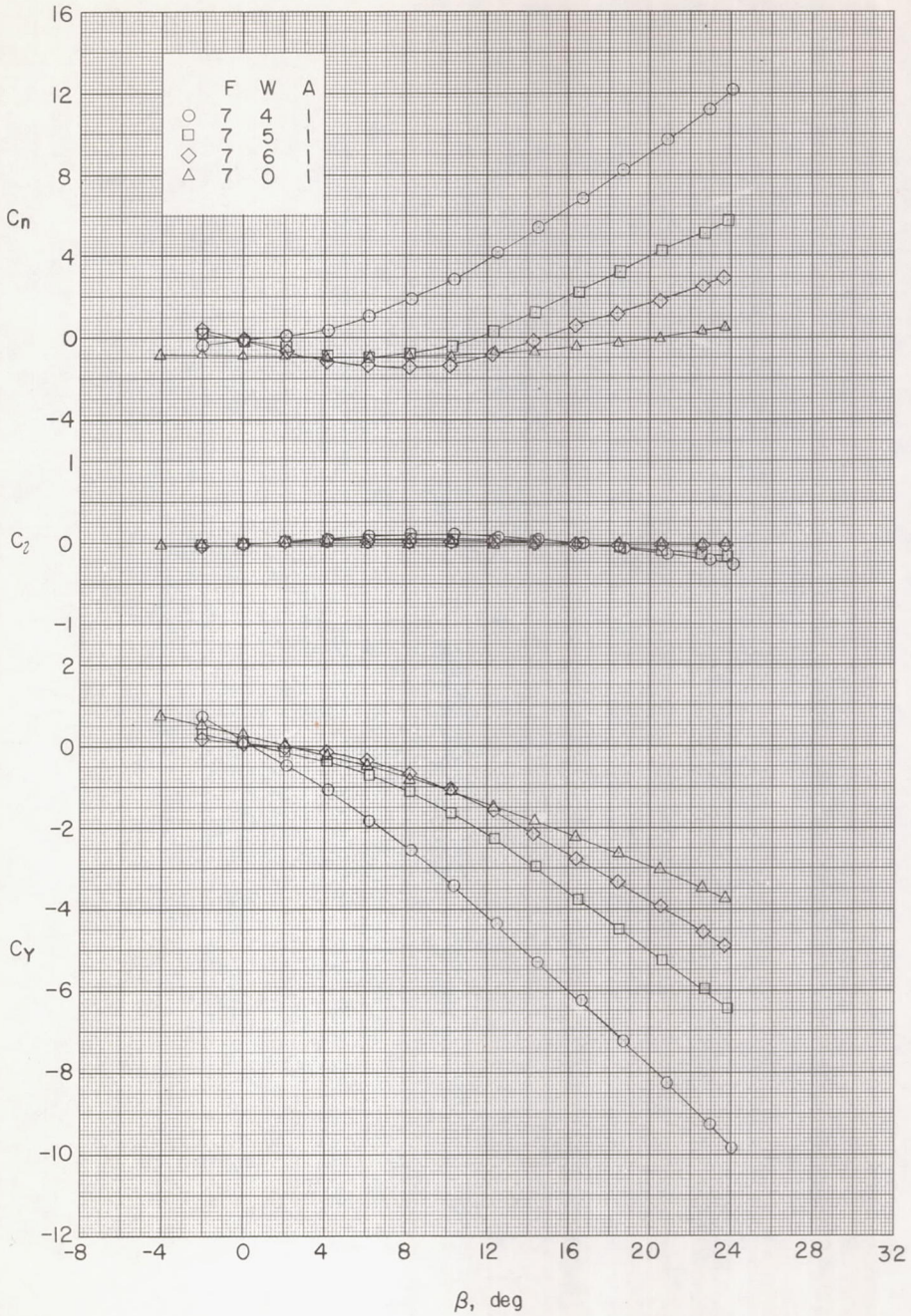
(c) $\alpha \approx 8.2^{\circ}$.

Figure 17.- Continued.



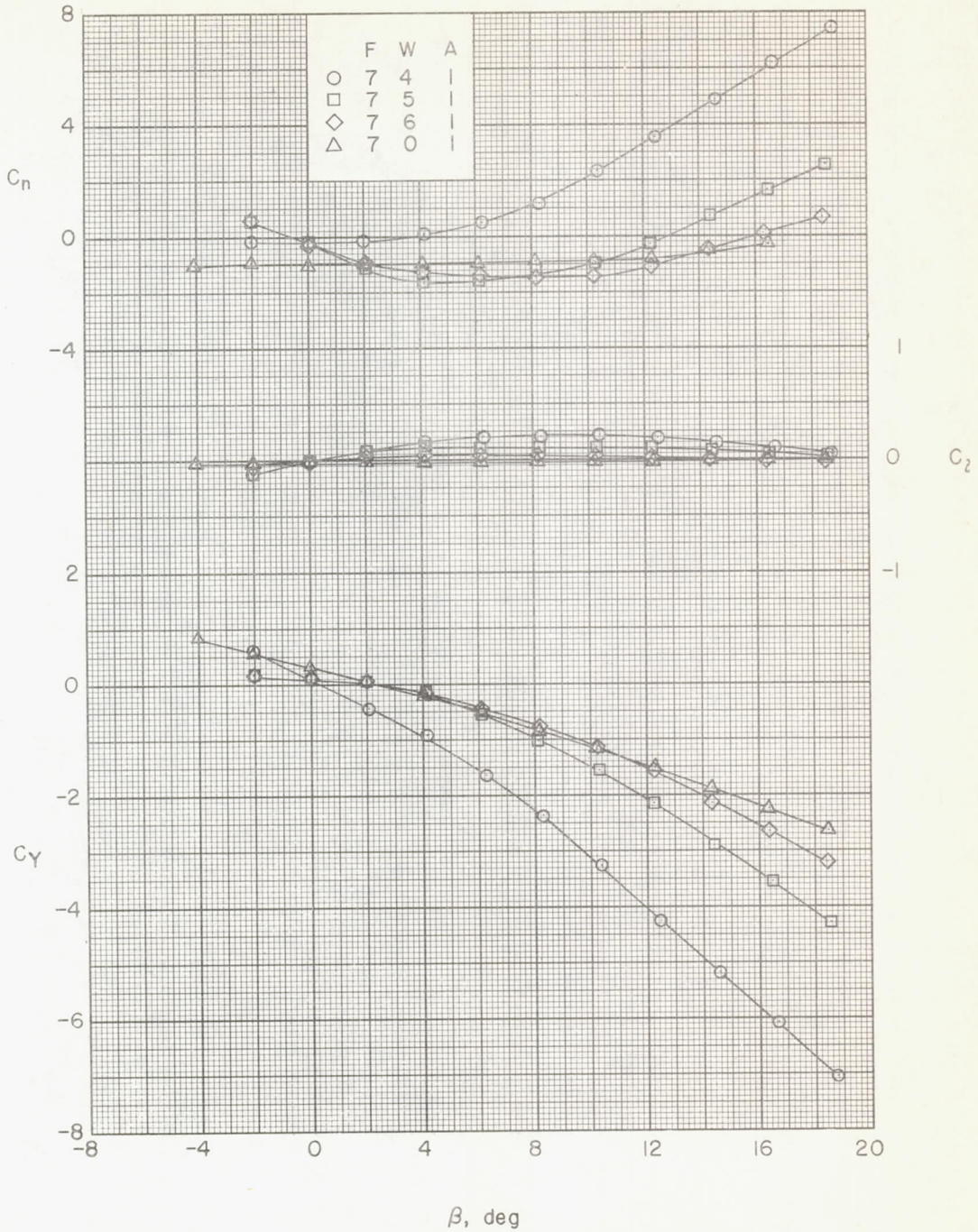
(d) $\alpha \approx 12.3^{\circ}$.

Figure 17.- Continued.



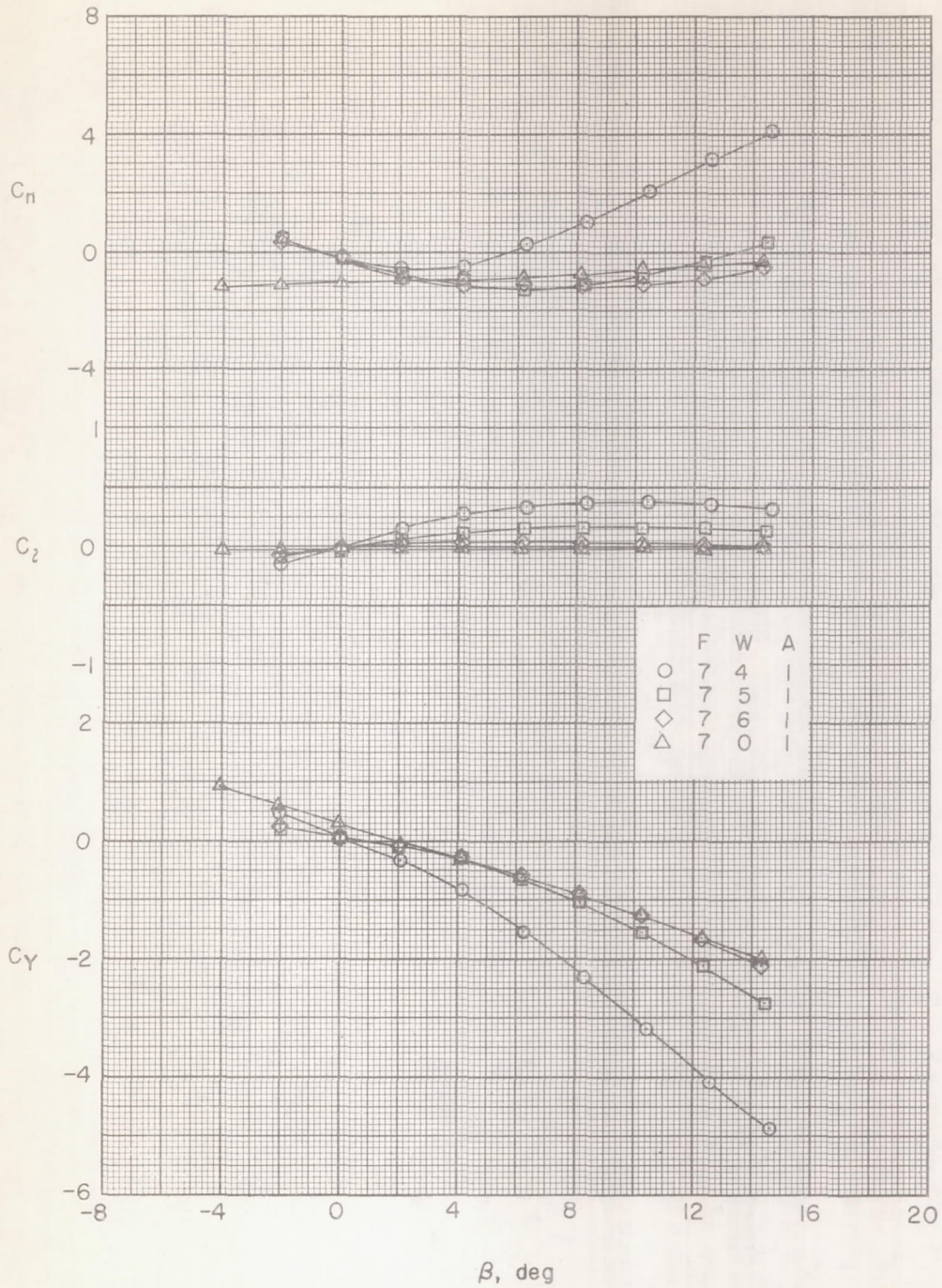
(e) $\alpha \approx 16.4^{\circ}$.

Figure 17.- Continued.



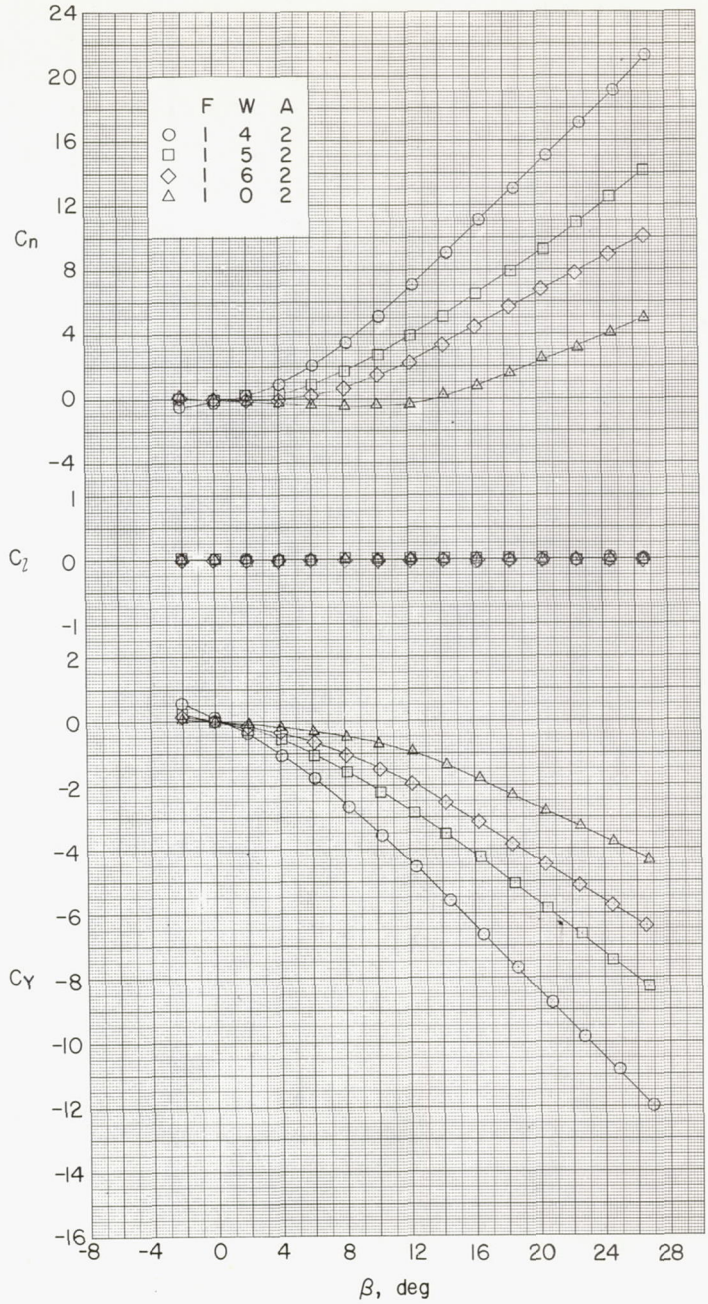
(f) $\alpha \approx 20.5^\circ$.

Figure 17.- Continued.



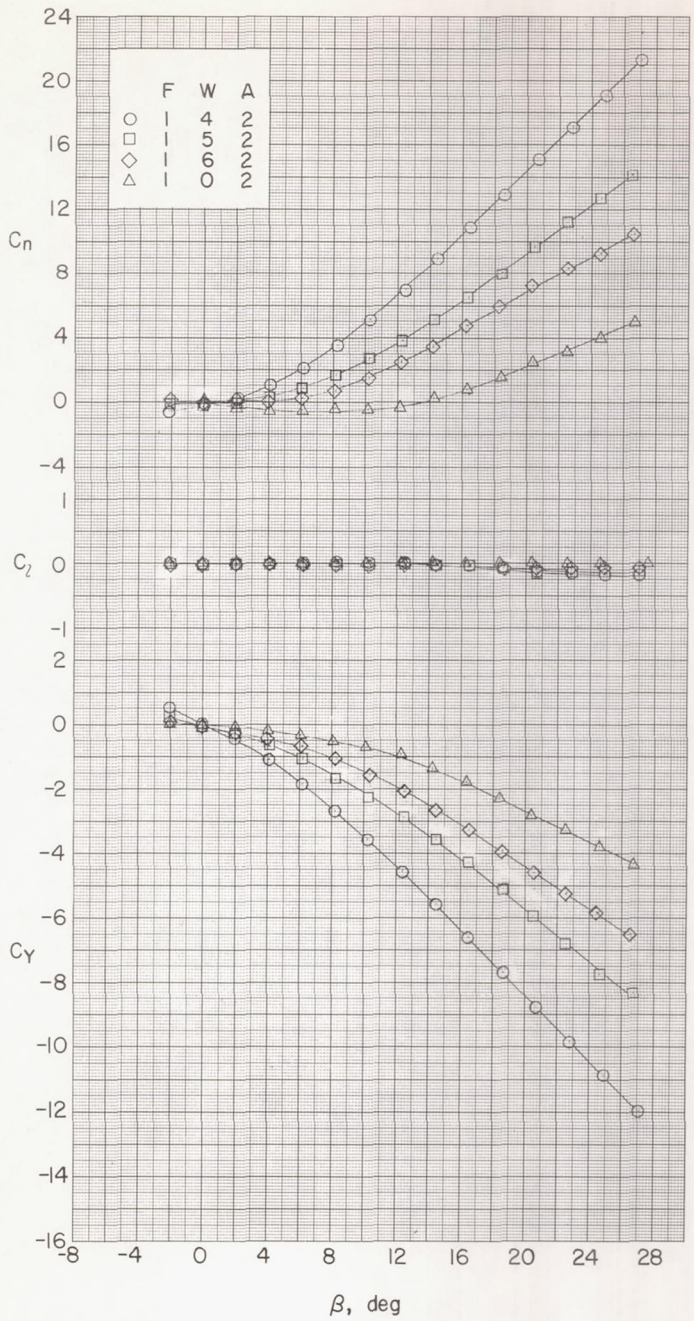
(g) $\alpha \approx 24.7^{\circ}$.

Figure 17.- Concluded.



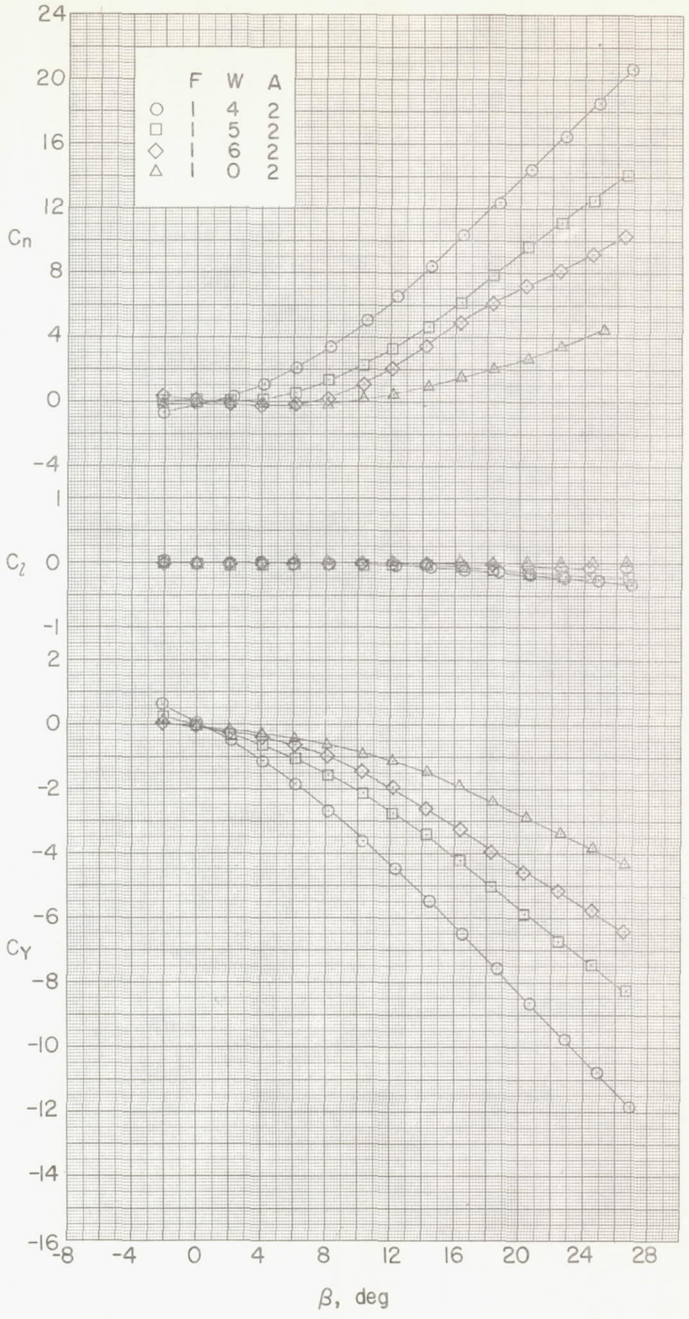
(a) $\alpha \approx 0^{\circ}$.

Figure 18.- Effect of rectangular wings on aerodynamic characteristics in sideslip. Two-caliber cylindrical afterbody; $l/d = 10$.



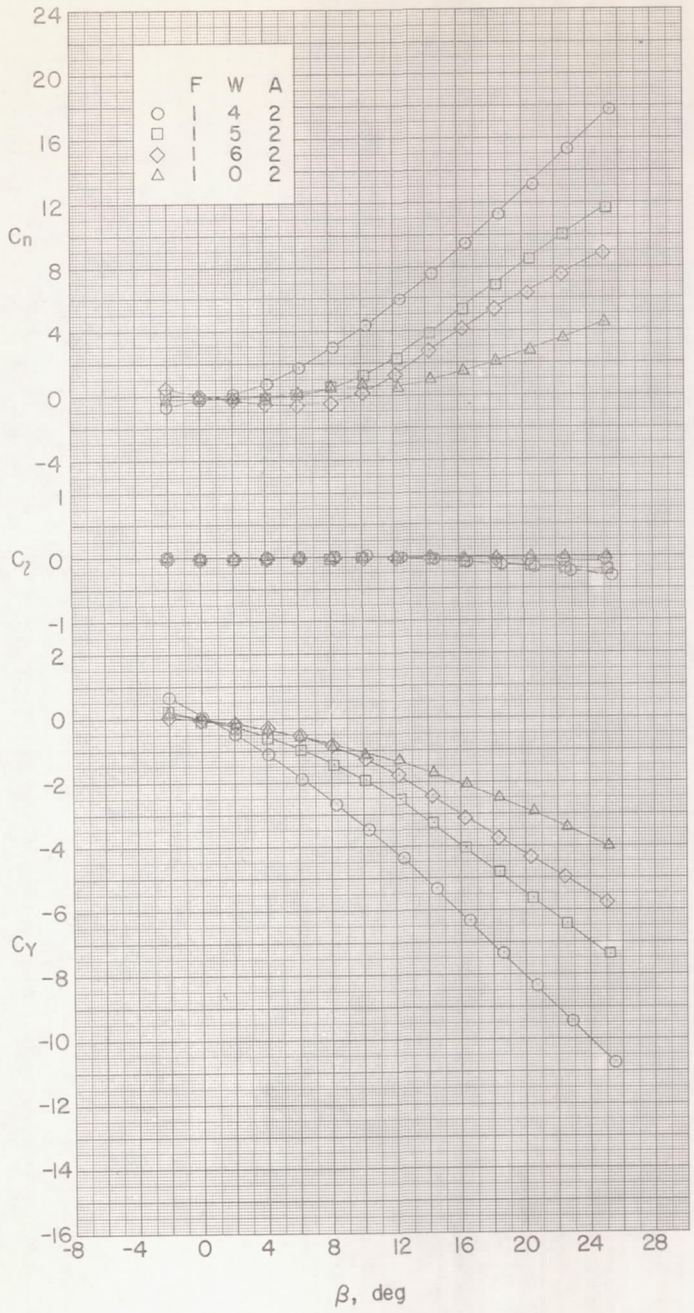
(b) $\alpha \approx 4.1^{\circ}$.

Figure 18.- Continued.



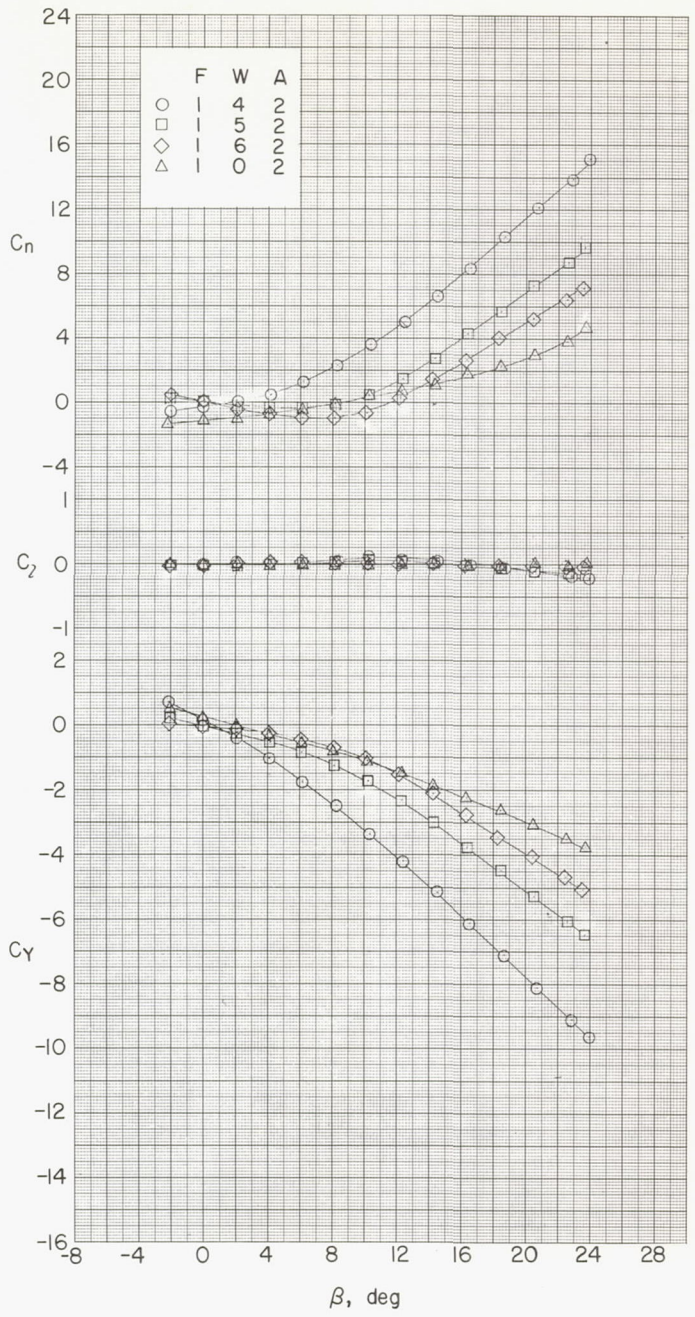
(c) $\alpha \approx 8.2^{\circ}$.

Figure 18.- Continued.



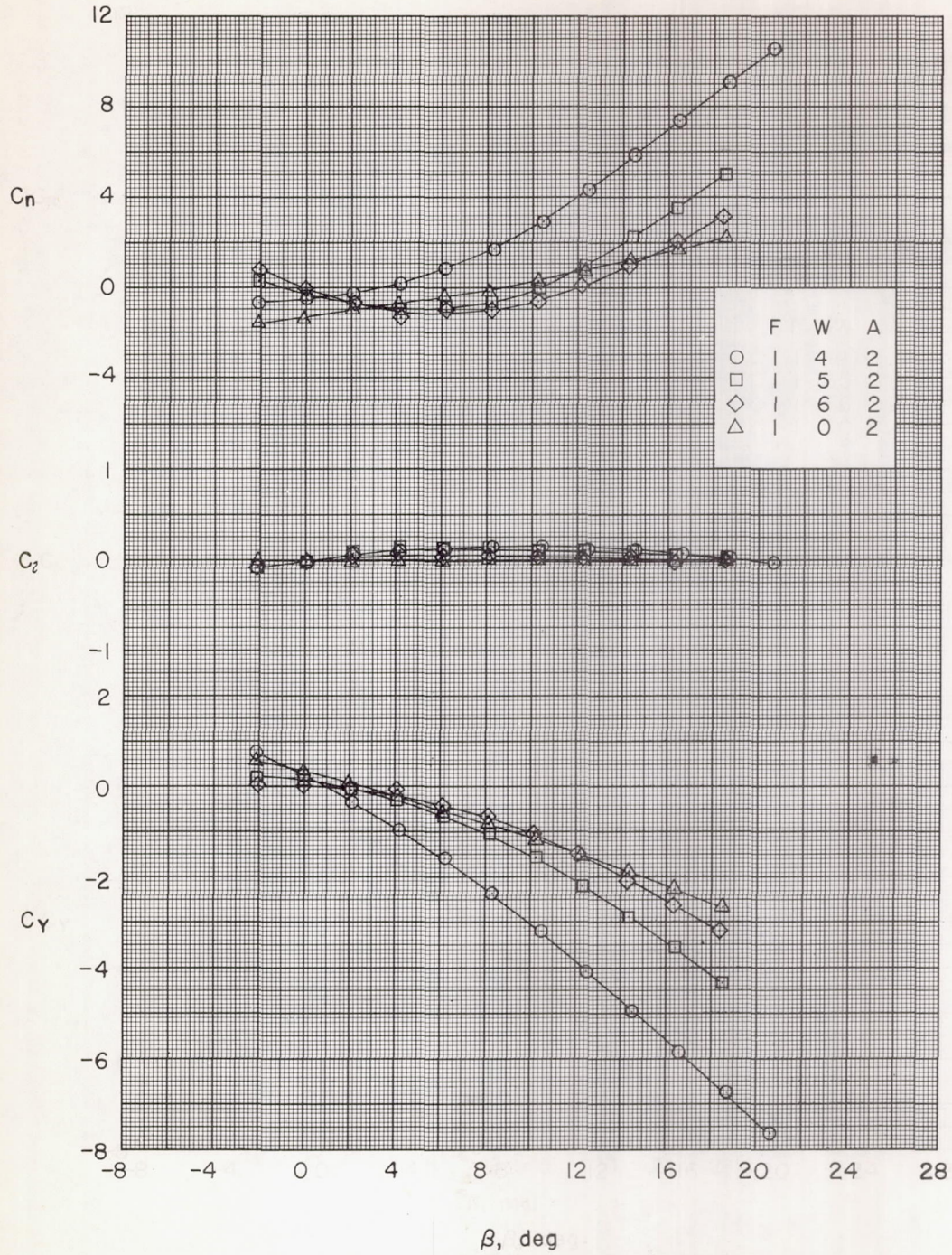
(d) $\alpha \approx 12.3^\circ$.

Figure 18.- Continued.



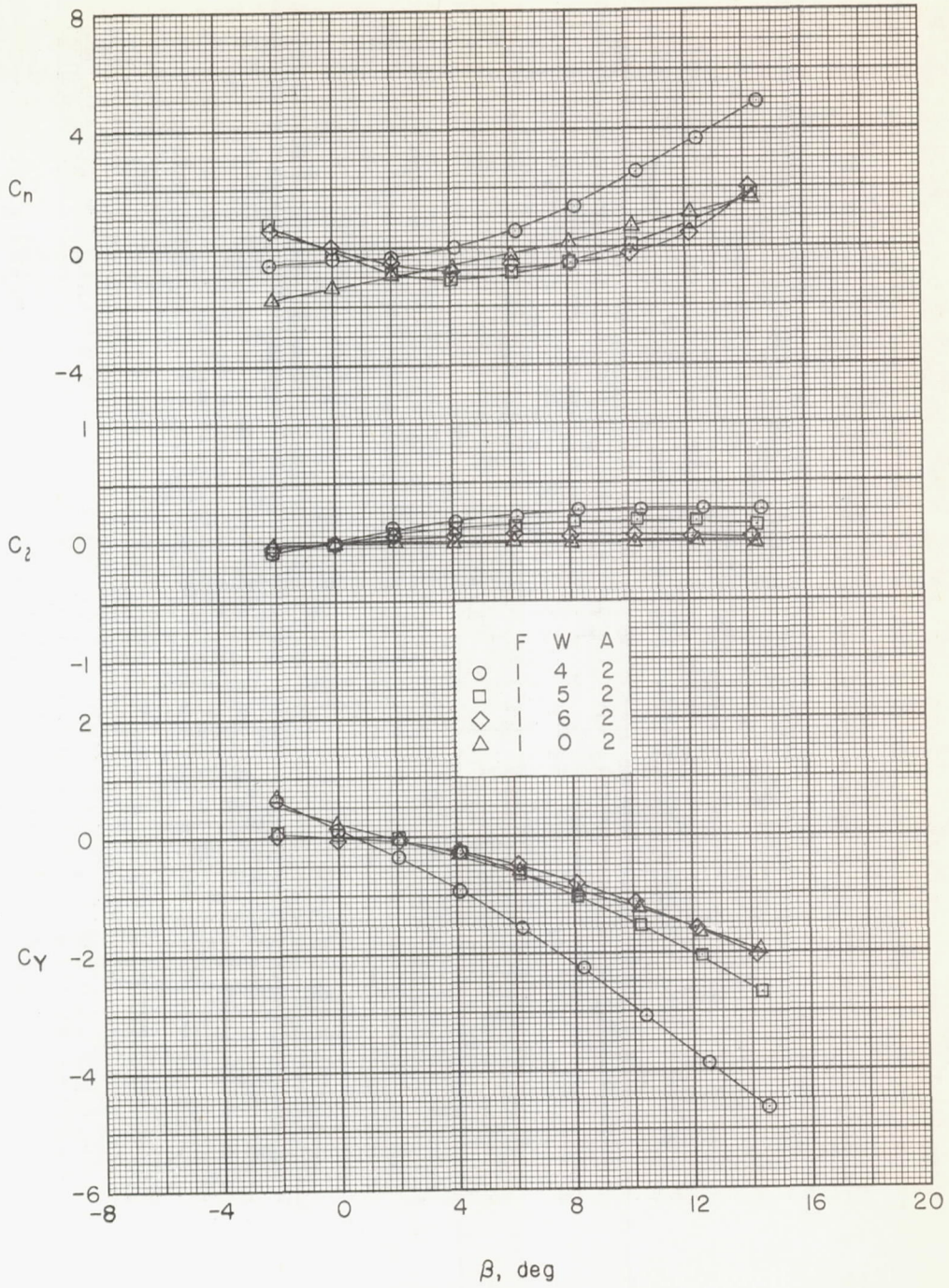
(e) $\alpha \approx 16.4^{\circ}$.

Figure 18.- Continued.



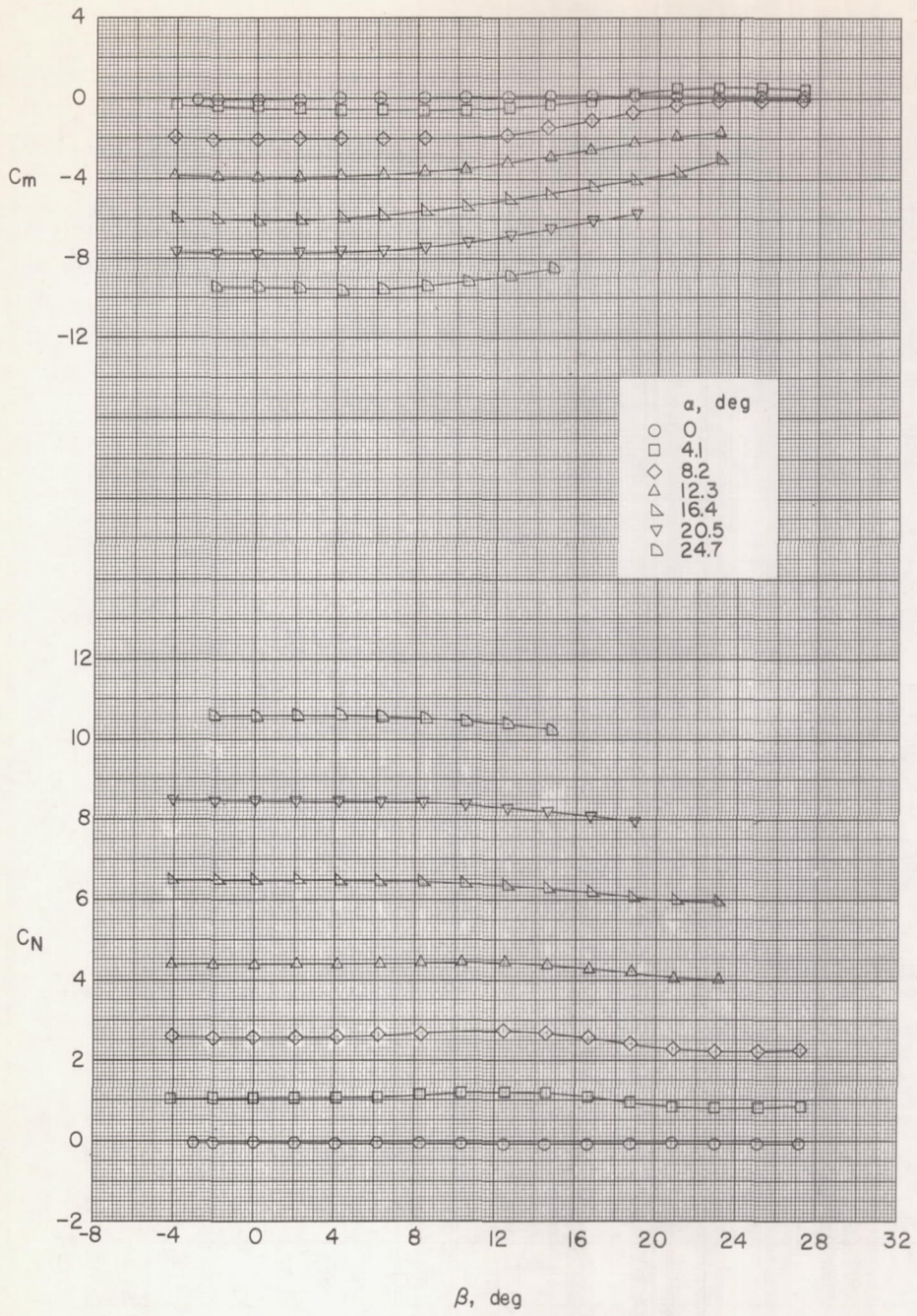
(f) $\alpha \approx 20.5°$.

Figure 18.- Continued.



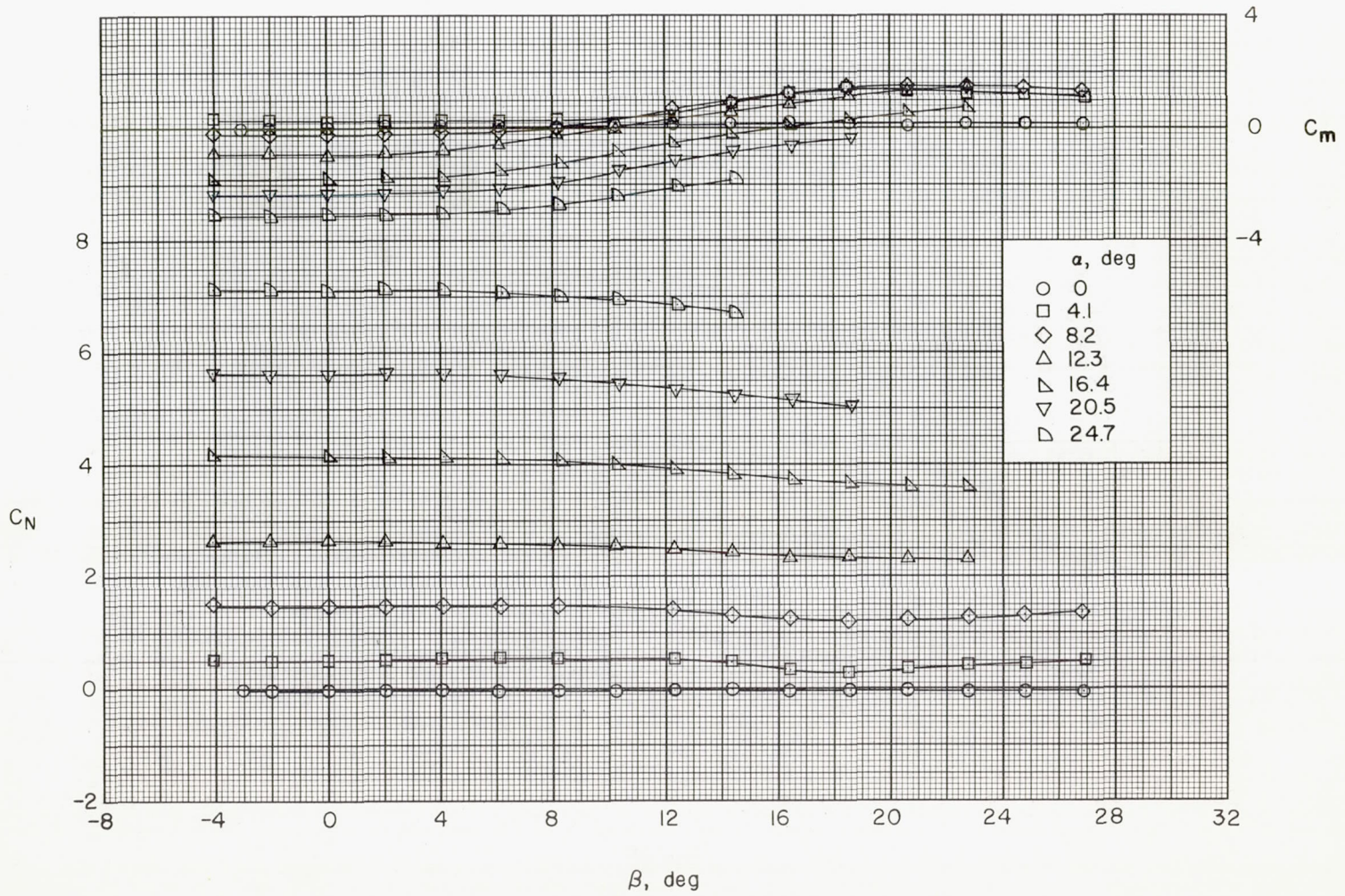
(g) $\alpha \approx 24.7^{\circ}$.

Figure 18.- Concluded.



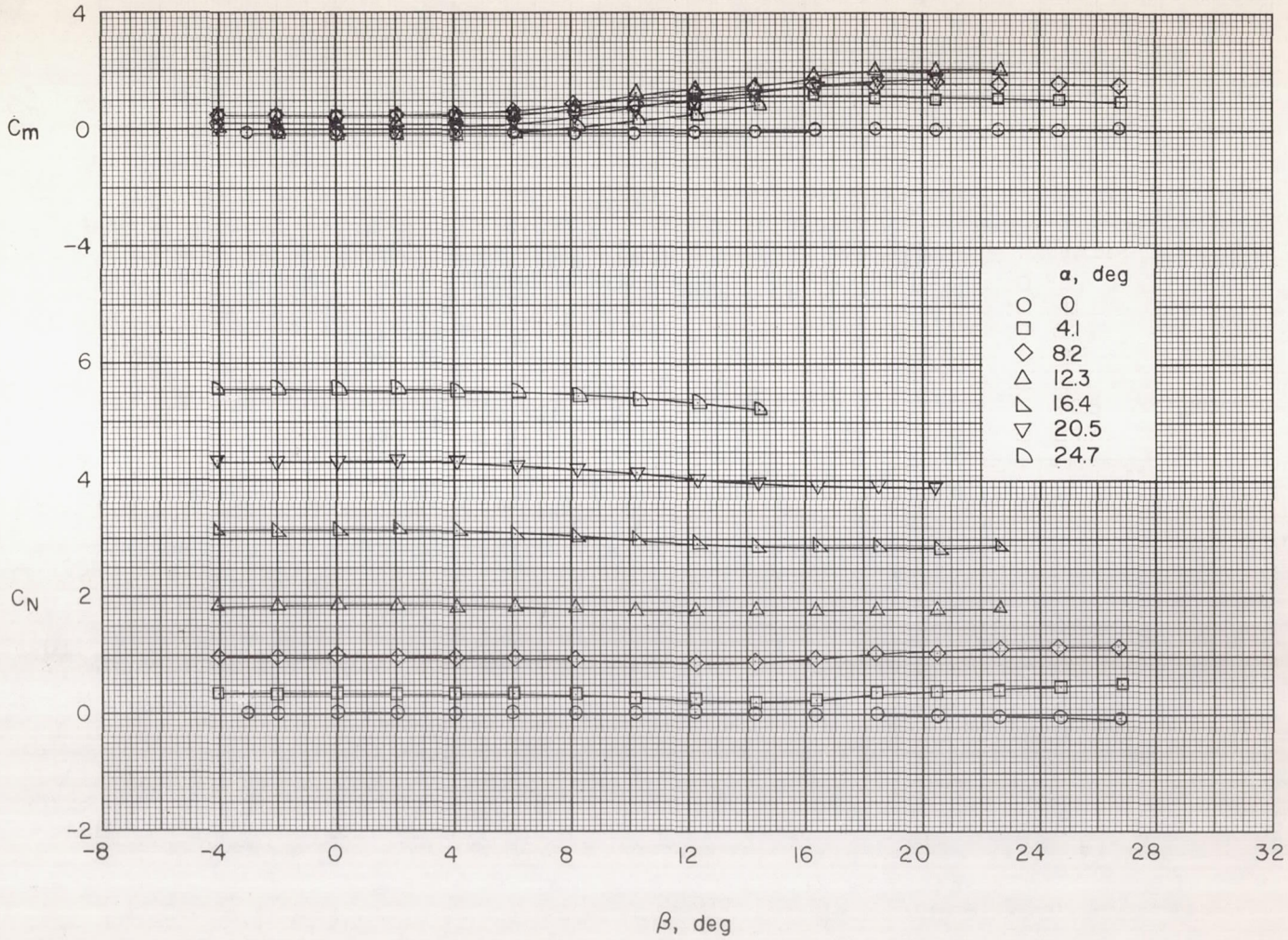
(a) Large rectangular wing, $F_8W_4A_0$.

Figure 19.- Variation of C_m and C_N with β for various angles of attack. Rectangular wings; no afterbody; l/d = 10.



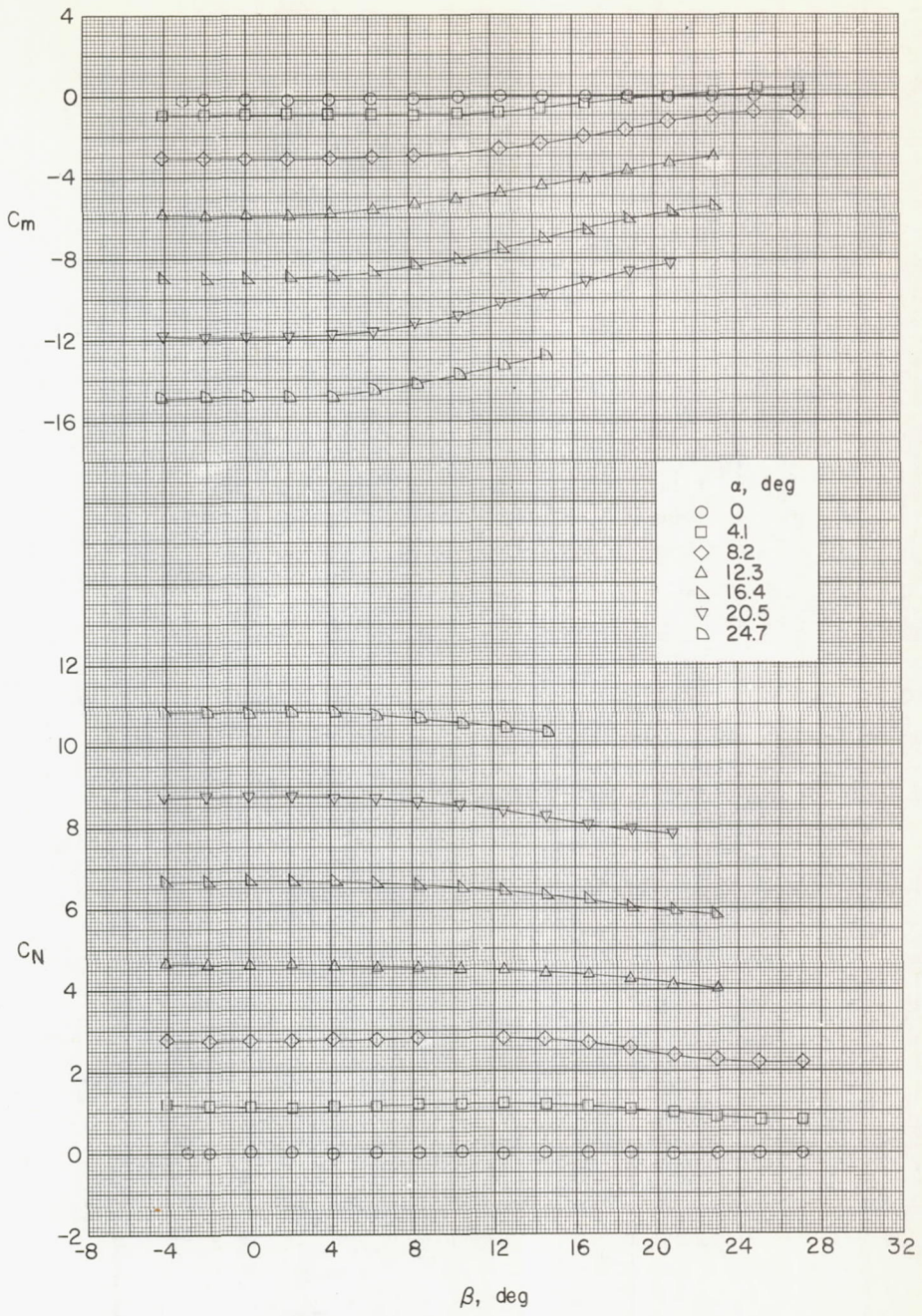
(b) Medium rectangular wing, $F_8W_5A_0$.

Figure 19.- Continued.



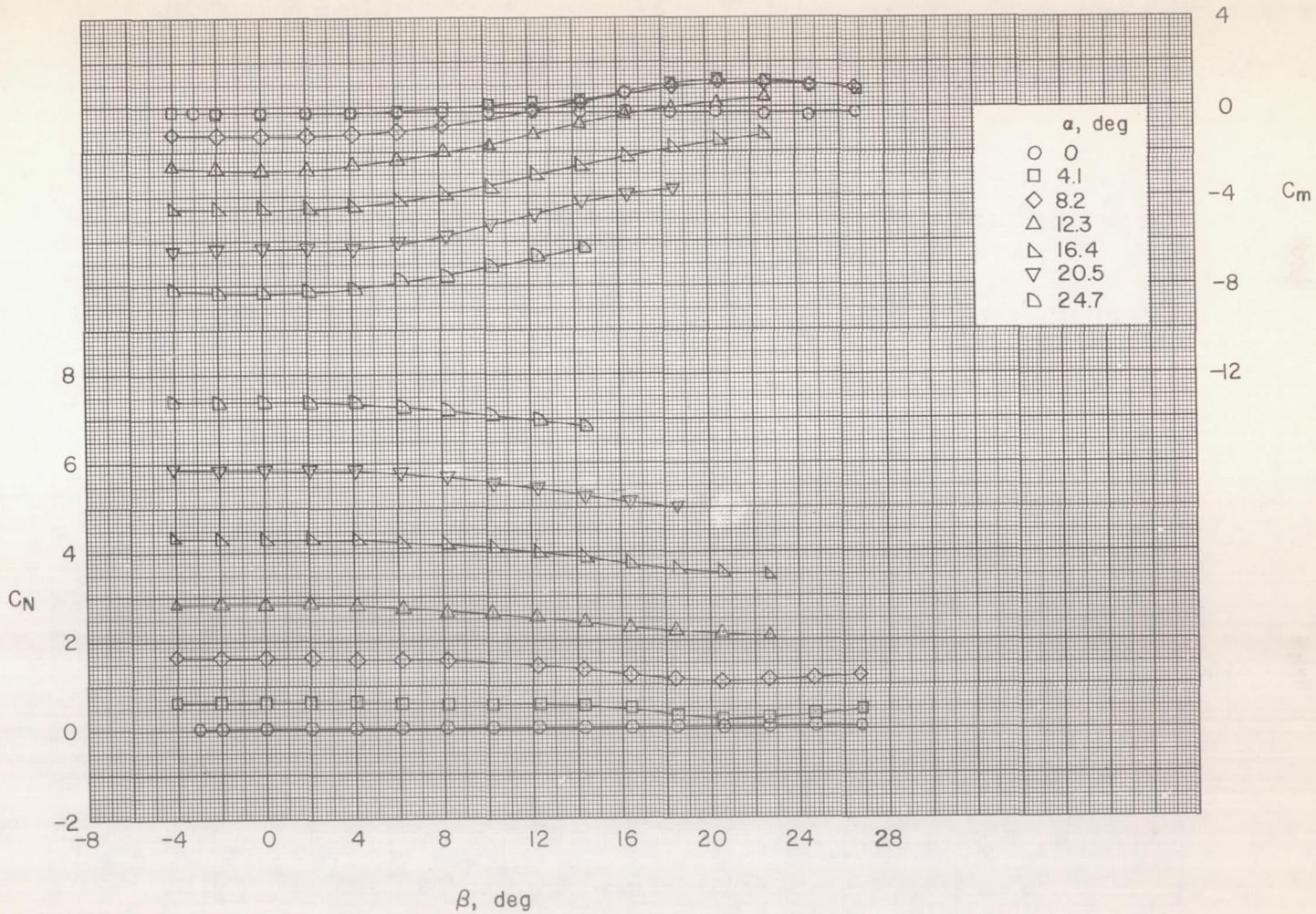
(c) Small rectangular wing, $F_8W_6A_0$.

Figure 19.- Concluded.



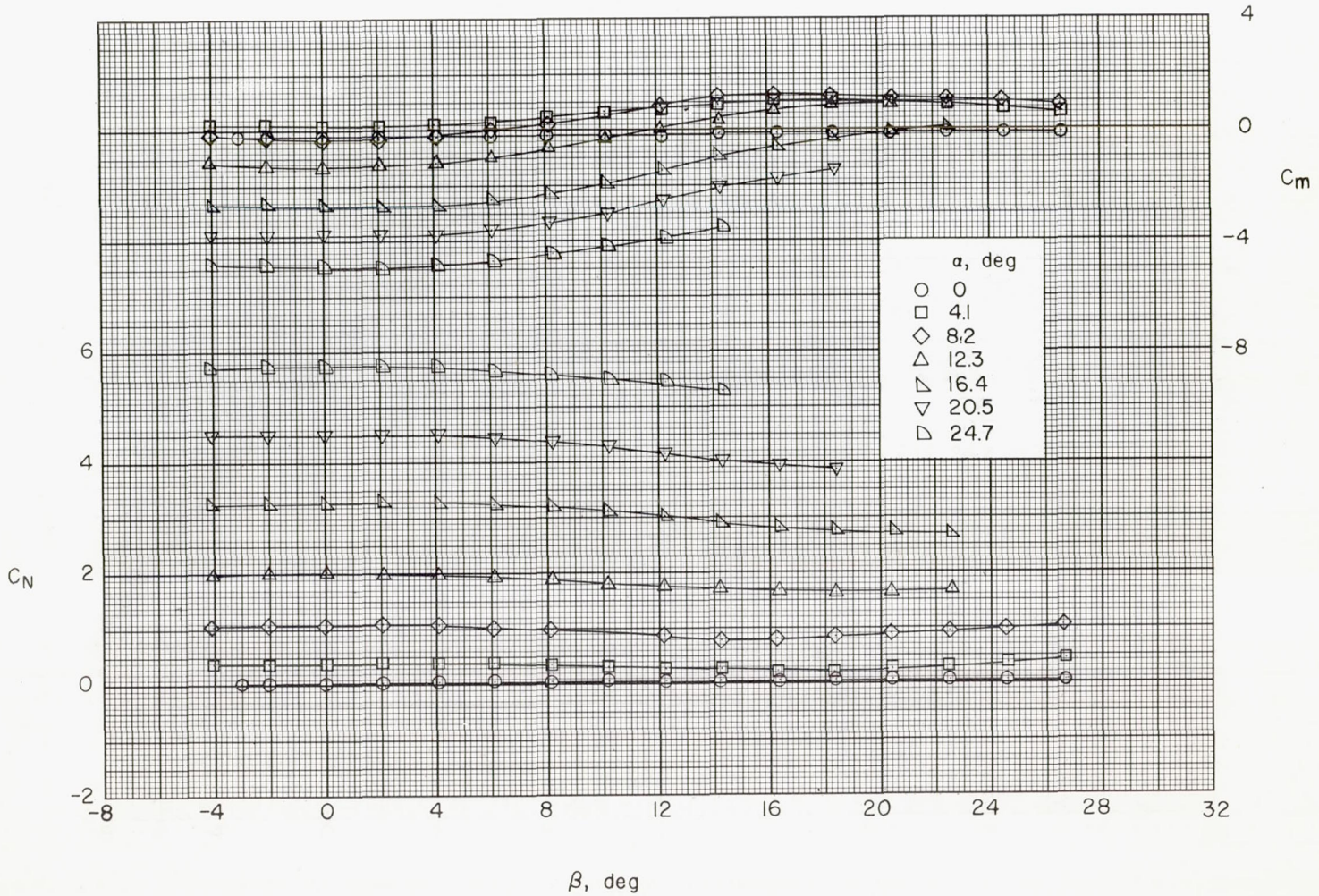
(a) Large rectangular wing, $F_7W_4A_1$.

Figure 20.- Variation of C_m and C_N with β for various angles of attack. Rectangular wings; 1-caliber cylindrical afterbody; l/d = 10.



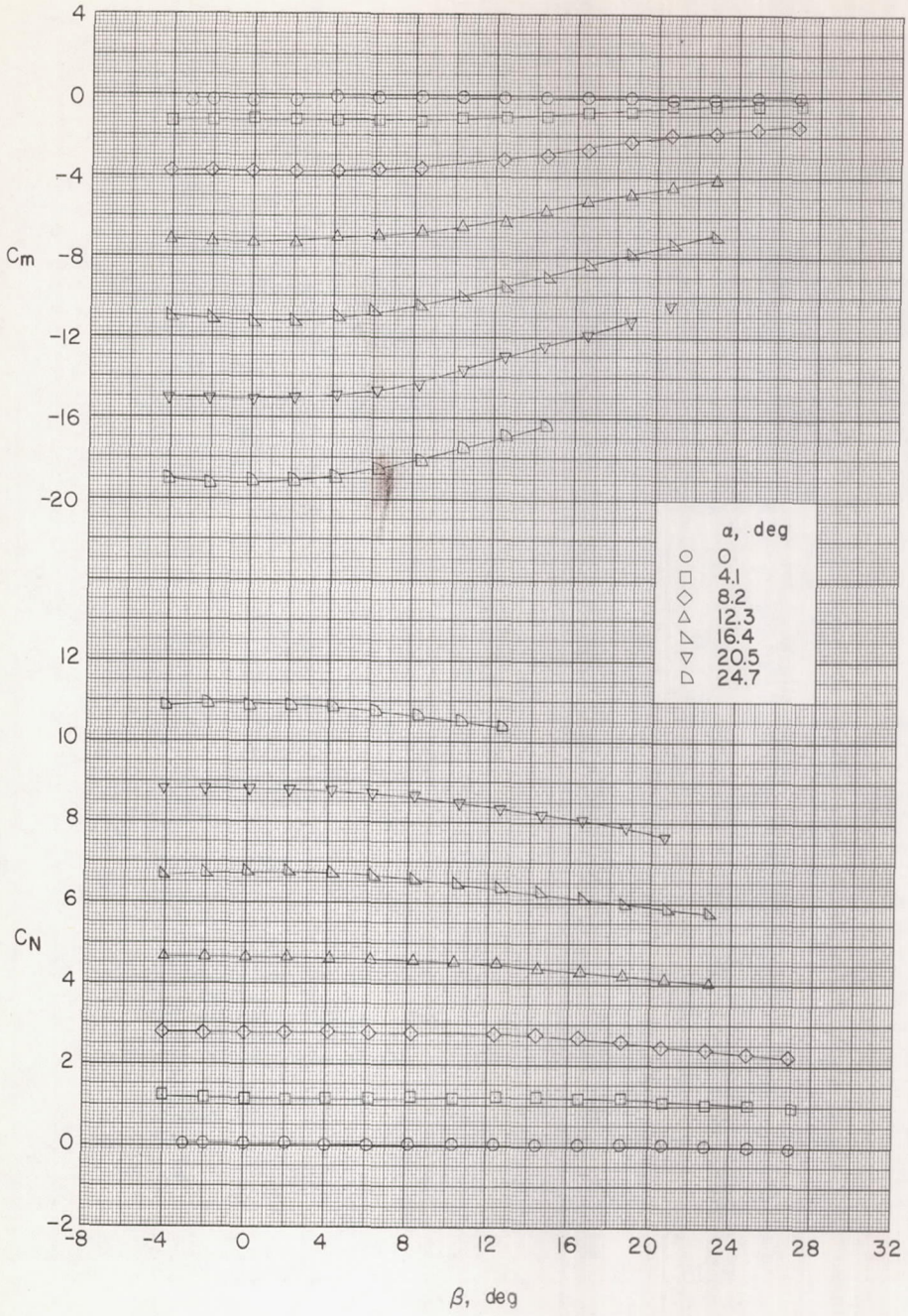
(b) Medium rectangular wing, $F_7W_5A_1$.

Figure 20.- Continued.



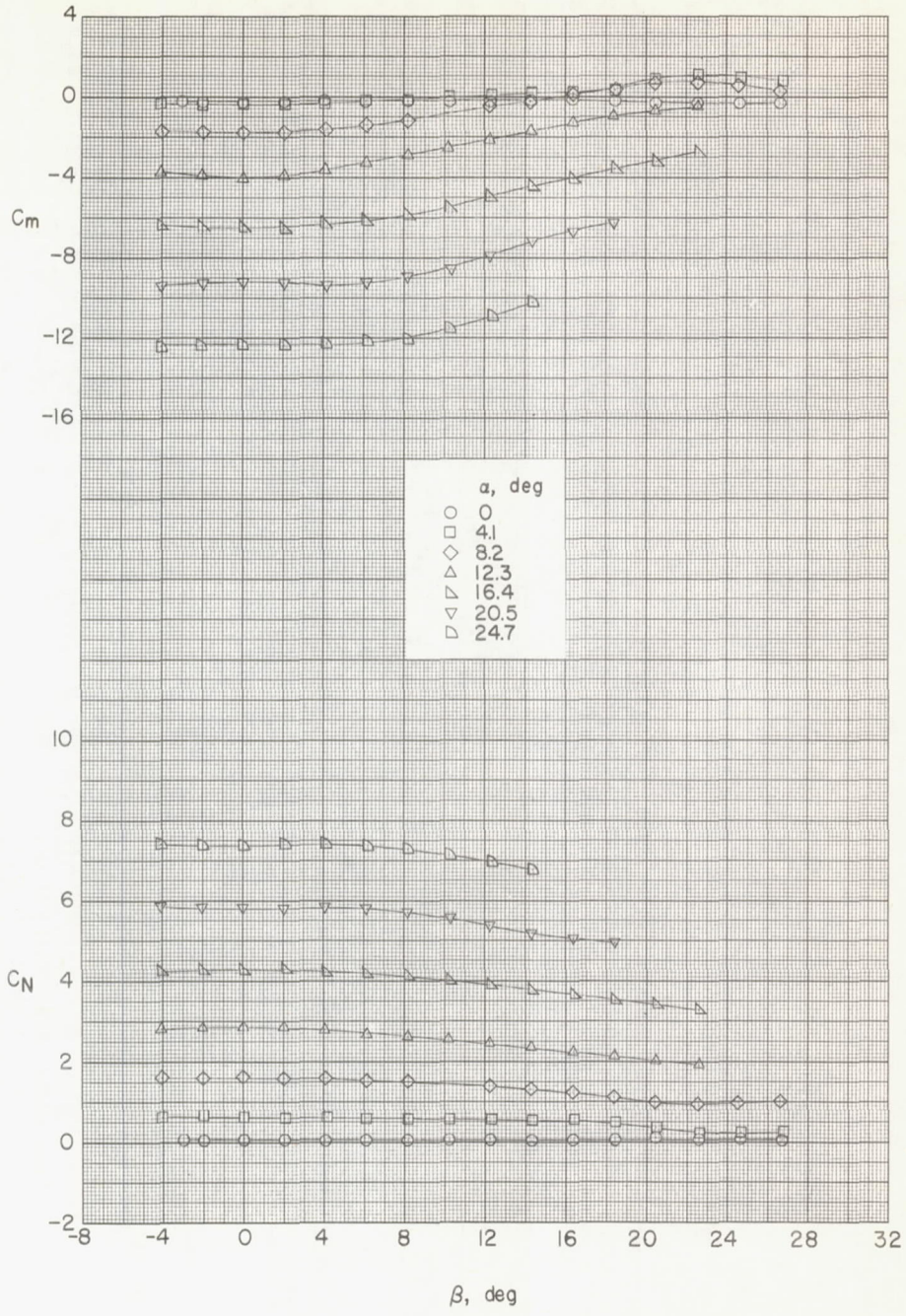
(c) Small rectangular wings, $F_7W_6A_1$.

Figure 20.- Concluded.



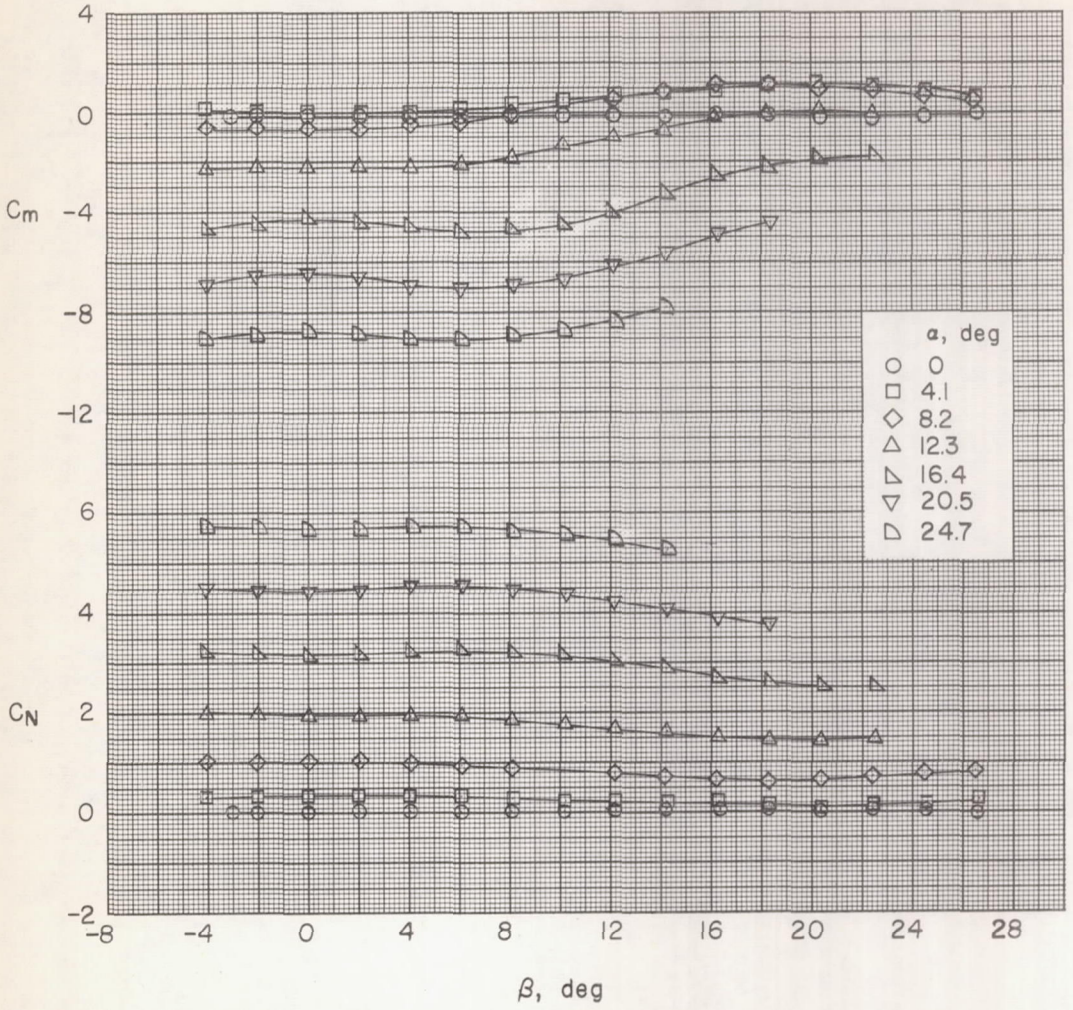
(a) Large rectangular wing, $F_1W_4A_2$.

Figure 21.- Variation of C_m and C_N with β for various angles of attack. Rectangular wings; 2-caliber cylindrical afterbody; $l/d = 10$.



(b) Medium rectangular wing, $F_1W_6A_2$.

Figure 21.- Continued.



(c) Small rectangular wing, $F_1W_6A_2$.

Figure 21.- Concluded.

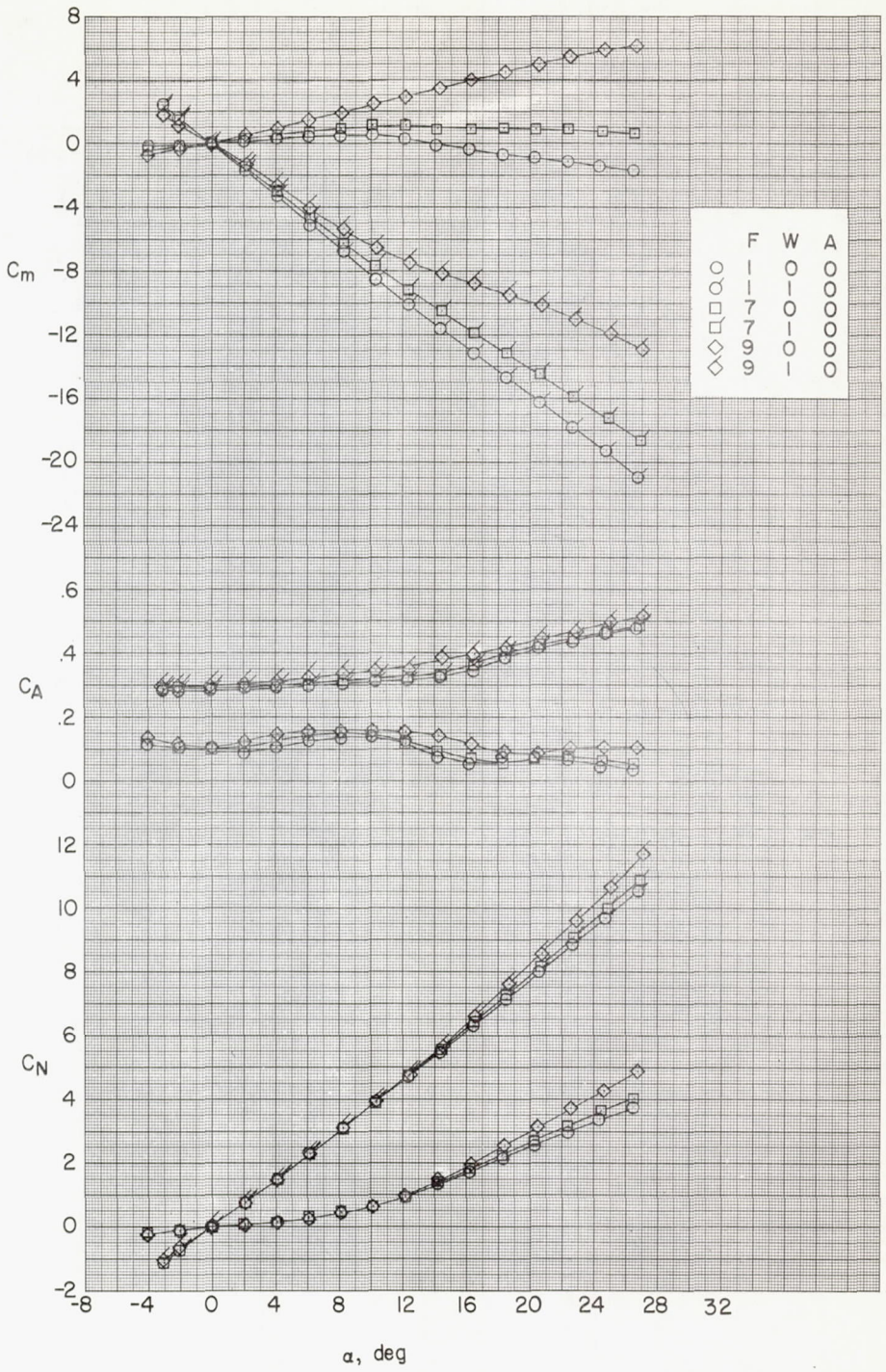


Figure 22.- Effect of forebody length on aerodynamic characteristics in pitch. Large delta wing; no afterbody.

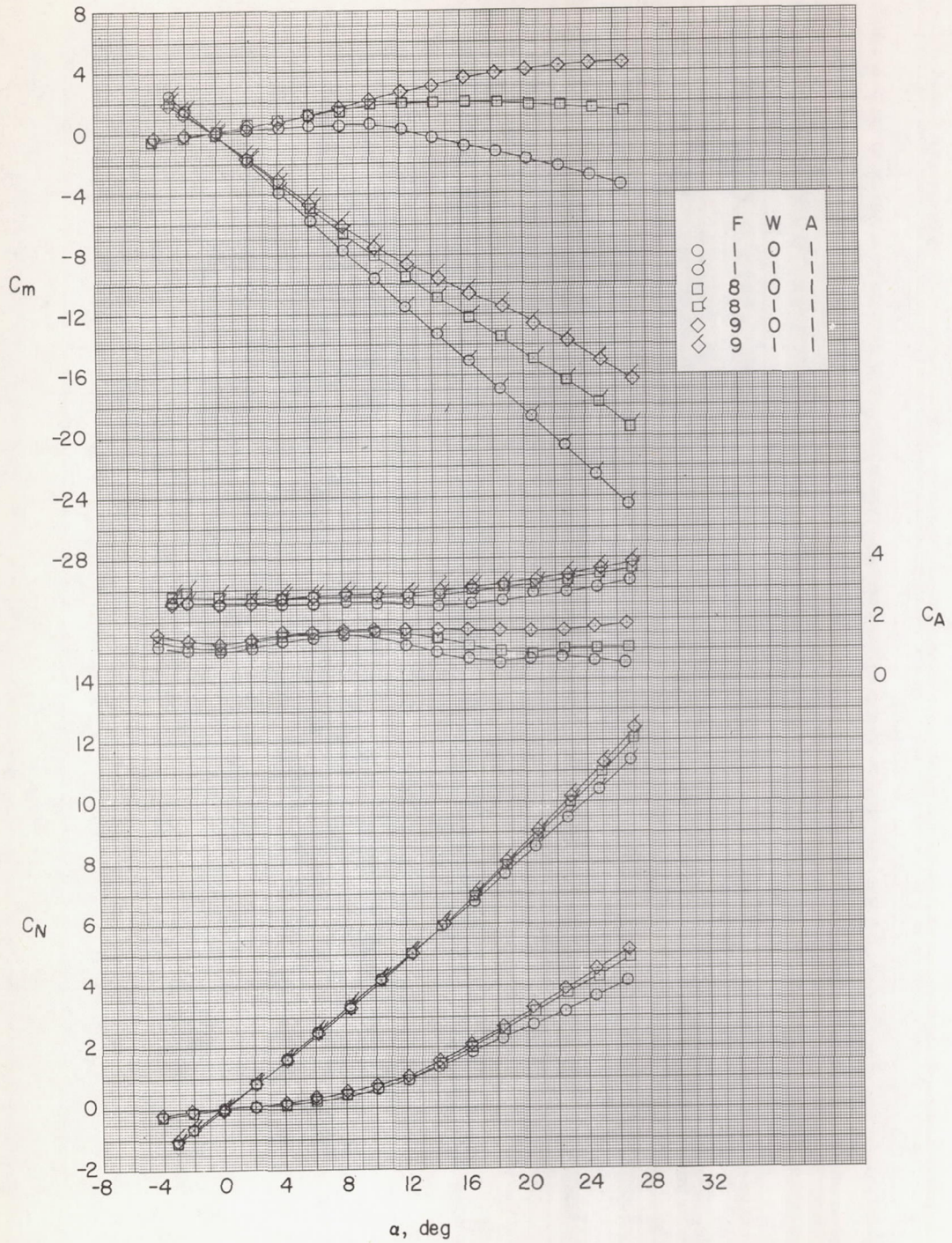


Figure 23.- Effects of forebody length on aerodynamic characteristics in pitch. Large delta wings; 1-caliber cylindrical afterbody.

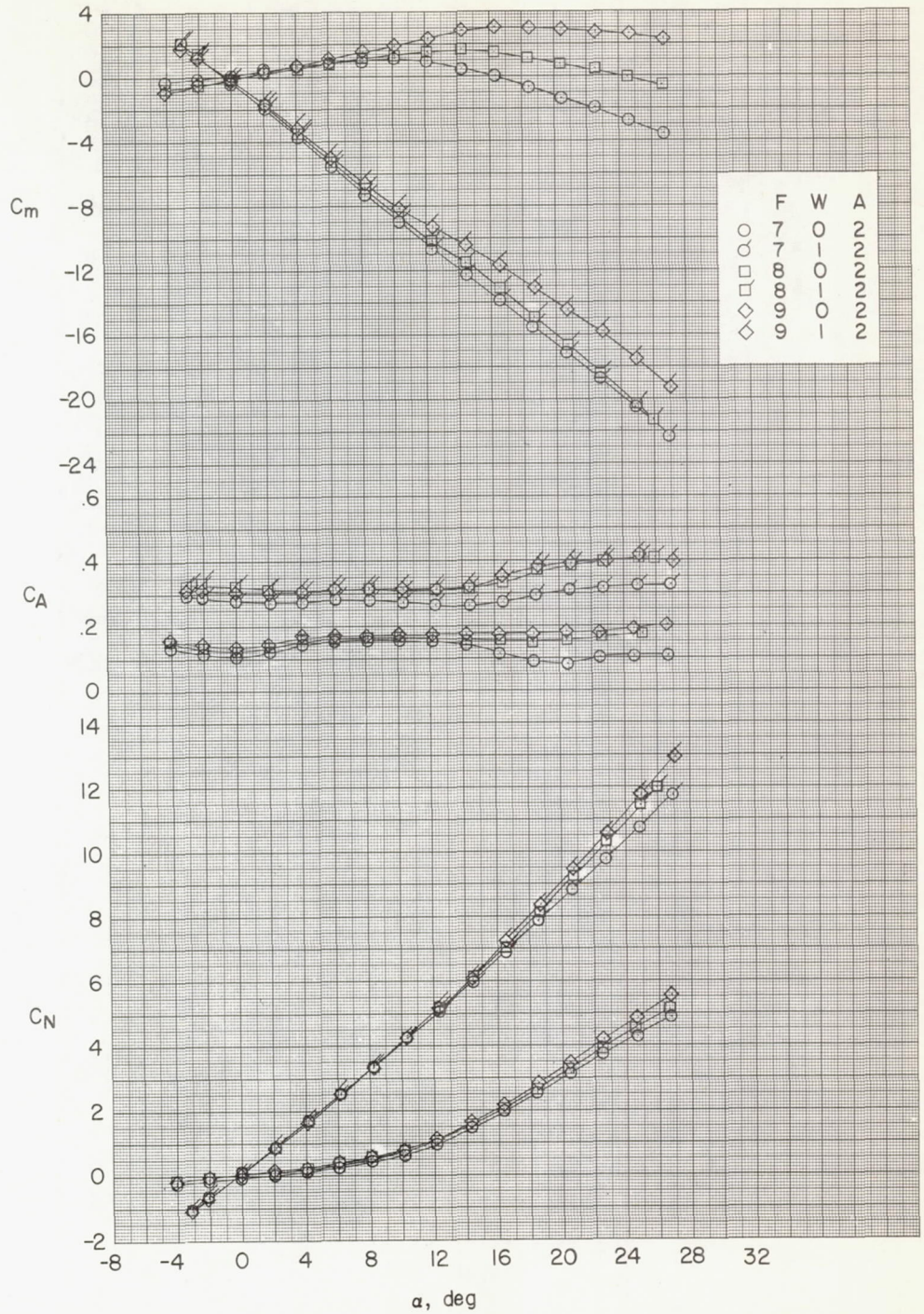
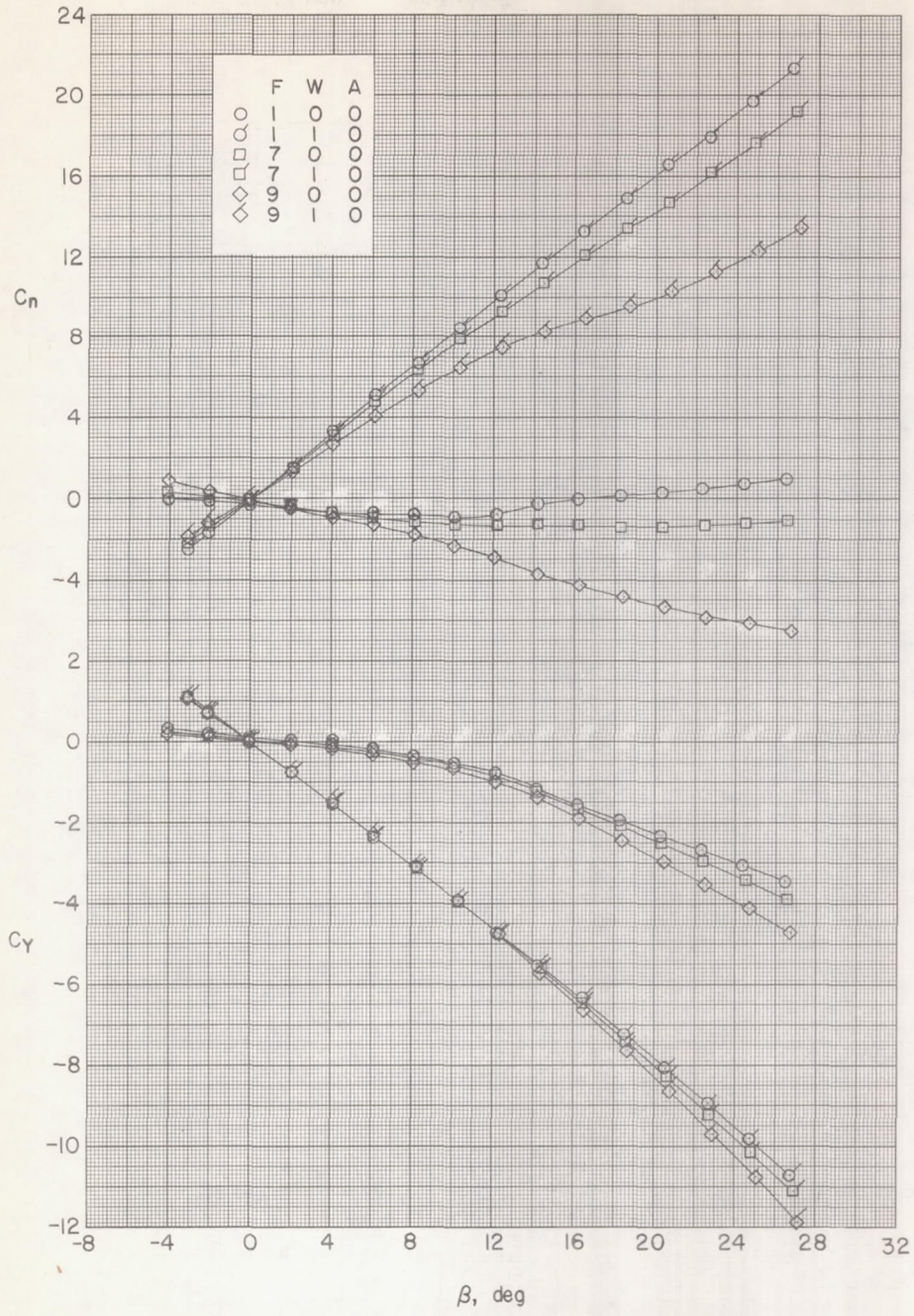
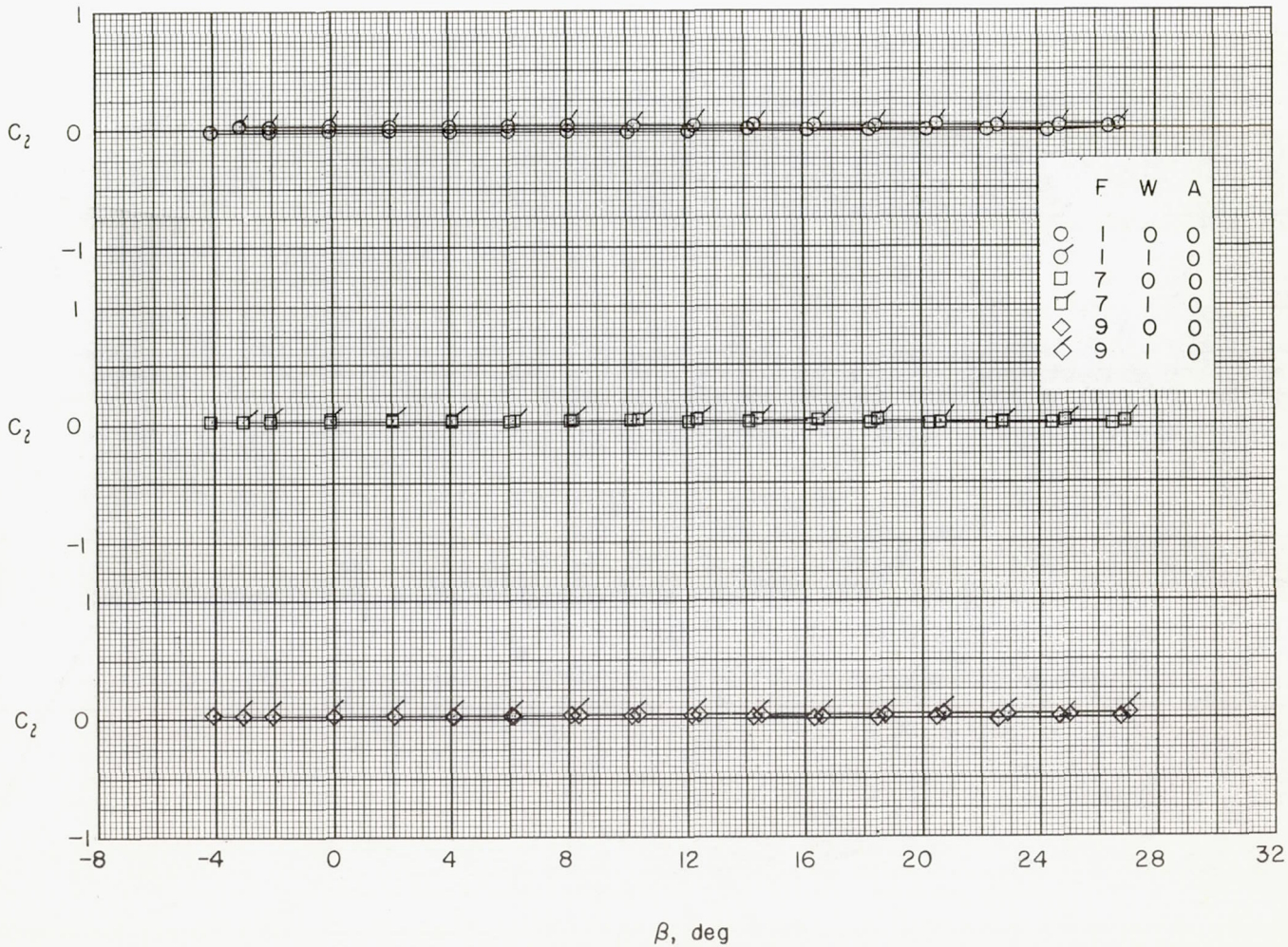


Figure 24.- Effects of forebody length on aerodynamic characteristics in pitch. Large delta wings; 2-caliber cylindrical afterbody.



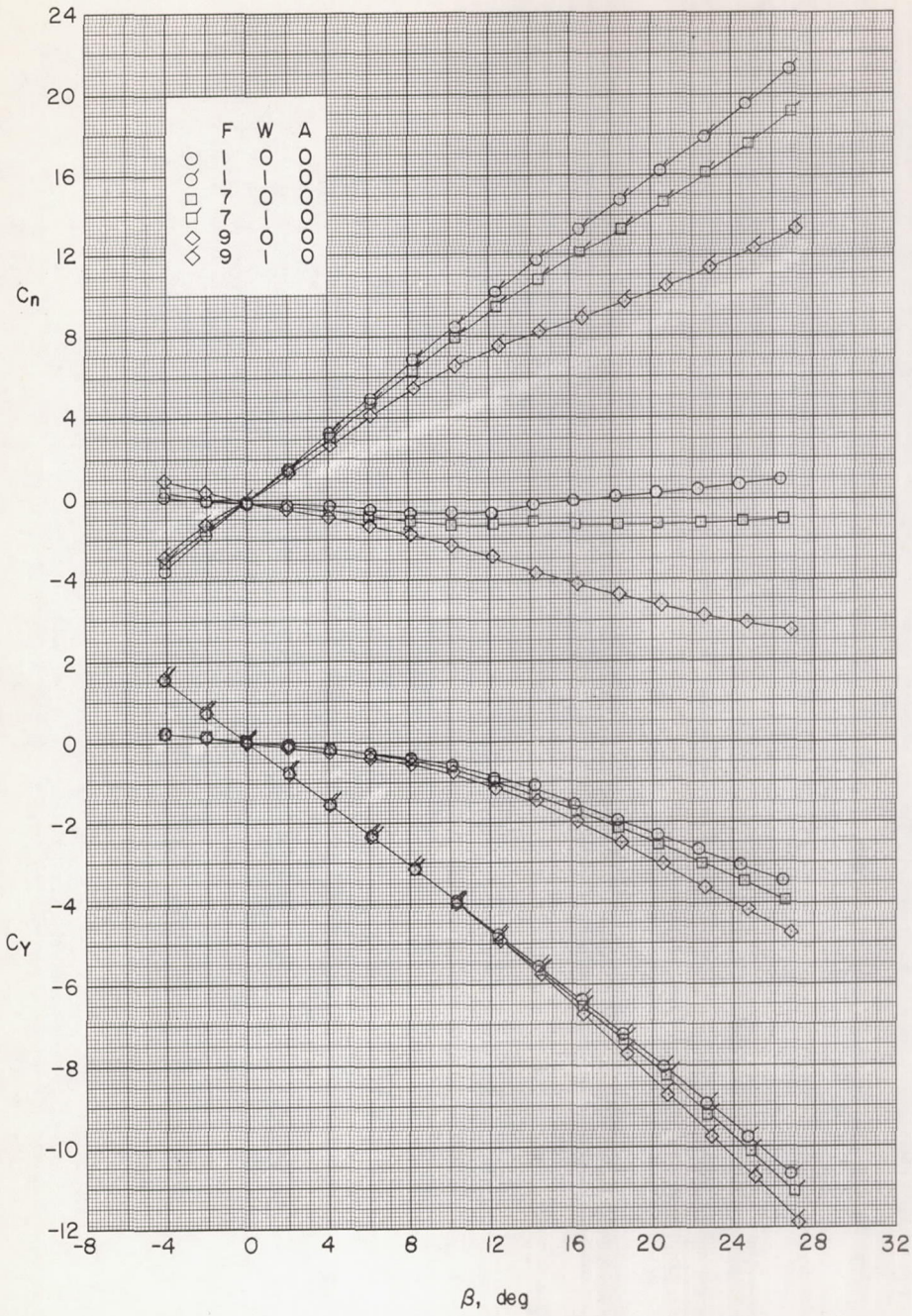
(a) $\alpha \approx 0^{\circ}$.

Figure 25.- Effect of forebody length on aerodynamic characteristics in sideslip. Large delta wings; no afterbody.



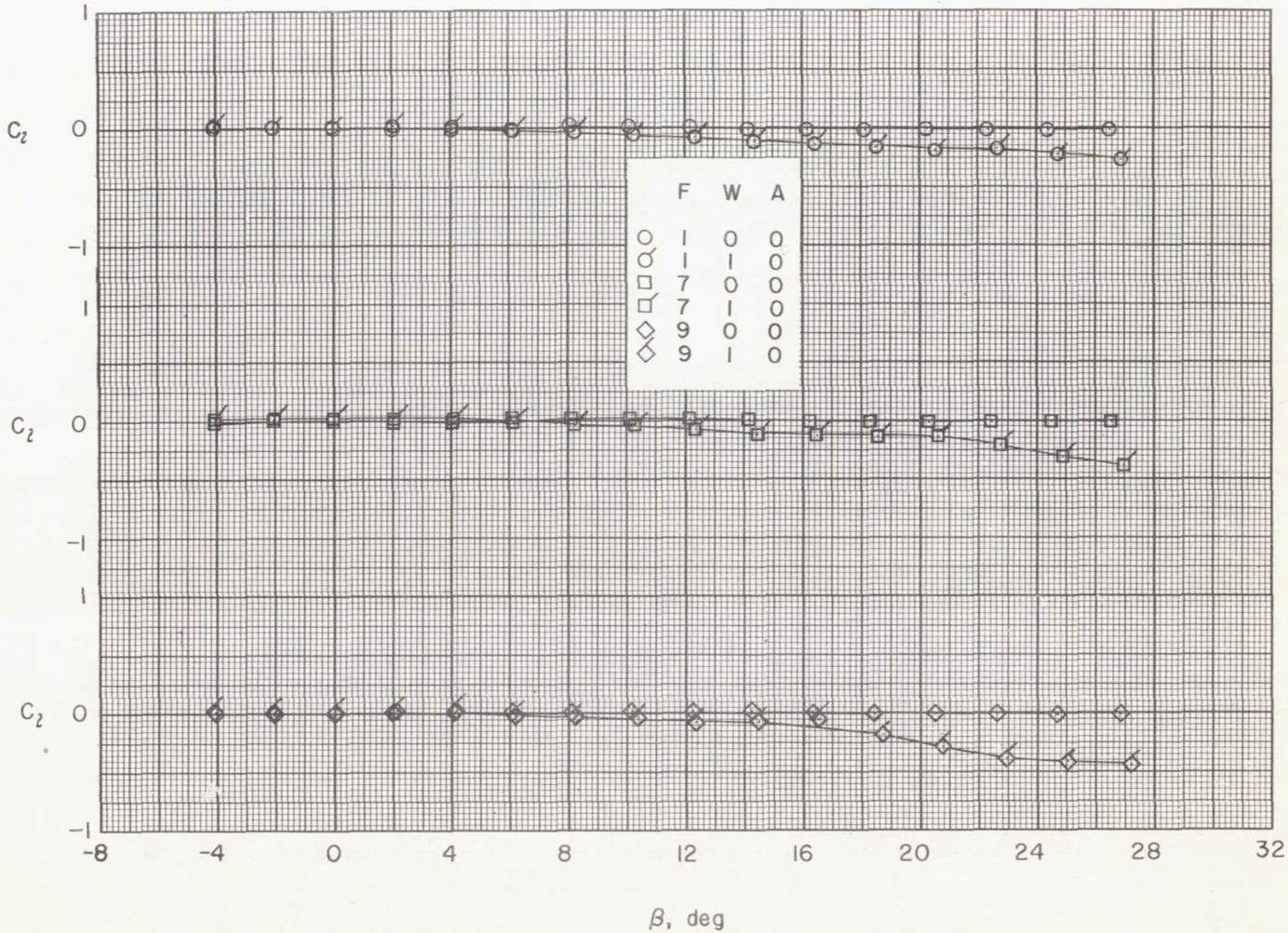
(a) Concluded.

Figure 25.- Continued.



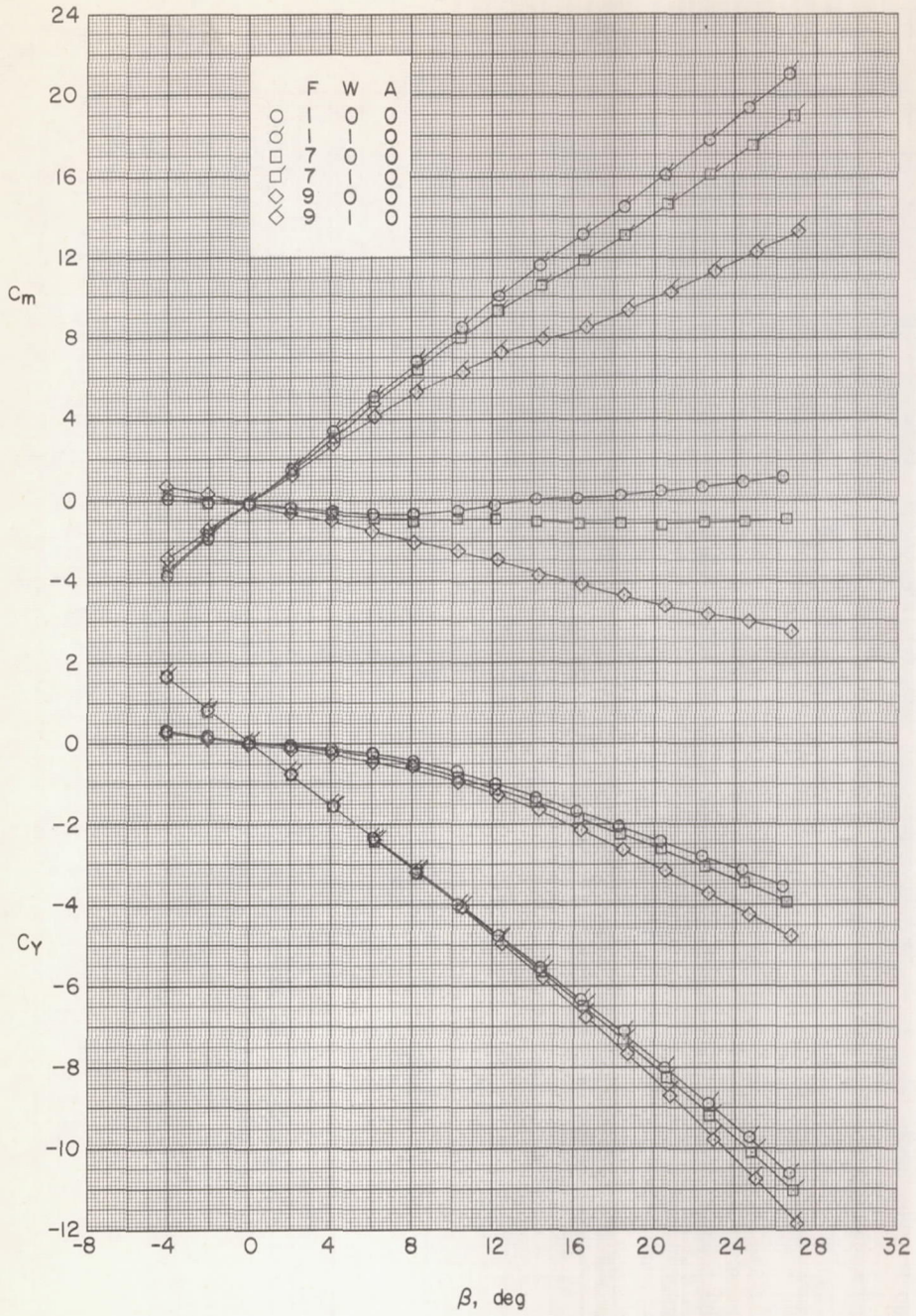
(b) $\alpha \approx 4.1^\circ$.

Figure 25.- Continued.



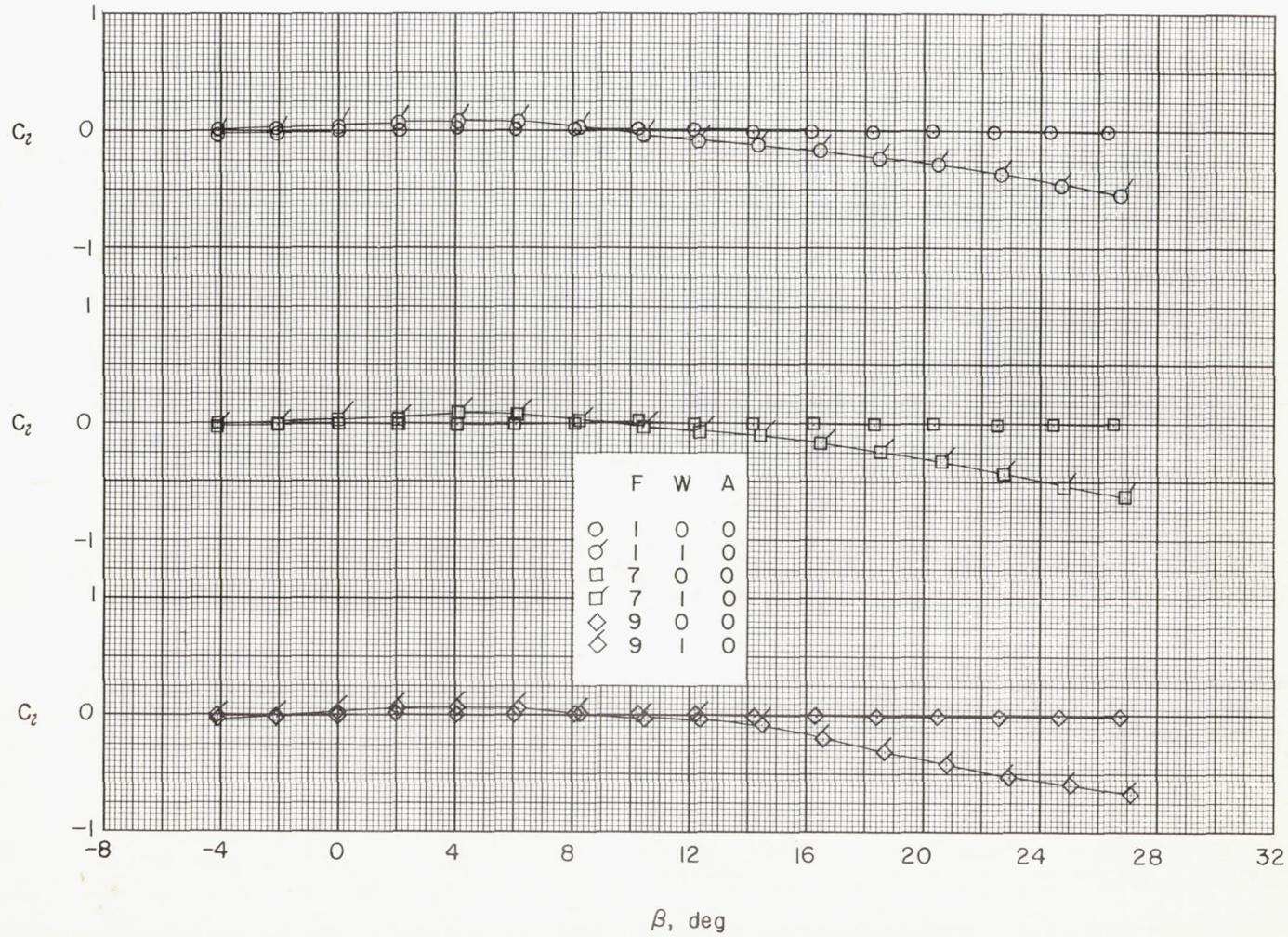
(b) Concluded.

Figure 25.- Continued.



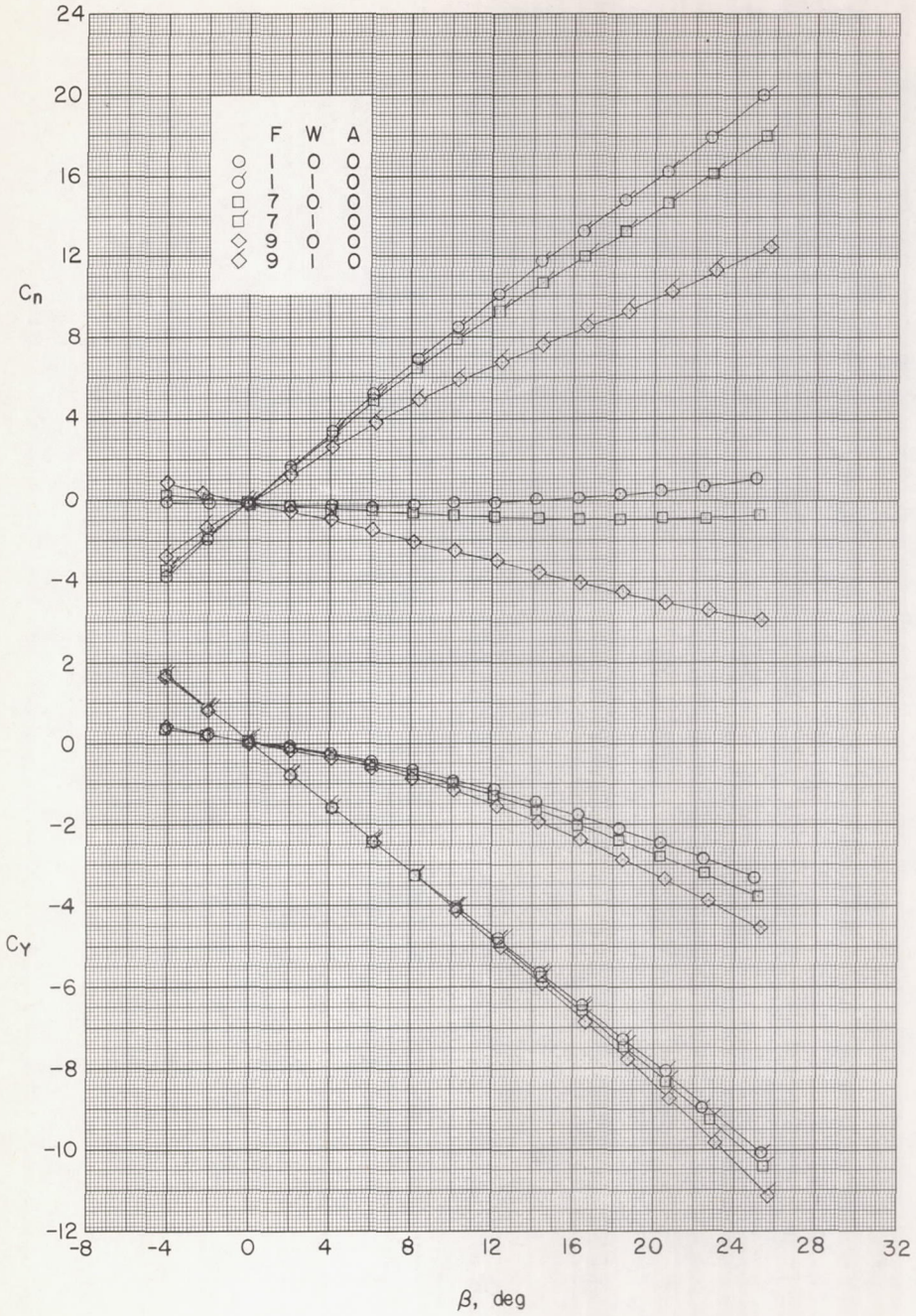
(c) $\alpha \approx 8.2^{\circ}$.

Figure 25.- Continued.



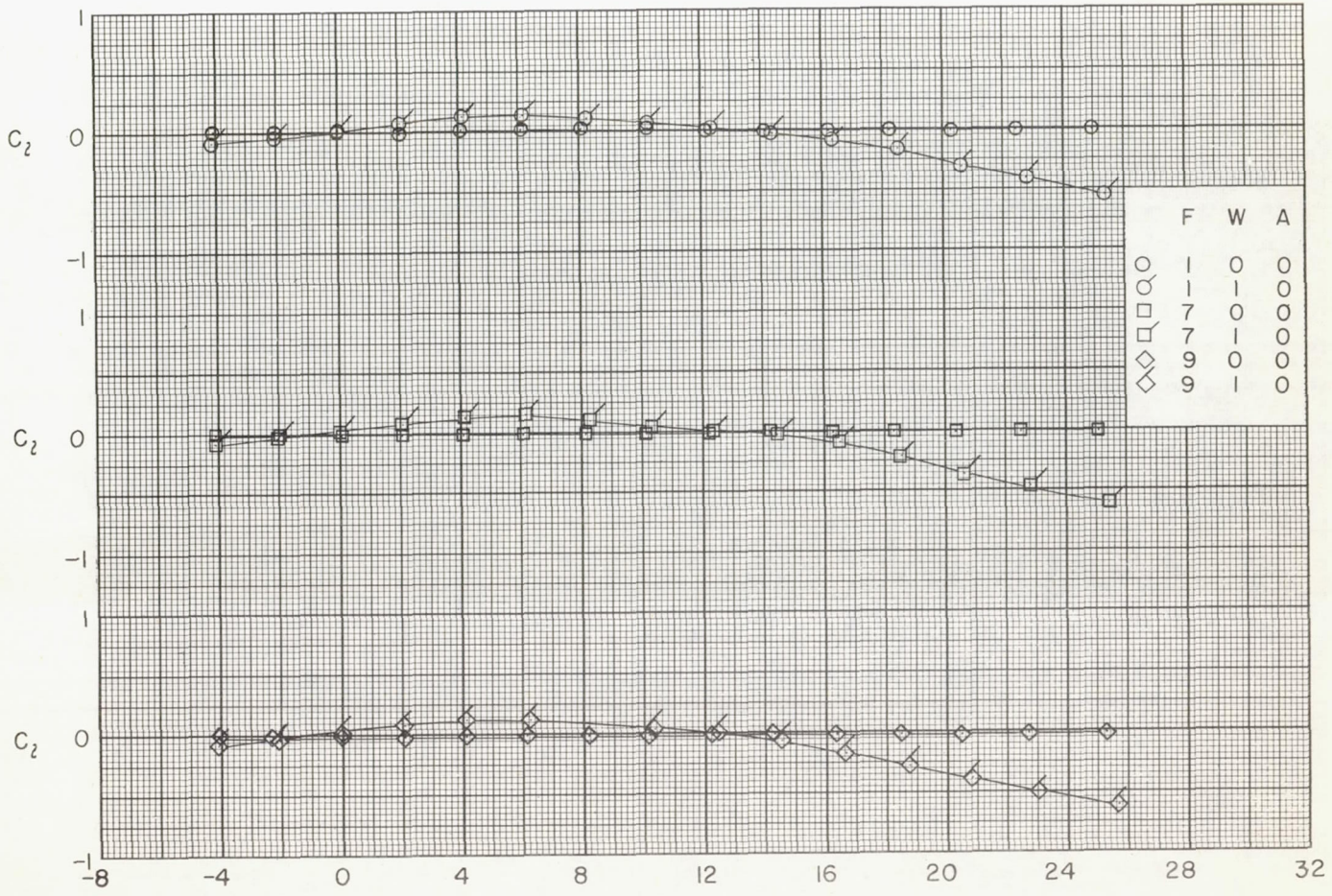
(c) Concluded.

Figure 25.- Continued.



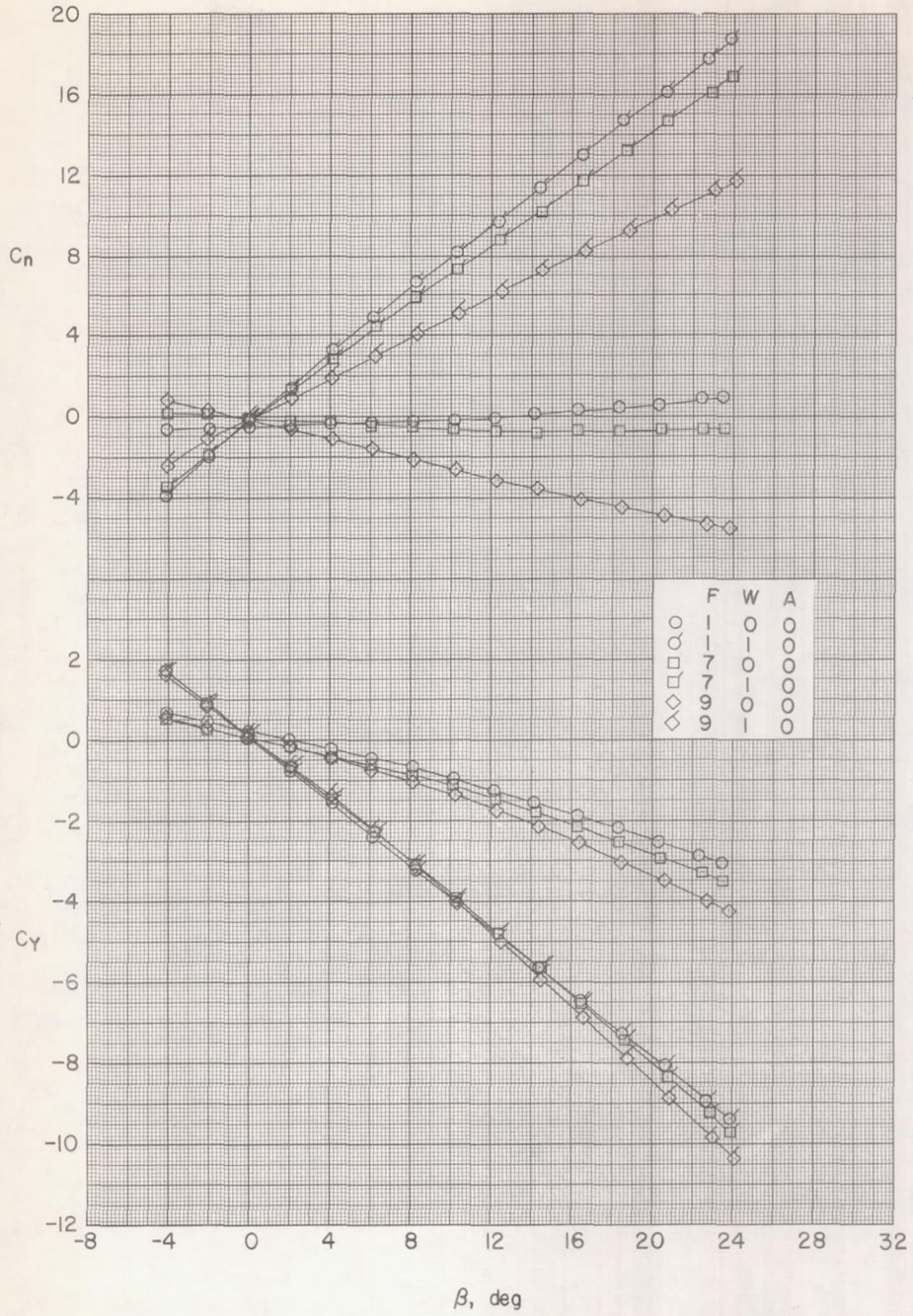
(d) $\alpha \approx 12.3^{\circ}$.

Figure 25.- Continued.



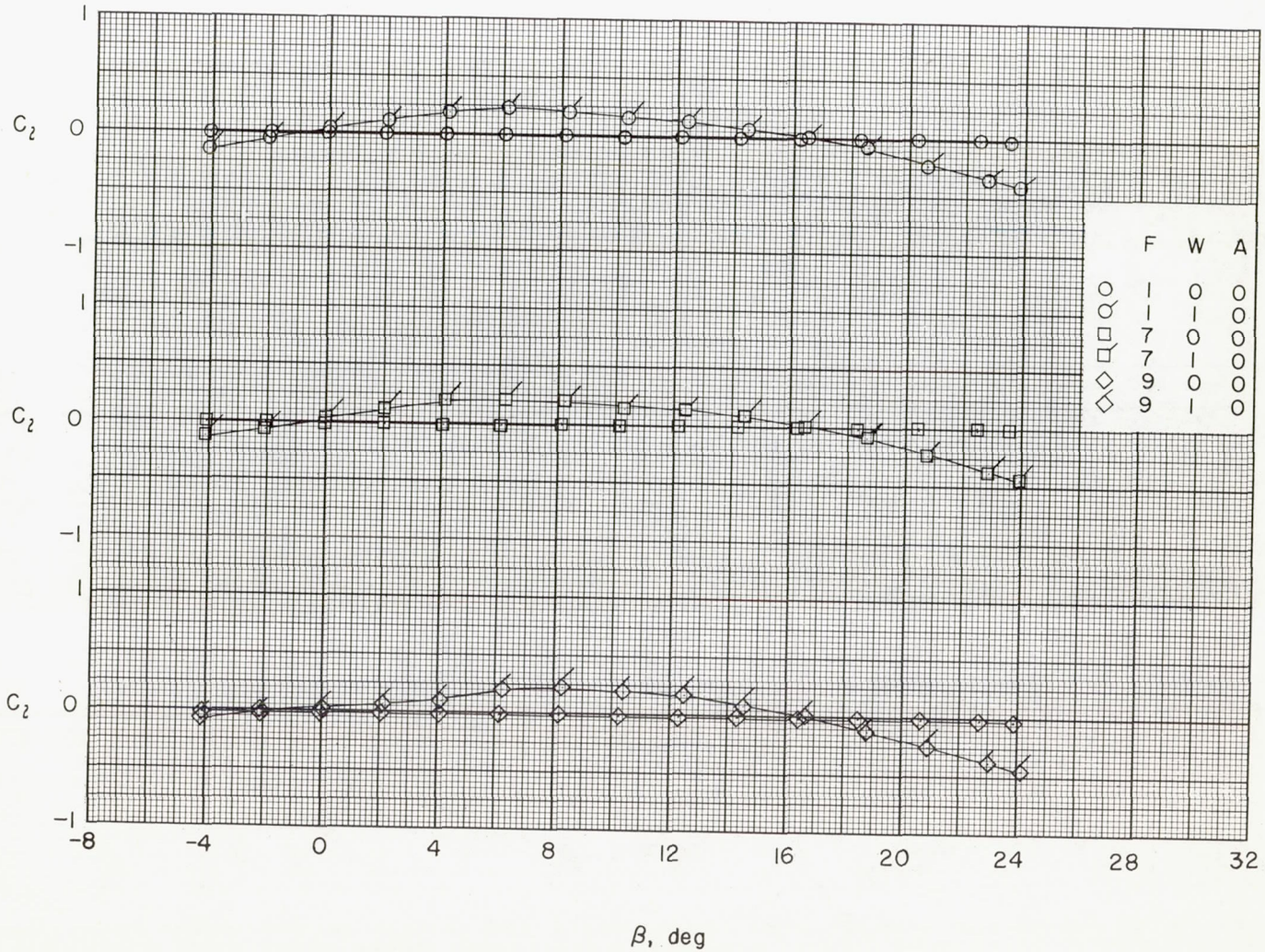
(d) Concluded.

Figure 25.- Continued.



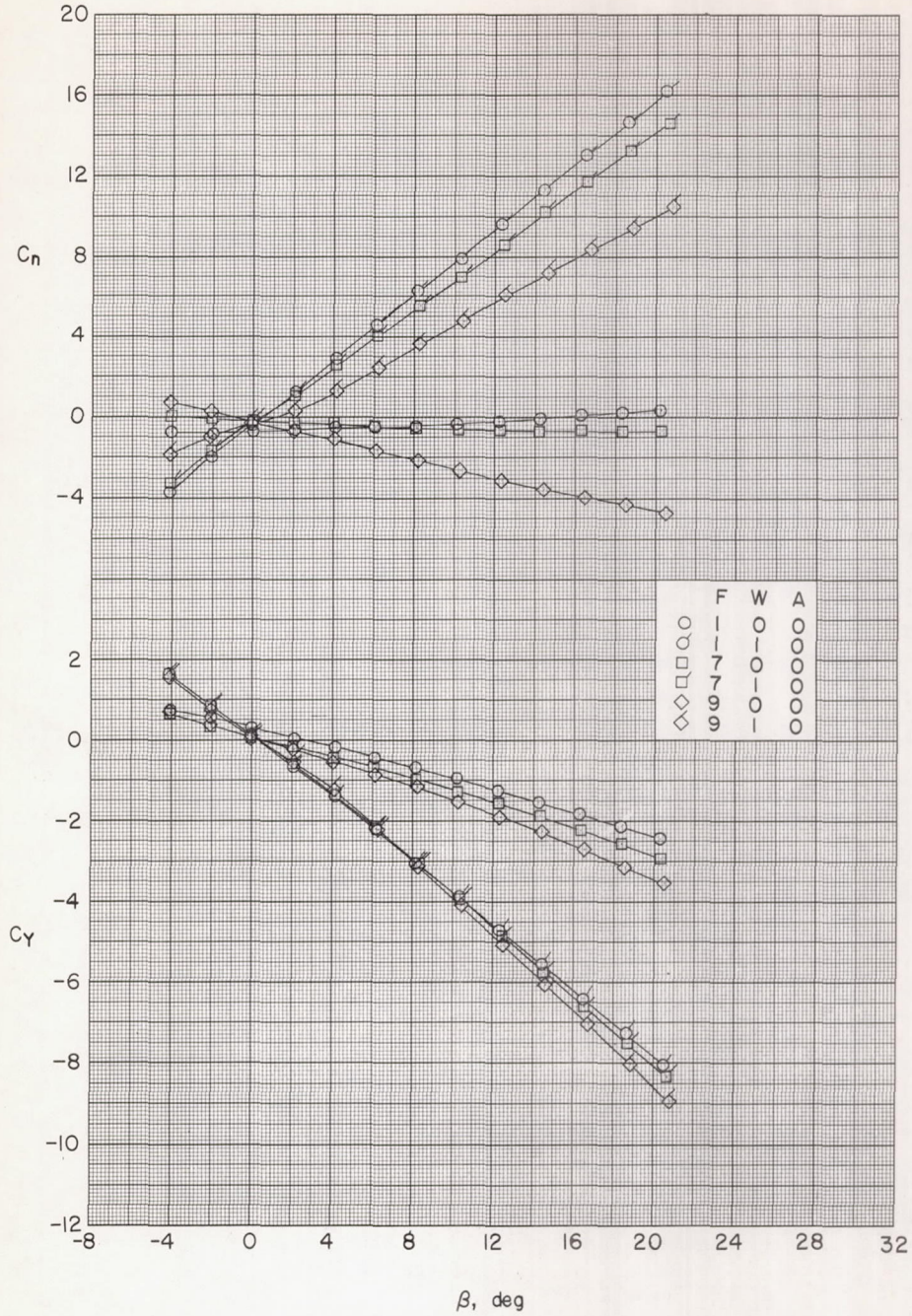
(e) $\alpha \approx 16.4^\circ$.

Figure 25.- Continued.



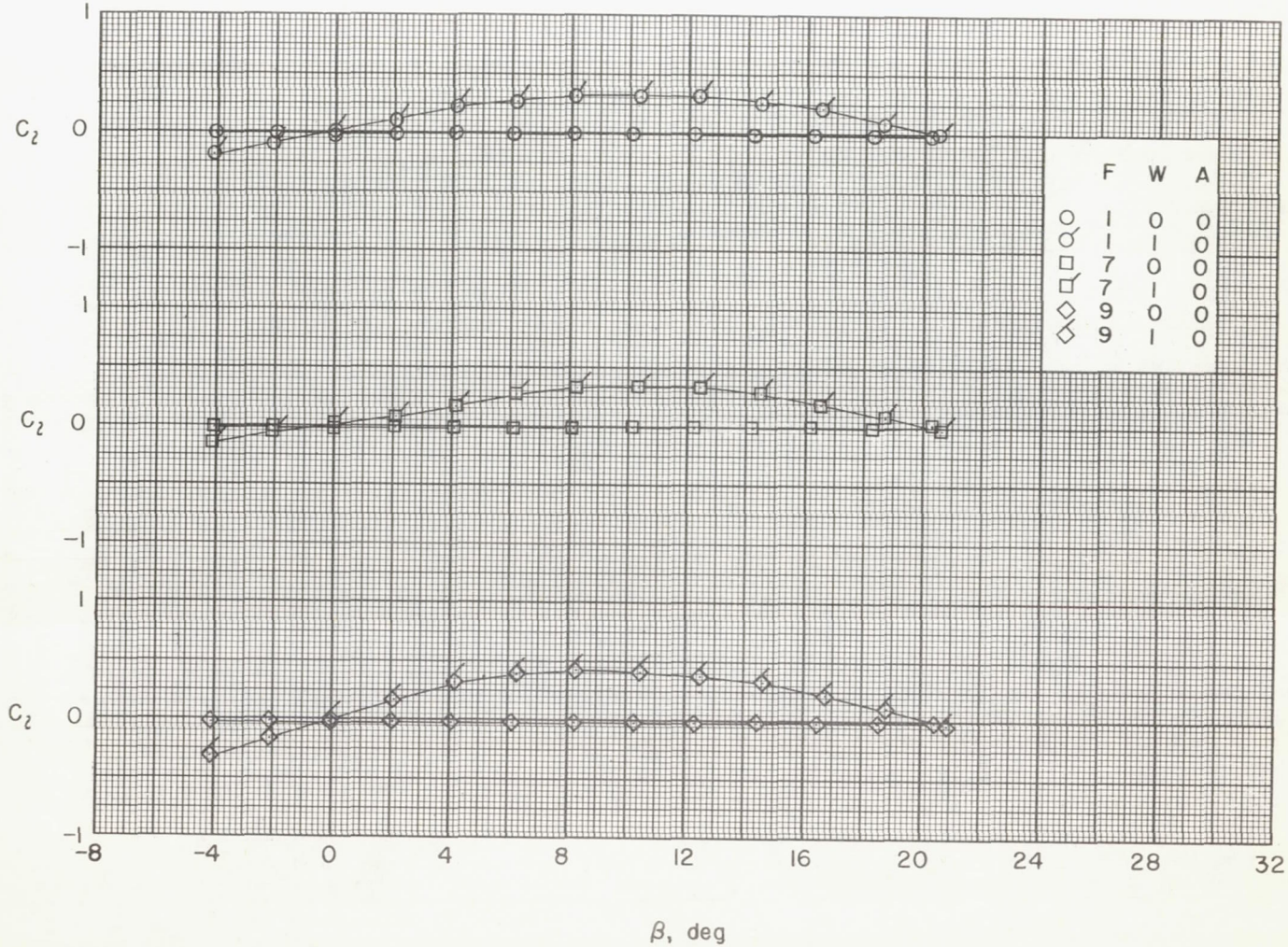
(e) Concluded.

Figure 25.- Continued.



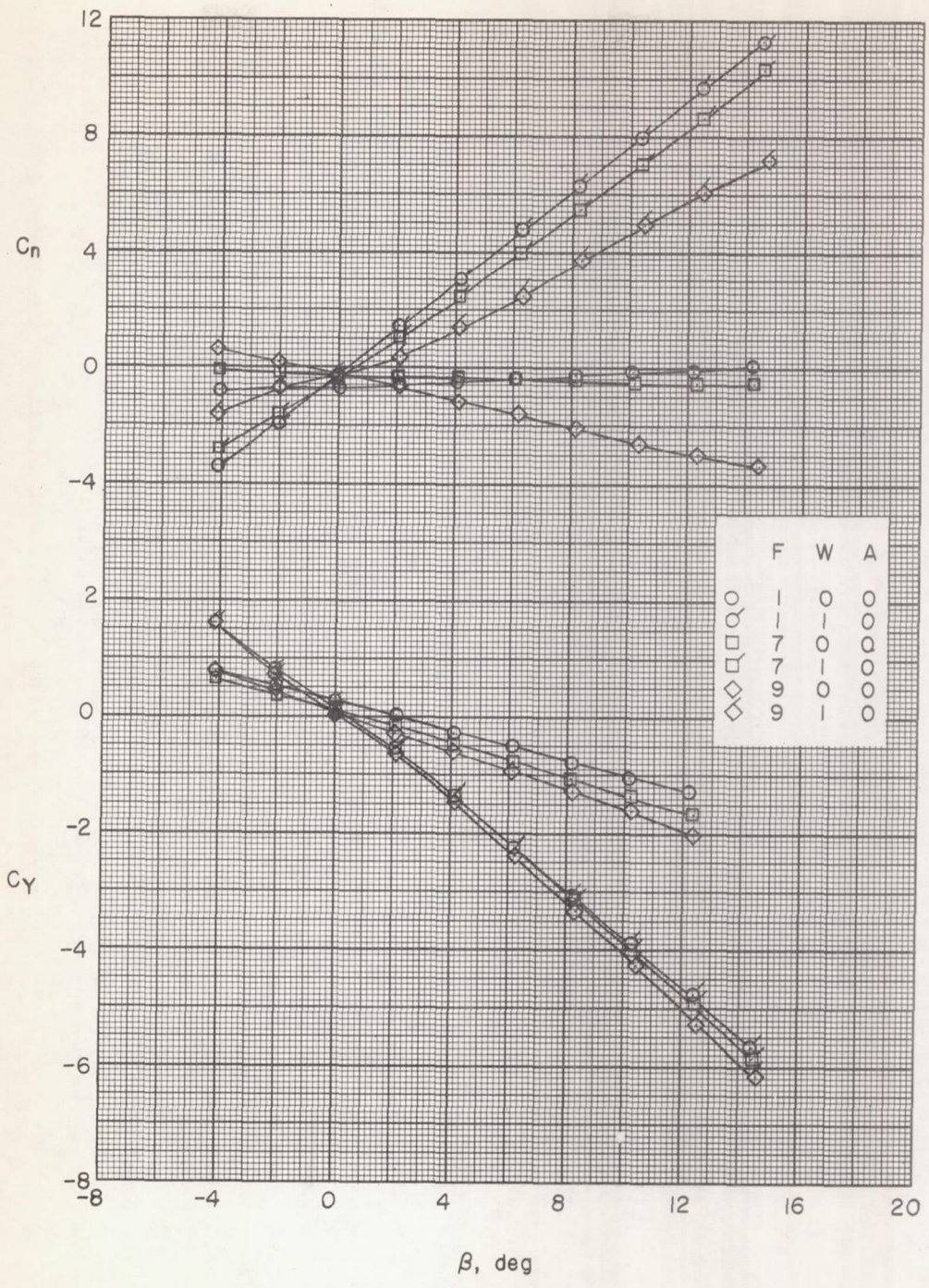
(f) $\alpha \approx 20.5^{\circ}$.

Figure 25.- Continued.



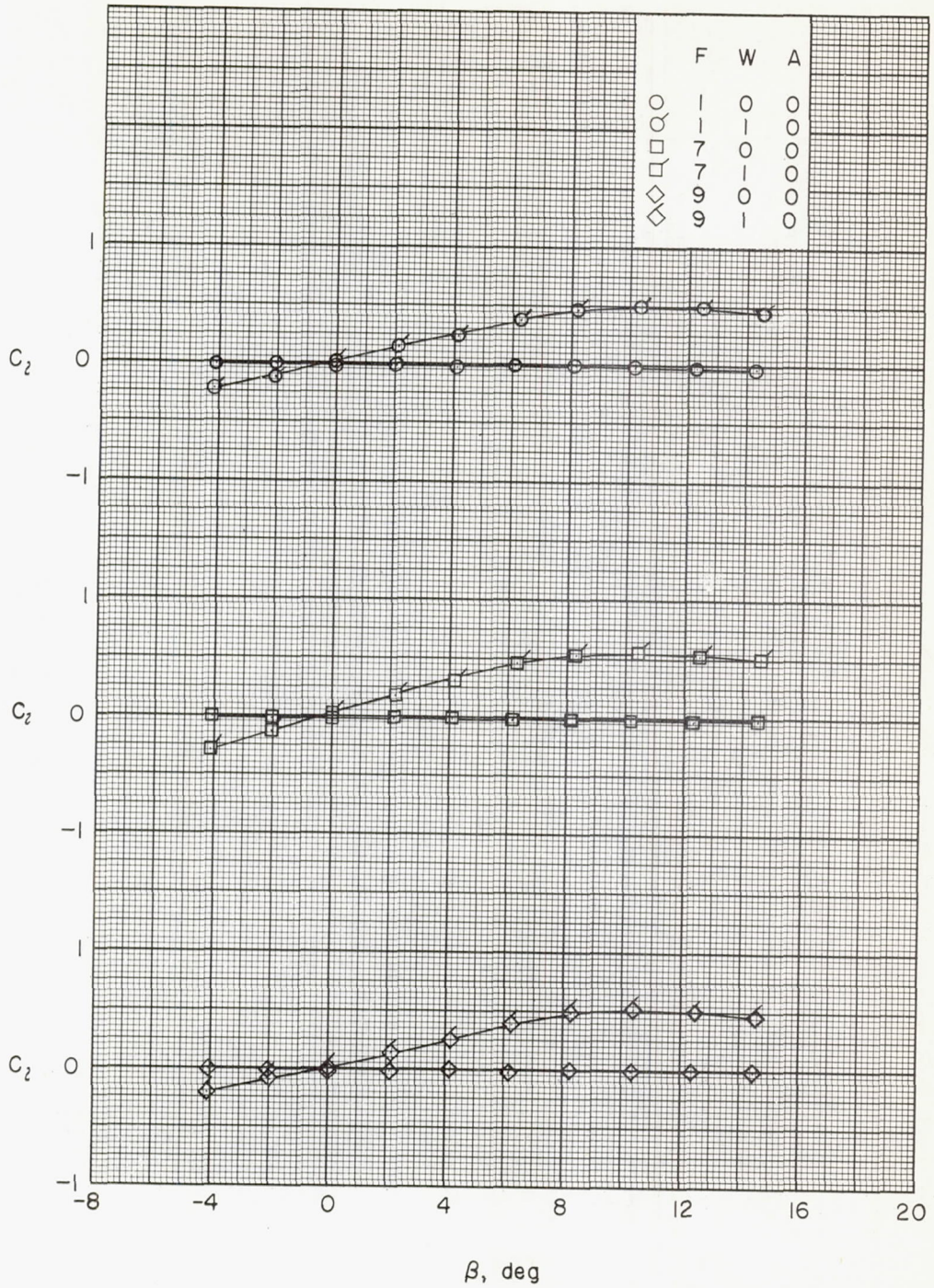
(f) Concluded.

Figure 25.- Continued.



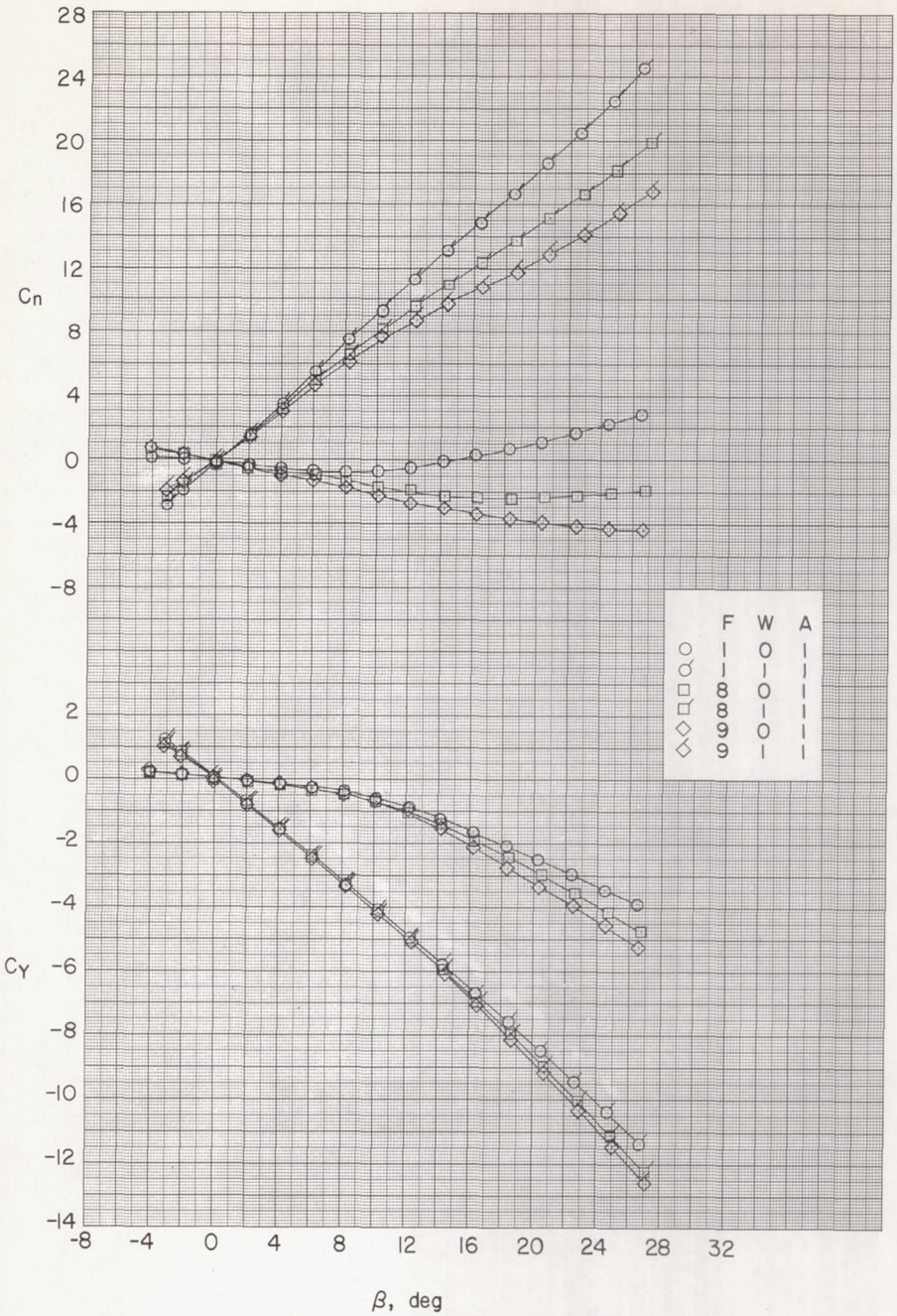
(g) $\alpha \approx 24.7^\circ$.

Figure 25.- Continued.



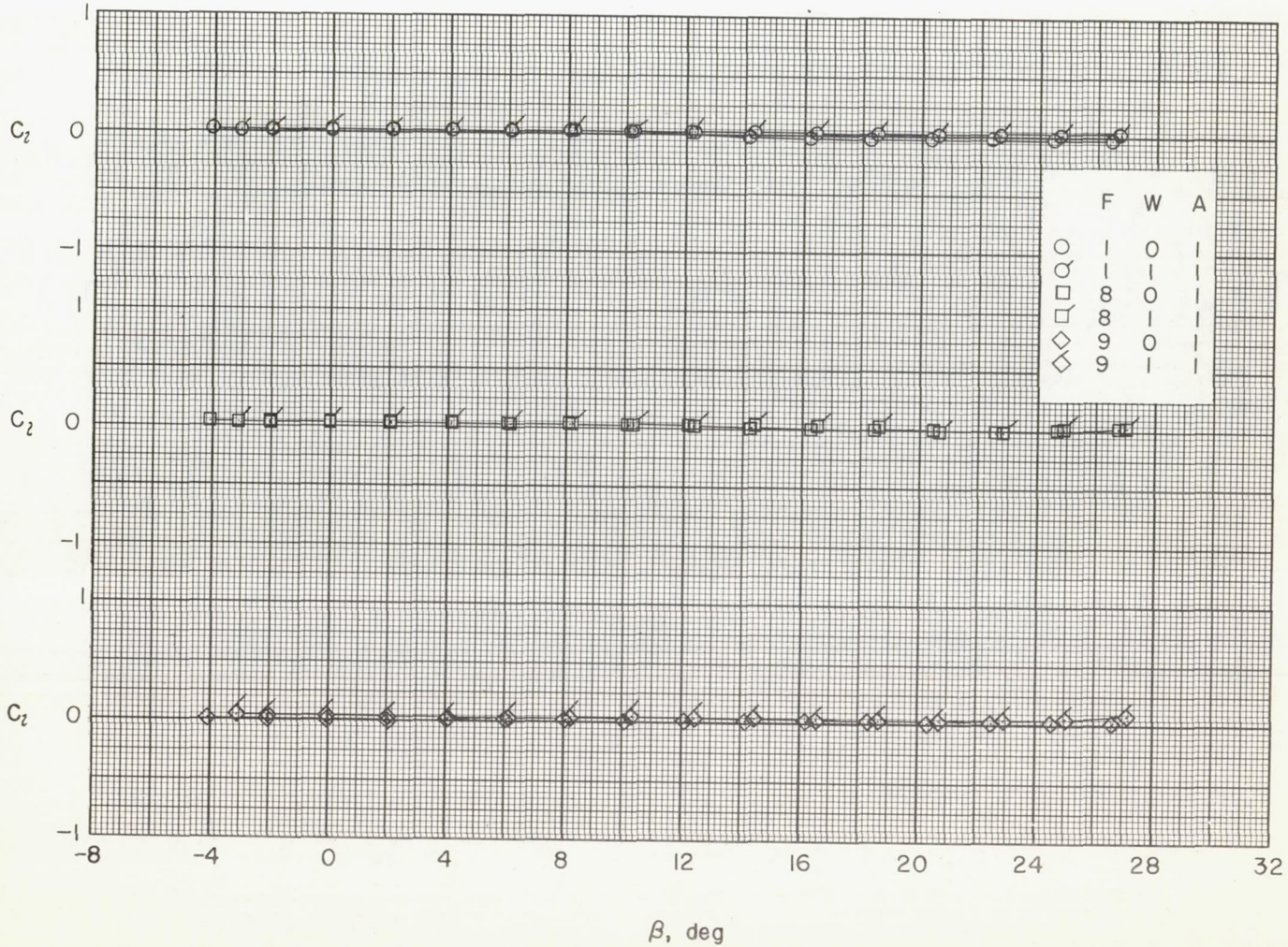
(g) Concluded.

Figure 25.- Concluded.



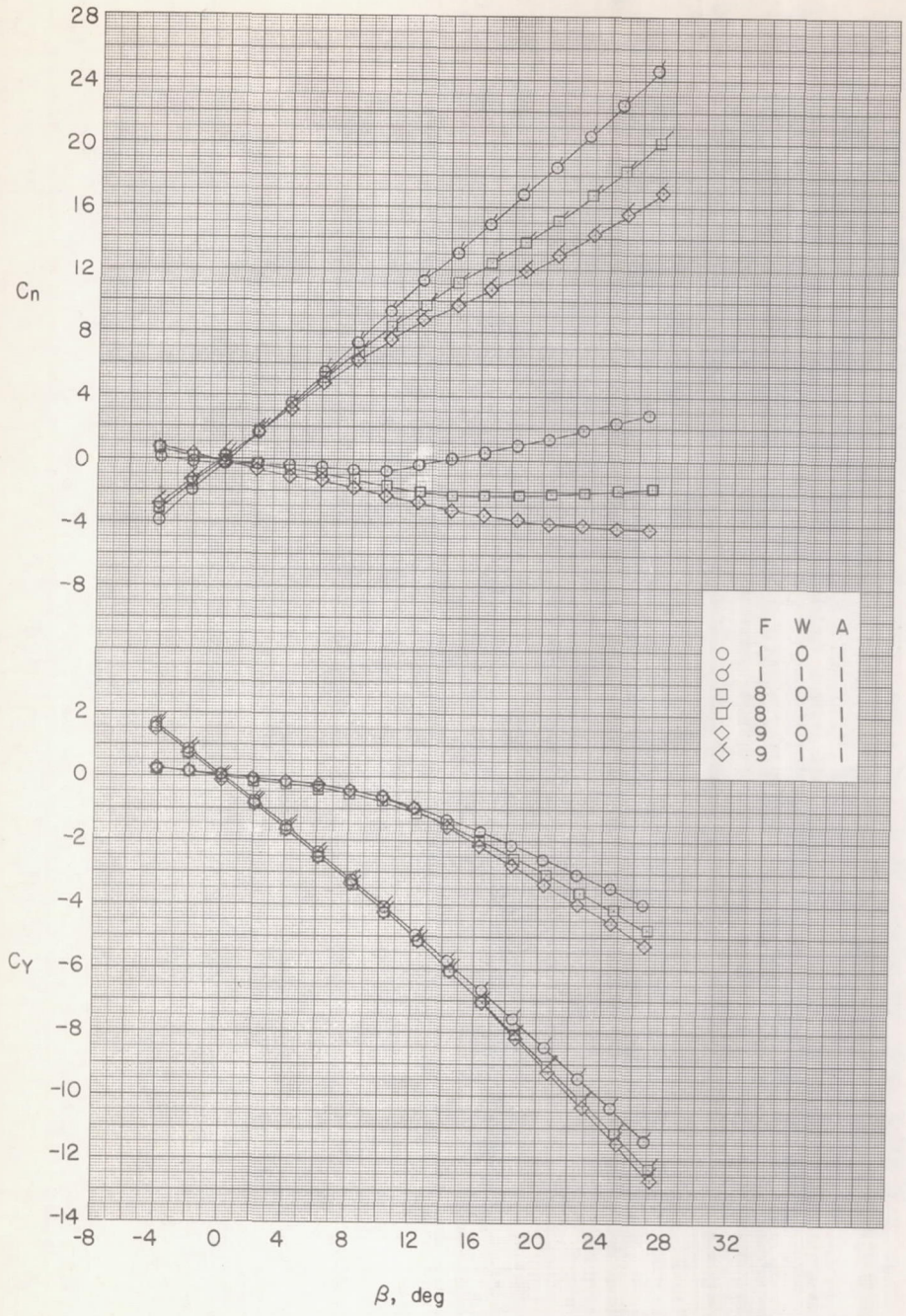
(a) $\alpha \approx 0^{\circ}$.

Figure 26.- Effect of forebody length on aerodynamic characteristics in sideslip. Large delta wings; 1-caliber cylindrical afterbody.



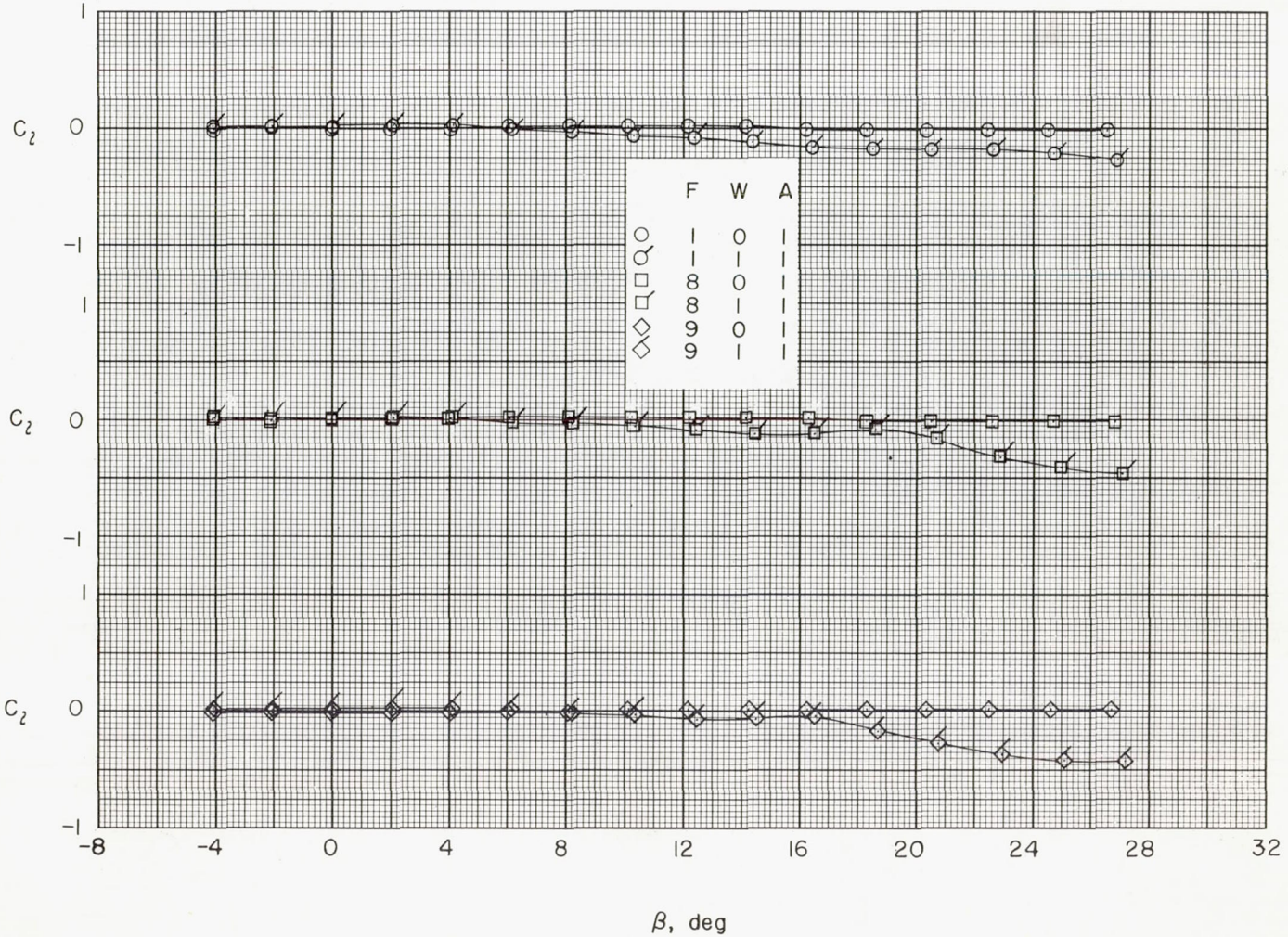
(a) Concluded.

Figure 26.- Continued.



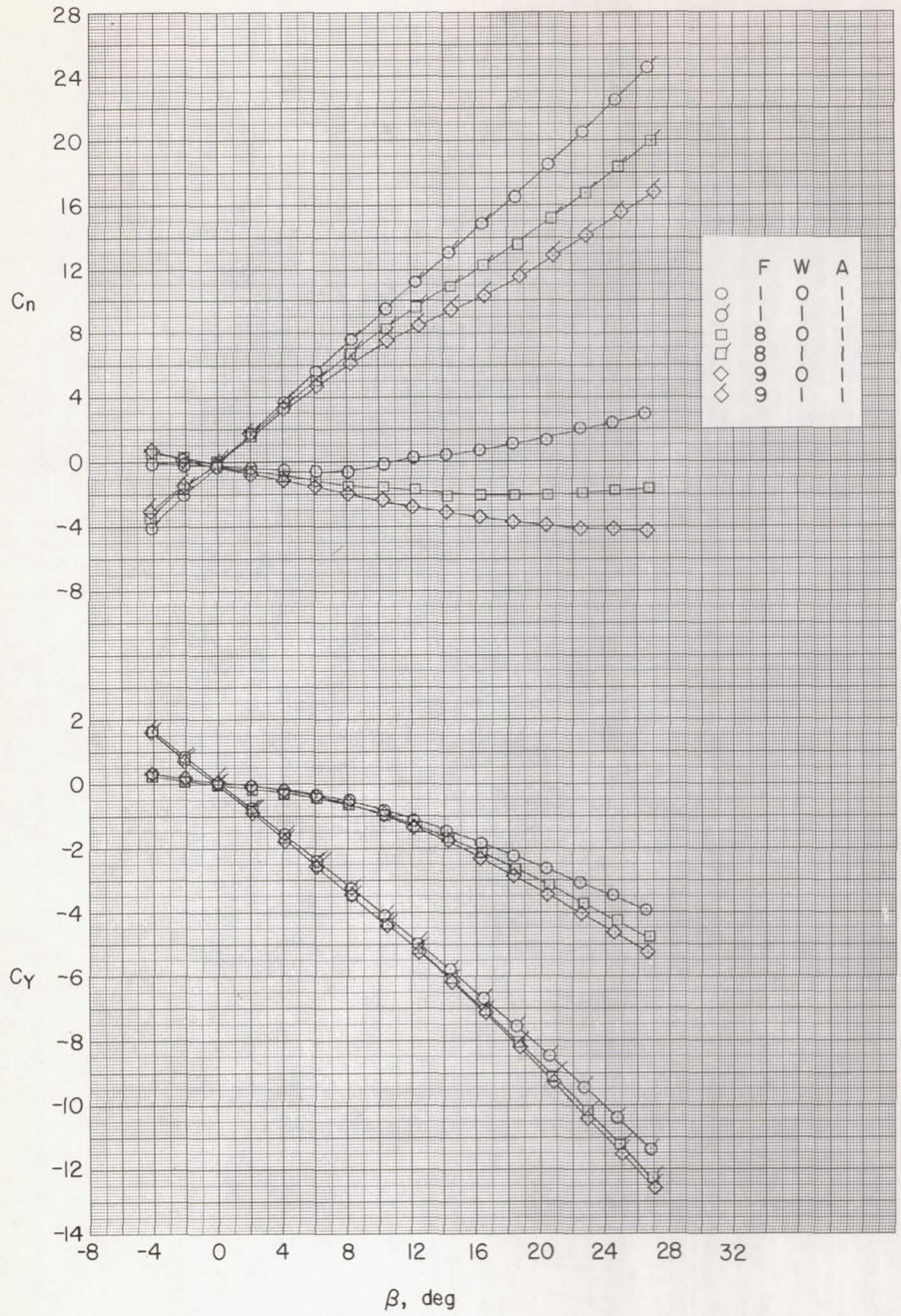
(b) $\alpha \approx 4.1^{\circ}$.

Figure 26.- Continued.



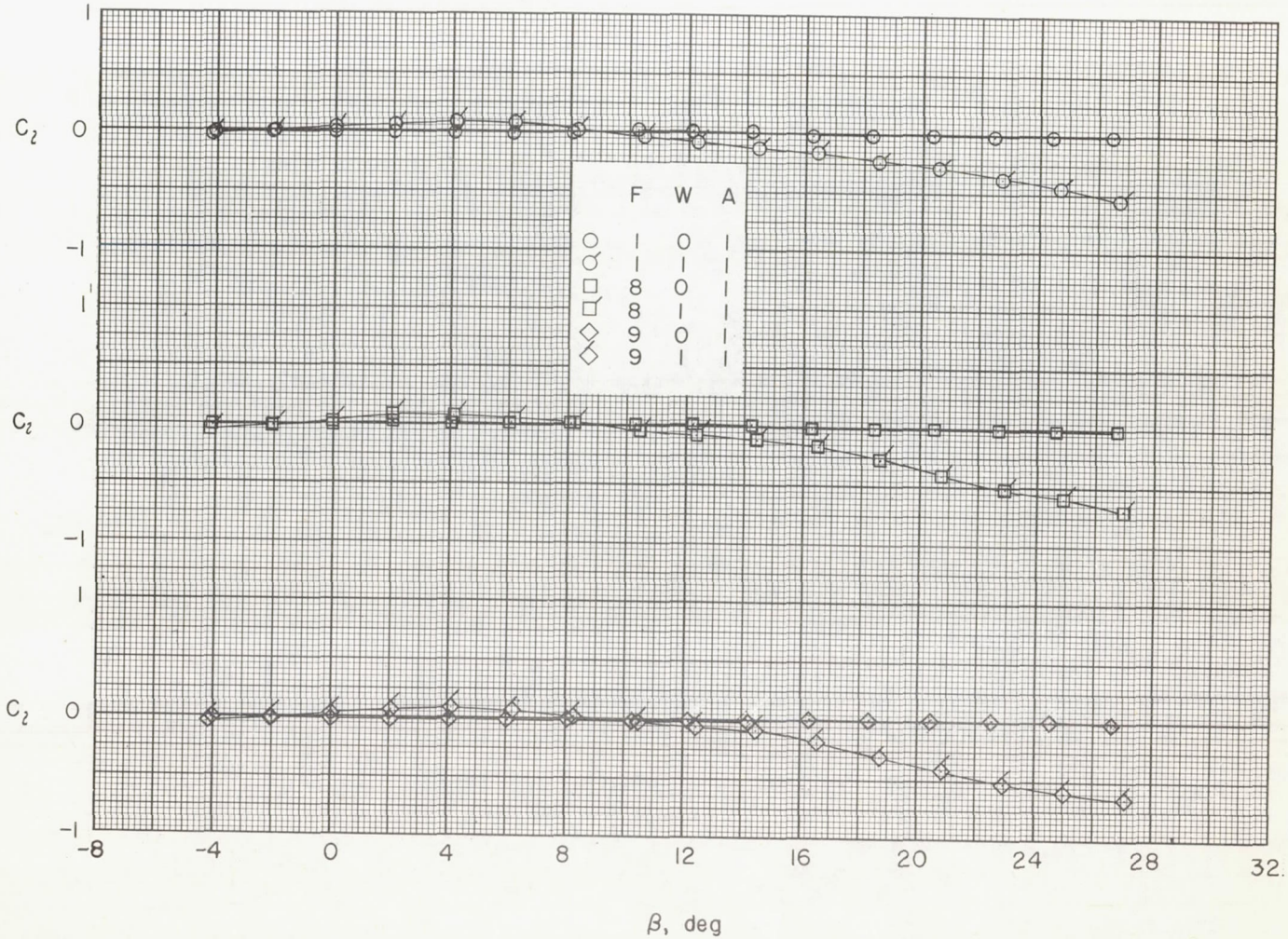
(b) Concluded.

Figure 26.- Continued.



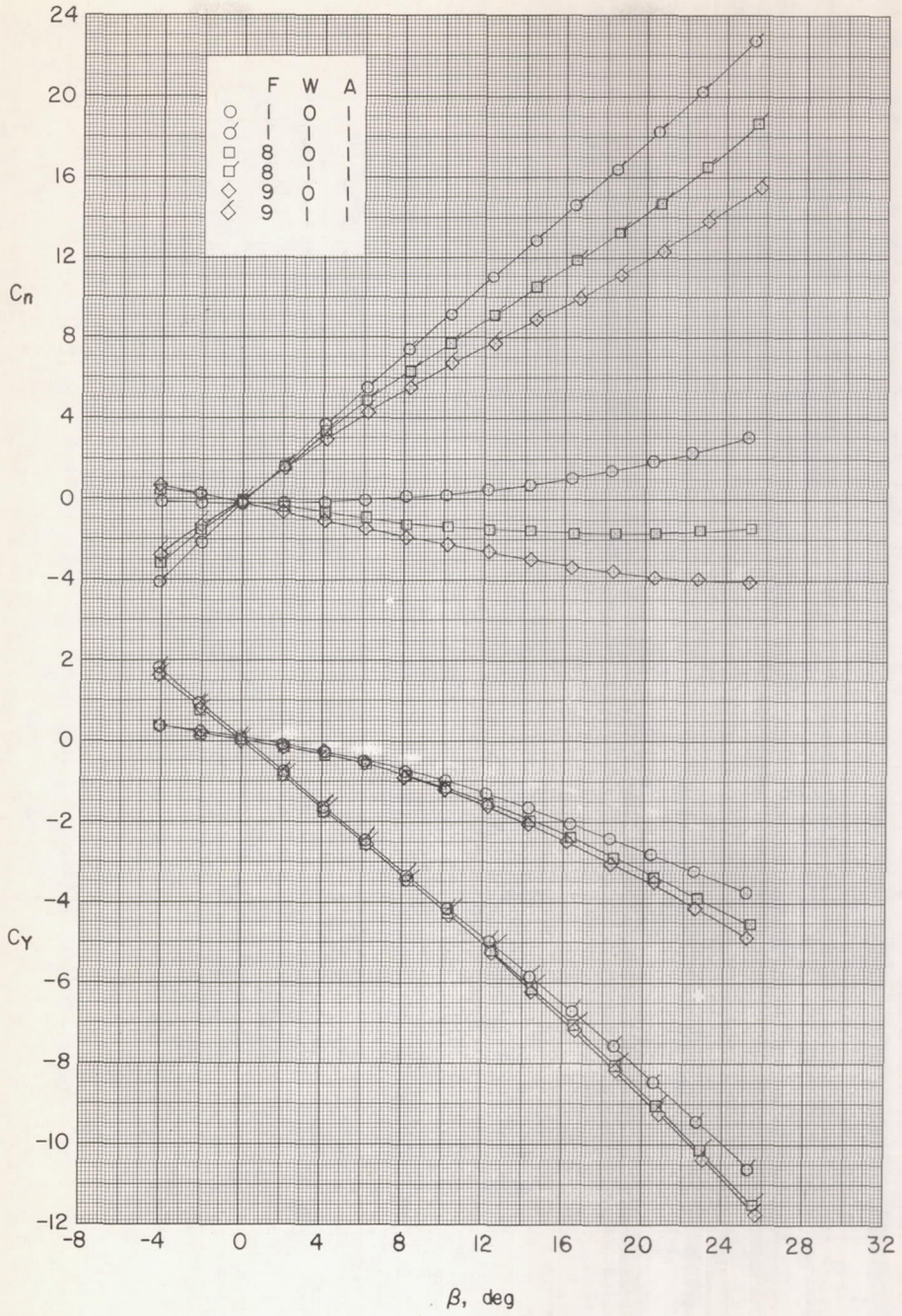
(c) $\alpha \approx 8.2^{\circ}$.

Figure 26.- Continued.



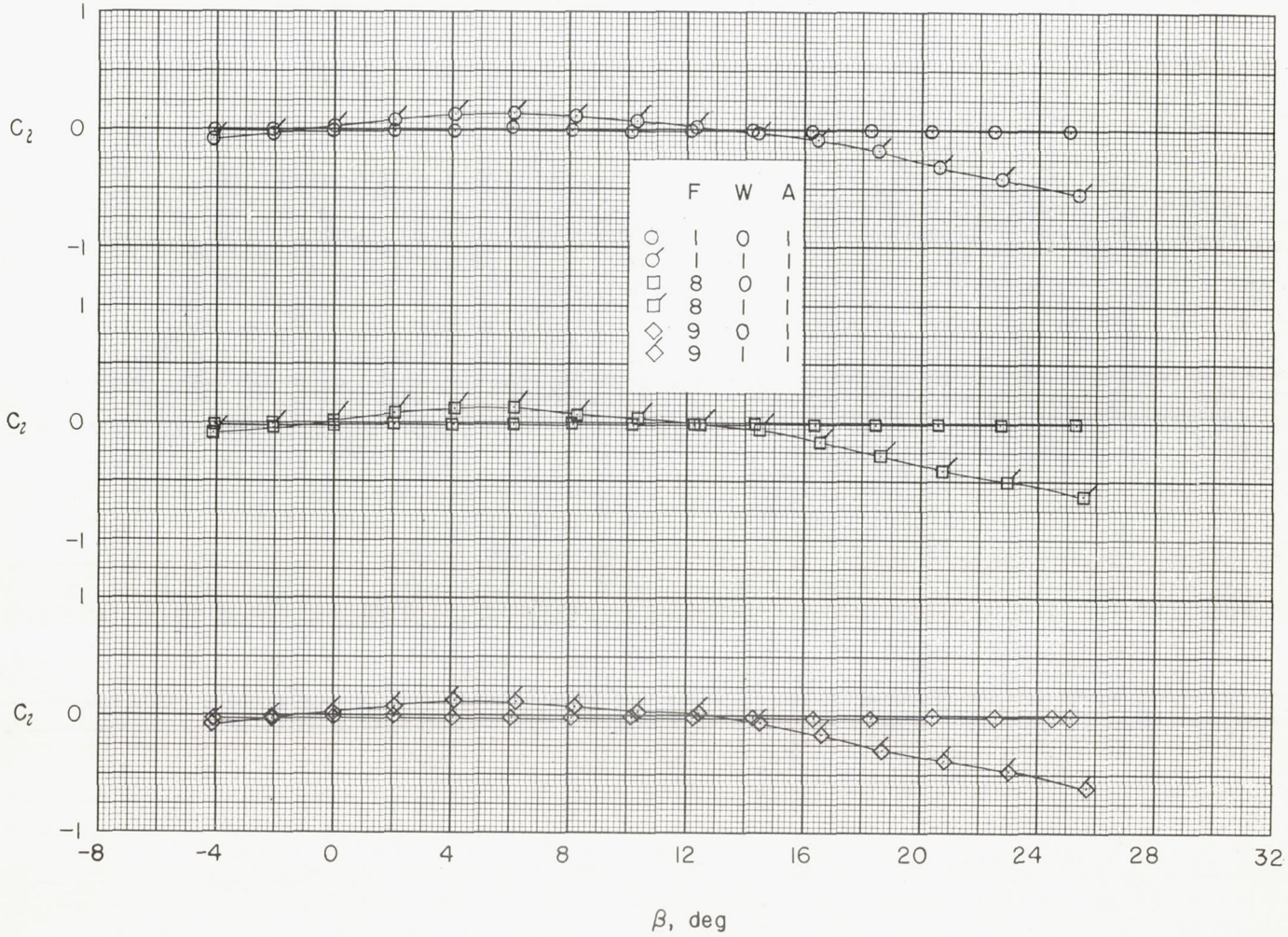
(c) Concluded.

Figure 26.- Continued.



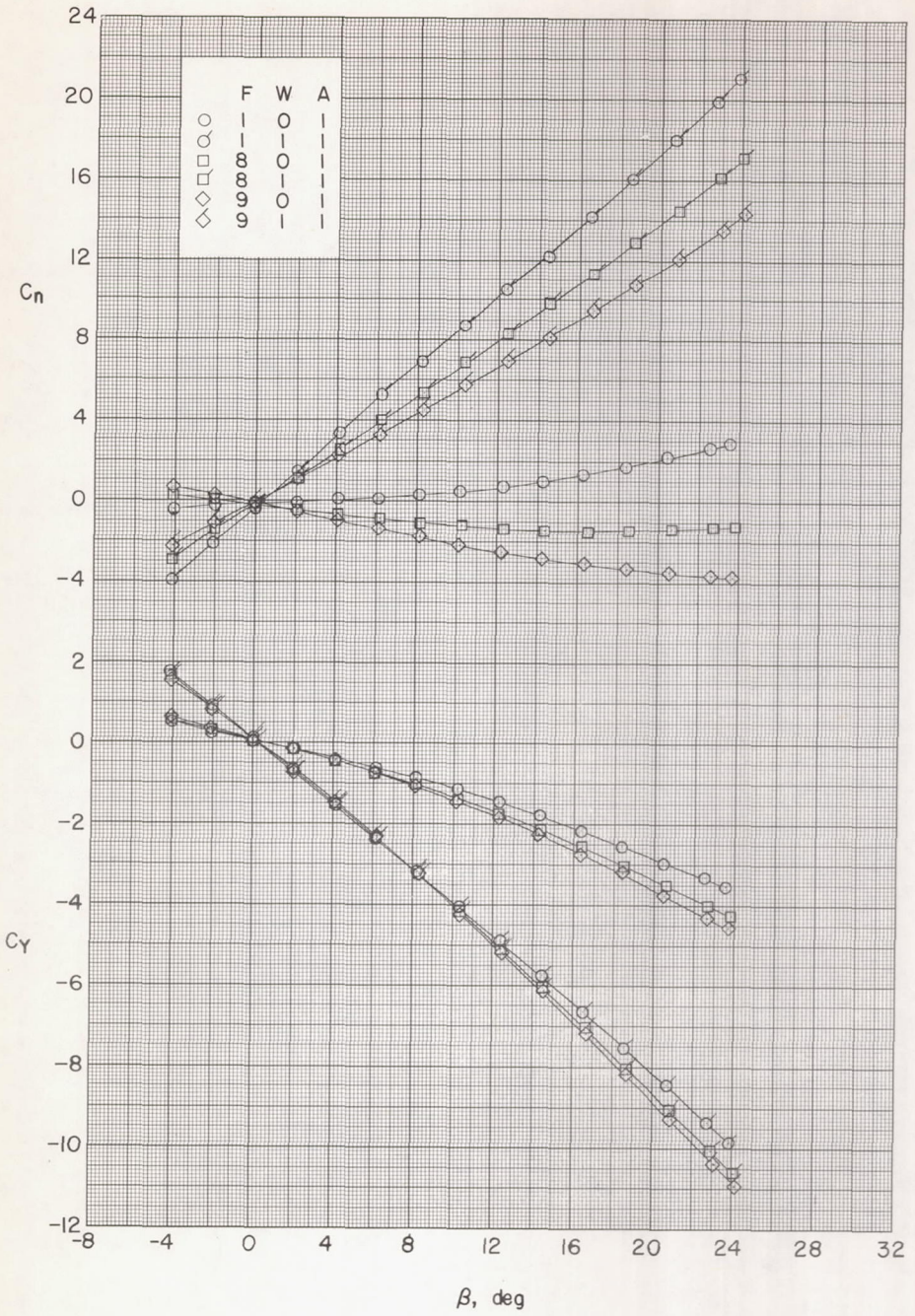
(d) $\alpha \approx 12.3^{\circ}$.

Figure 26.- Continued.



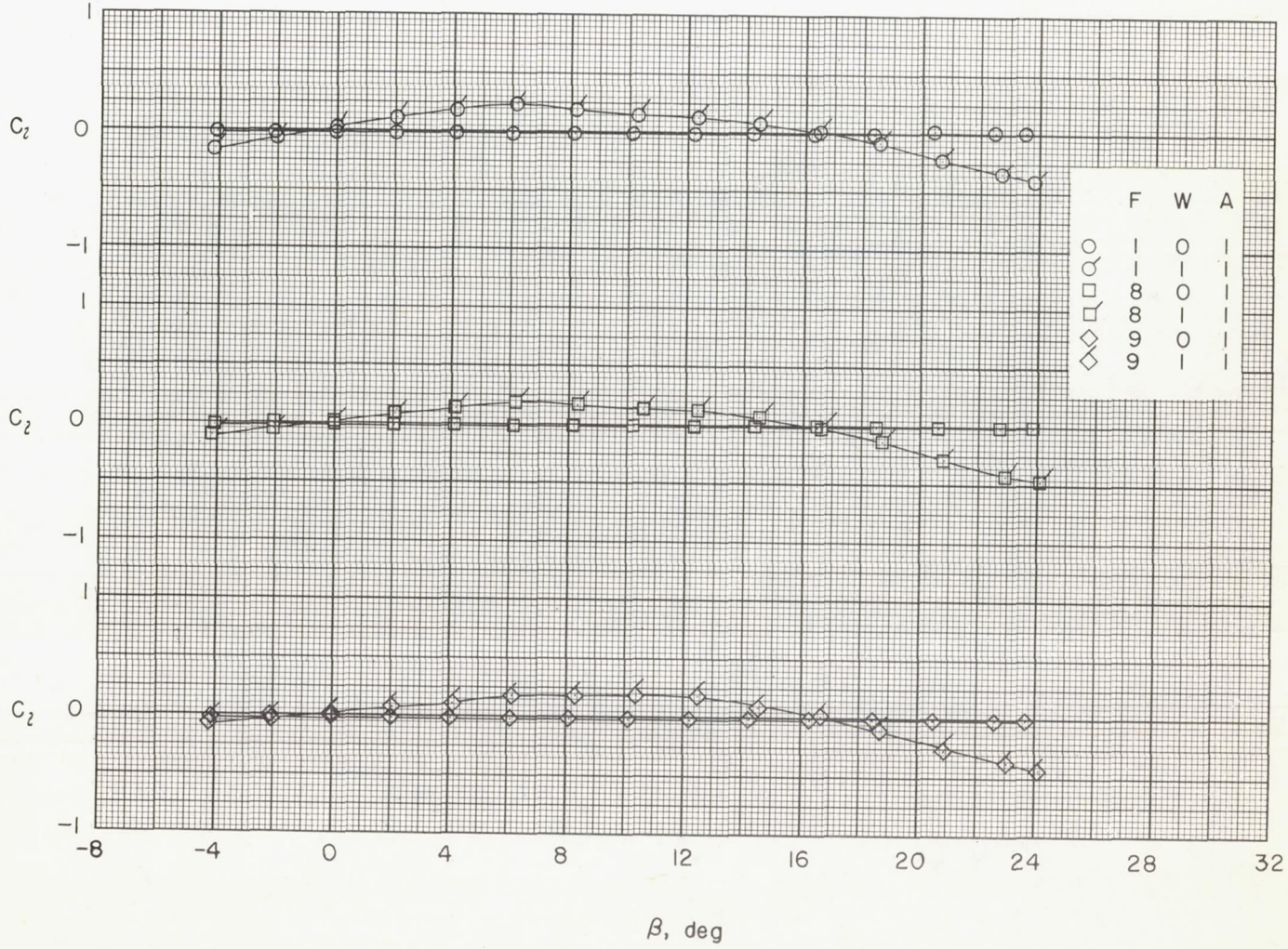
(d) Concluded.

Figure 26.- Continued.



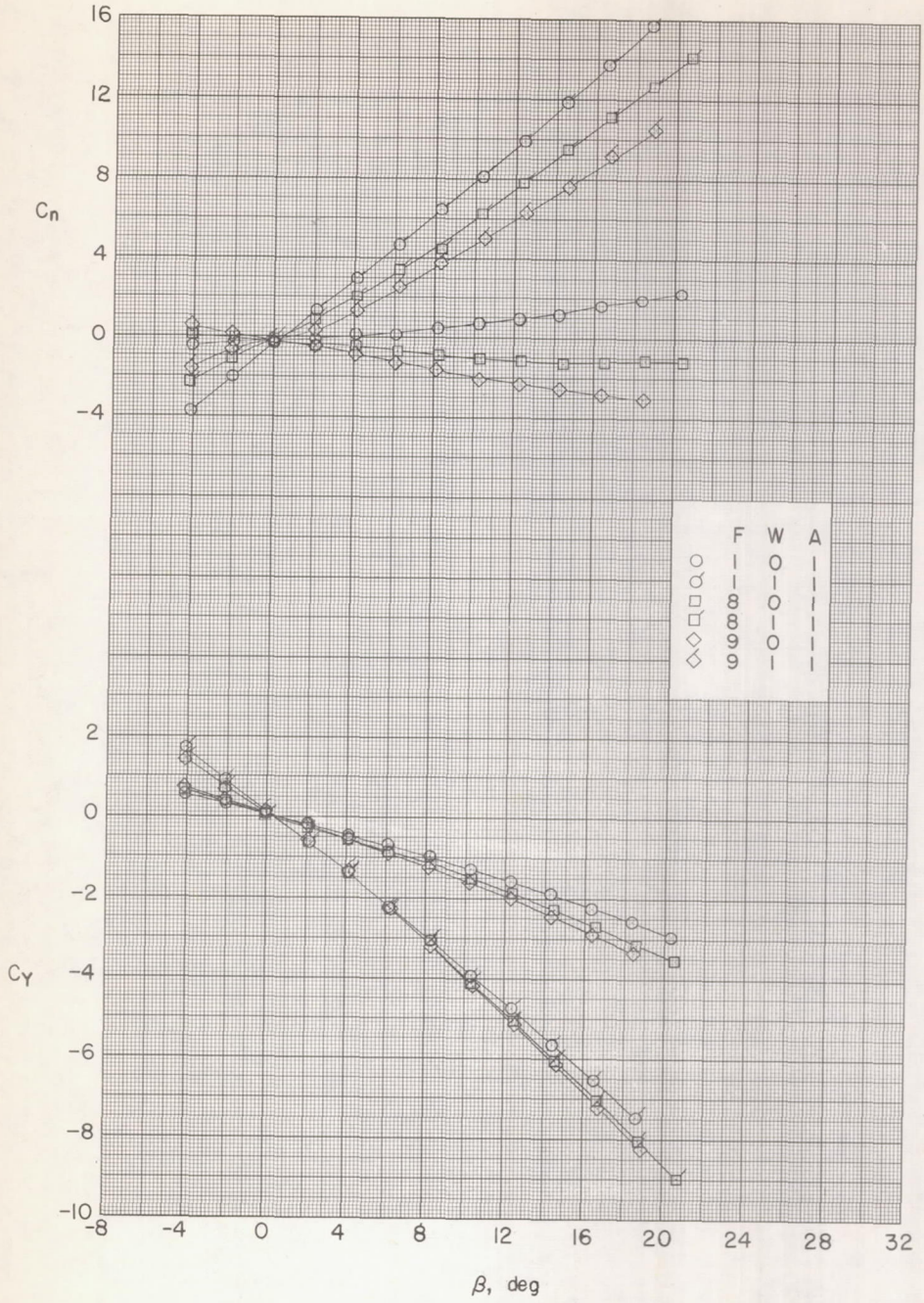
(e) $\alpha \approx 16.4^{\circ}$.

Figure 26.- Continued.



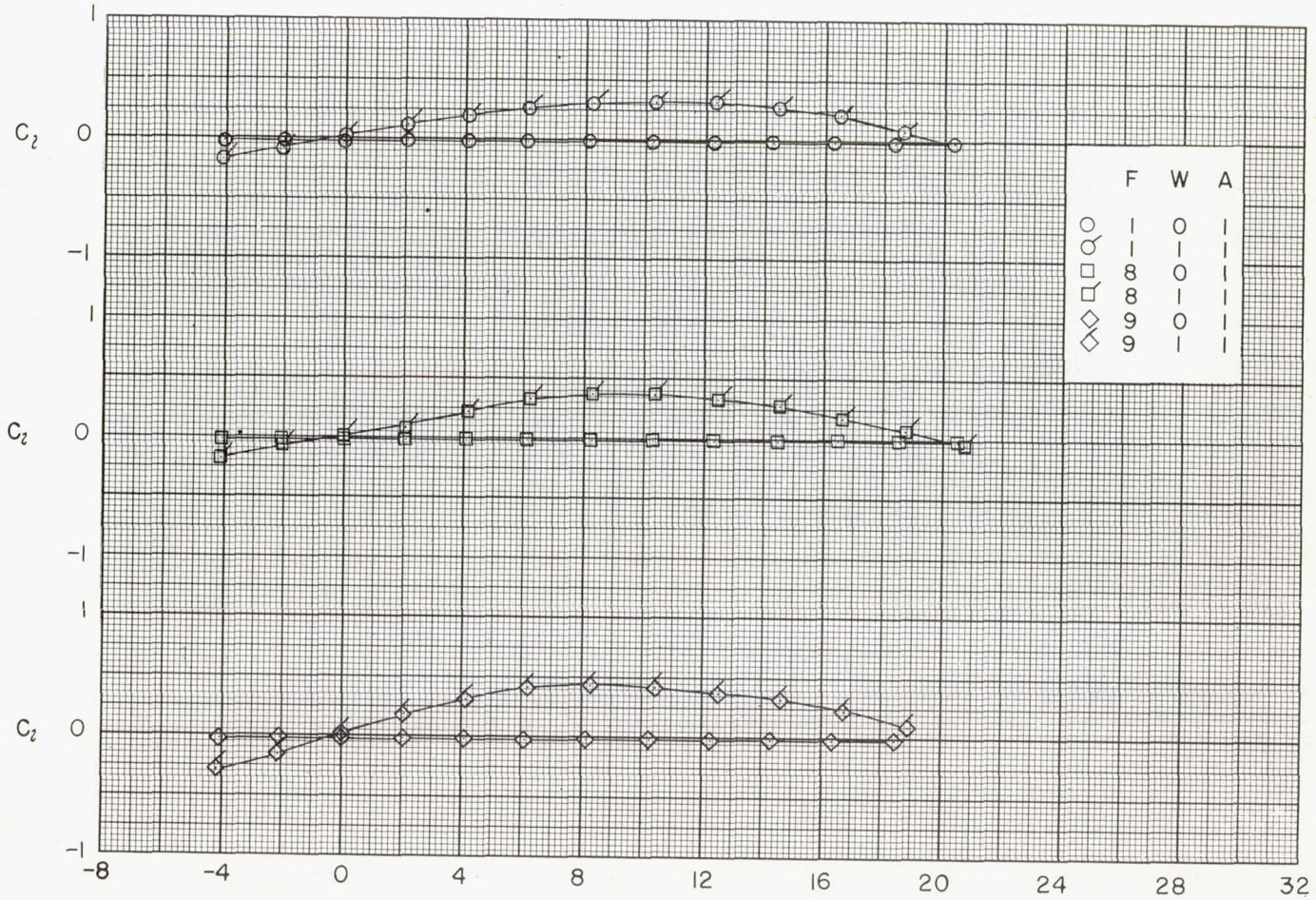
(e) Concluded.

Figure 26.- Continued.



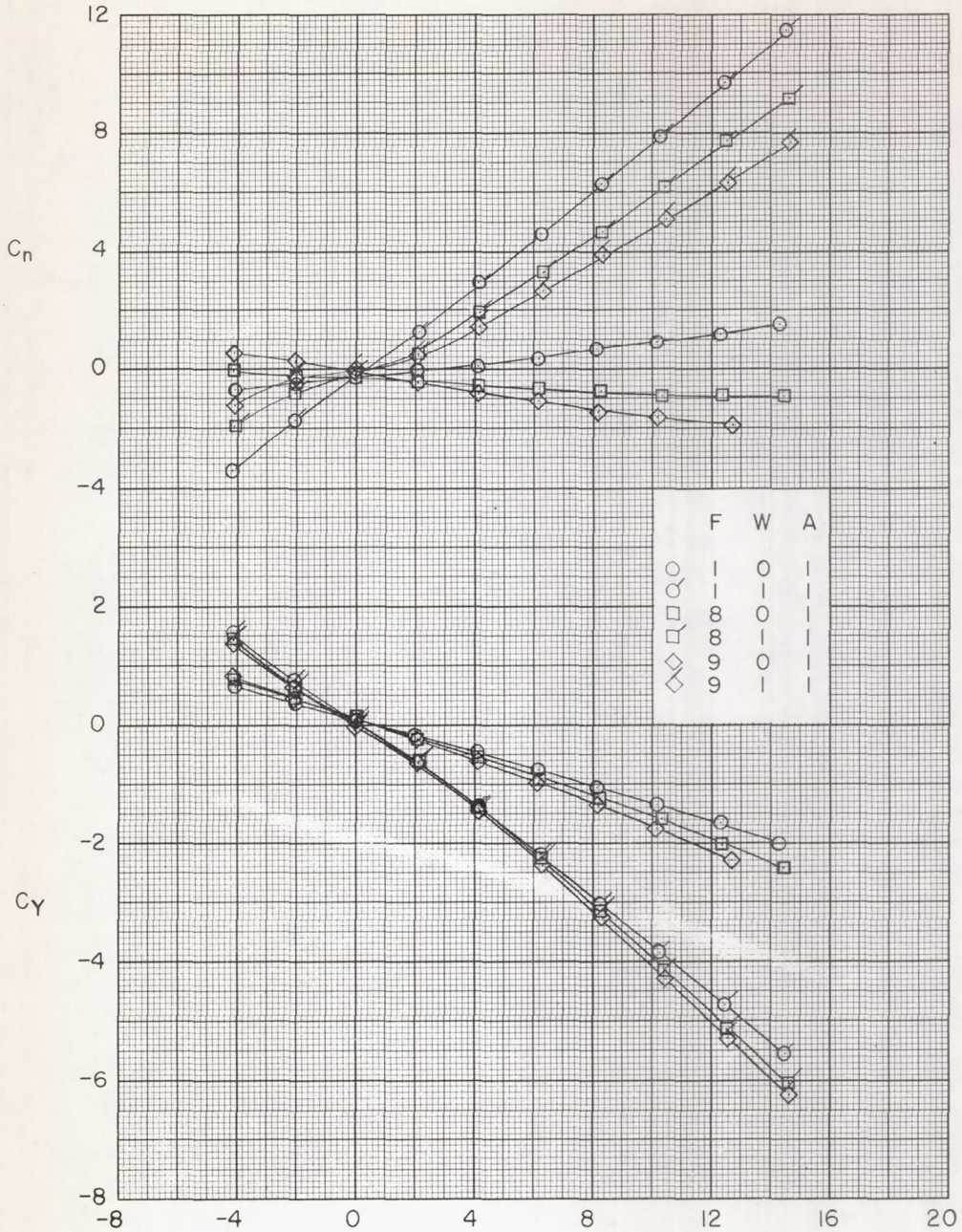
(f) $\alpha \approx 20.5^{\circ}$.

Figure 26.- Continued.



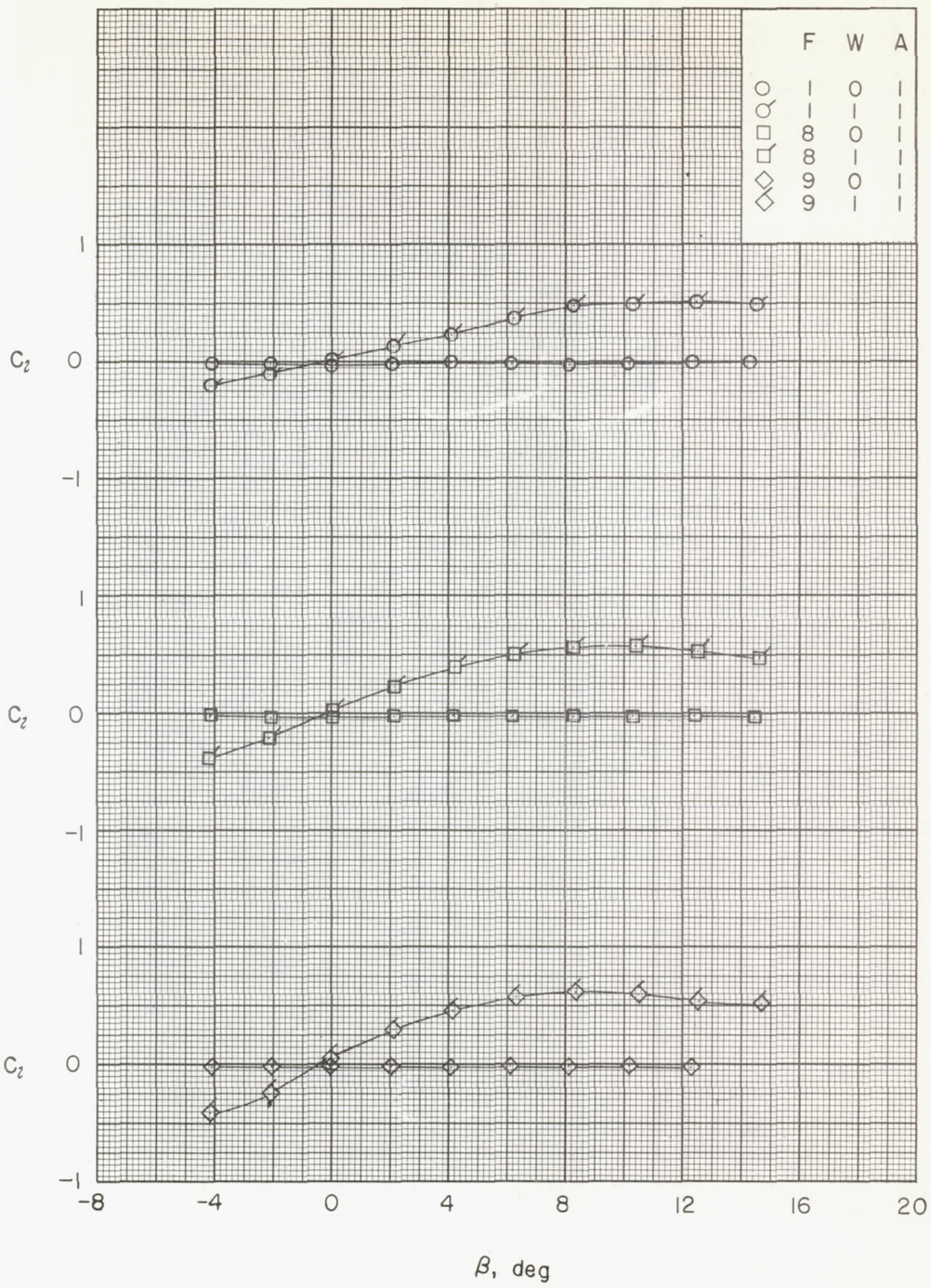
(f) Concluded.

Figure 26.- Continued.



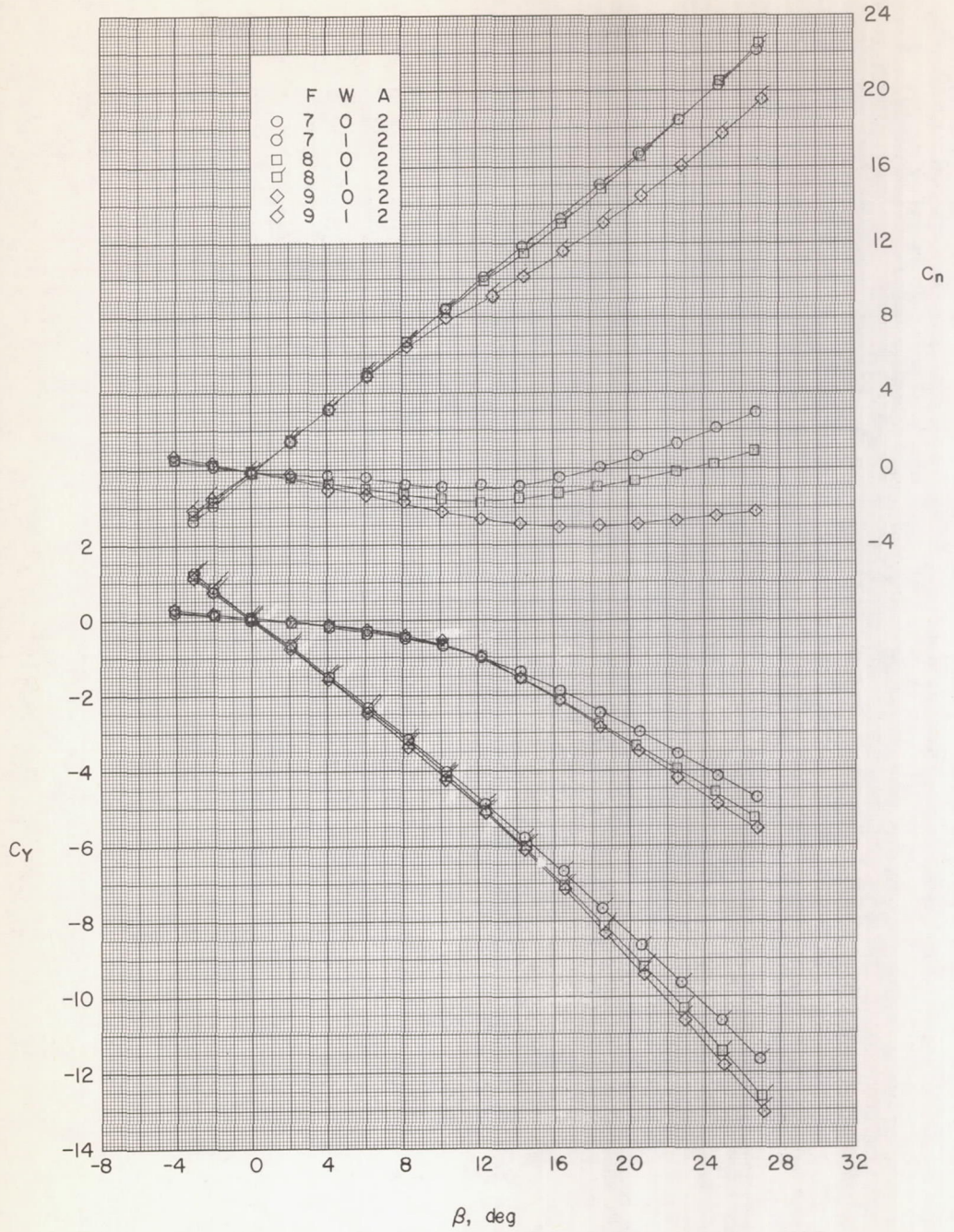
(g) $\alpha \approx 24.7^\circ$.

Figure 26.- Continued.



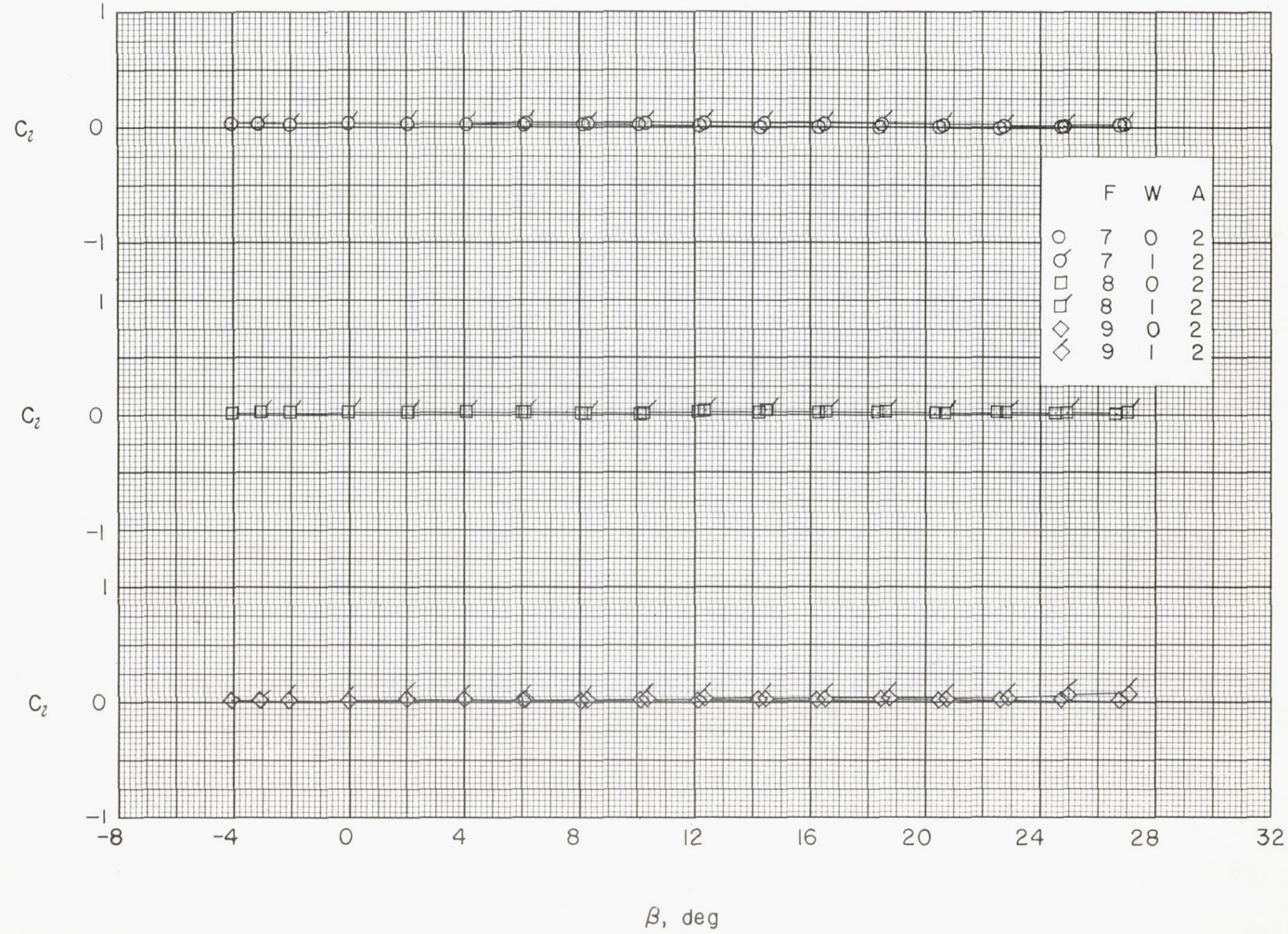
(g) Concluded.

Figure 26.- Concluded.



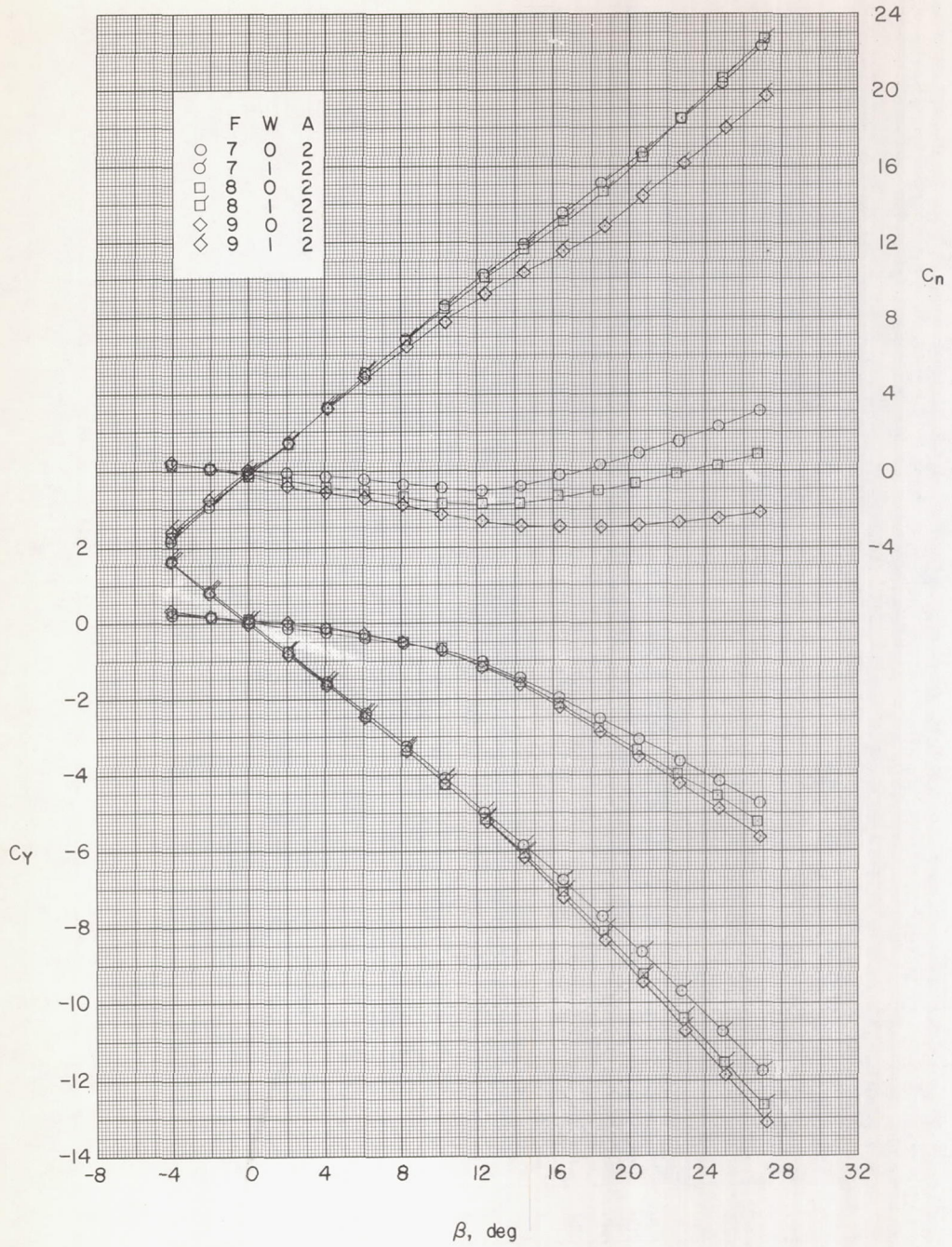
(a) $\alpha \approx 0^{\circ}$.

Figure 27.- Effects of forebody length on aerodynamic characteristics in sideslip. Large delta wings; 2-caliber cylindrical afterbody.



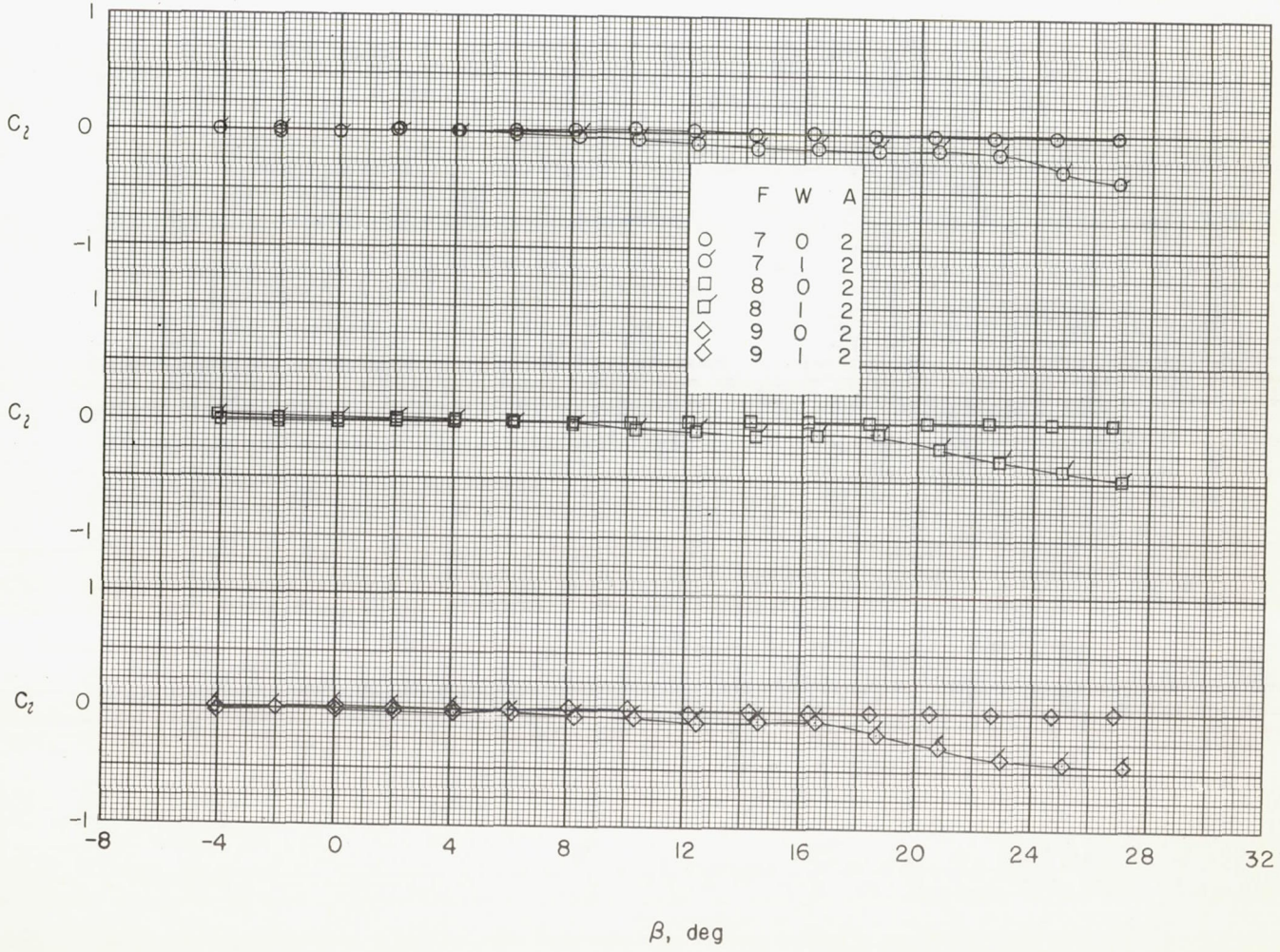
(a) Concluded.

Figure 27.- Continued.



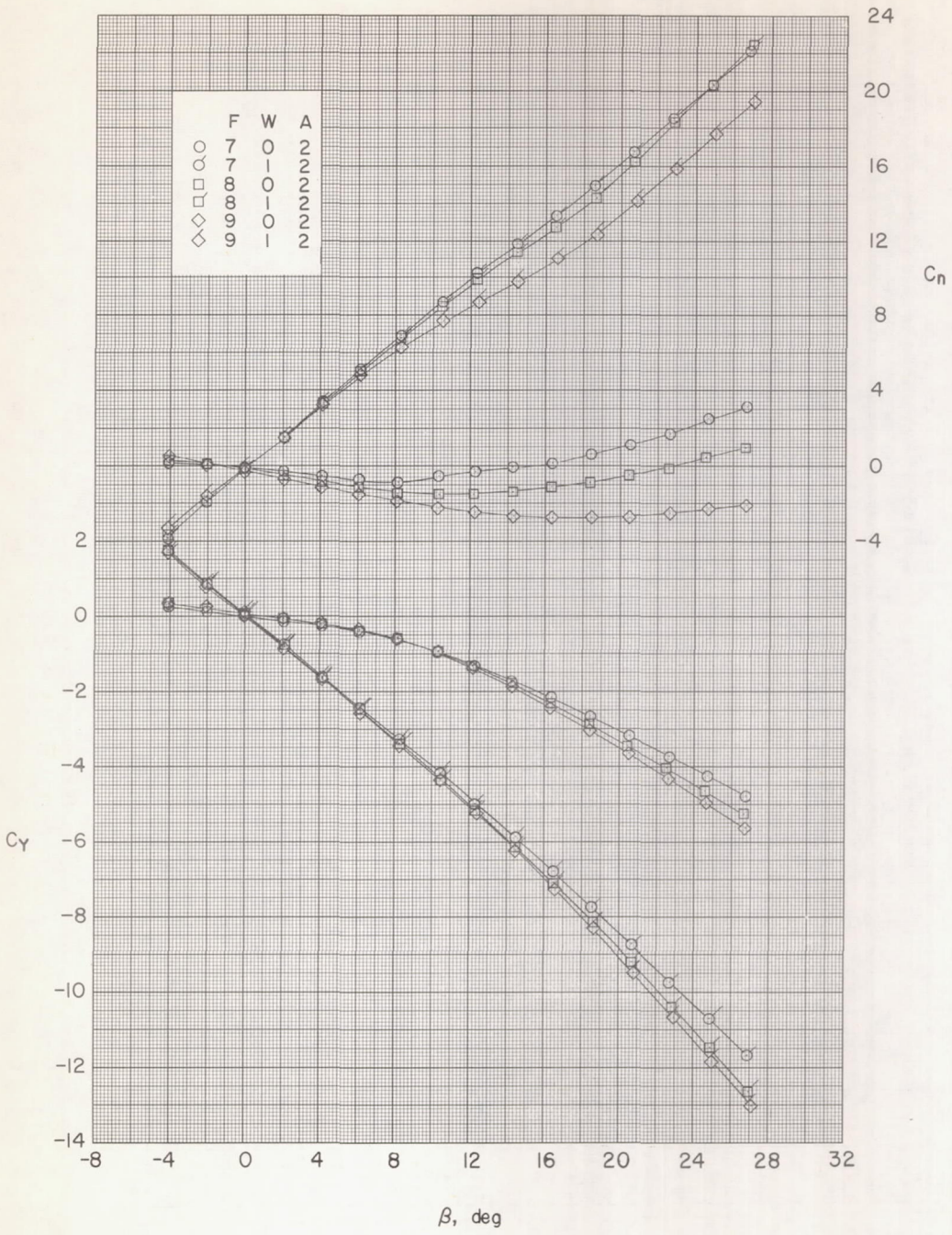
(b) $\alpha \approx 4.1^{\circ}$.

Figure 27.- Continued.



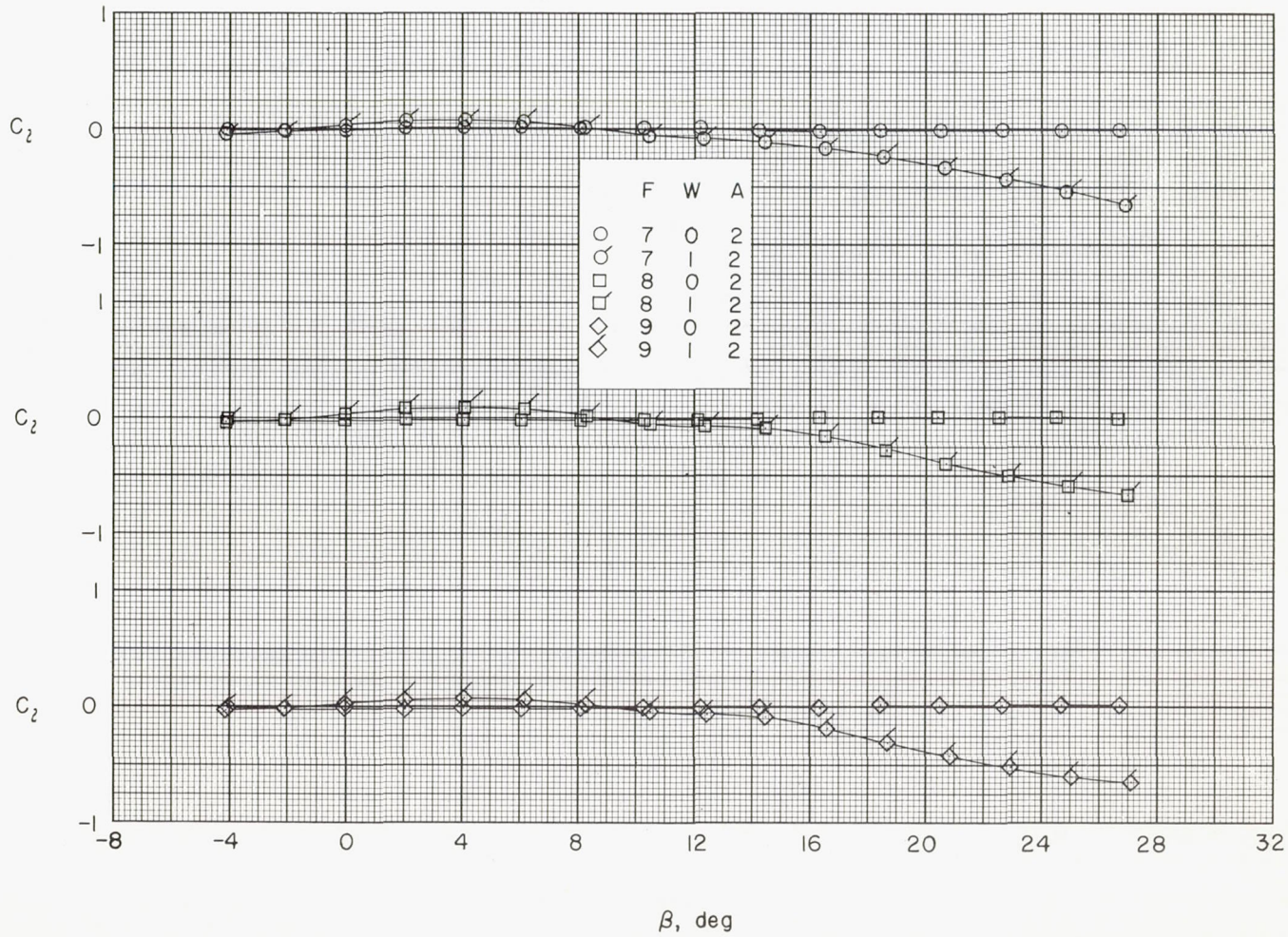
(b) Concluded.

Figure 27.- Continued.



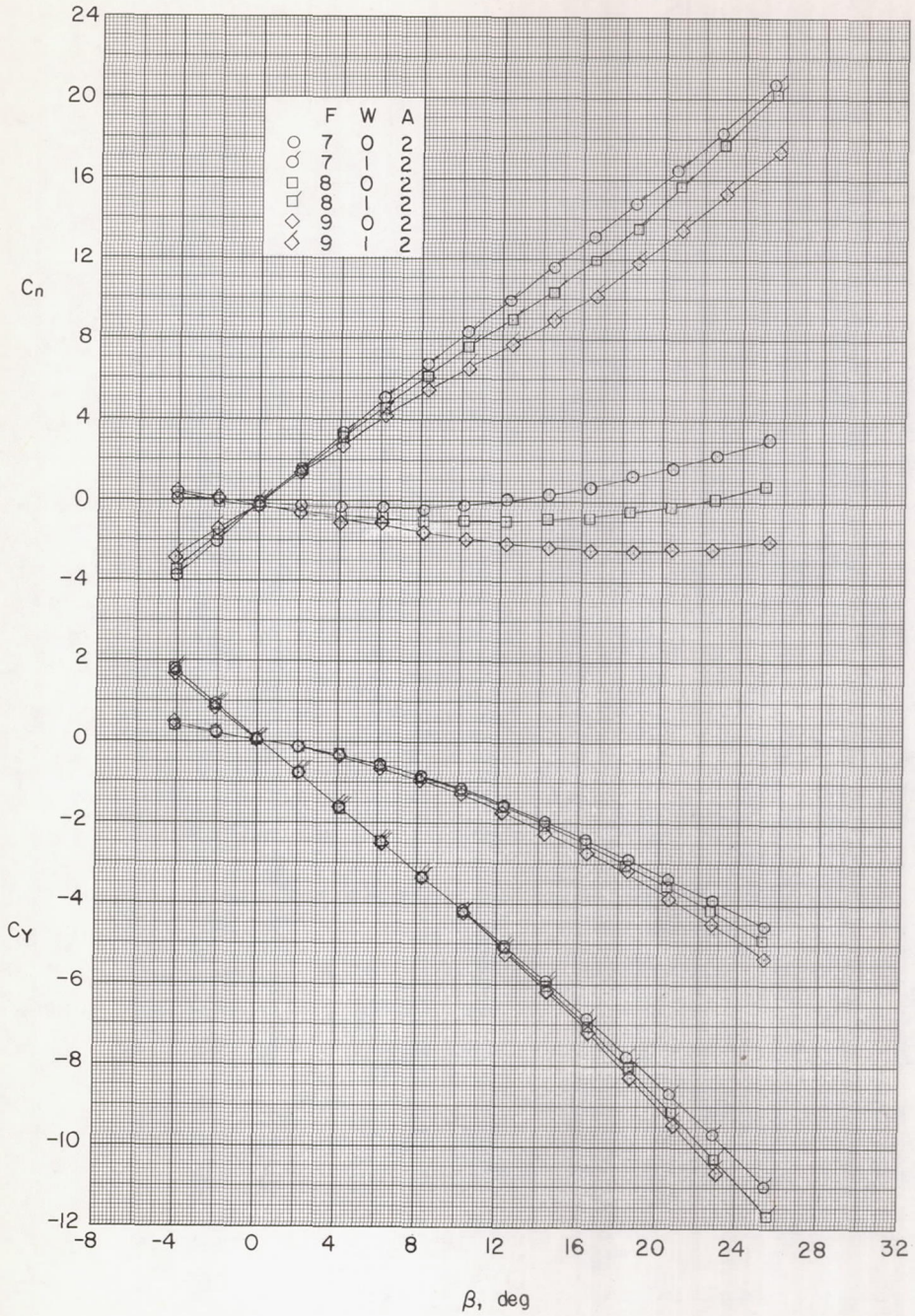
(c) $\alpha \approx 8.2^{\circ}$.

Figure 27.- Continued.



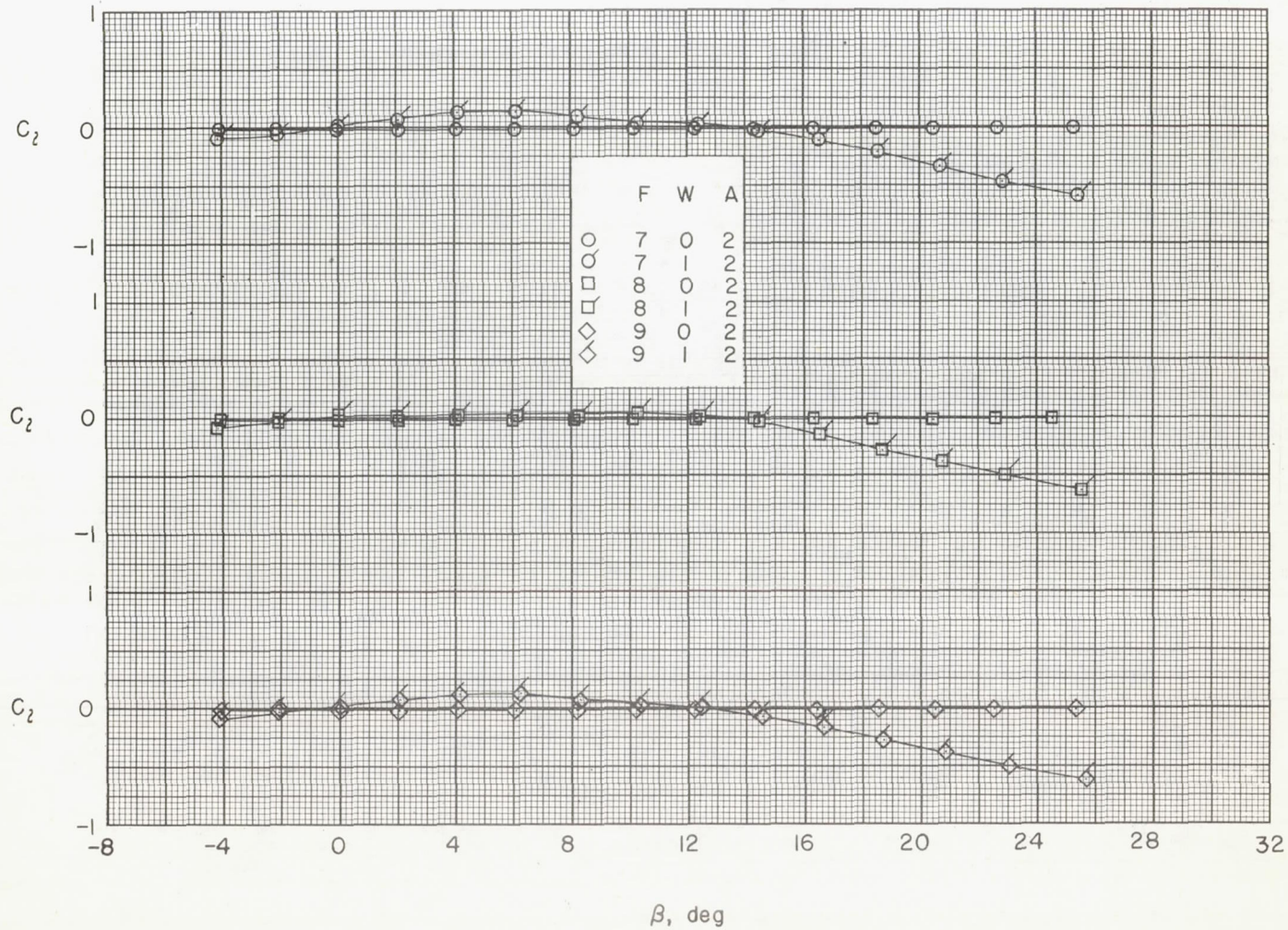
(c) Concluded.

Figure 27.- Continued.



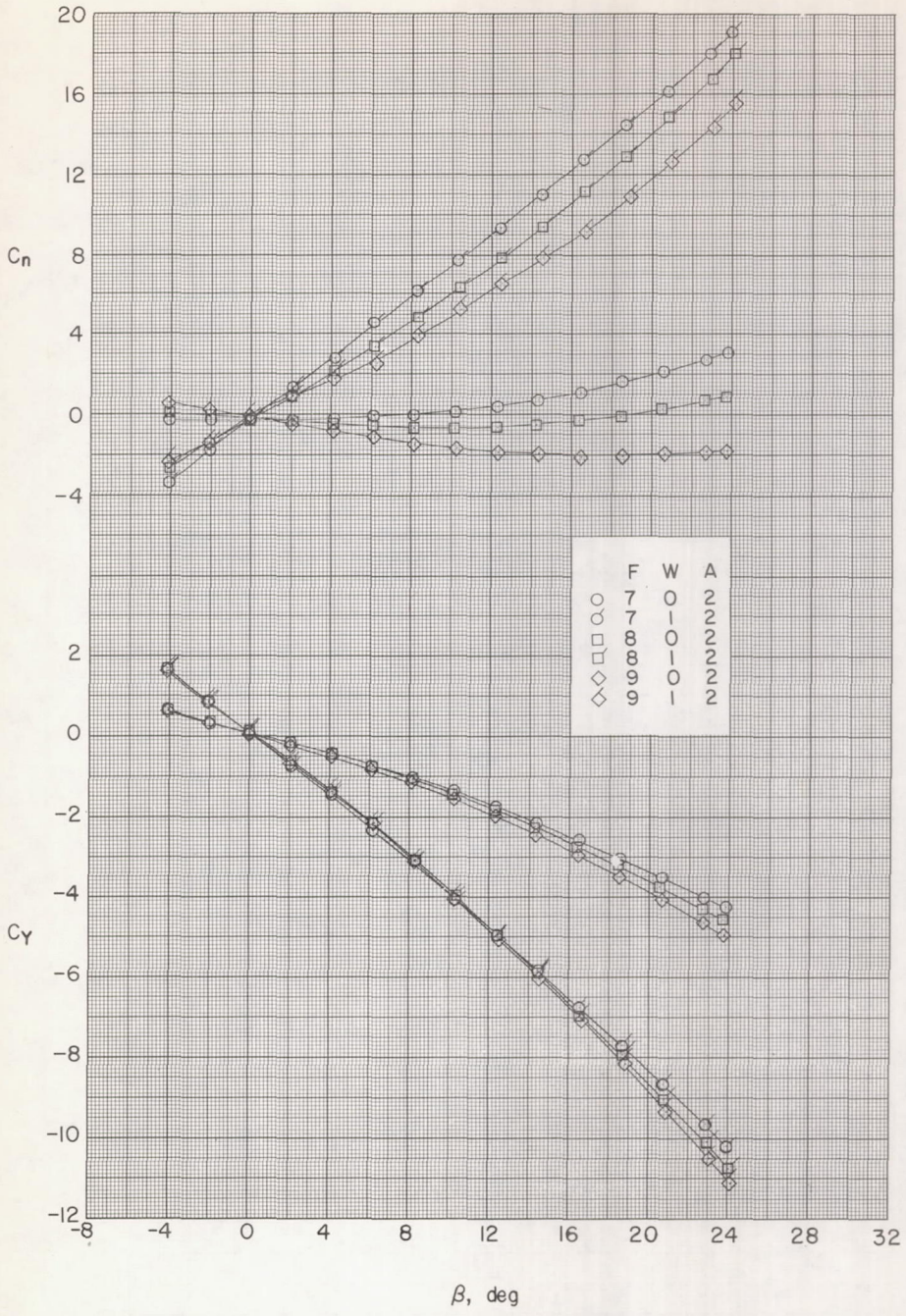
(d) $\alpha \approx 12.3^{\circ}$.

Figure 27.- Continued.



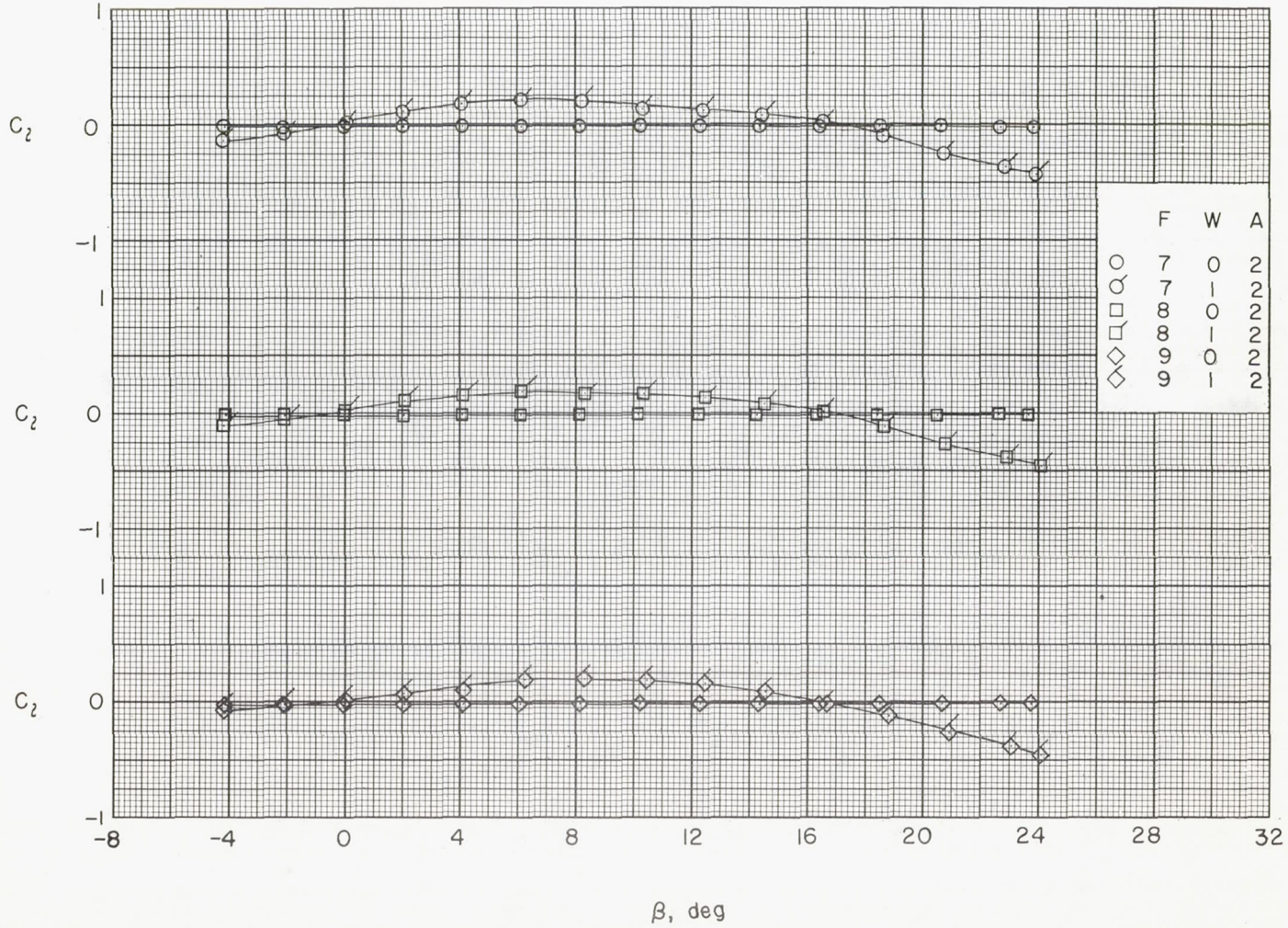
(d) Concluded.

Figure 27.- Continued.



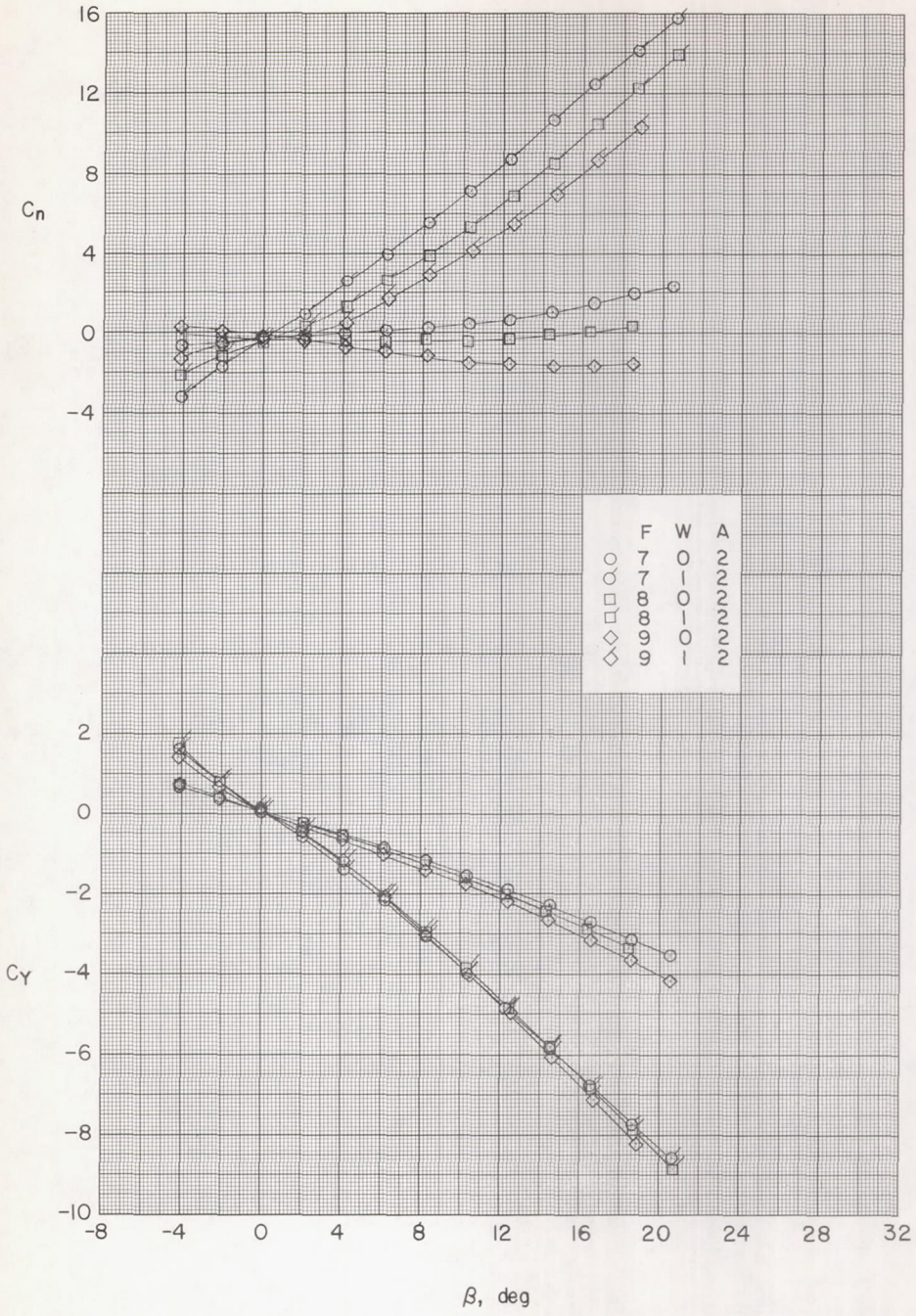
(e) $\alpha \approx 16.4^\circ$.

Figure 27.- Continued.



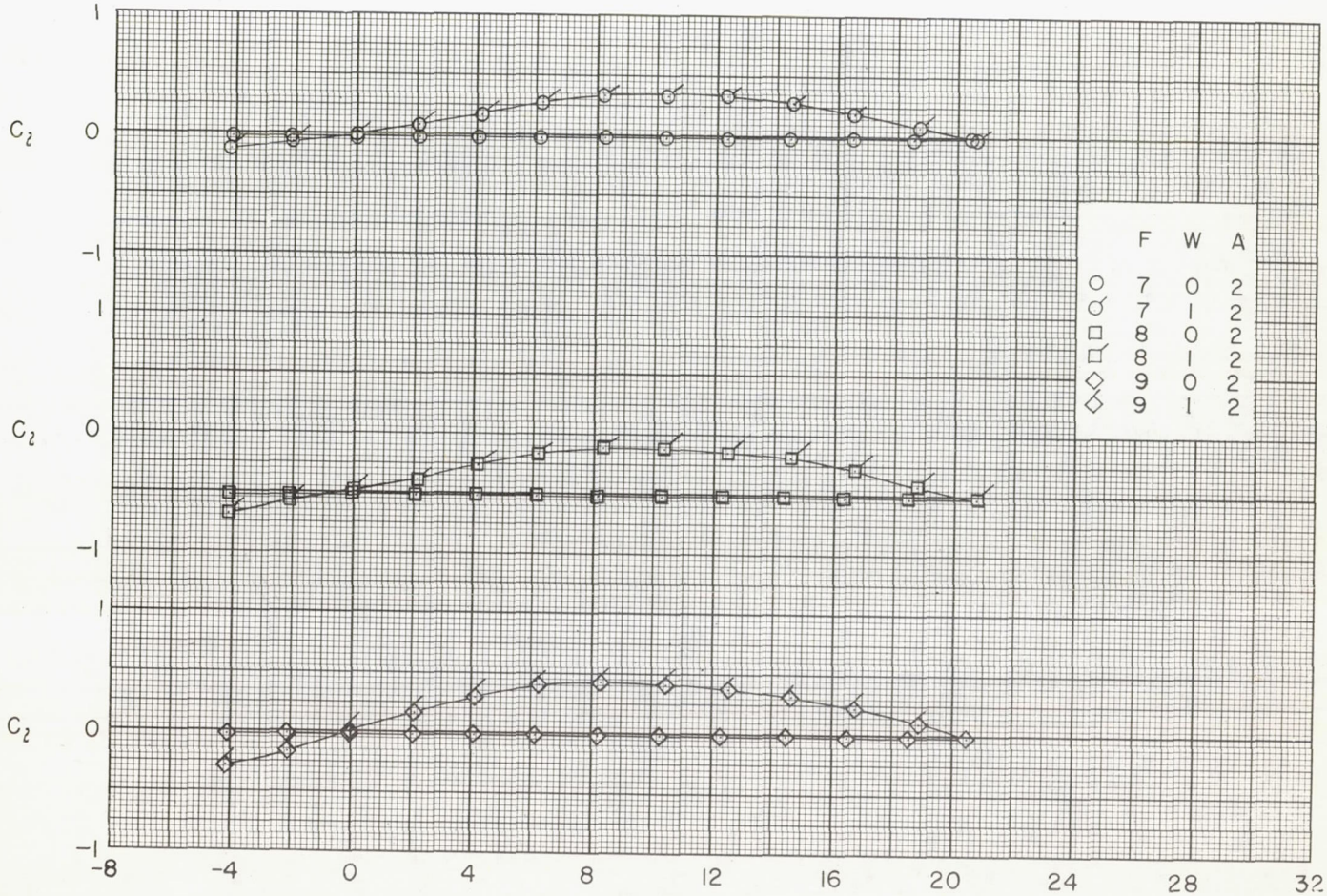
(e) Concluded.

Figure 27.- Continued.



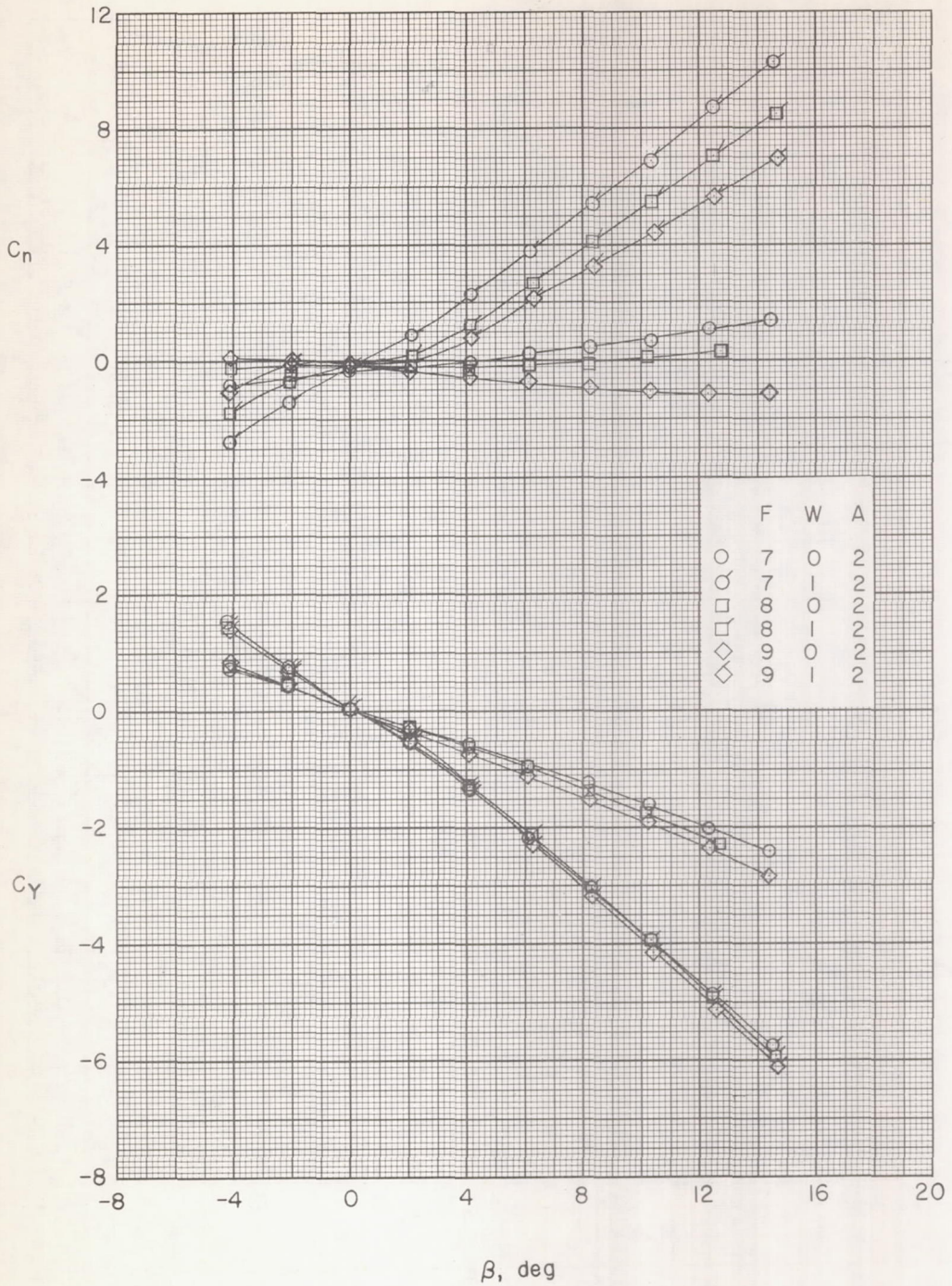
(f) $\alpha \approx 20.5^{\circ}$.

Figure 27.- Continued.



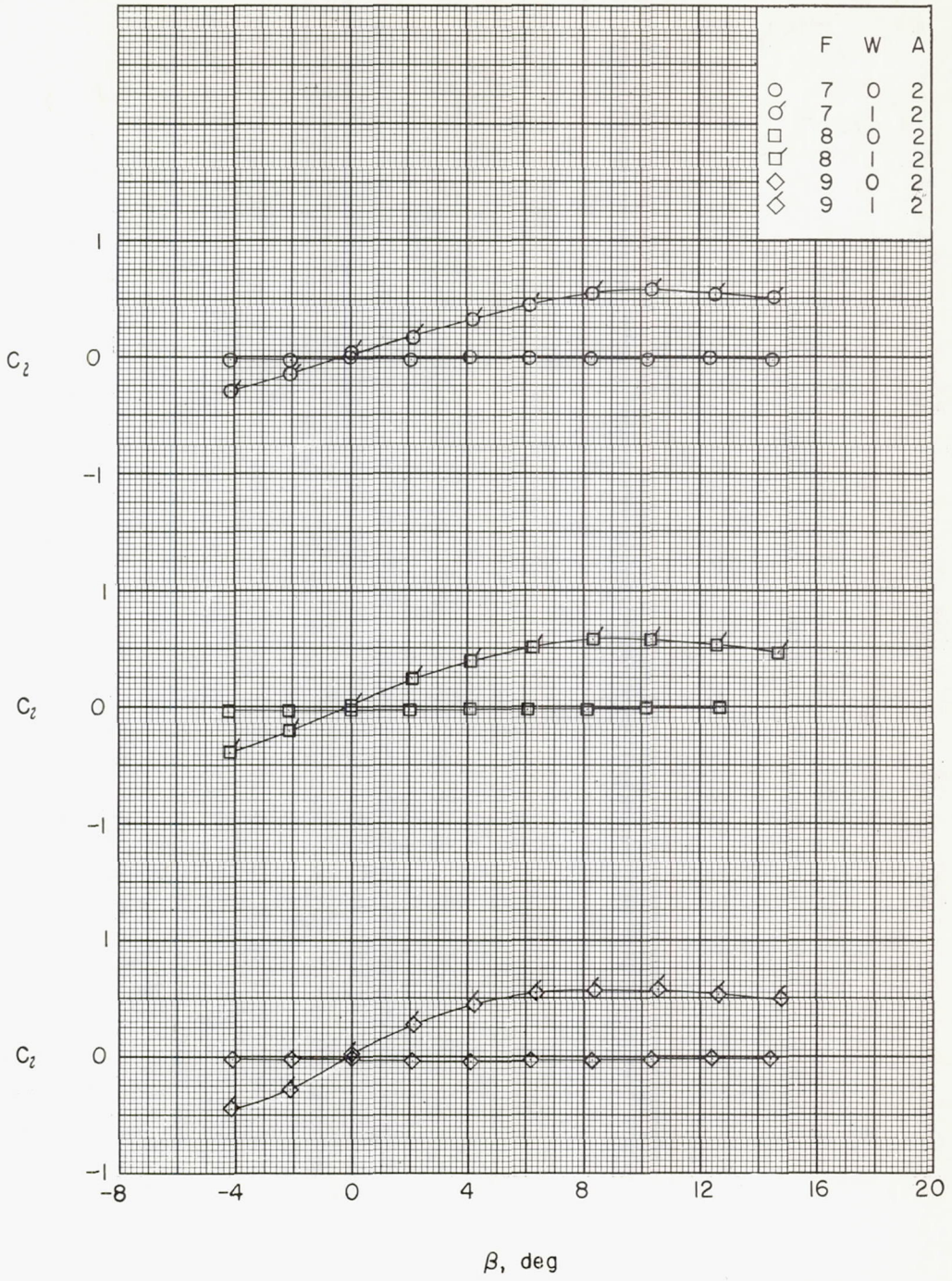
(f) Concluded.

Figure 27.- Continued.



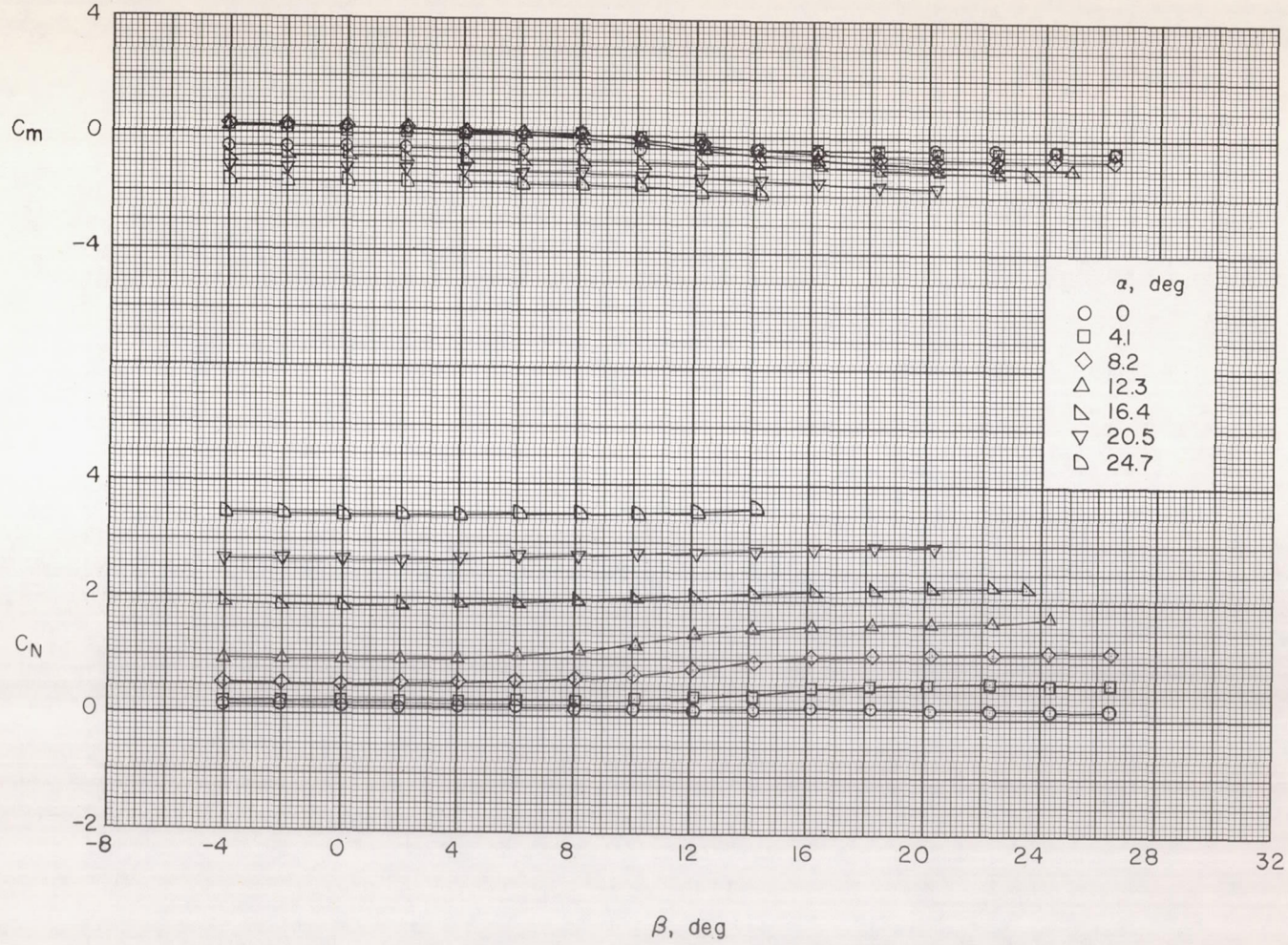
(g) $\alpha \approx 24.7°$.

Figure 27.- Continued.



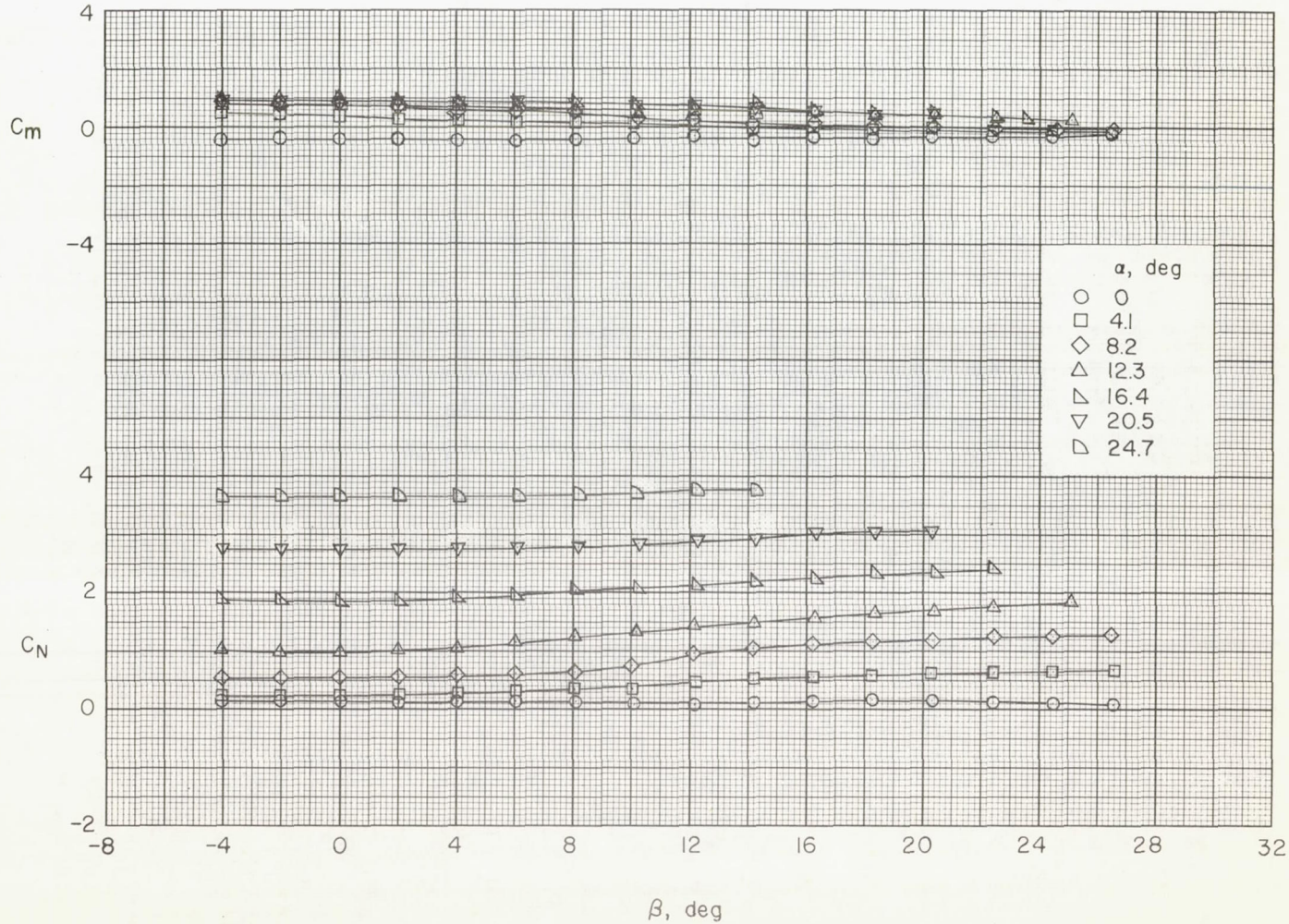
(g) Concluded.

Figure 27.- Concluded.



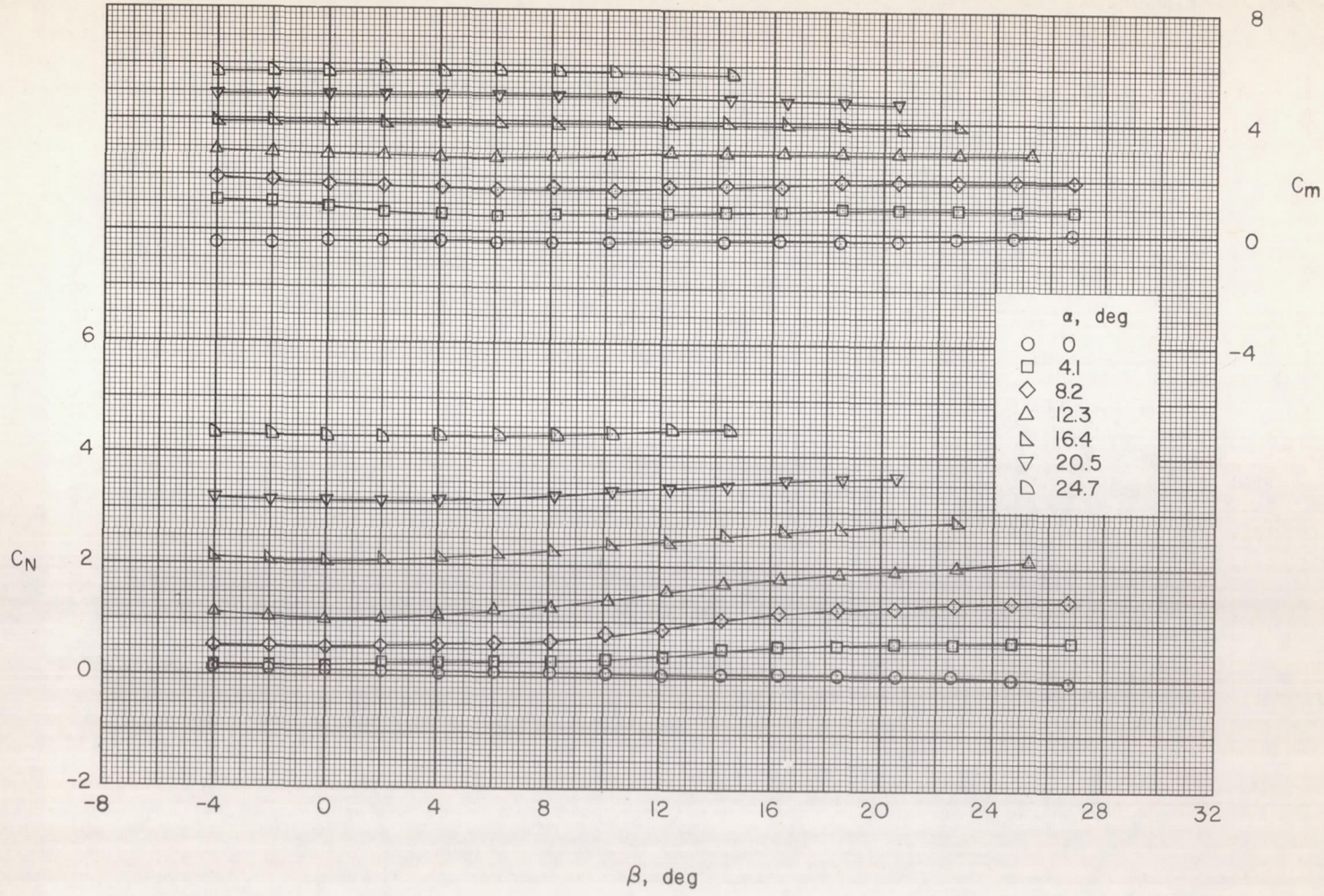
(a) Body alone, $F_1W_0A_0$.

Figure 28.- Variation of C_m and C_N with β for various angles of attack. Various forebody lengths; large delta wings; no afterbody.



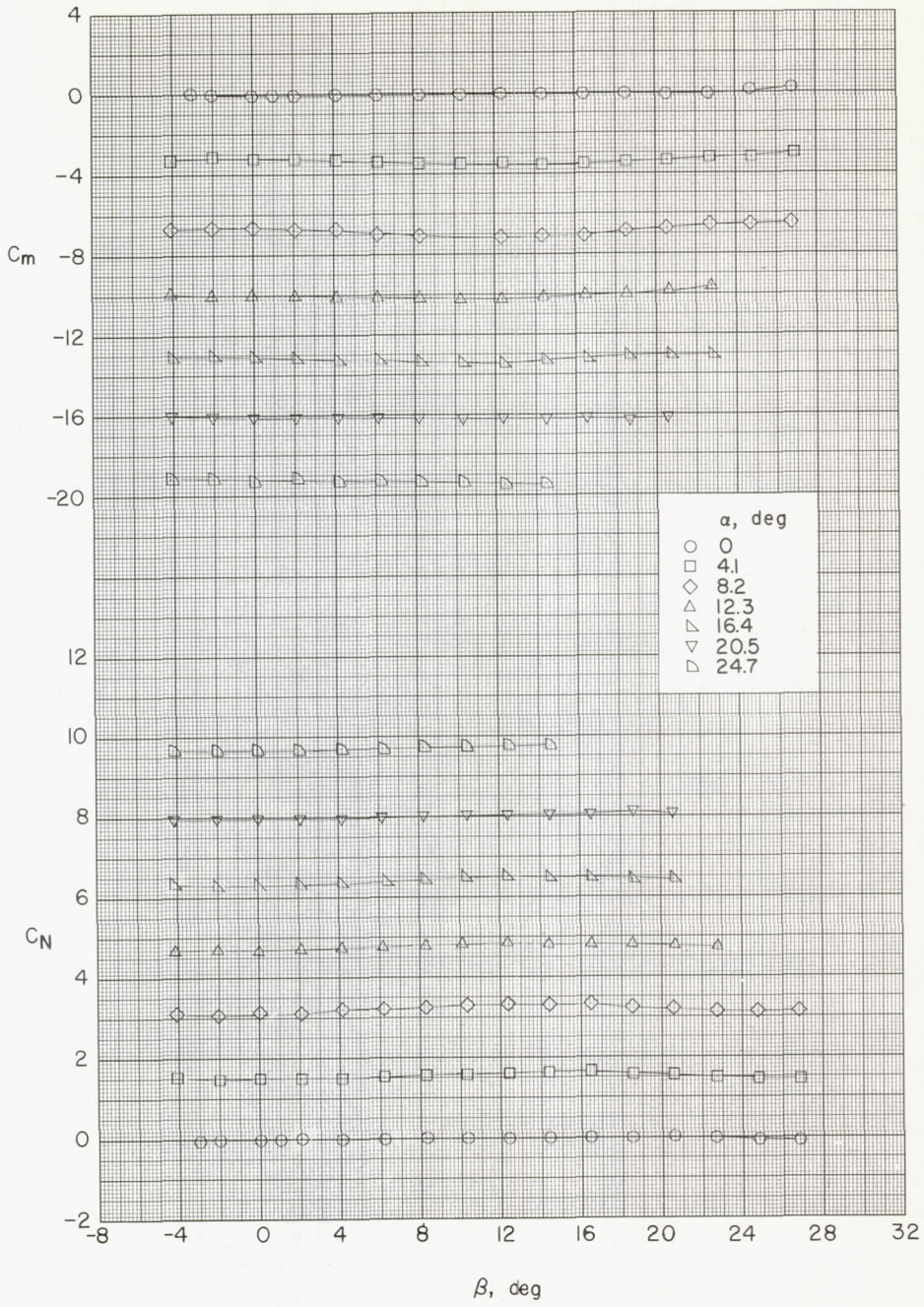
(b) Body alone, $F_7W_0A_0$.

Figure 28.- Continued.



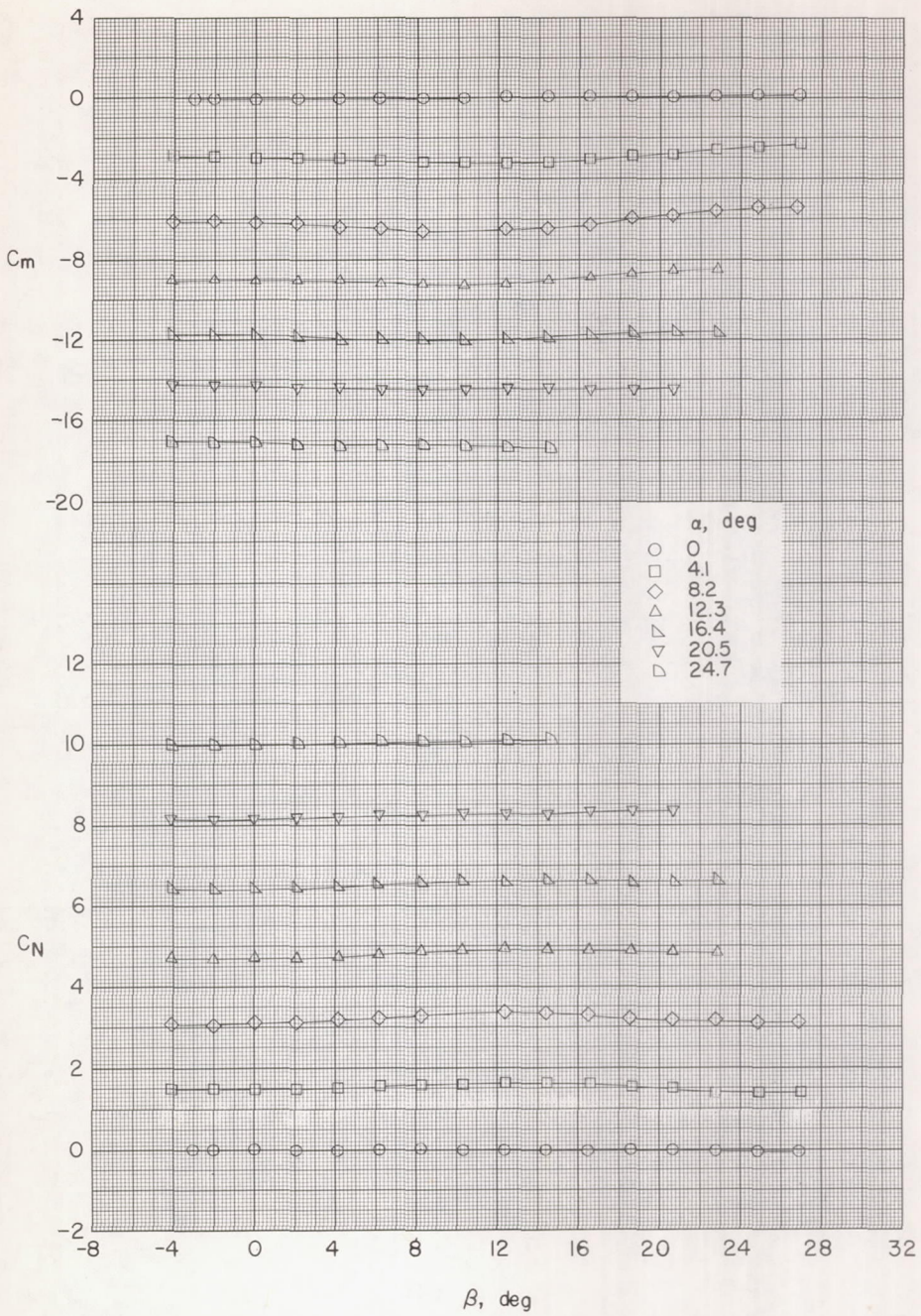
(c) Body alone, $F_9W_0A_0$.

Figure 28.- Continued.



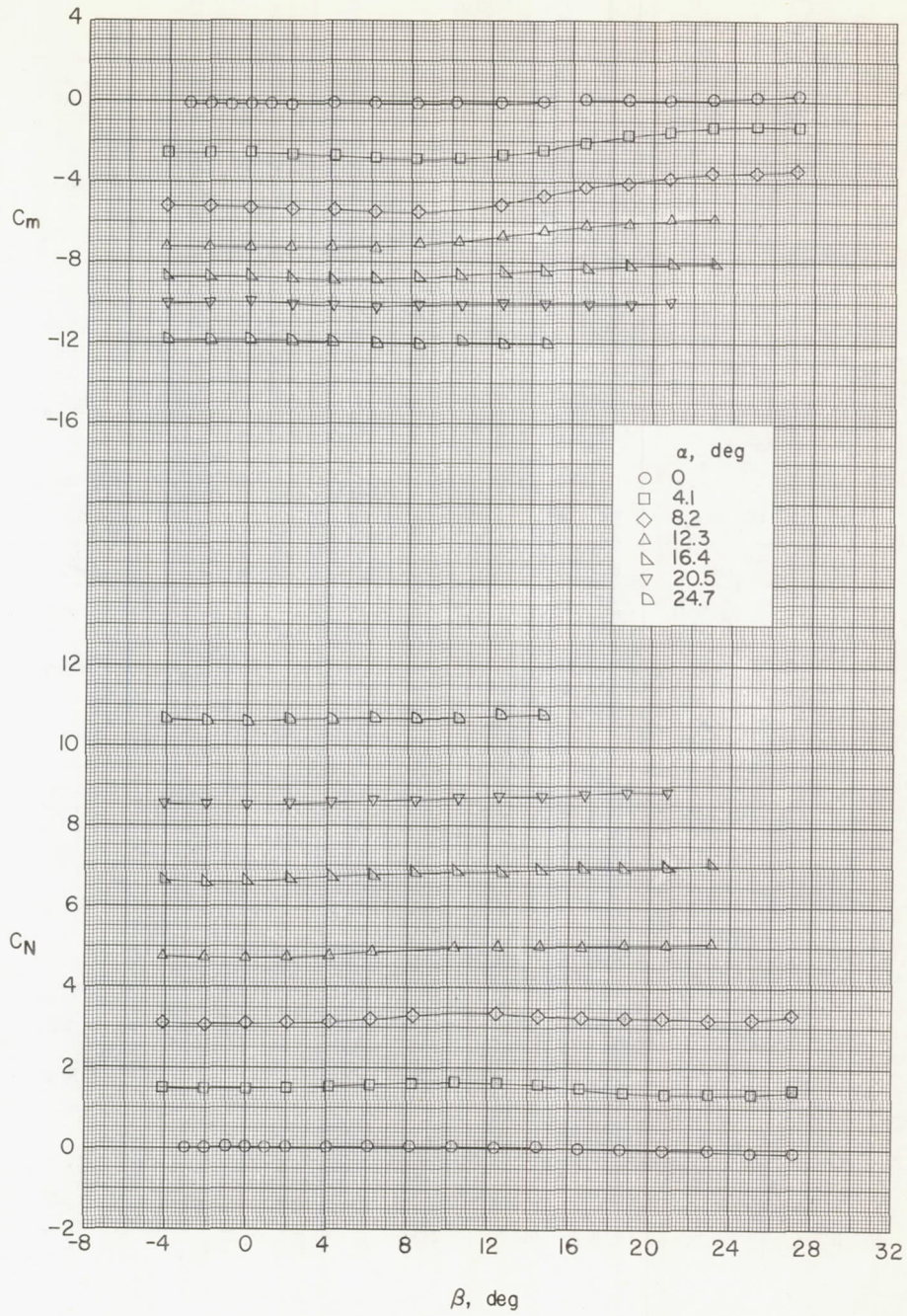
(d) Large delta wing, $F_1W_1A_0$.

Figure 28.- Continued.



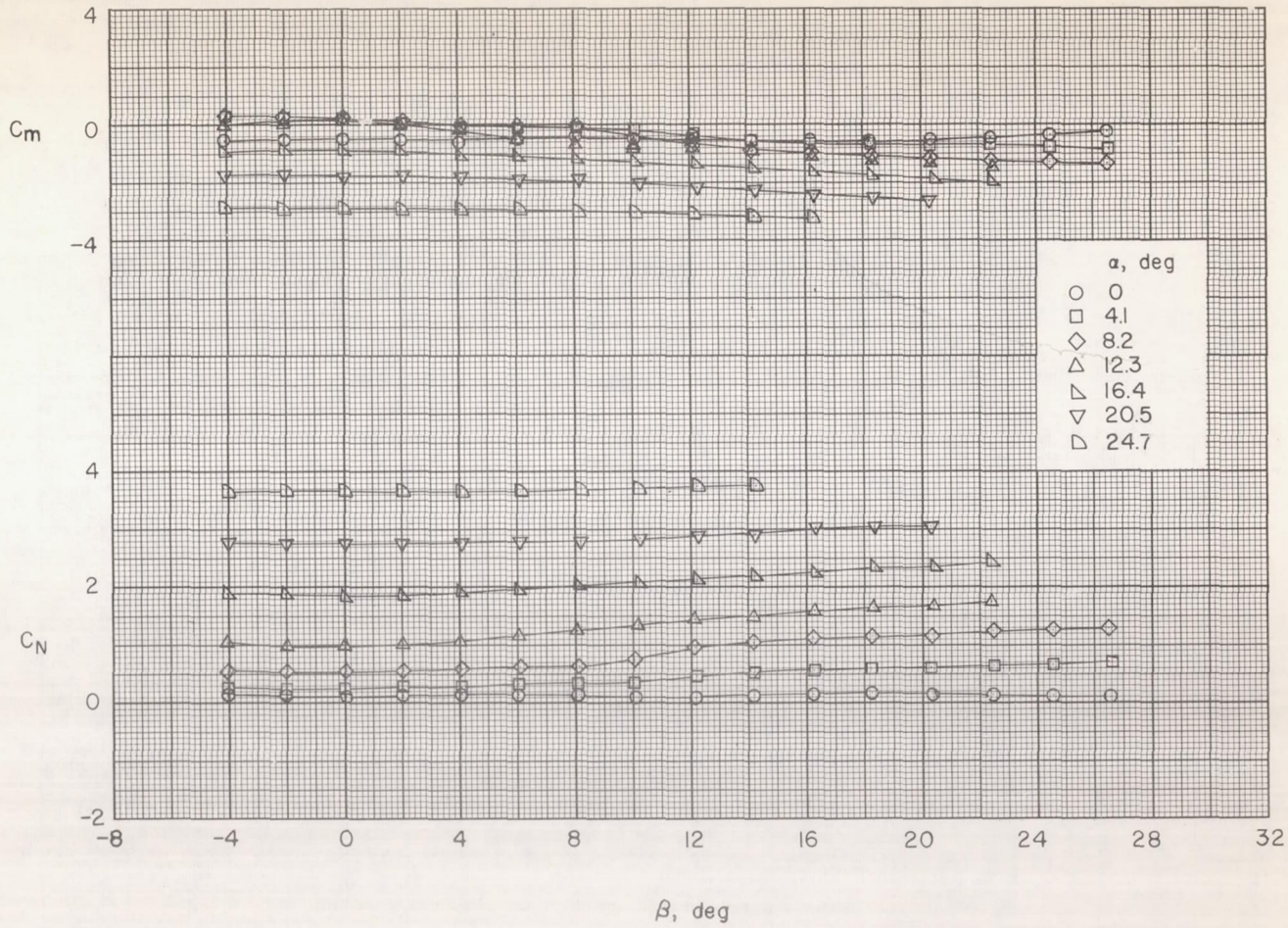
(e) Large delta wing, $F_7W_1A_0$.

Figure 28.- Continued.



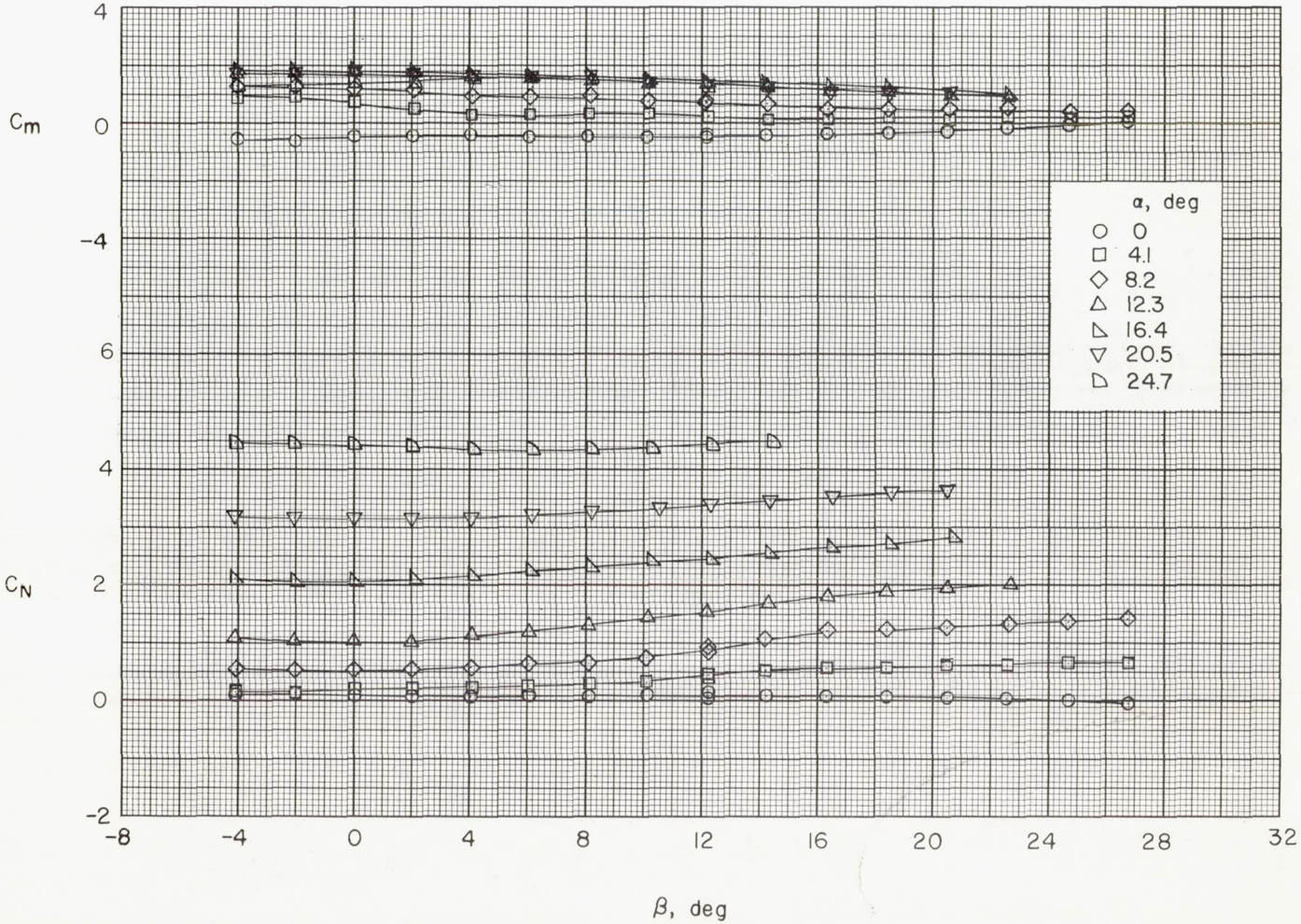
(f) Large delta wing, $F_9W_1A_0$.

Figure 28.- Concluded.



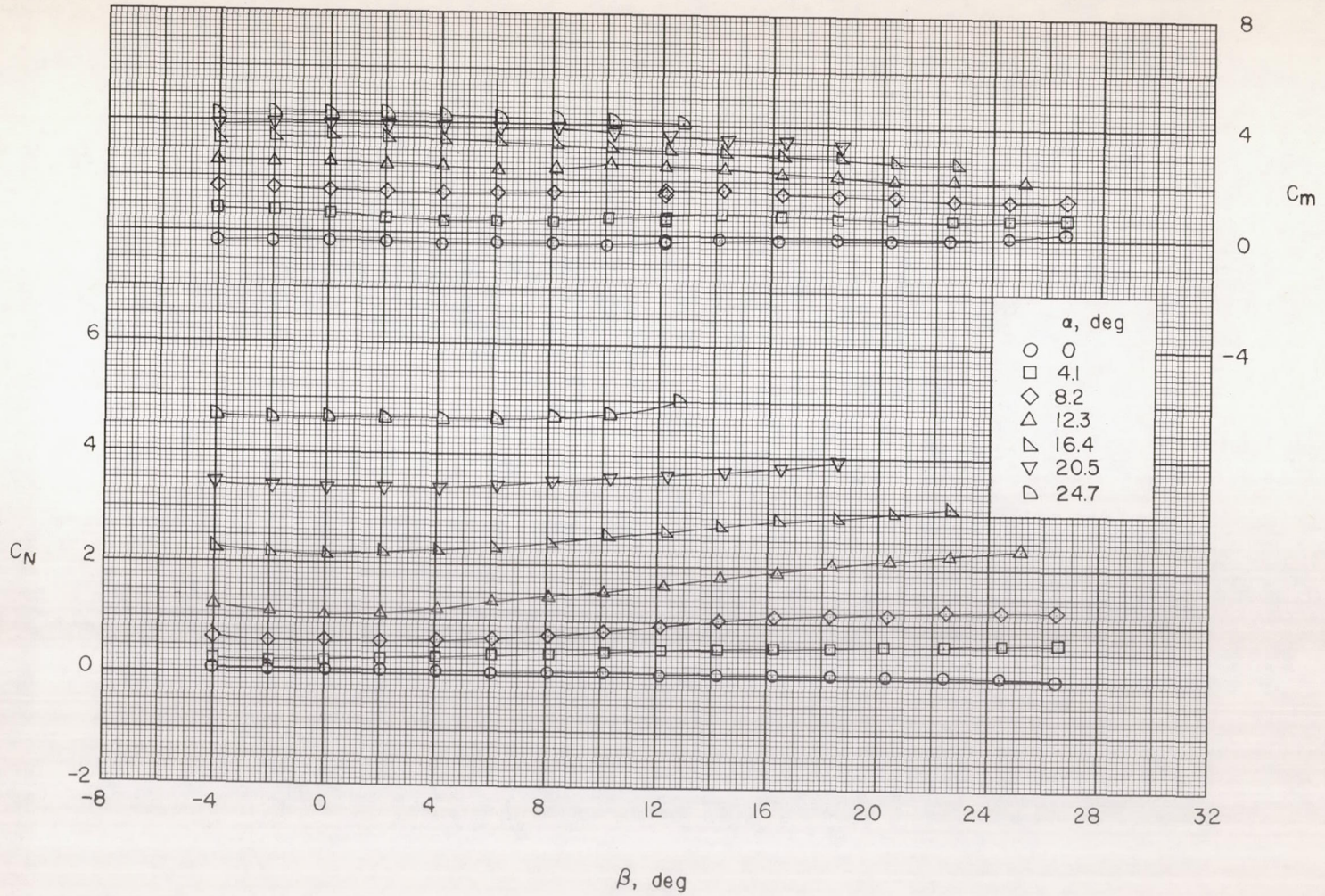
(a) Body alone, $F_1W_0A_1$.

Figure 29.- Variation of C_m and C_N with β for various angles of attack. Various forebody lengths; large delta wings; 1-caliber cylindrical afterbody.



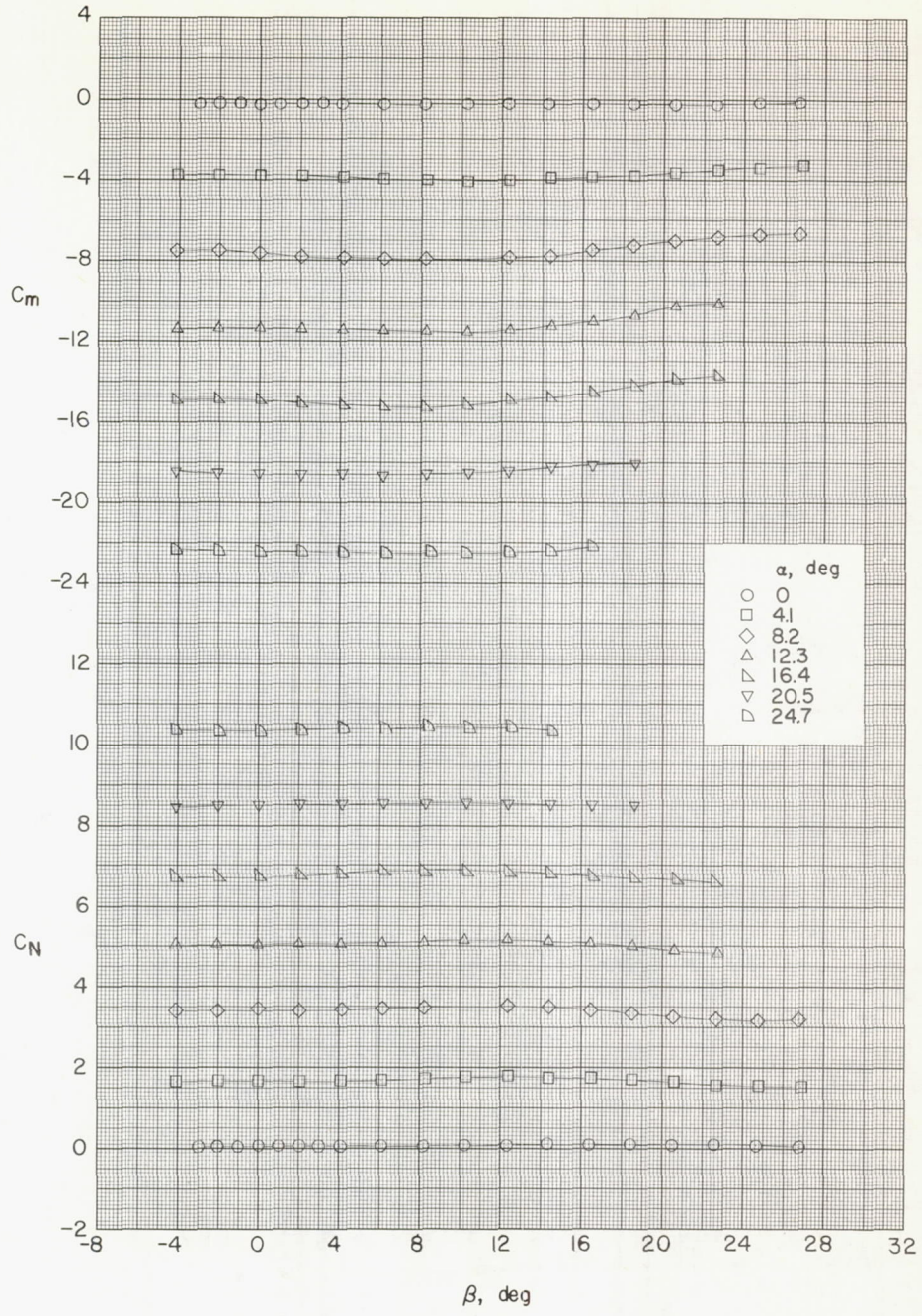
(b) Body alone, $F_8W_0A_1$.

Figure 29.- Continued.



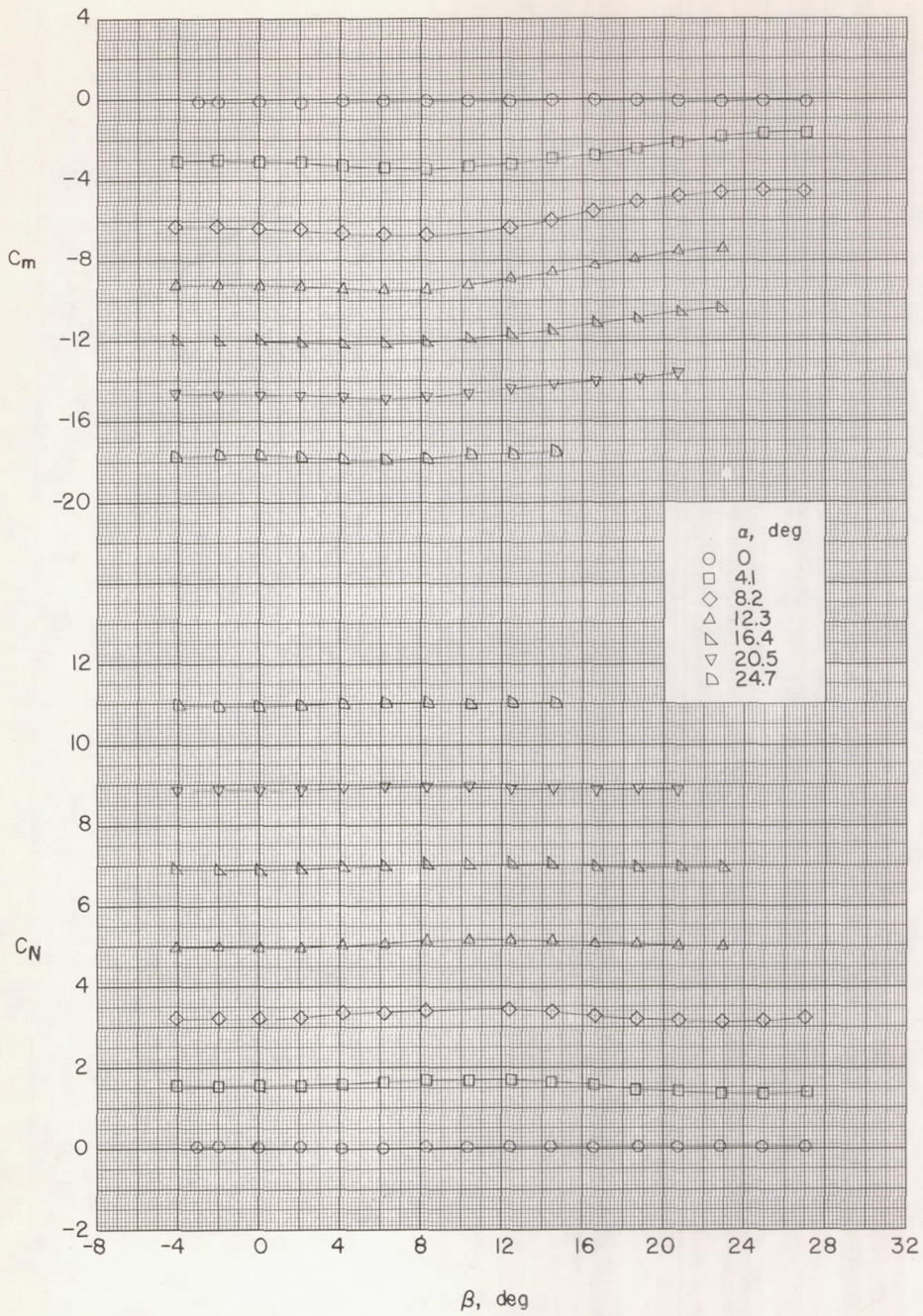
(c) Body alone, $F_9W_0A_1$.

Figure 29.- Continued.



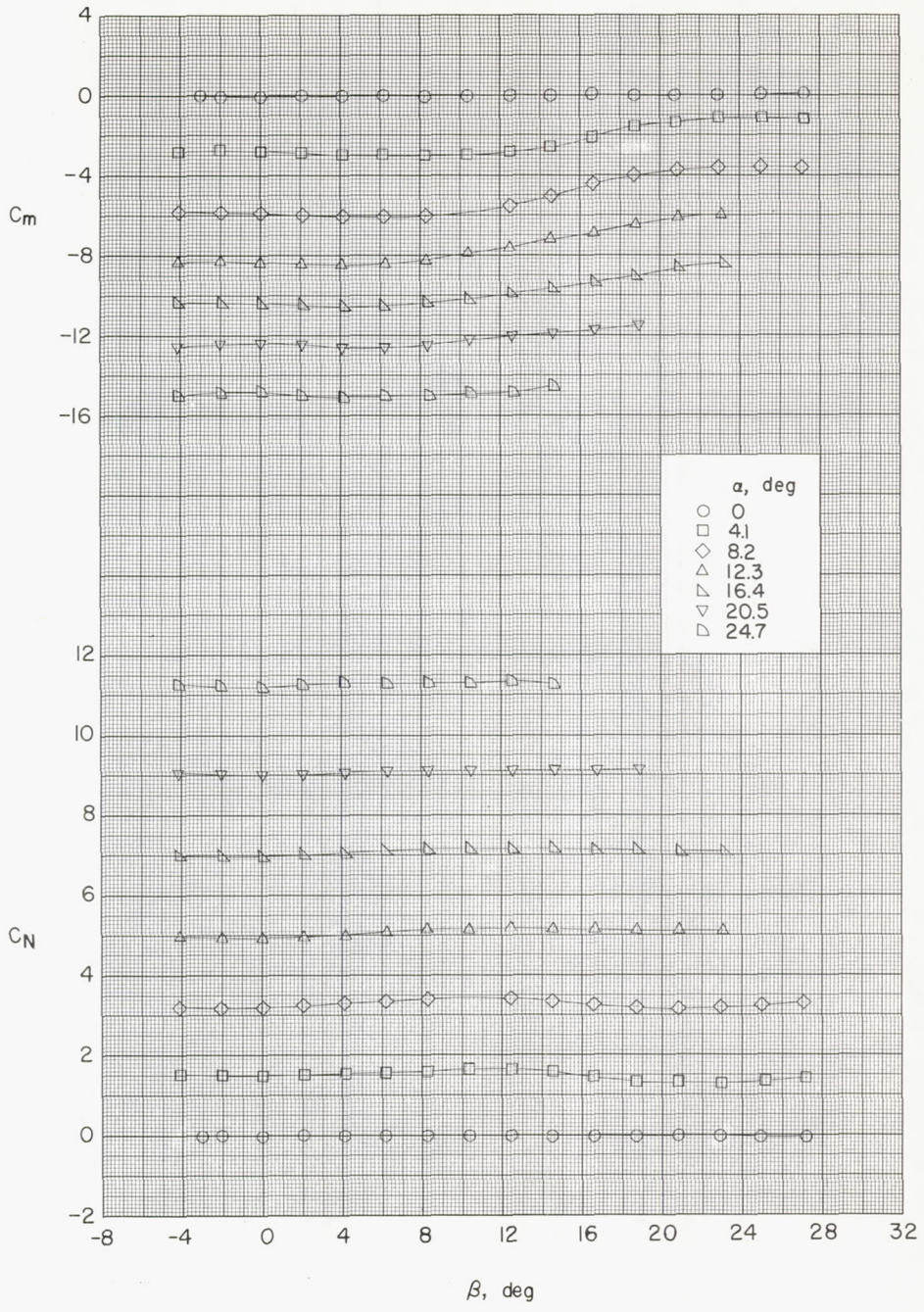
(d) Large delta wing, $F_1W_1A_1$.

Figure 29.- Continued.



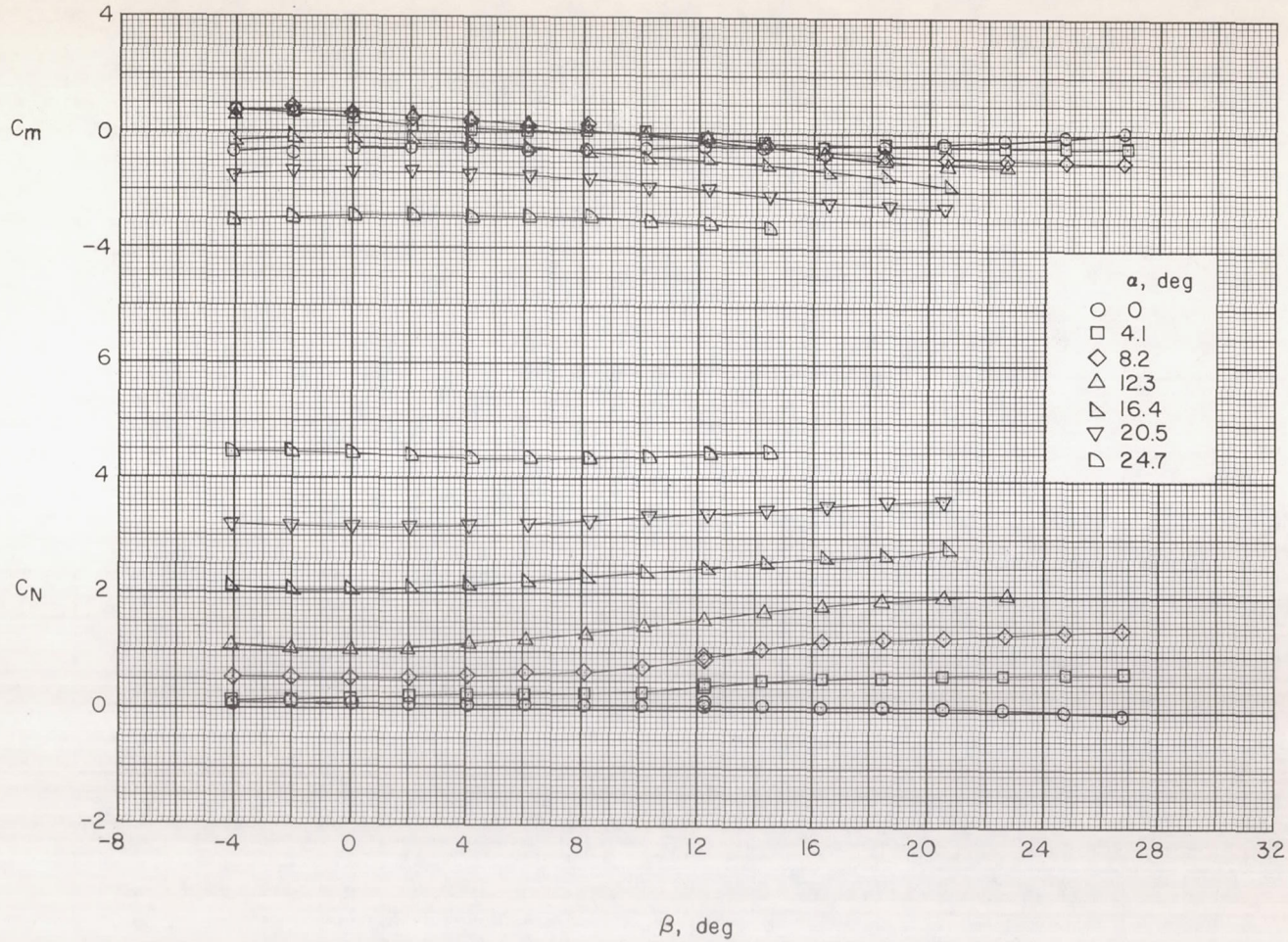
(e) Large delta wing, $F_8W_1A_1$.

Figure 29.- Continued.



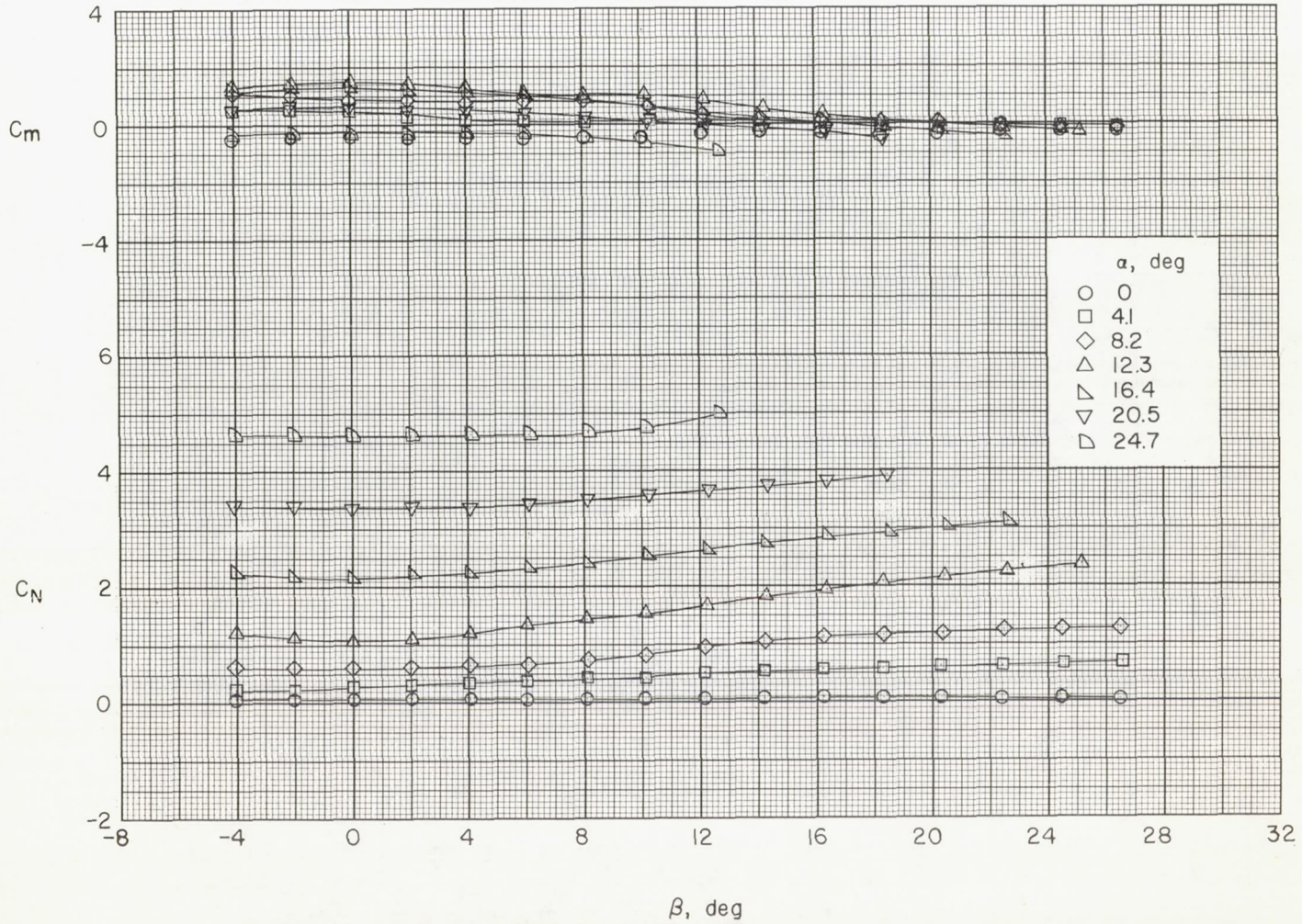
(f) Large delta wing, $F_9W_1A_1$.

Figure 29.- Concluded.



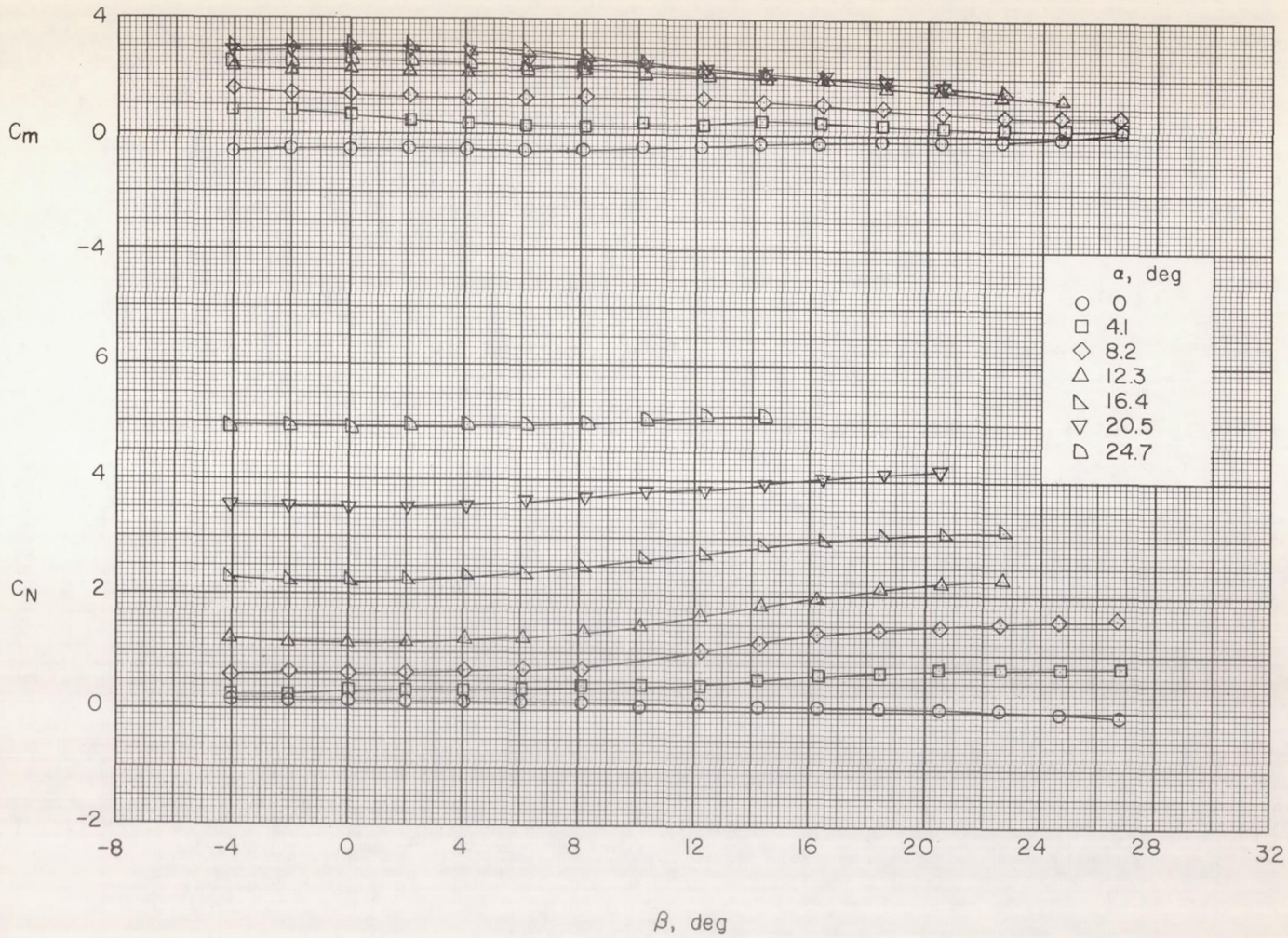
(a) Body alone, $F_7W_0A_2$.

Figure 30.- Variation of C_m and C_N with β for various angles of attack. Various forebody lengths; large delta wings; 2-caliber cylindrical afterbody.



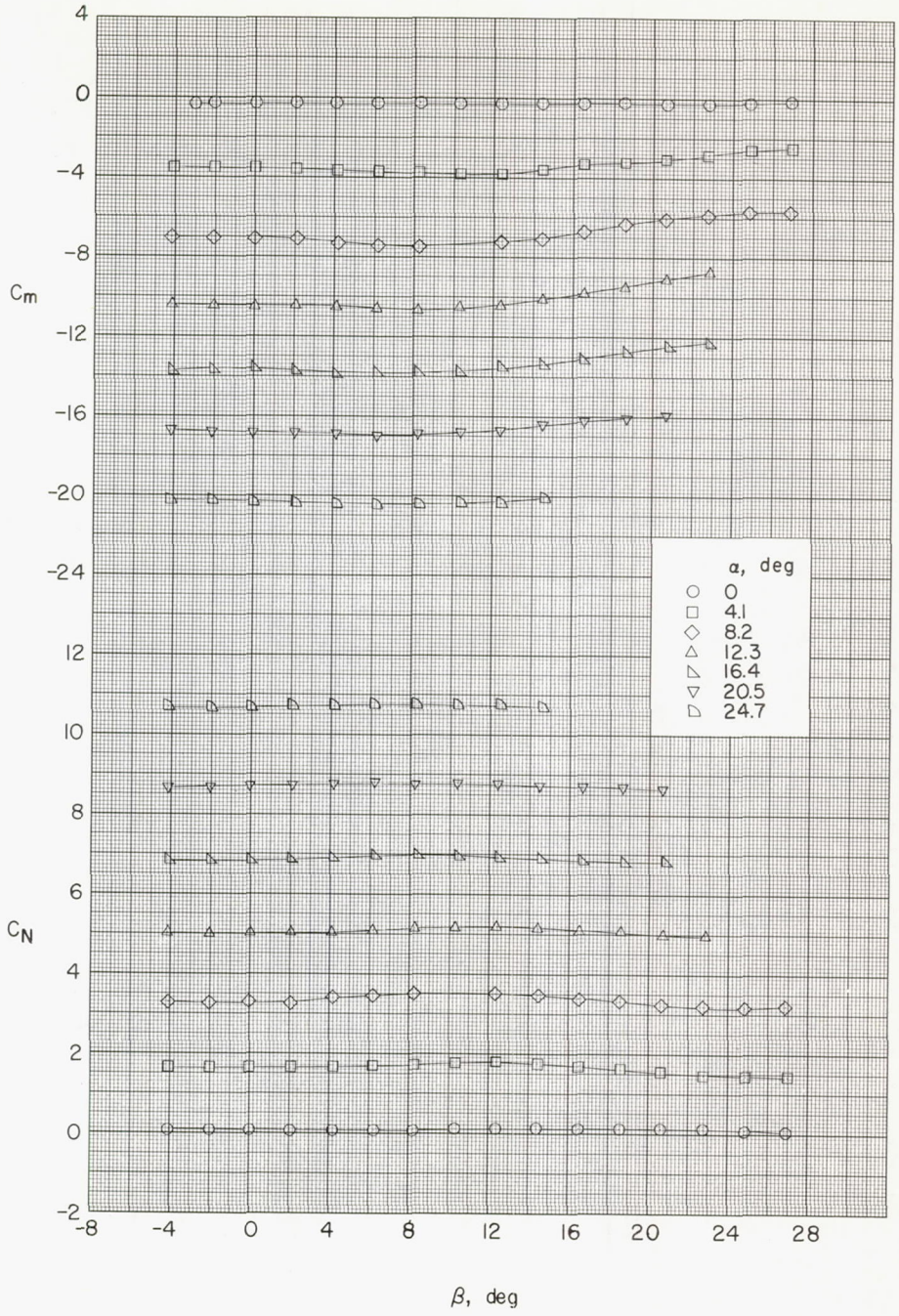
(b) Body alone, $F_8W_0A_2$.

Figure 30.- Continued.



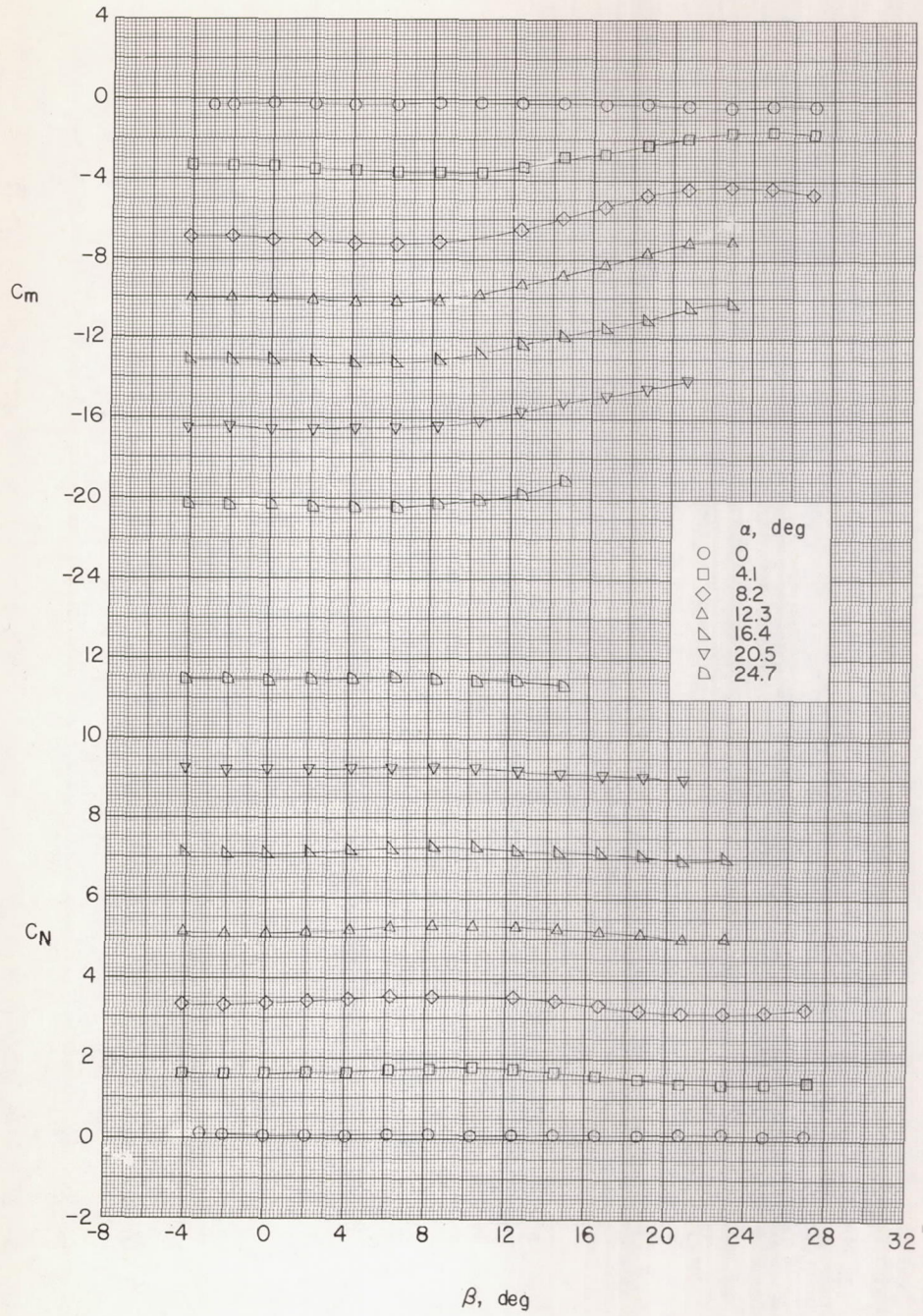
(c) Body alone, $F_9W_1A_2$.

Figure 30.- Continued.



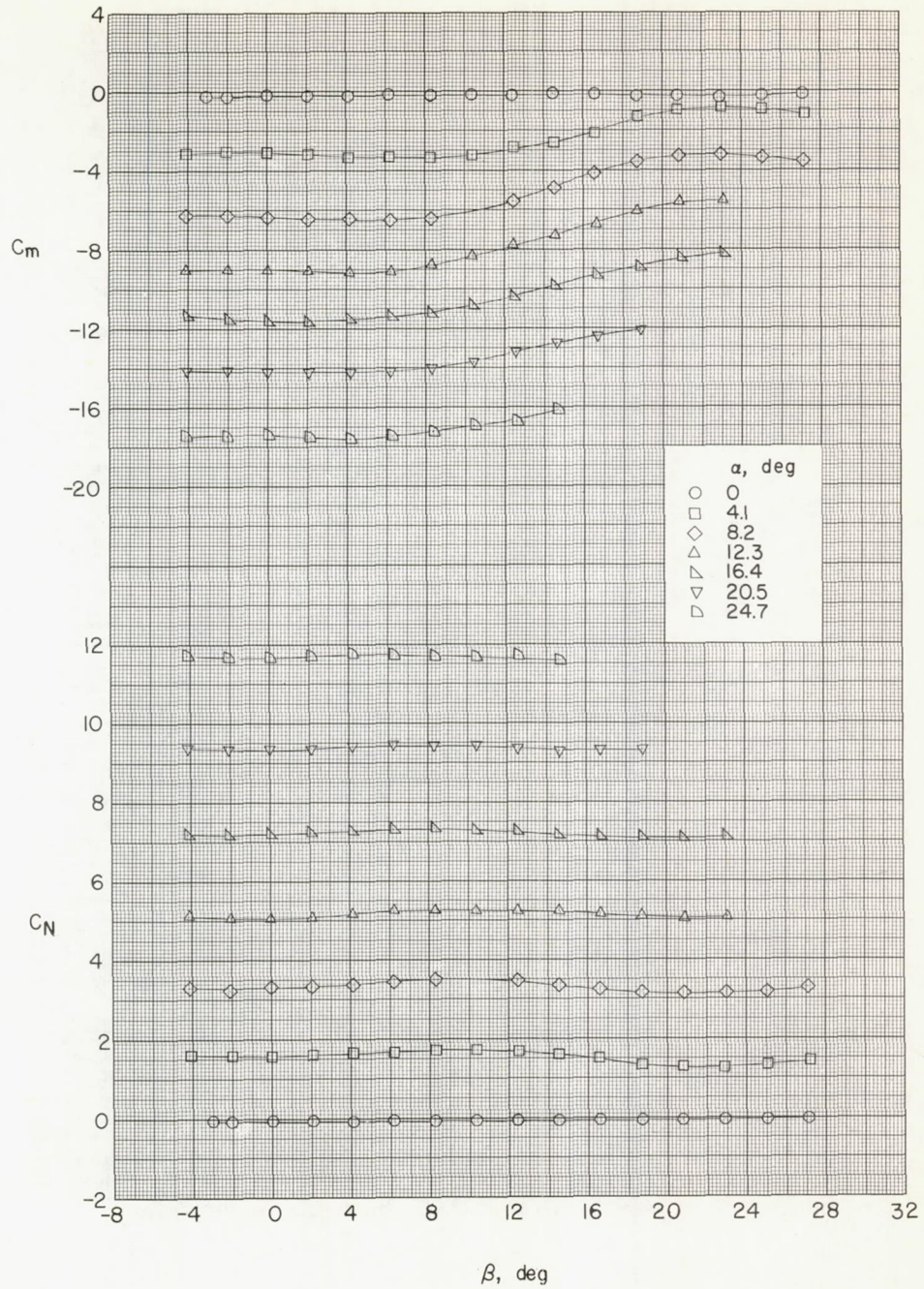
(d) Large delta wing, $F_7W_1A_2$.

Figure 30.- Continued.



(e) Large delta wing, $F_8W_1A_2$.

Figure 30.- Continued.



(f) Large delta wing, $F_9W_1A_2$.

Figure 30.- Concluded.

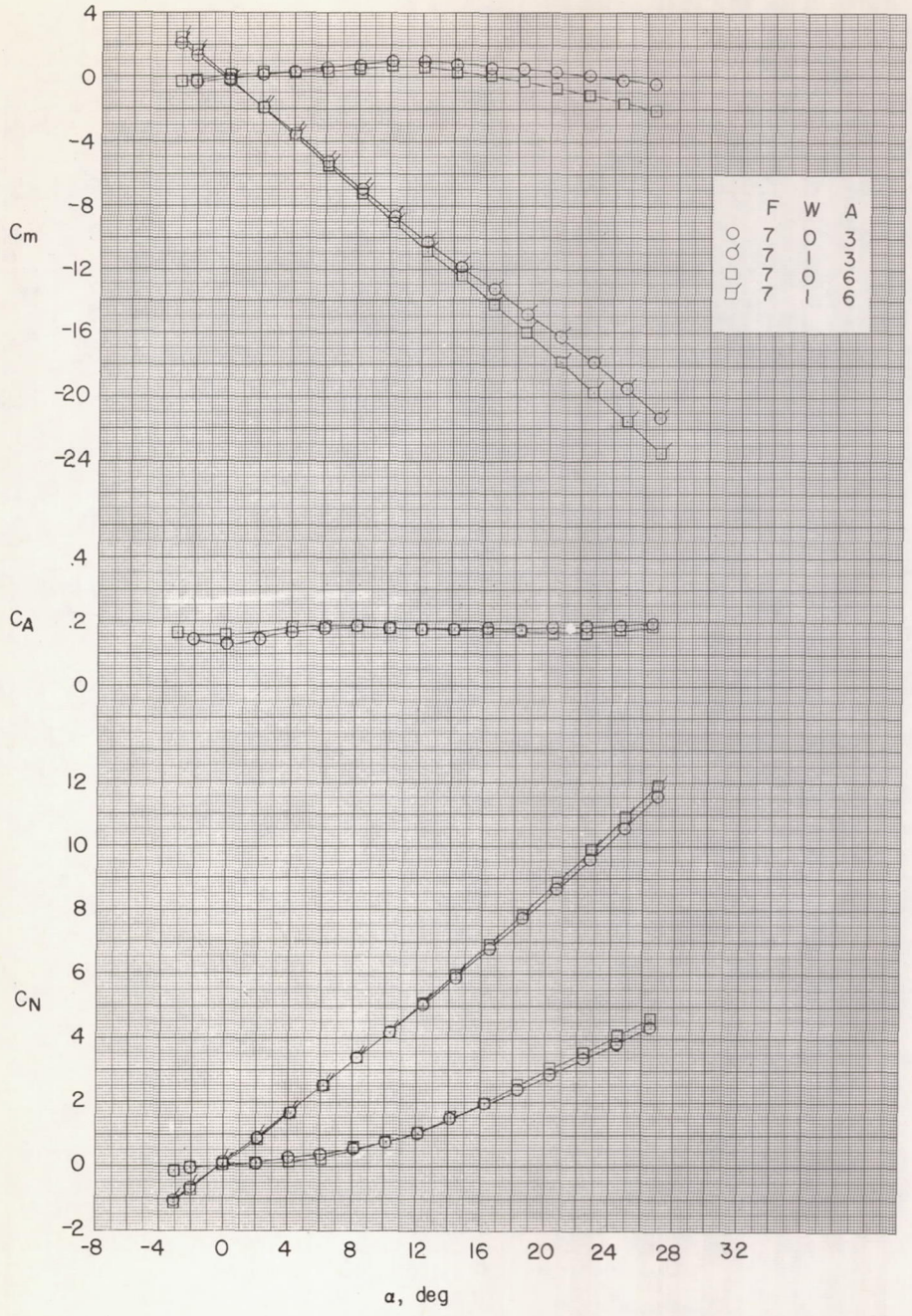


Figure 31.- Effects of 1-caliber boattail (A_3) and 1-caliber flare (A_6) afterbodies on aerodynamic characteristics in pitch. Large delta wings; l/d = 10.

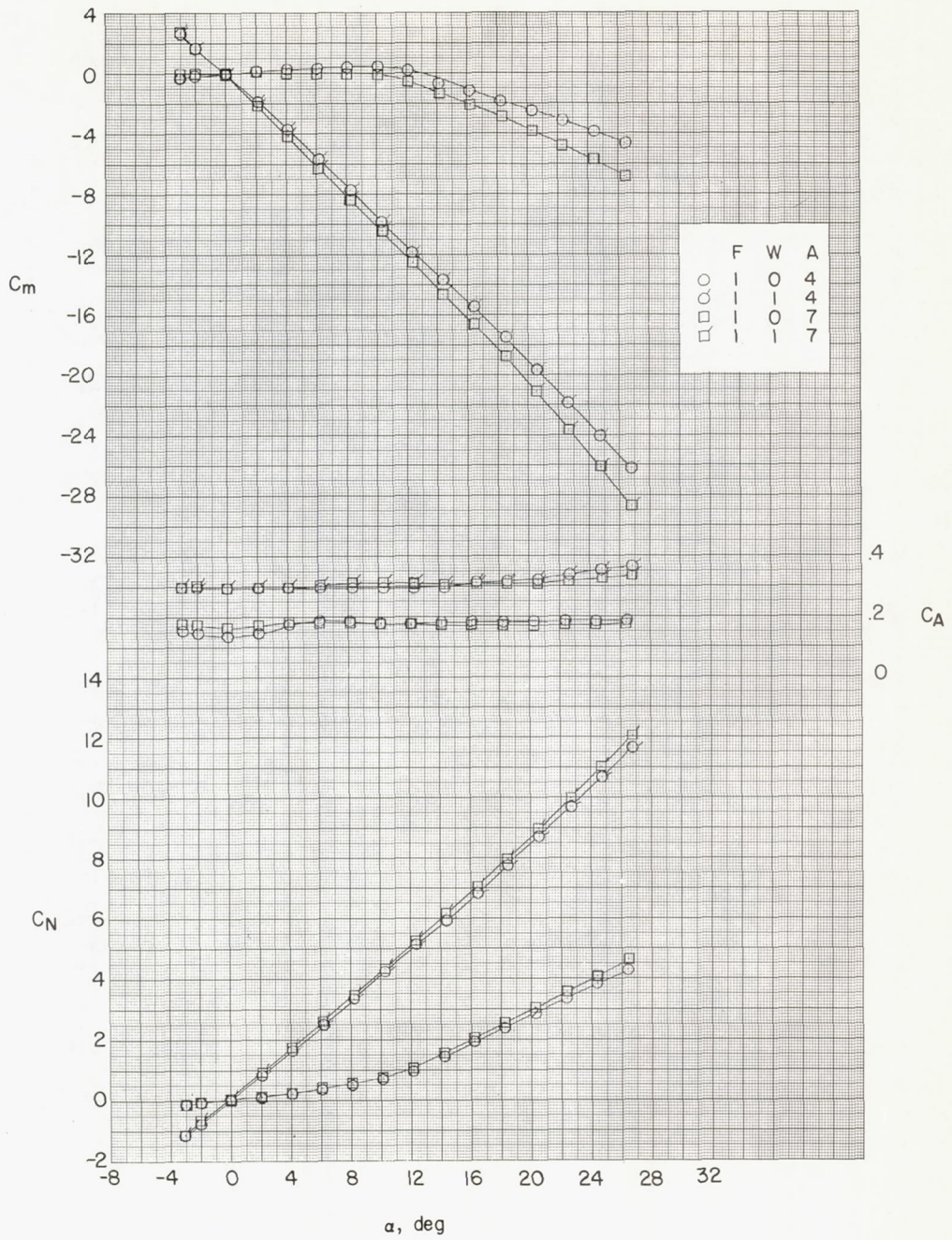


Figure 32.- Effects of 2-caliber cylinder-boattail (A_4) and 2-caliber cylinder-flare (A_7) afterbodies on aerodynamic characteristics in pitch. Large delta wings; $l/d = 10$.

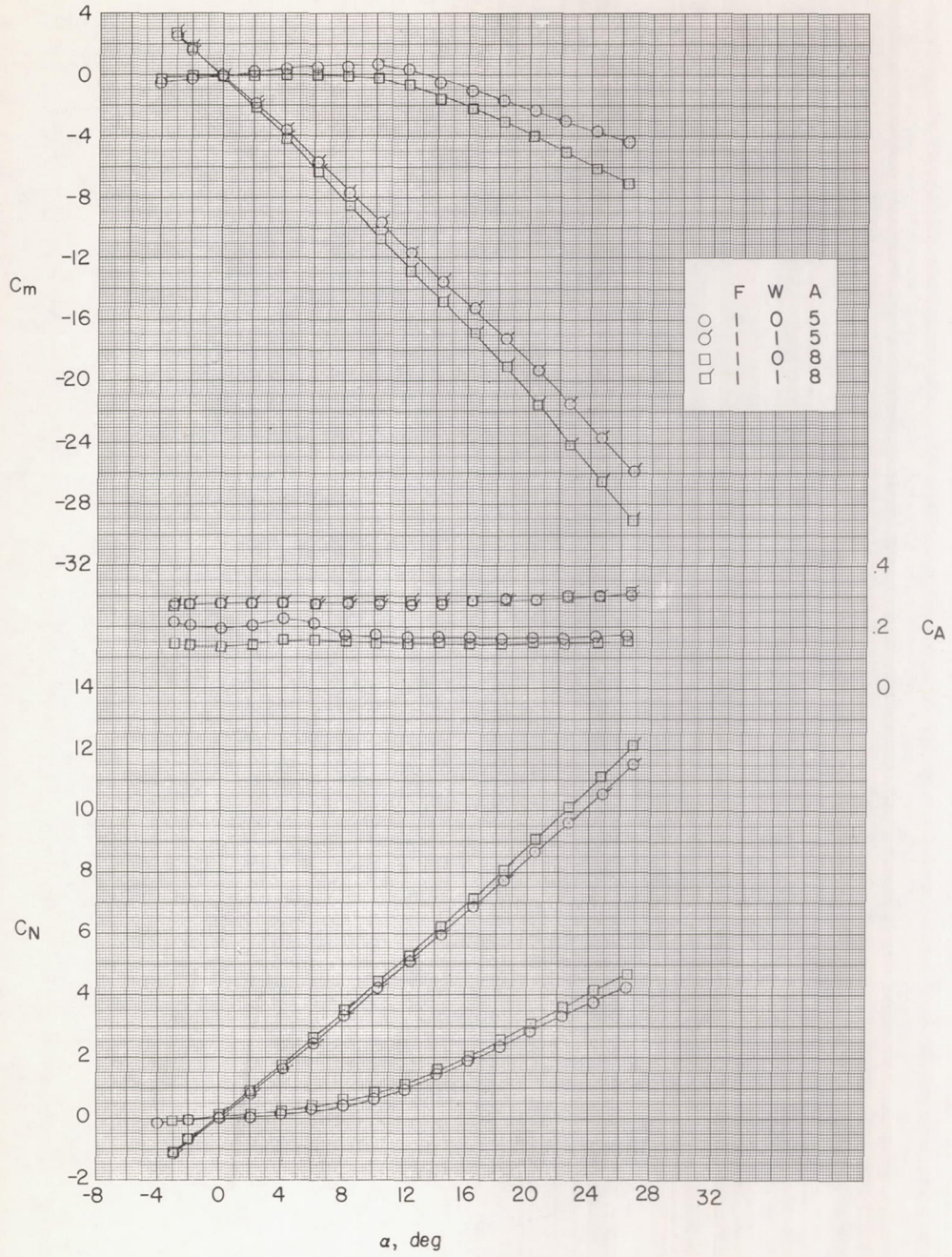
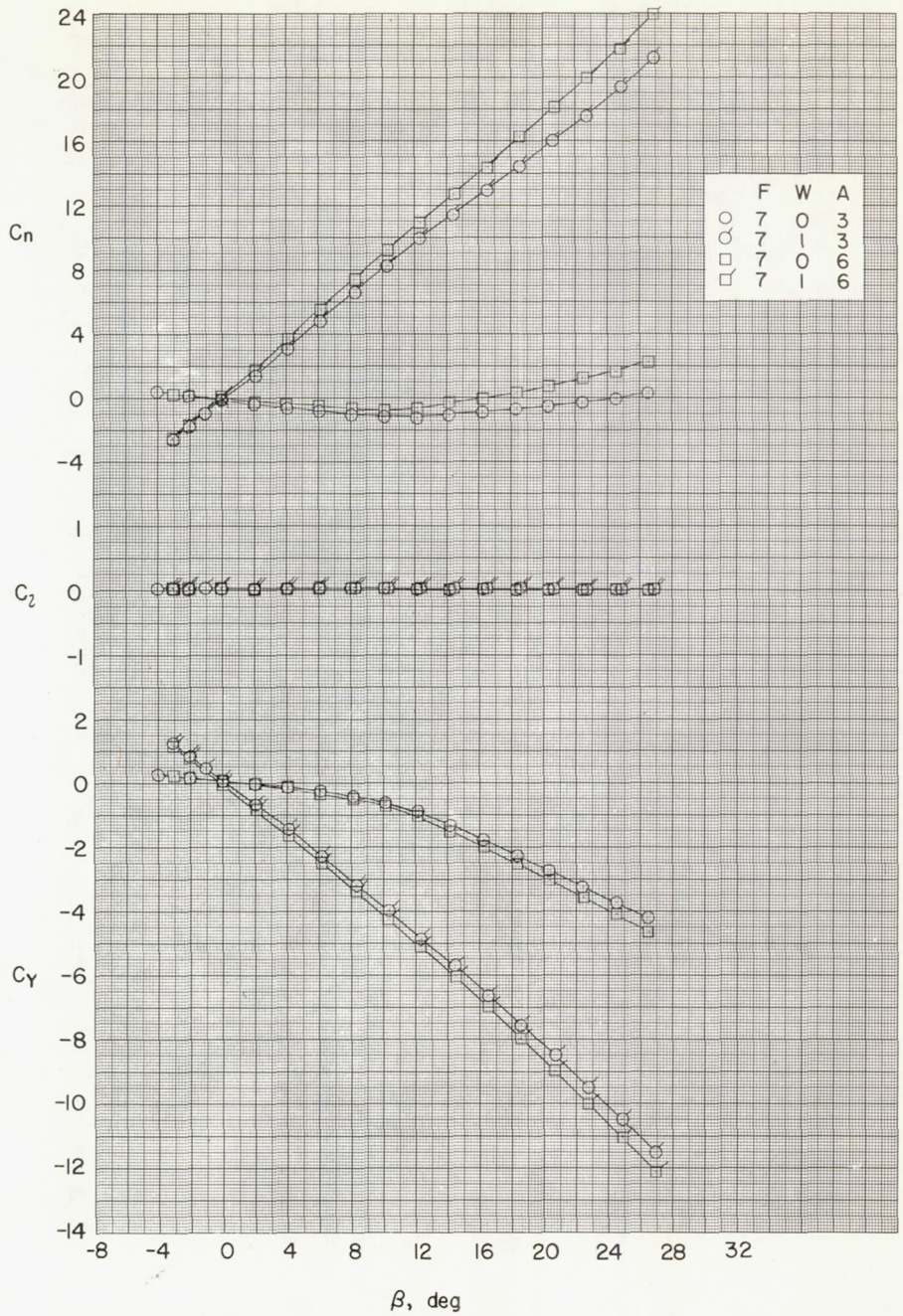
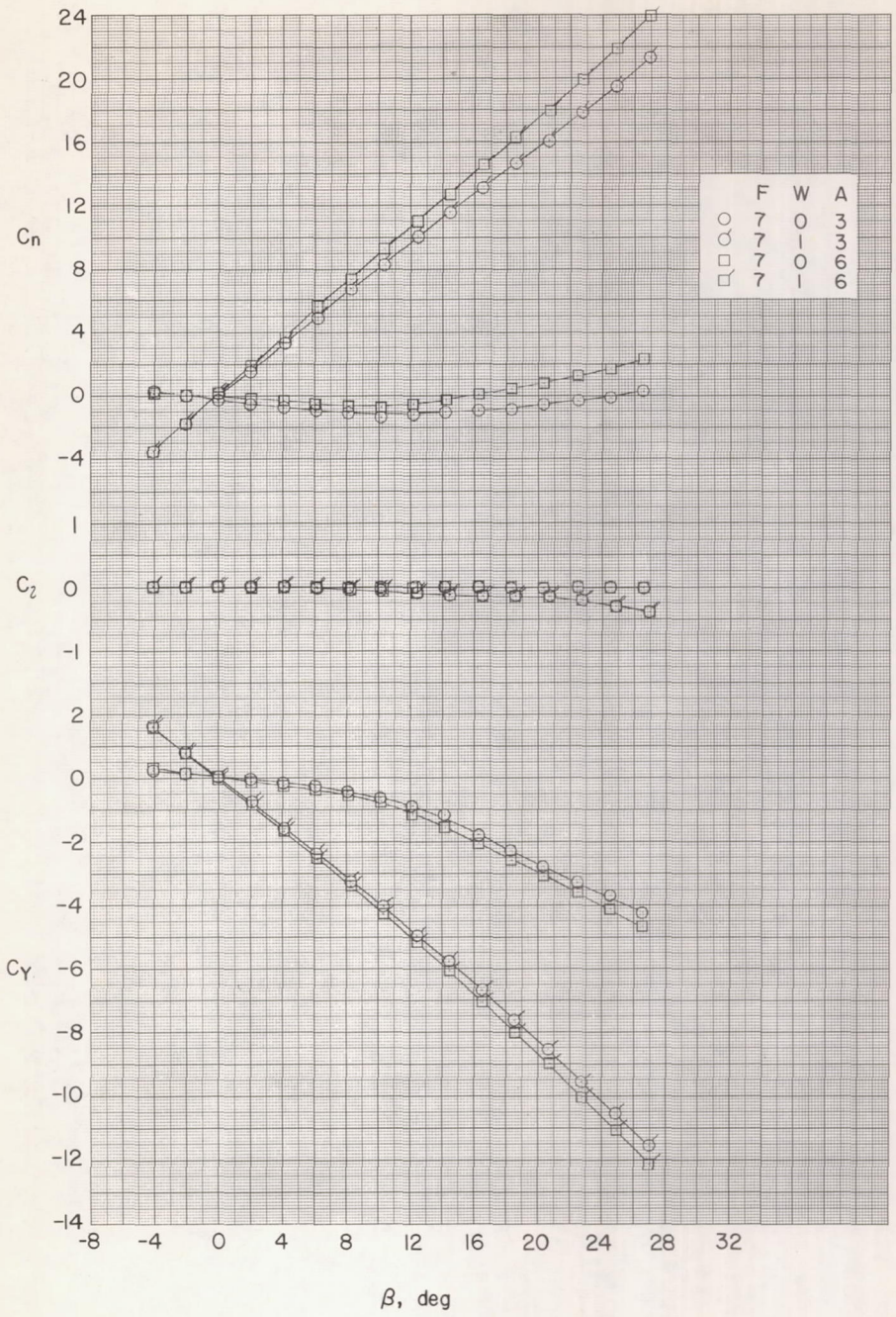


Figure 33.- Effects of 2-diameter boattail (A_5) and 2-caliber flare (A_8) afterbodies on aerodynamic characteristics in pitch. Large delta wings; $l/d = 10$.



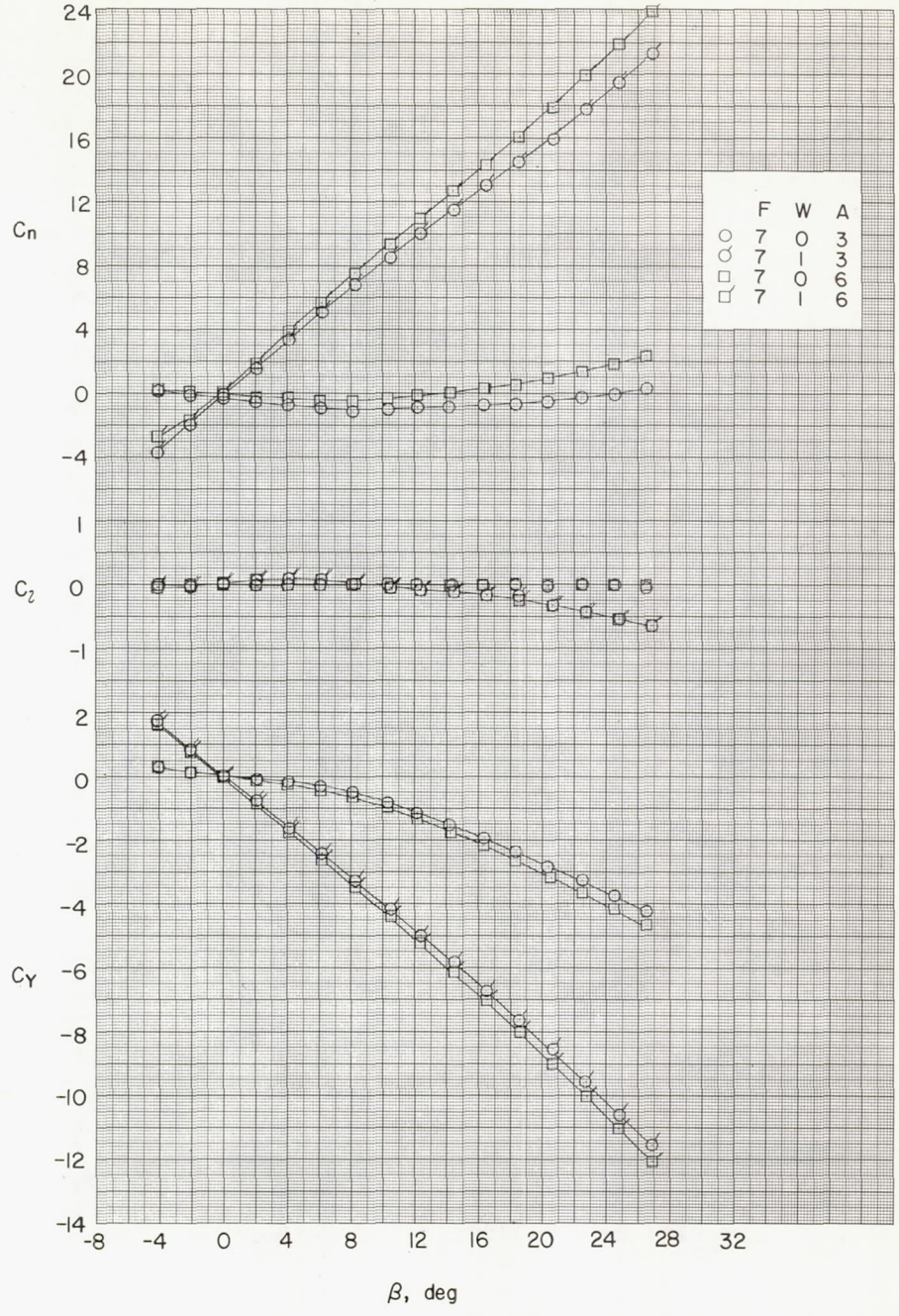
(a) $\alpha \approx 0^{\circ}$.

Figure 34.- Effects of 1-caliber boattail (A_3) and 1-caliber flare (A_6) afterbodies on aerodynamic characteristics in sideslip. Large delta wings; $l/d = 10$.



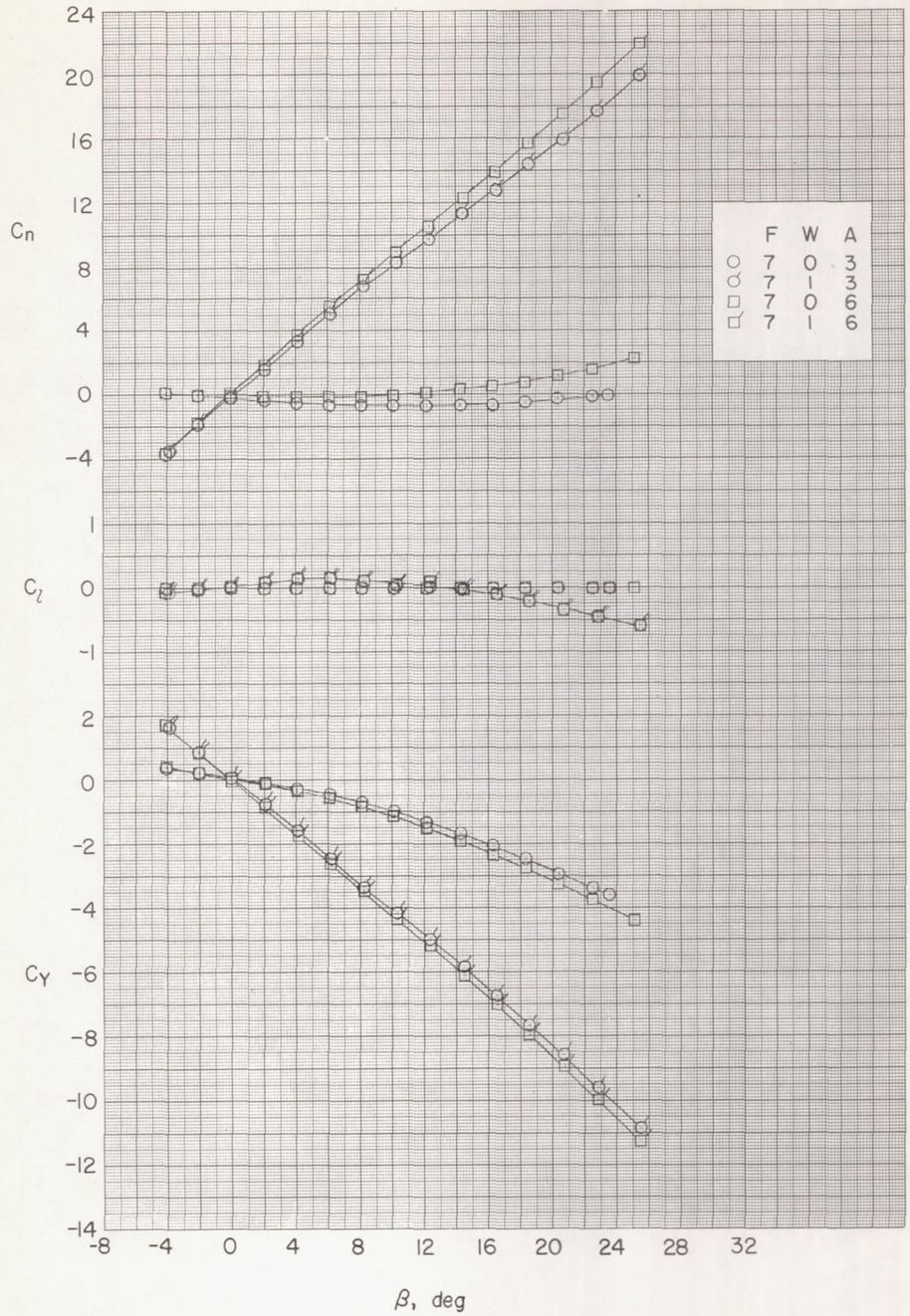
(b) $\alpha \approx 4.1°$.

Figure 34.- Continued.



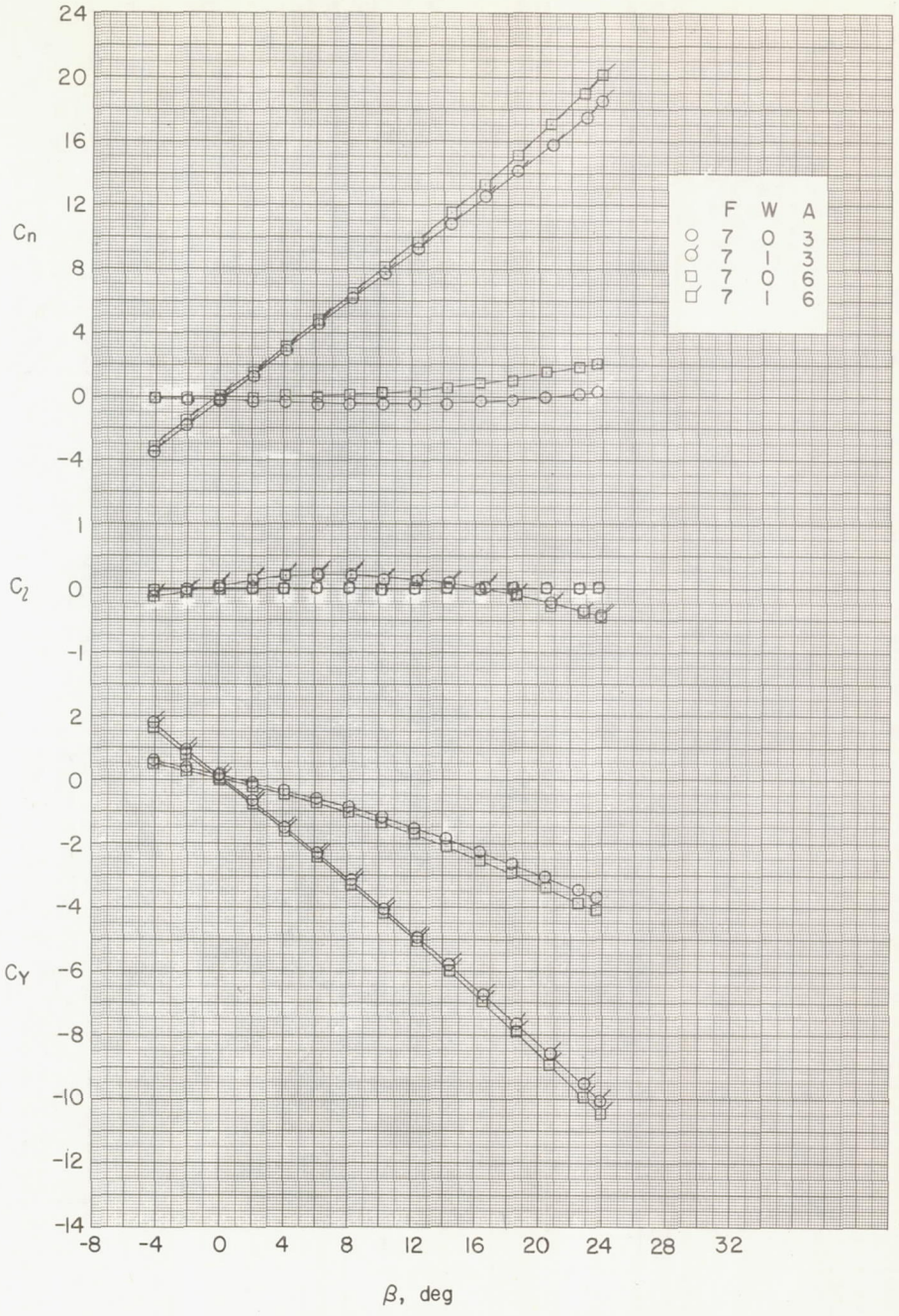
(c) $\alpha \approx 8.2^{\circ}$.

Figure 34.- Continued.



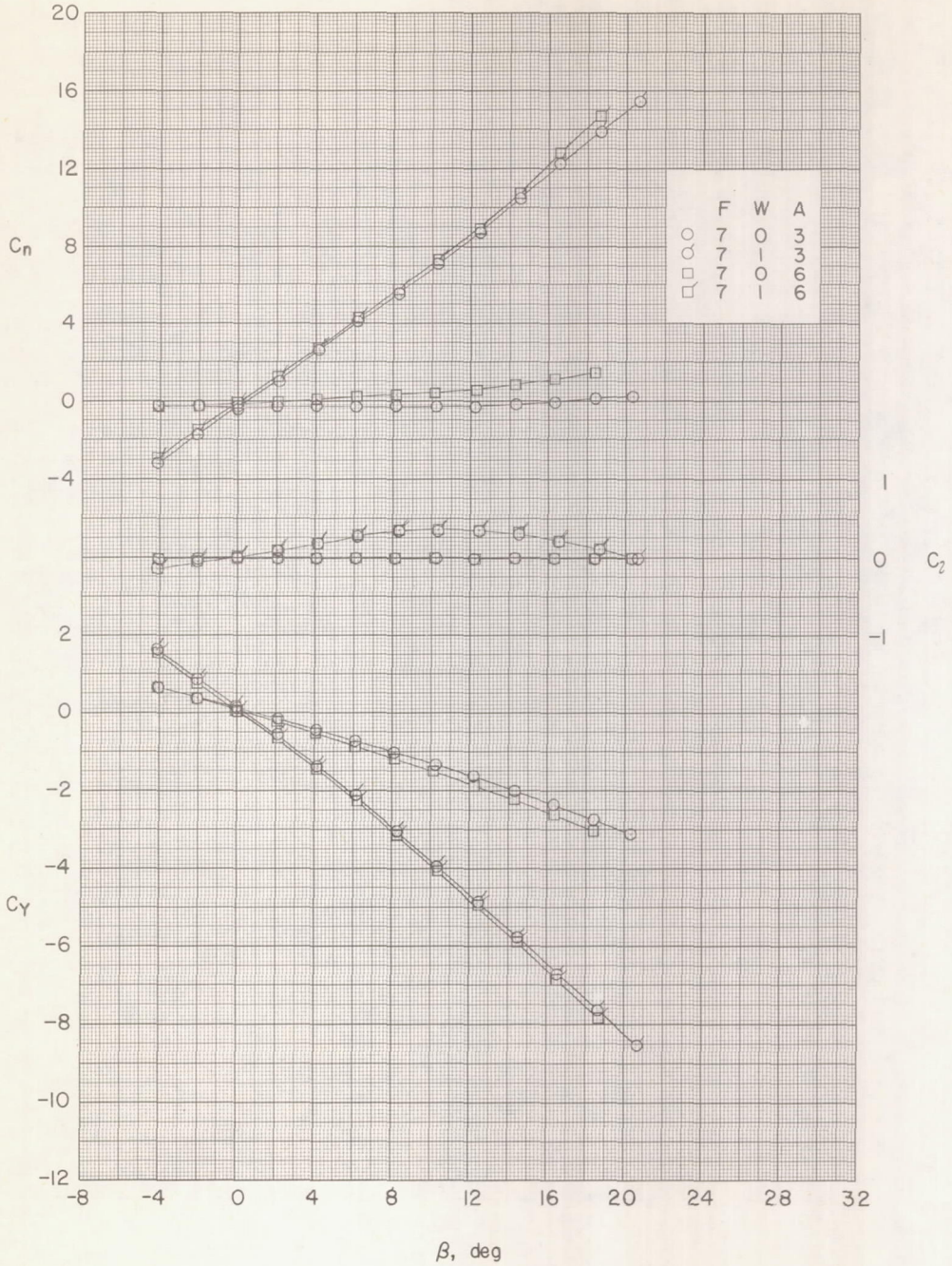
(d) $\alpha \approx 12.3^\circ$.

Figure 34.- Continued.



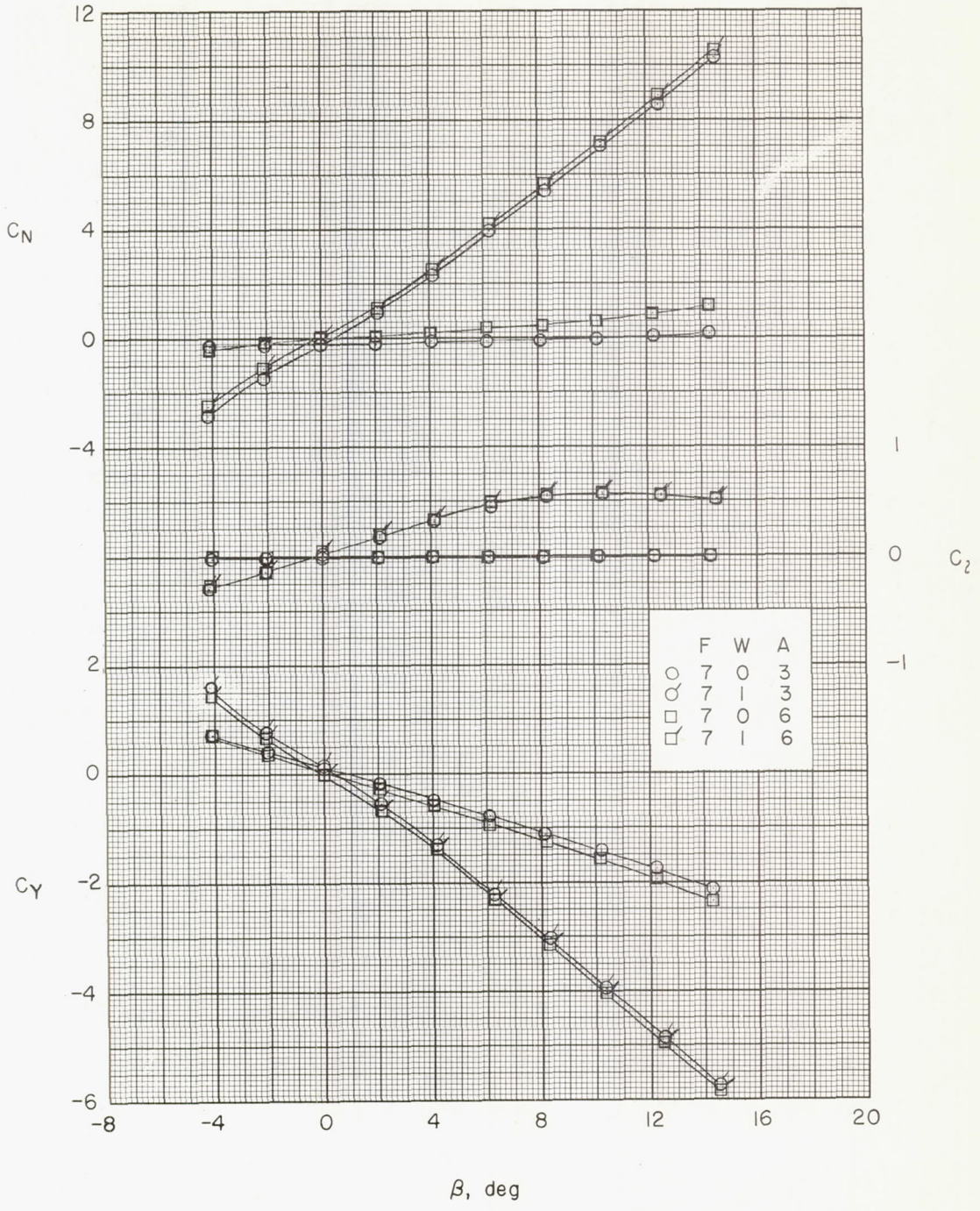
(e) $\alpha \approx 16.4^{\circ}$.

Figure 34.- Continued.



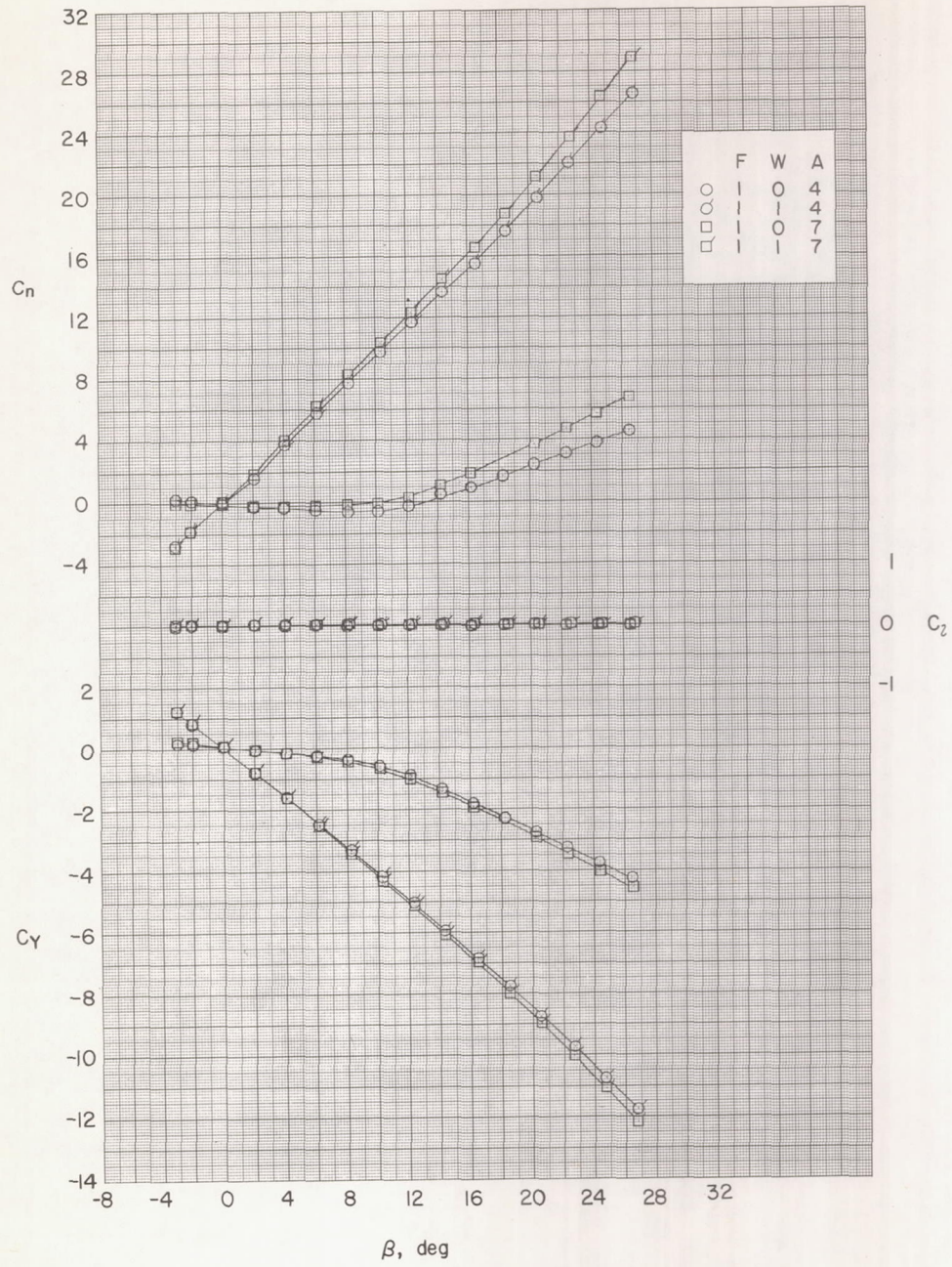
(f) $\alpha \approx 20.5^\circ$.

Figure 34.- Continued.



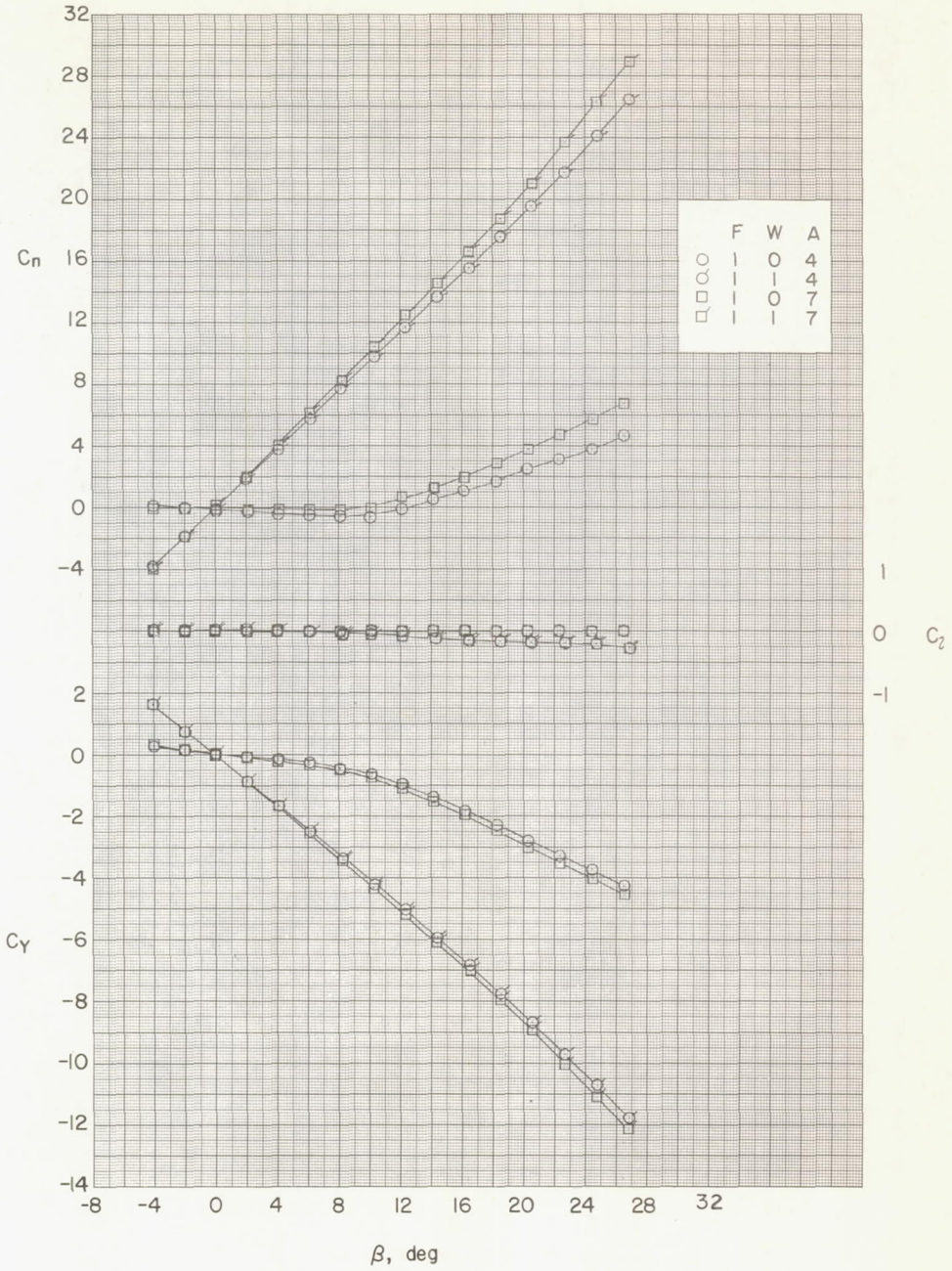
(g) $\alpha \approx 24.7°$.

Figure 34.- Concluded.



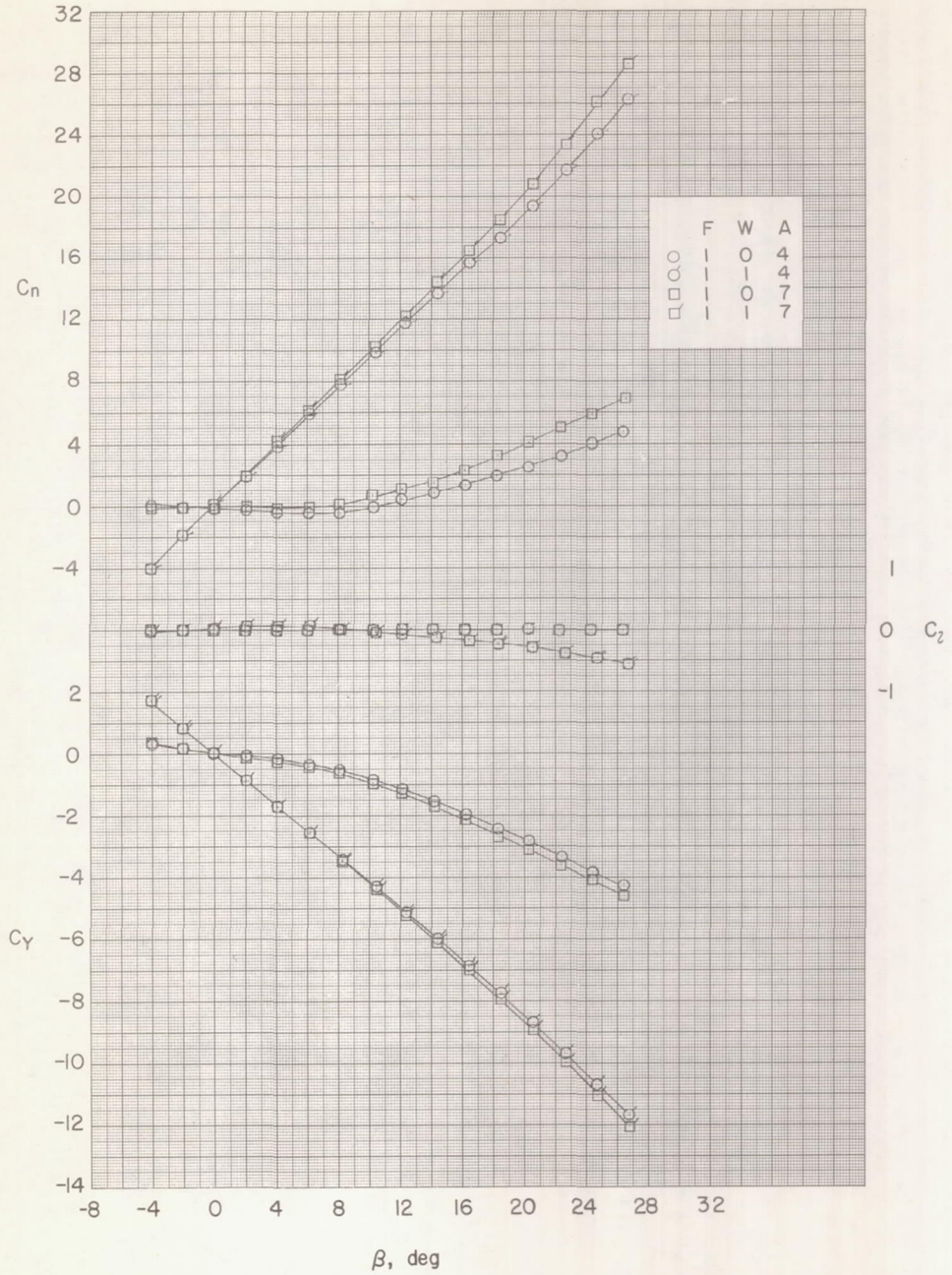
(a) $\alpha \approx 0^\circ$.

Figure 35.- Effects of 2-caliber cylinder-boattail (A_4) and 2-caliber cylinder-flare (A_6) afterbodies on aerodynamic characteristics in sideslip. Large delta wings; $l/d = 10$.



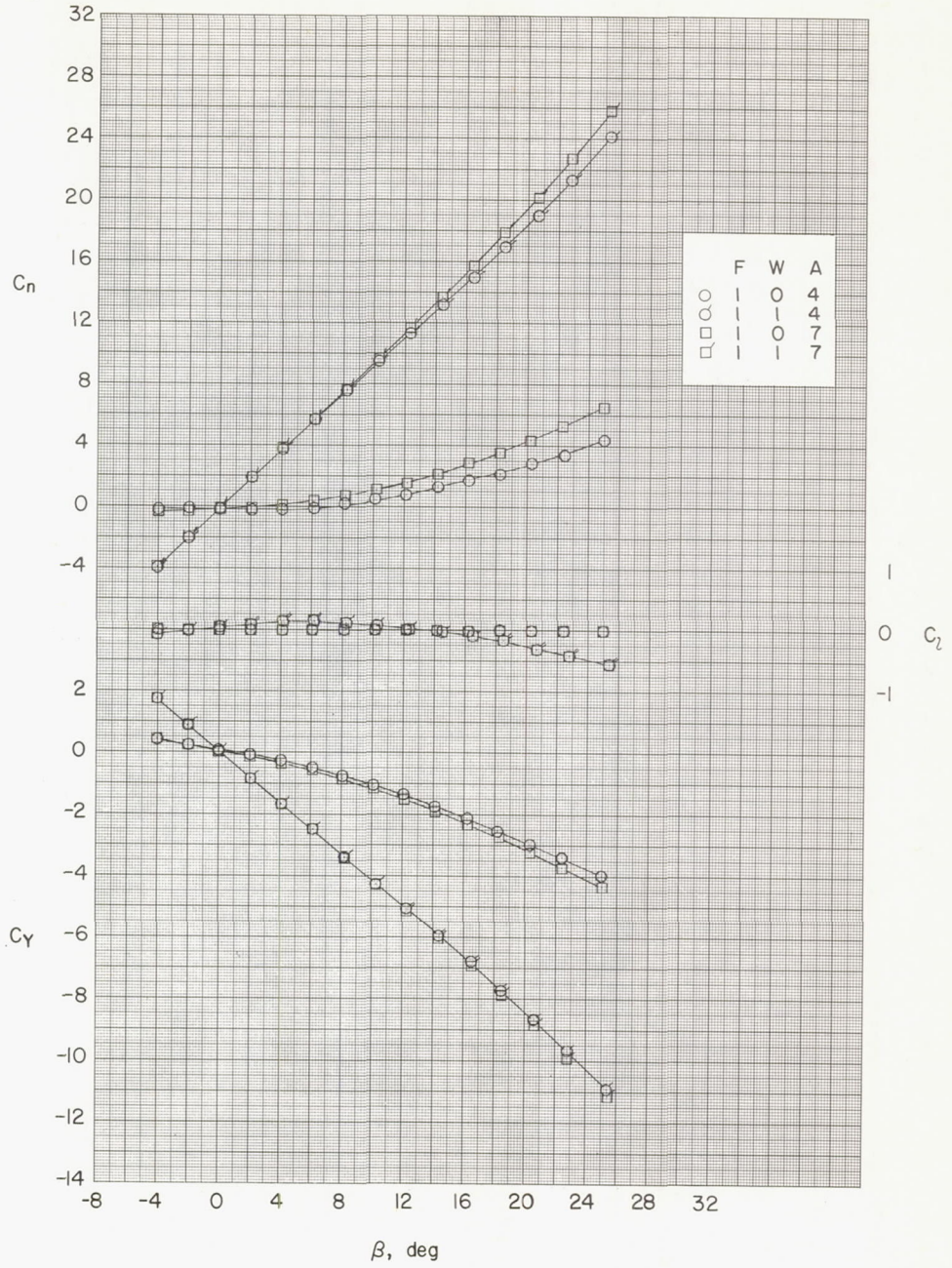
(b) $\alpha \approx 4.1^\circ$.

Figure 35.- Continued.



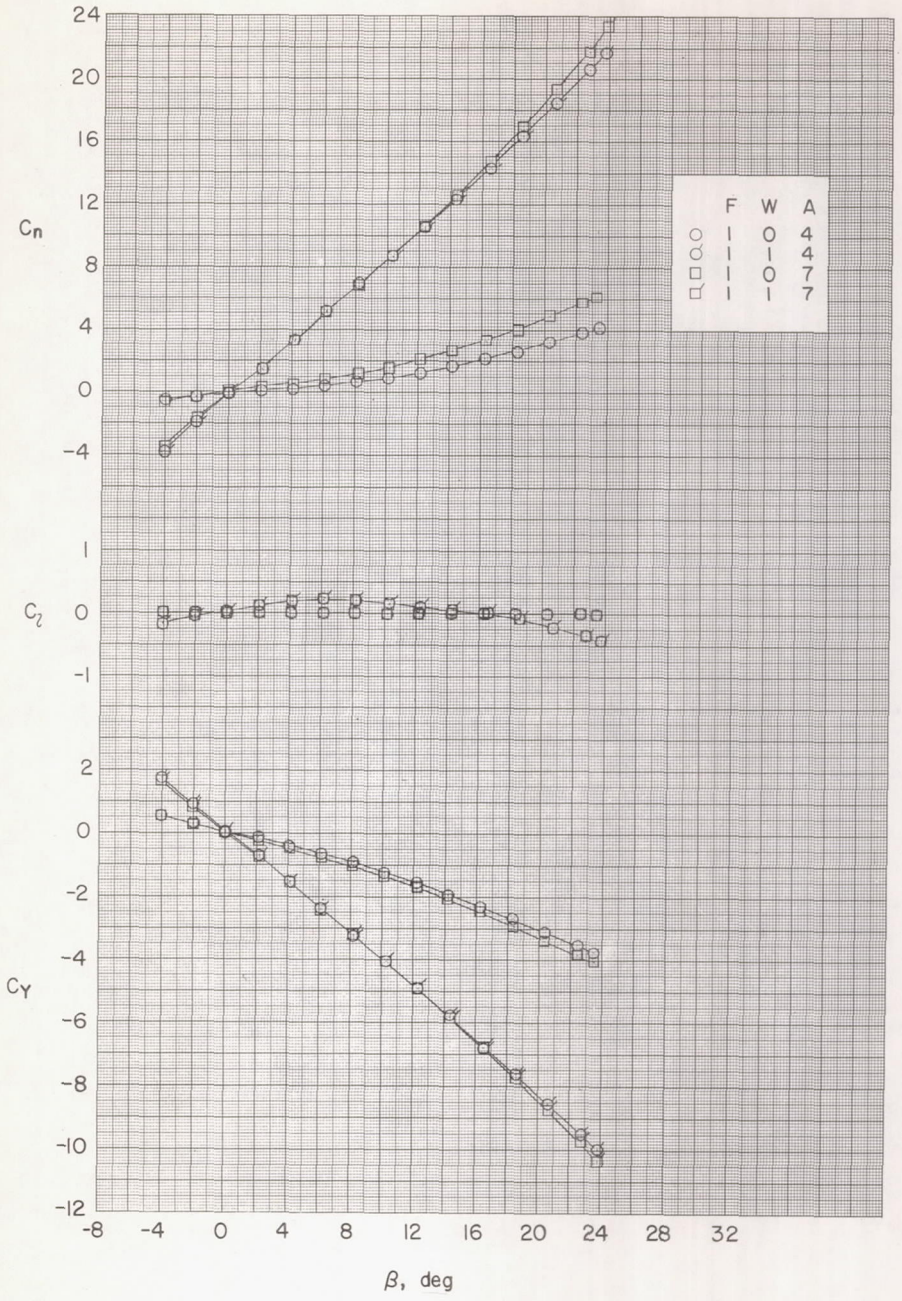
(c) $\alpha \approx 8.2^{\circ}$.

Figure 35.- Continued.



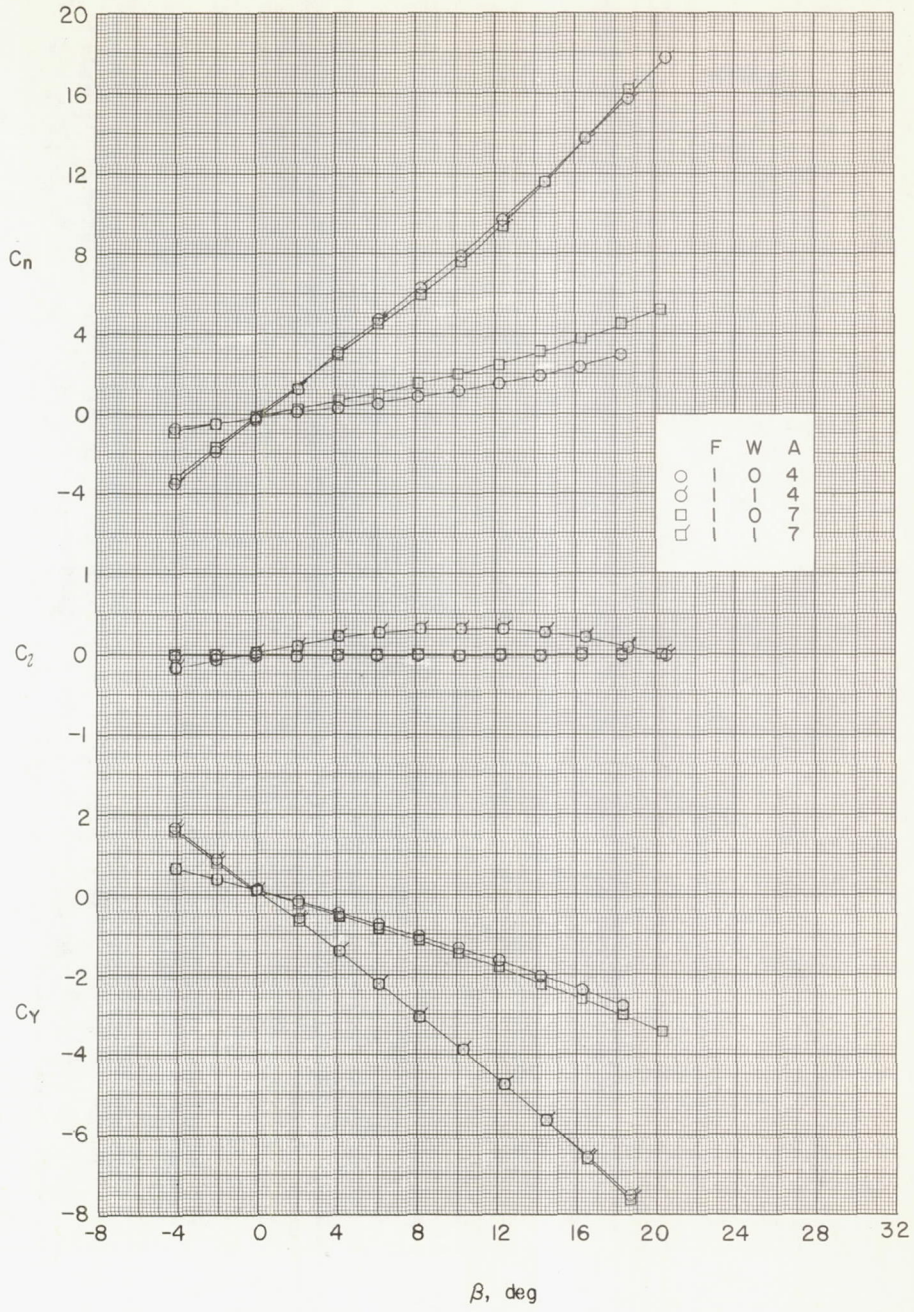
(d) $\alpha \approx 12.3^\circ$.

Figure 35.- Continued.



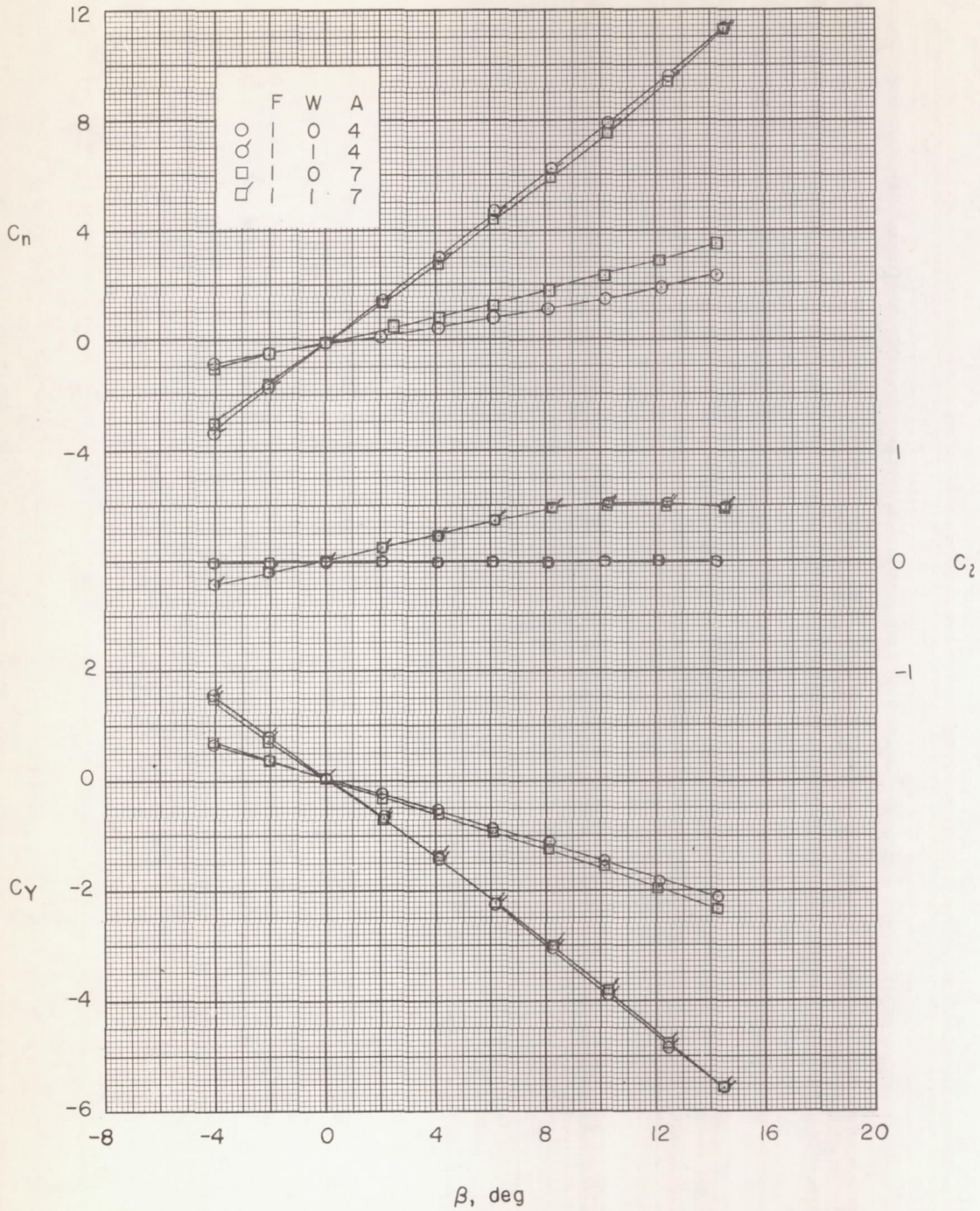
(e) $\alpha \approx 16.4^\circ$.

Figure 35.- Continued.



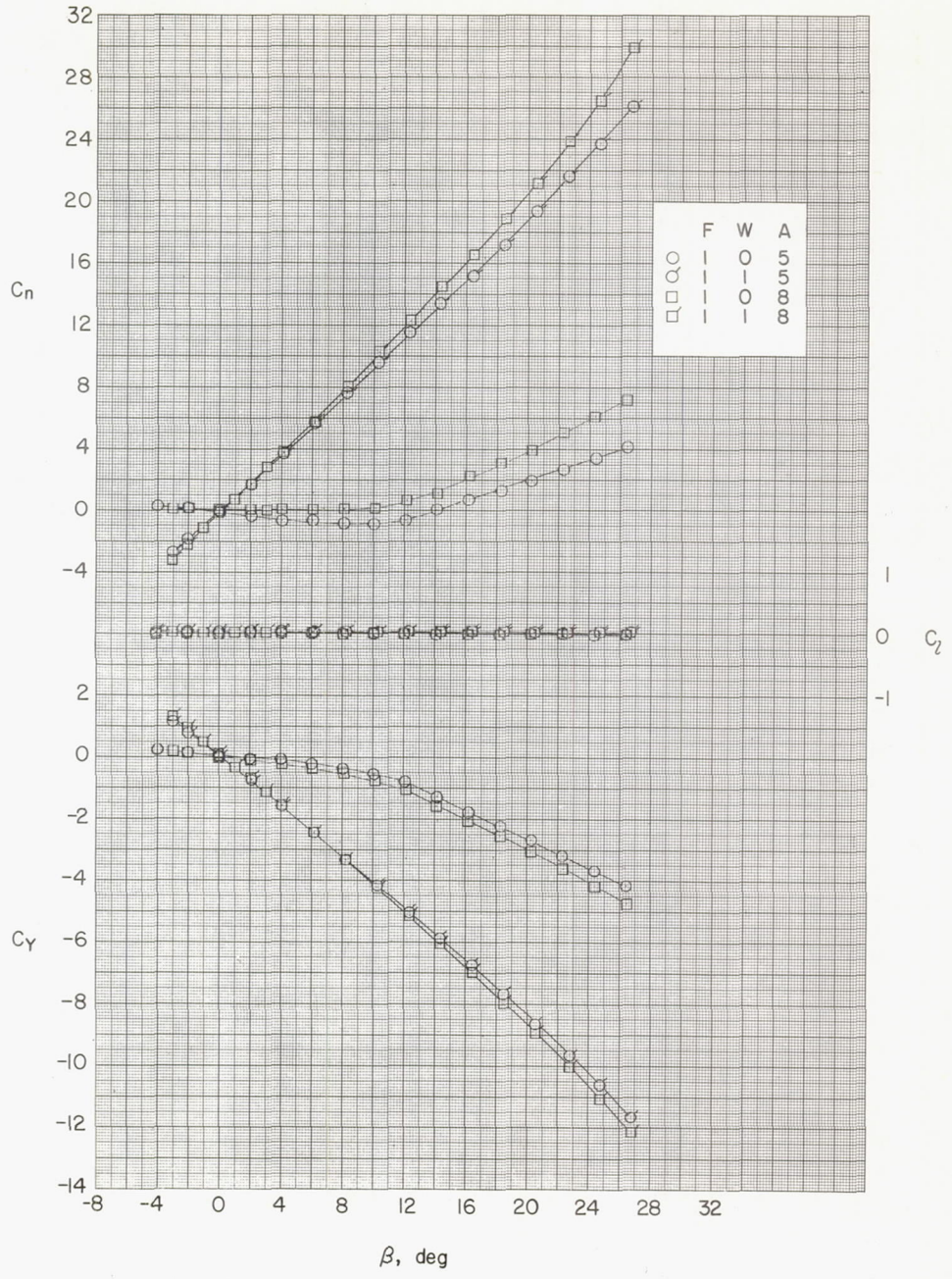
(f) $\alpha \approx 20.5^{\circ}$.

Figure 35.- Continued.



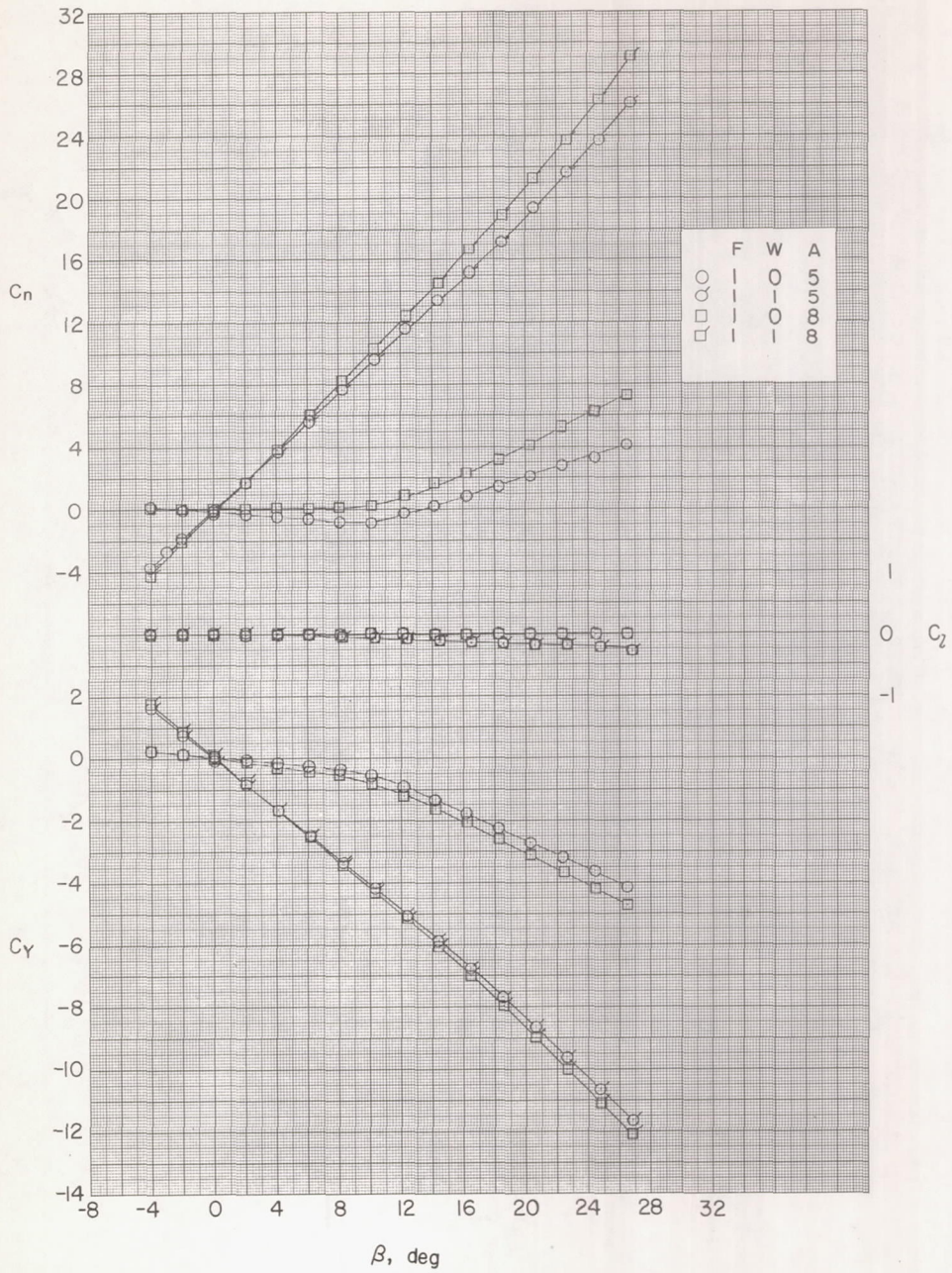
(g) $\alpha \approx 24.7^\circ$.

Figure 35.- Concluded.



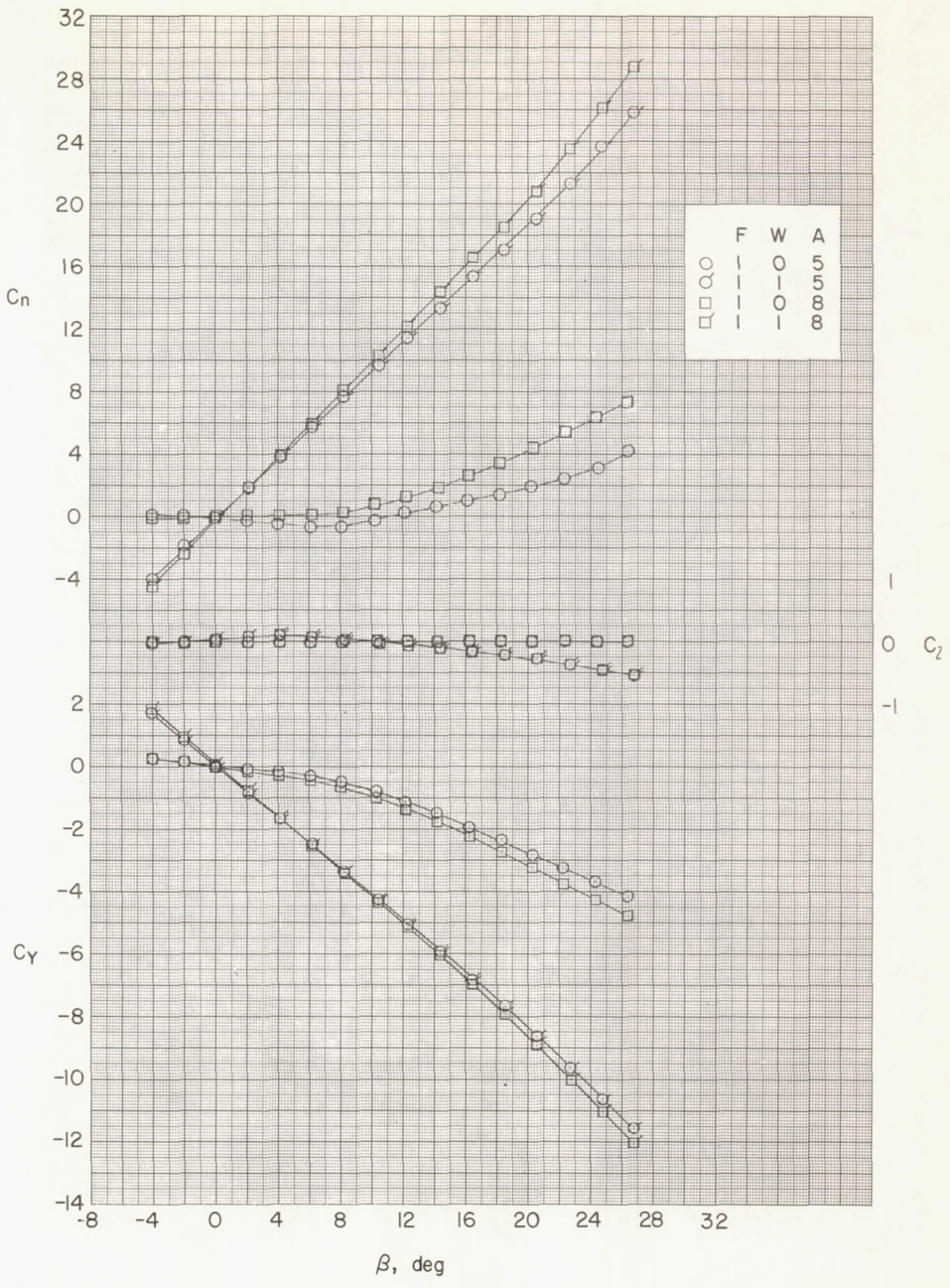
(a) $\alpha \approx 0^\circ$.

Figure 36.- Effects of 2-caliber boattail (A_5) and 2-caliber flare (A_8) afterbodies on the aerodynamic characteristics in sideslip. Large delta wings; $l/D = 10$.



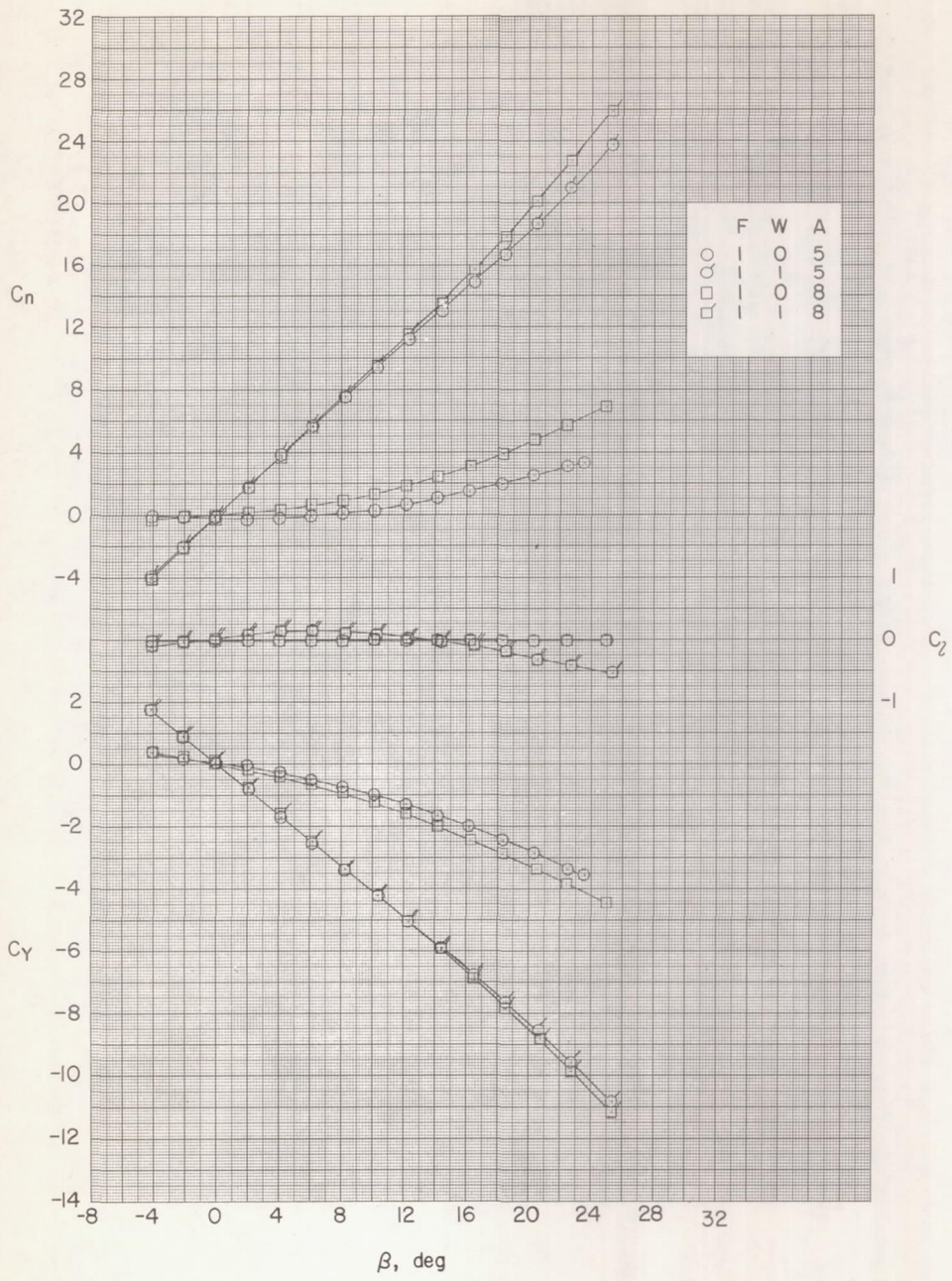
(b) $\alpha \approx 4.1^\circ$.

Figure 36.- Continued.



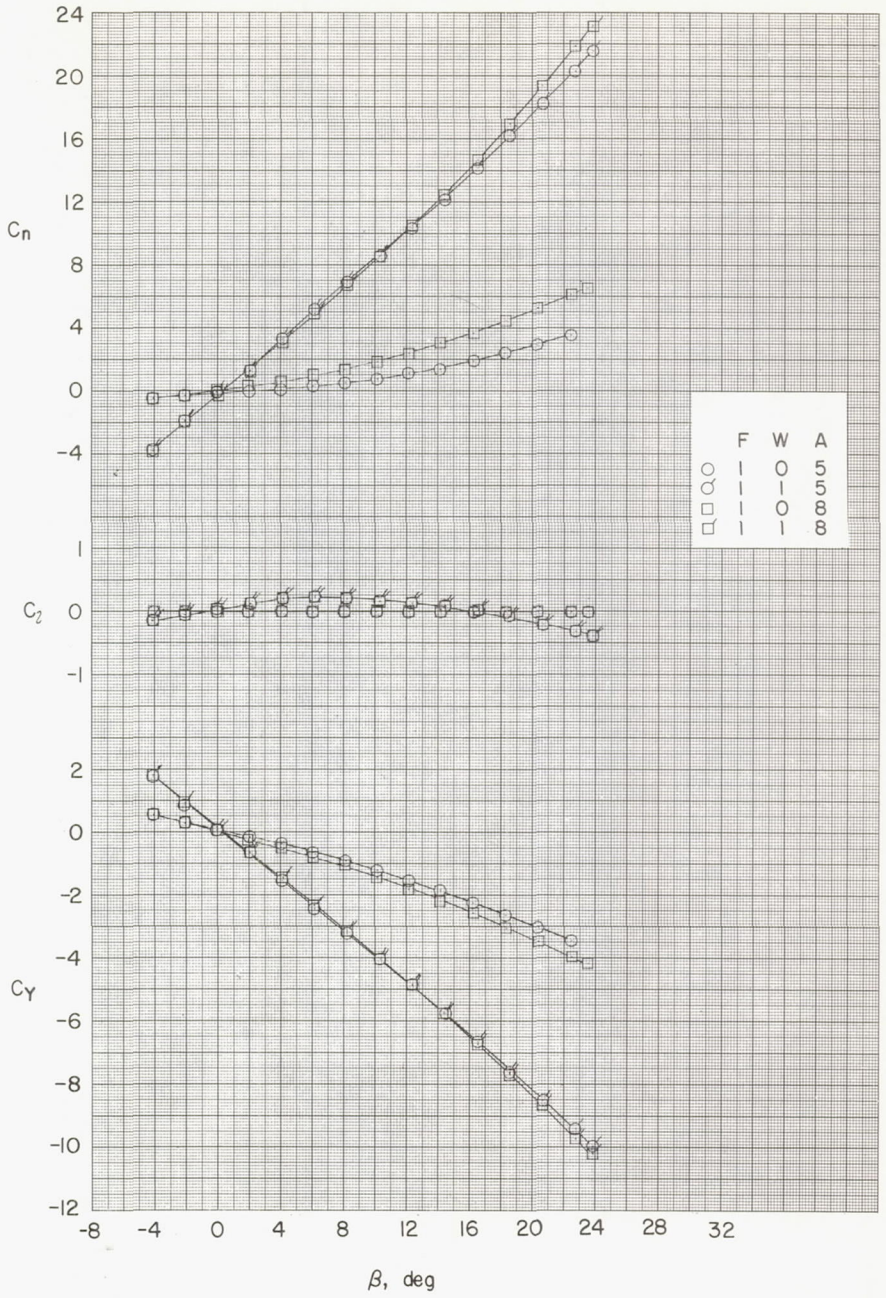
(c) $\alpha \approx 8.2^{\circ}$.

Figure 36.- Continued.



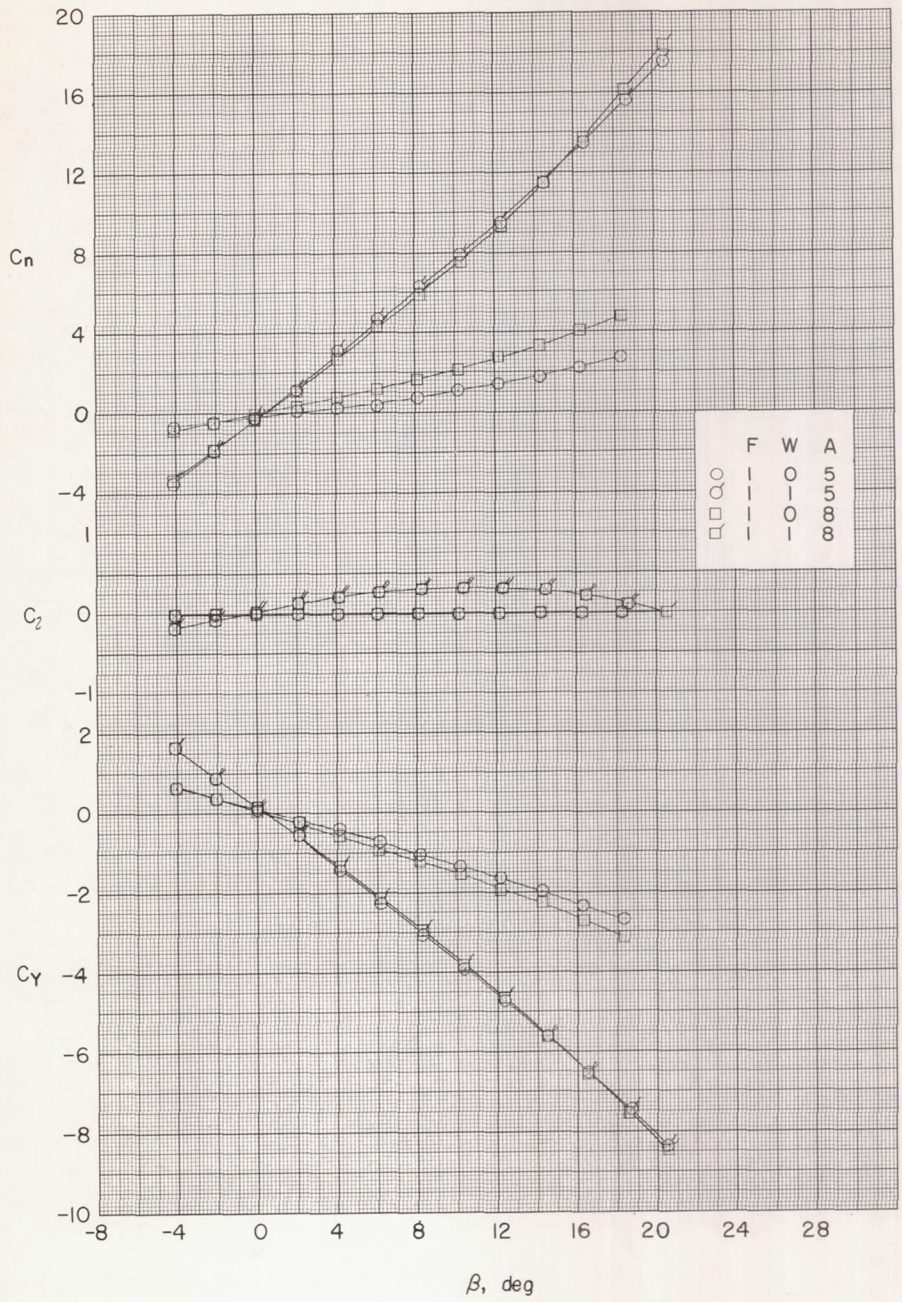
(d) $\alpha \approx 12.3^{\circ}$.

Figure 36.- Continued.



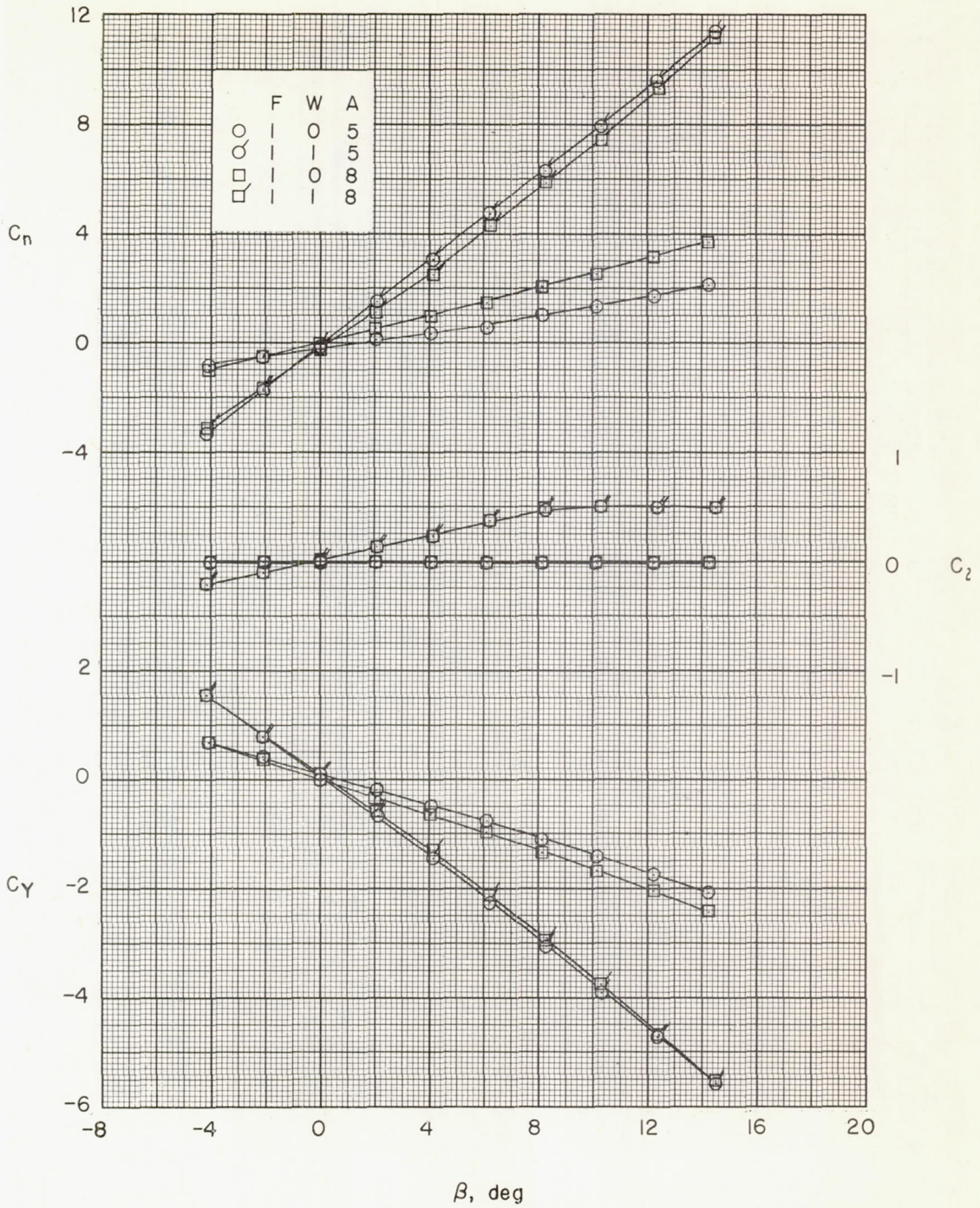
(e) $\alpha \approx 16.4^\circ$.

Figure 36.- Continued.



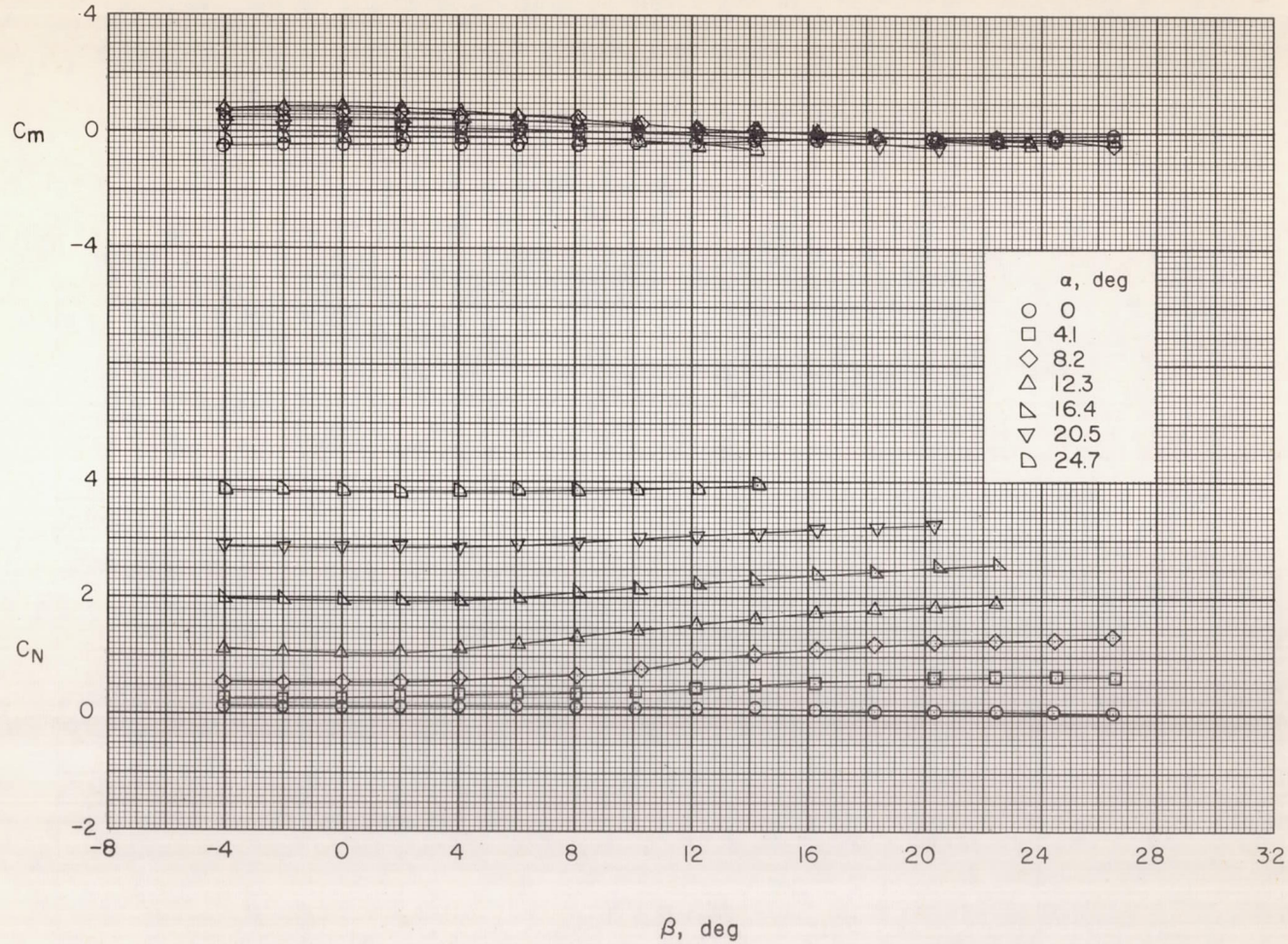
(f) $\alpha \approx 20.5^{\circ}$.

Figure 36.- Continued.



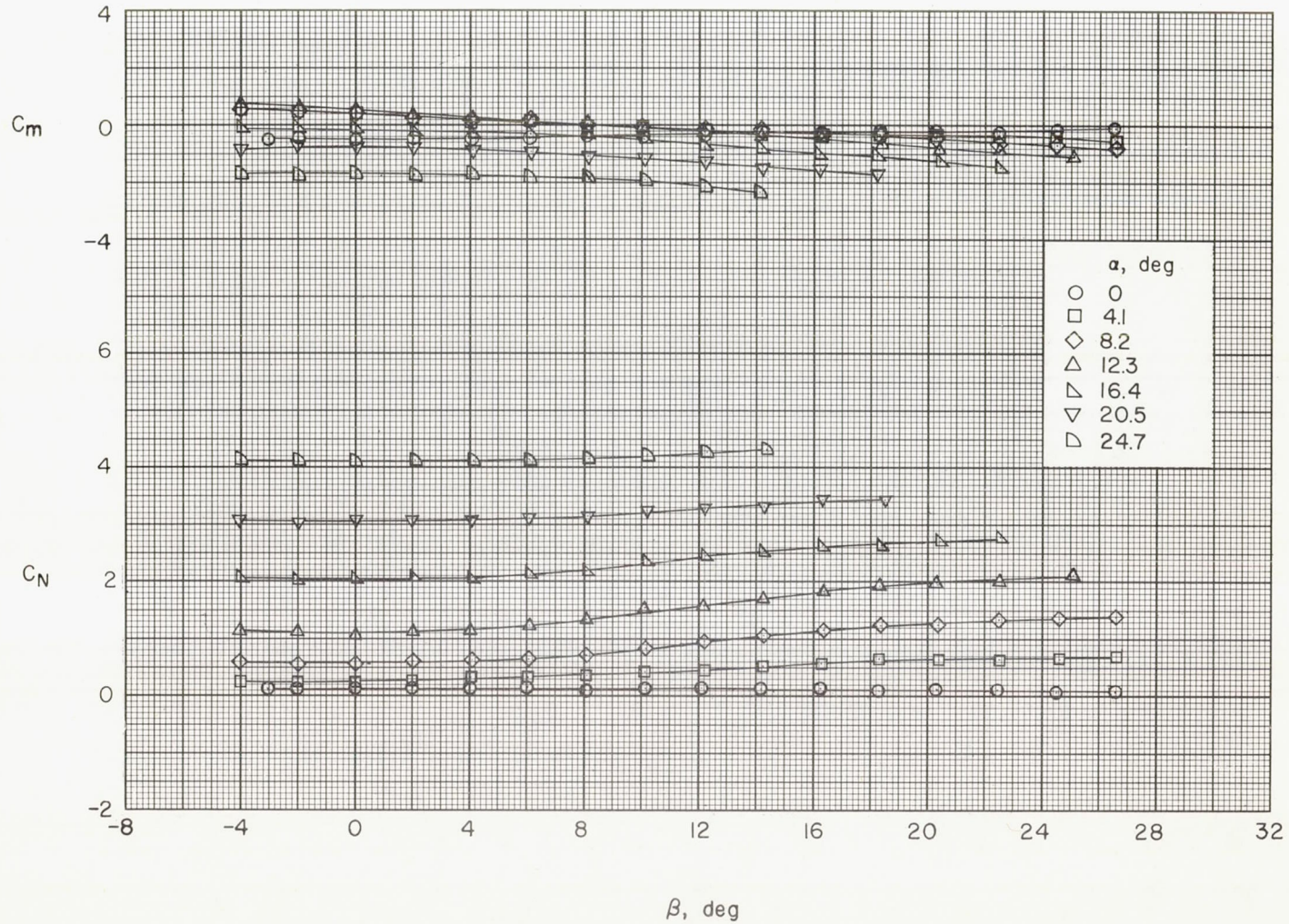
(g) $\alpha \approx 24.7^\circ$.

Figure 36.- Concluded.



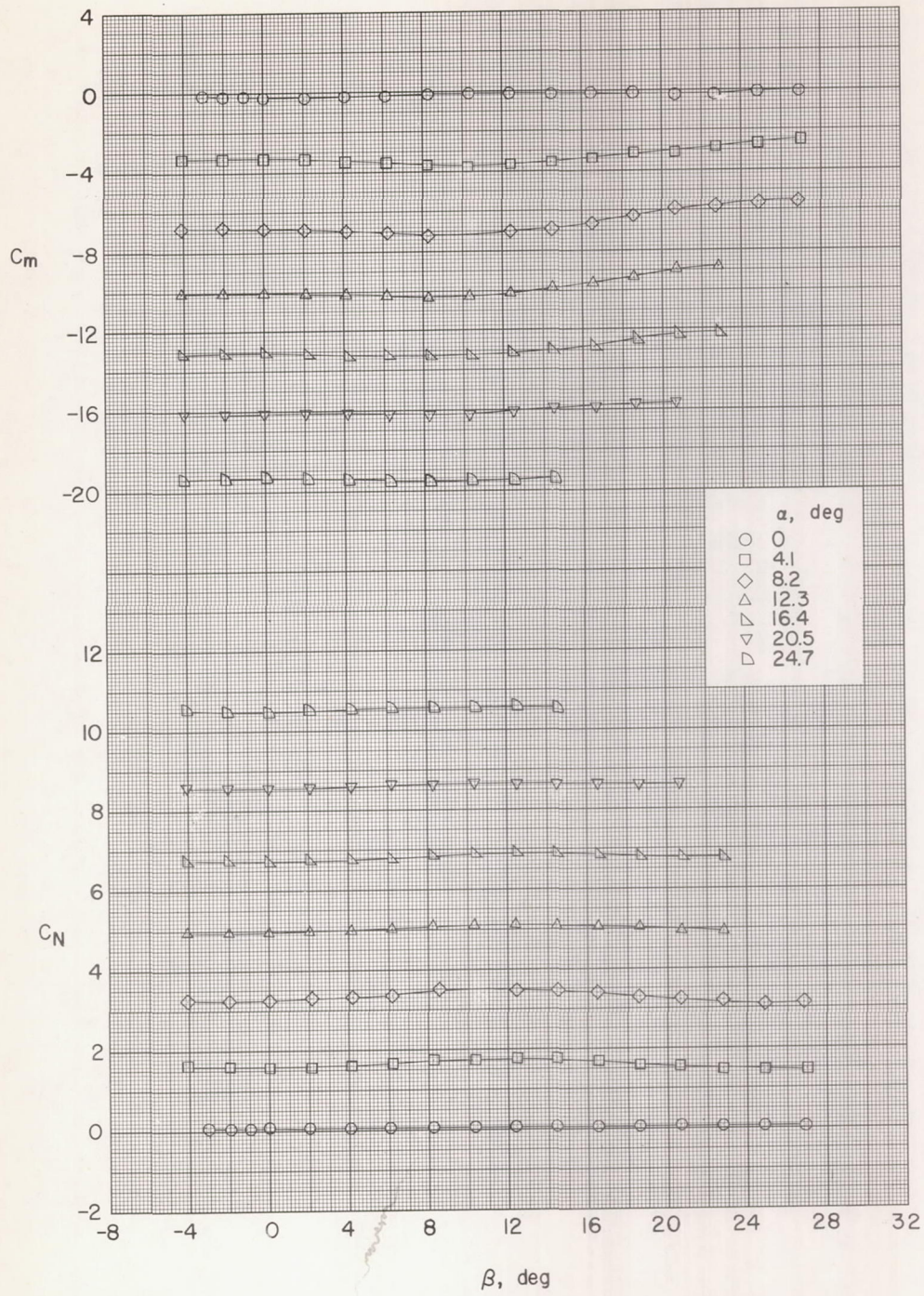
(a) Body alone, $F_7W_0A_3$.

Figure 37.- Variation of C_m and C_N with β for various angles of attack. One-caliber boattail (A_3) and 1-caliber flare (A_6) afterbodies; large delta wings; $l/d = 10$.



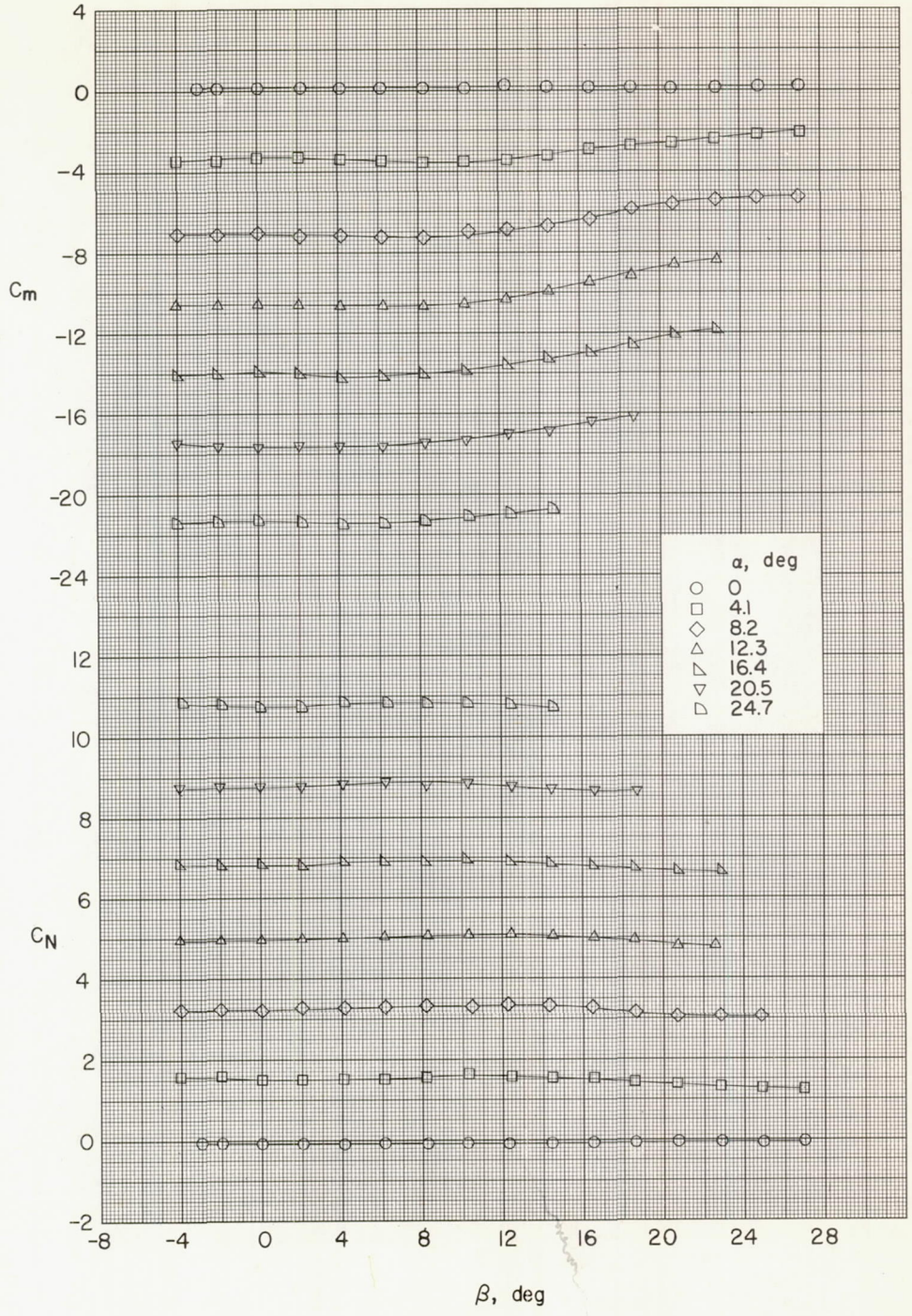
(b) Body alone, $F_7W_0A_6$.

Figure 37.- Continued.



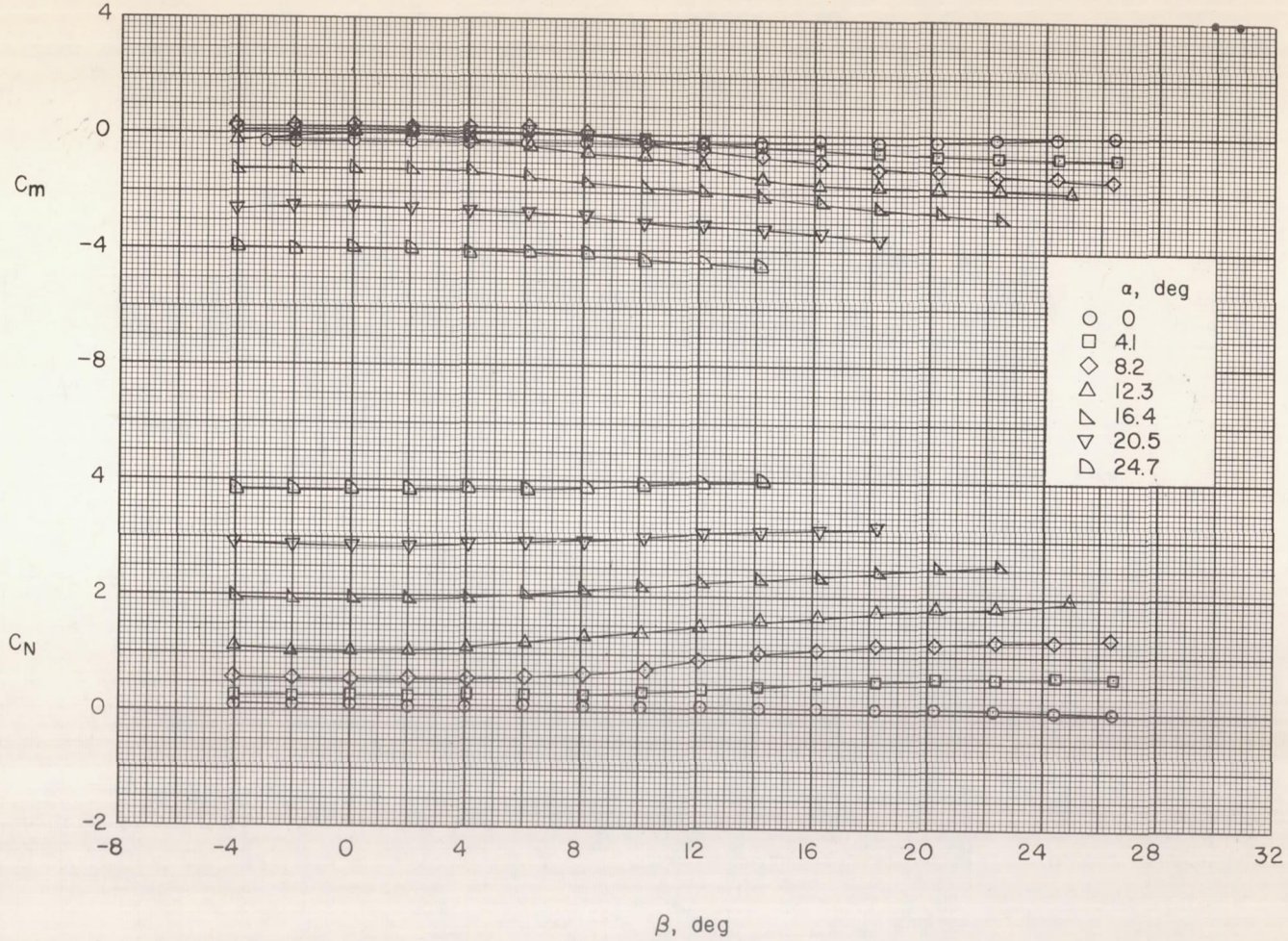
(c) Large delta wing, $F_7W_0A_3$.

Figure 37.- Continued.



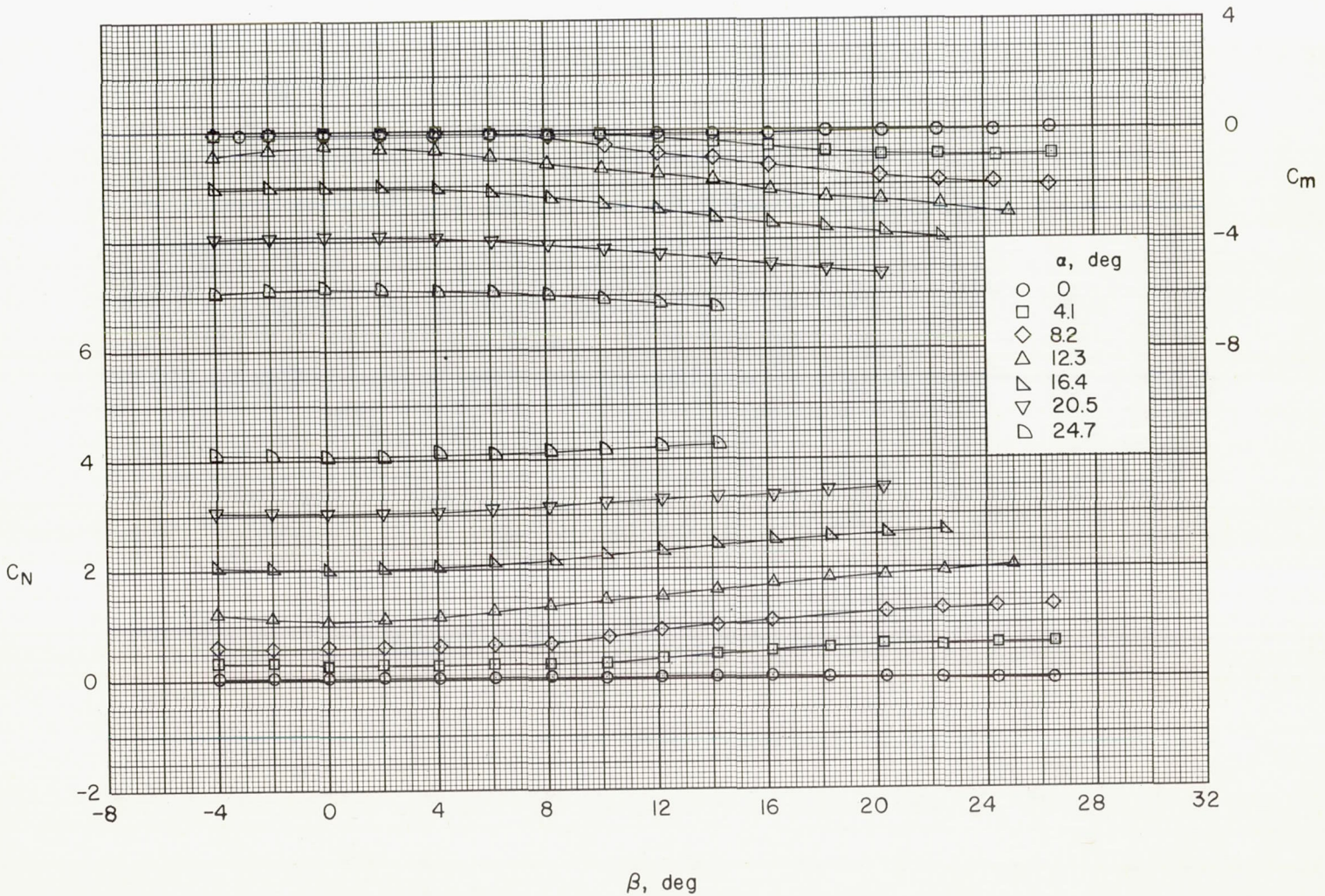
(d) Large delta wing, $F_7W_1A_6$.

Figure 37.- Concluded.



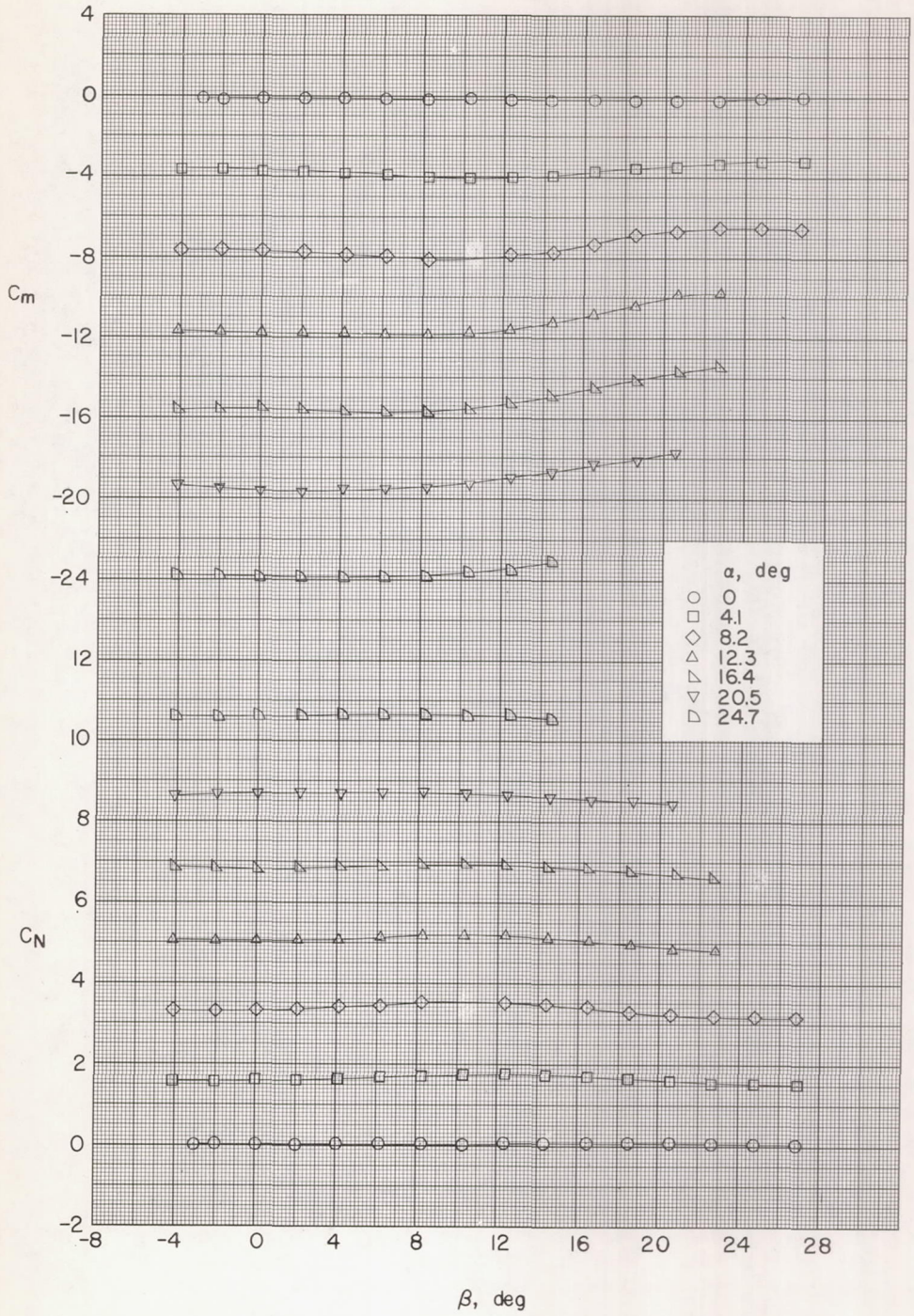
(a) Body alone, $F_1W_0A_4$.

Figure 38.- Variation of C_m and C_N with β for various angles of attack. Two-caliber cylinder-boattail (A_4) and 2-caliber cylinder-flare (A_7) afterbodies; large delta wings; $l/d = 10$.



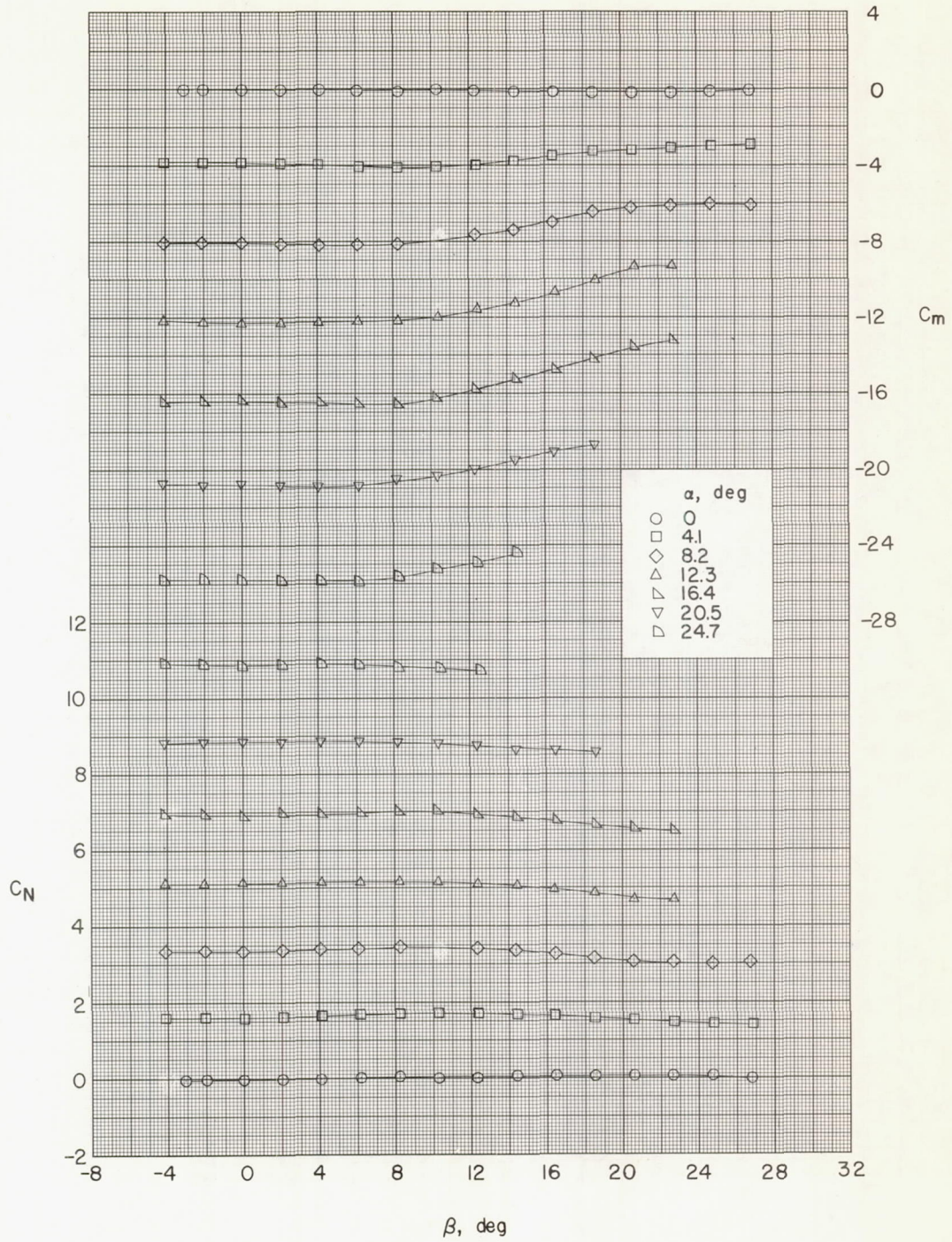
(b) Body alone, $F_1W_0A_7$.

Figure 38.- Continued.



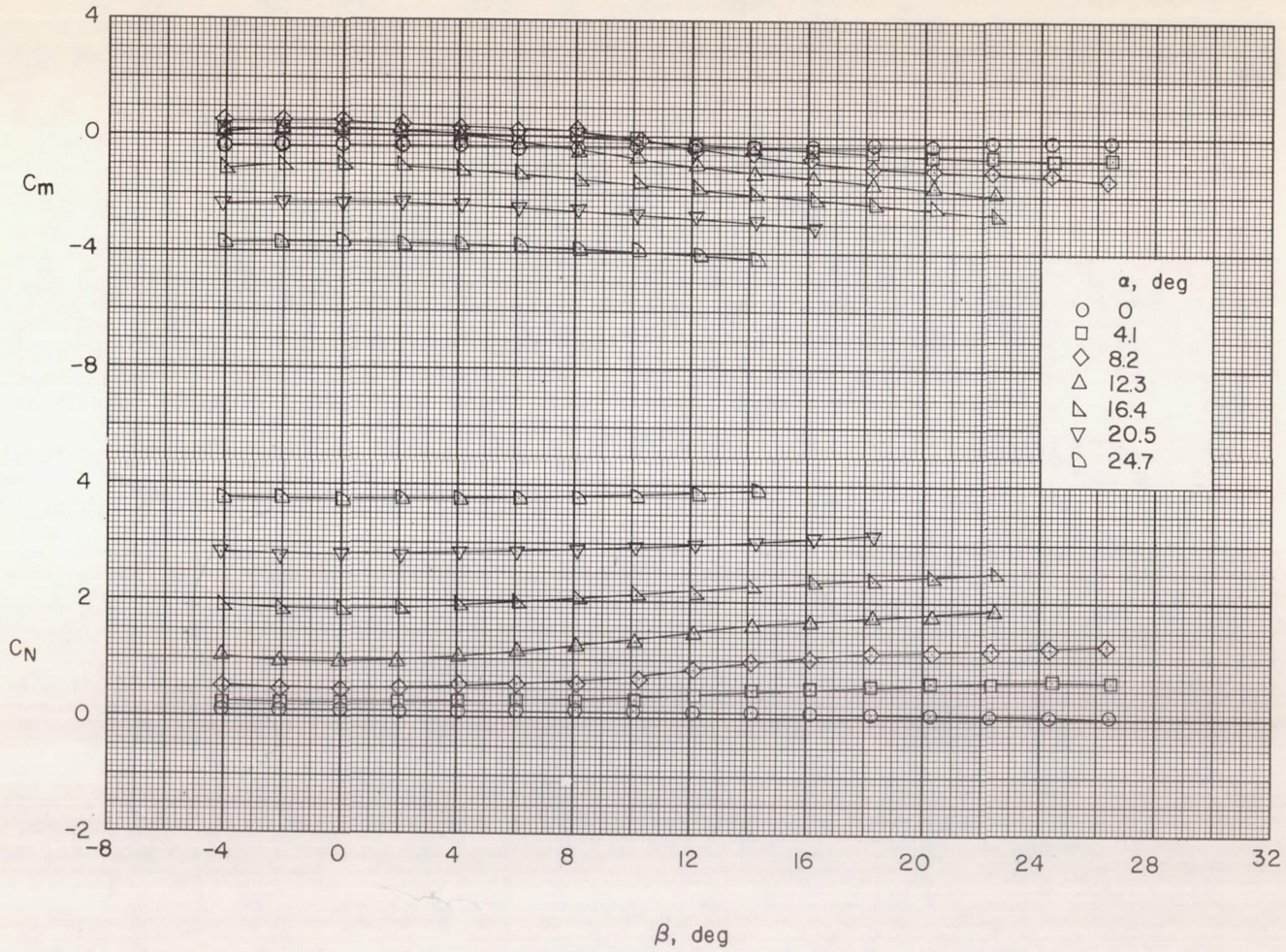
(c) Large delta wing, $F_1W_1A_4$.

Figure 38.- Continued.



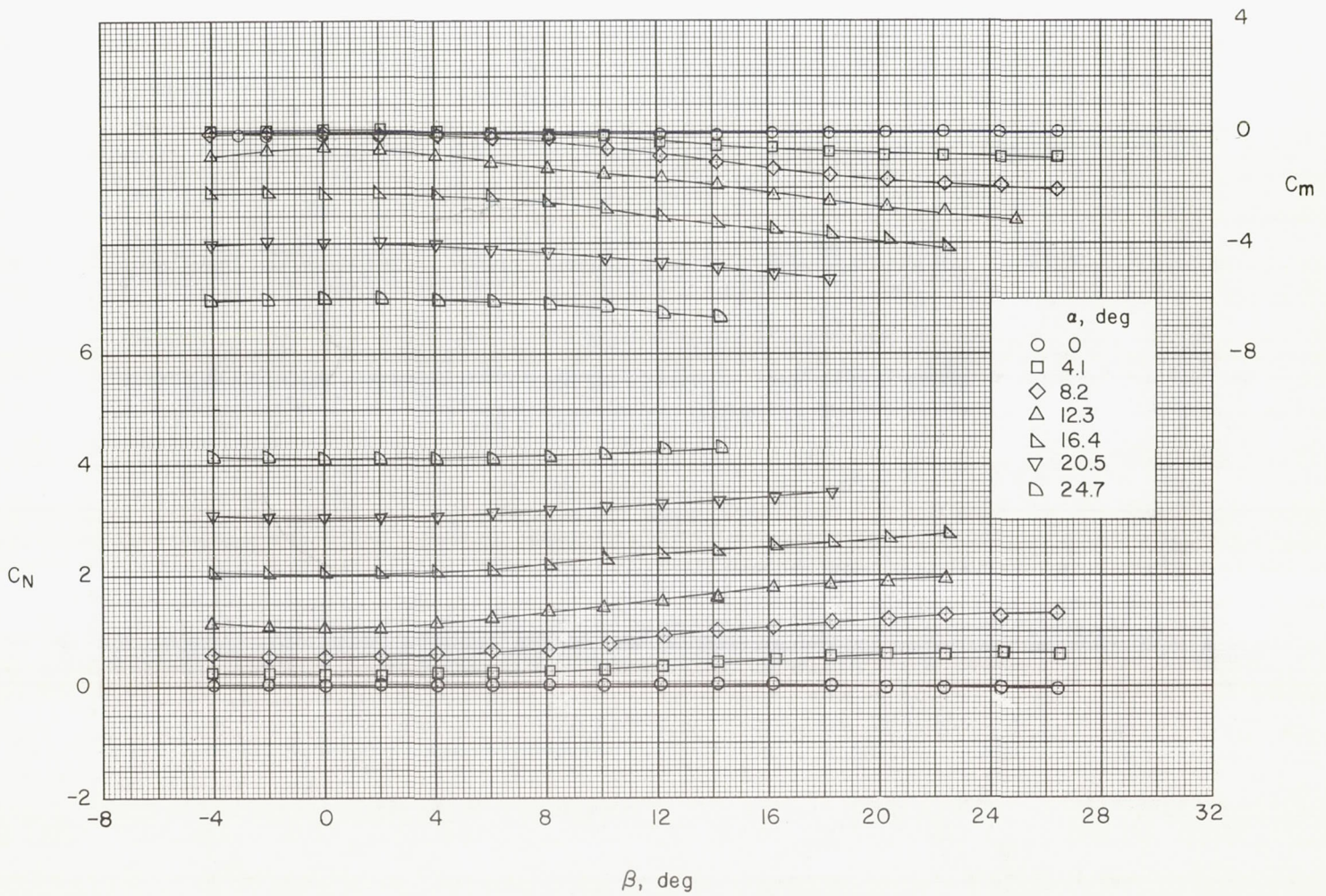
(d) Large delta wing, $F_1W_1A_7$.

Figure 38.- Concluded.



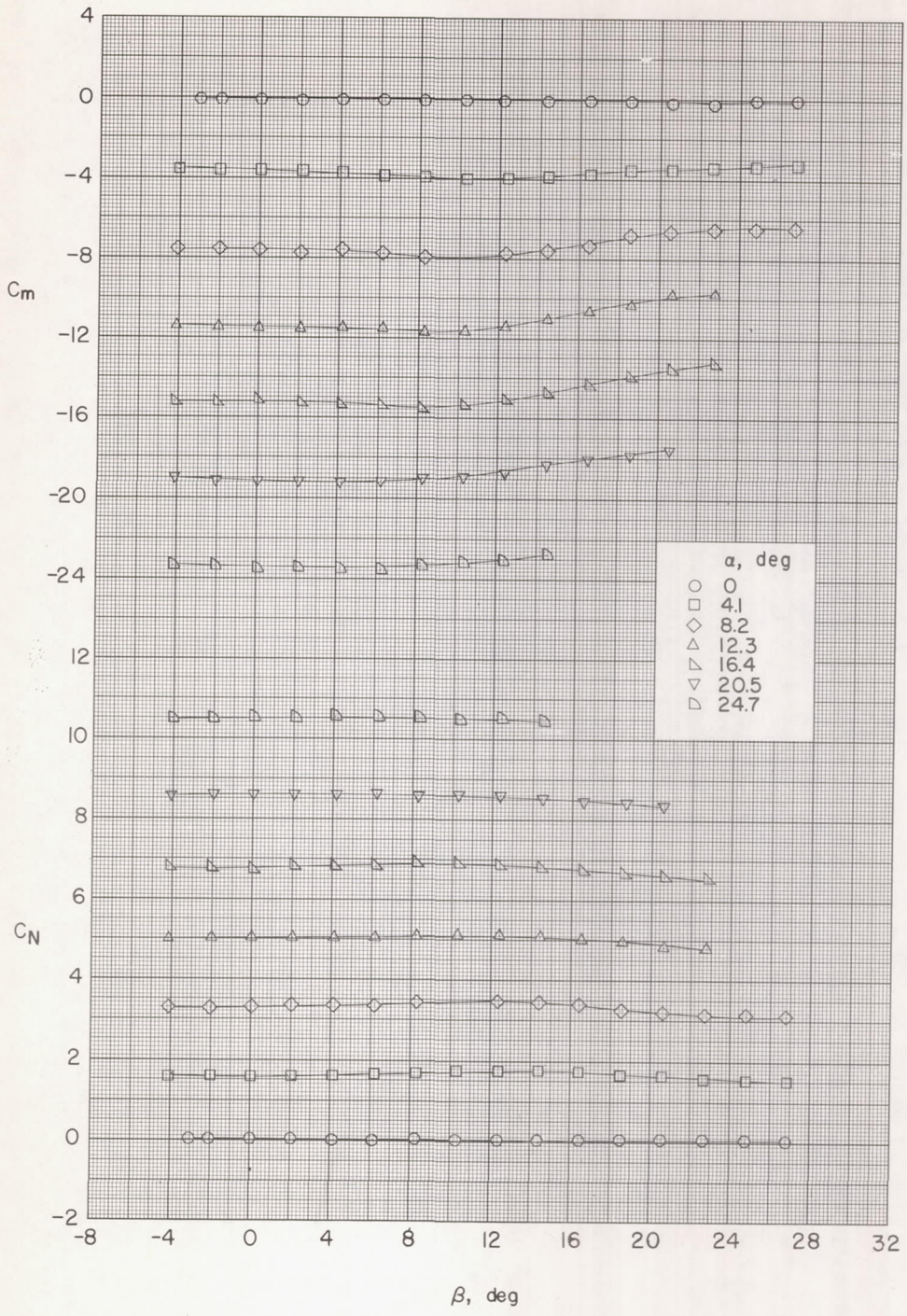
(a) Body alone, $F_1W_0A_5$.

Figure 39.- Variation of C_m and C_N with β for various angles of attack. Two-caliber boattail (A_5) and 2-caliber flare (A_8) afterbodies; large delta wings; l/d = 10.



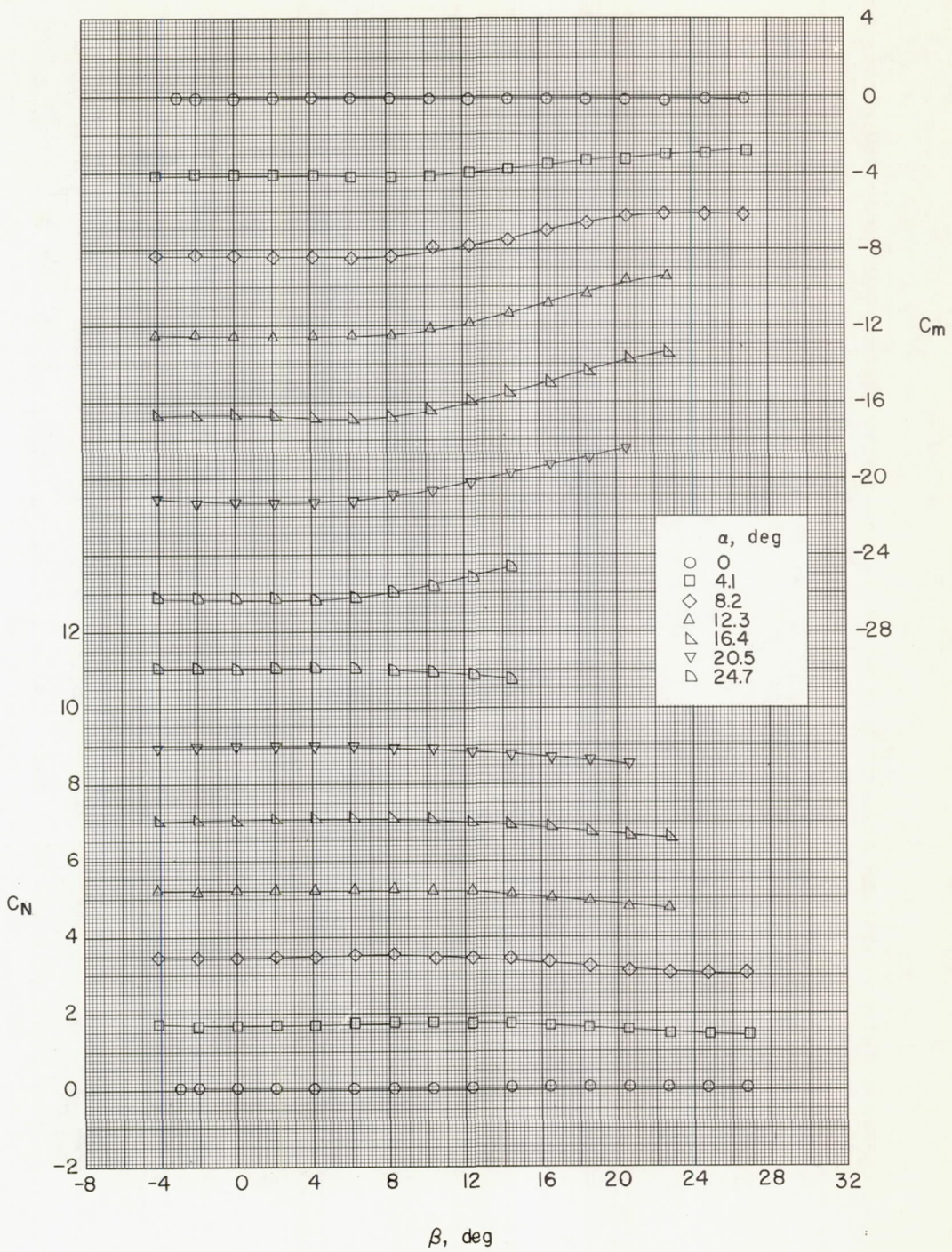
(b) Body alone, $F_1W_0A_8$.

Figure 39.- Continued.



(c) Large delta wing, $F_1W_1A_5$.

Figure 39.- Continued.



(d) Large delta wing, $F_1W_1A_8$.

Figure 39.- Concluded.

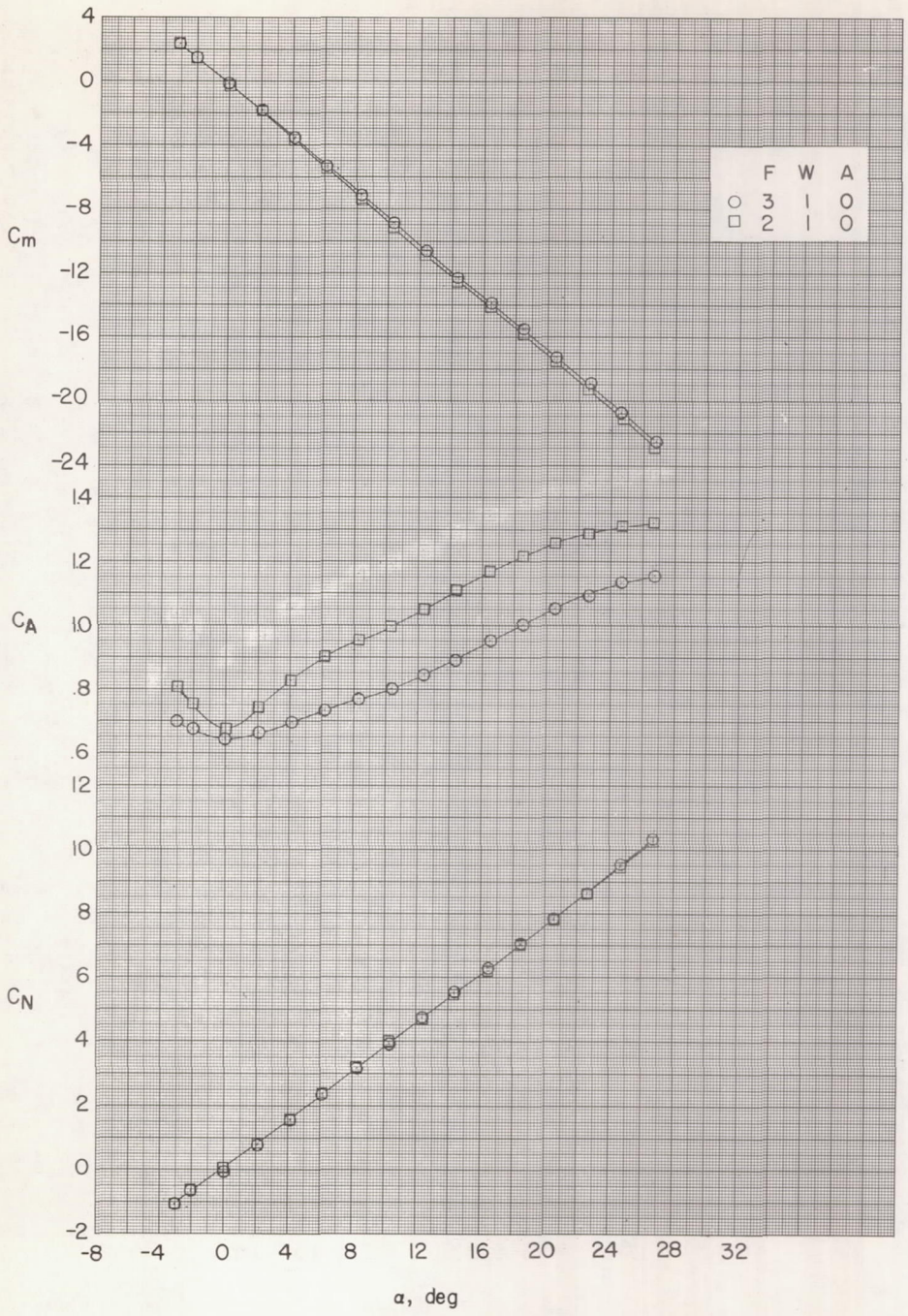


Figure 40.- Aerodynamic characteristics in pitch of tripod nose configuration with screen (F_3) and without screen (F_2). No afterbody; large delta wings.

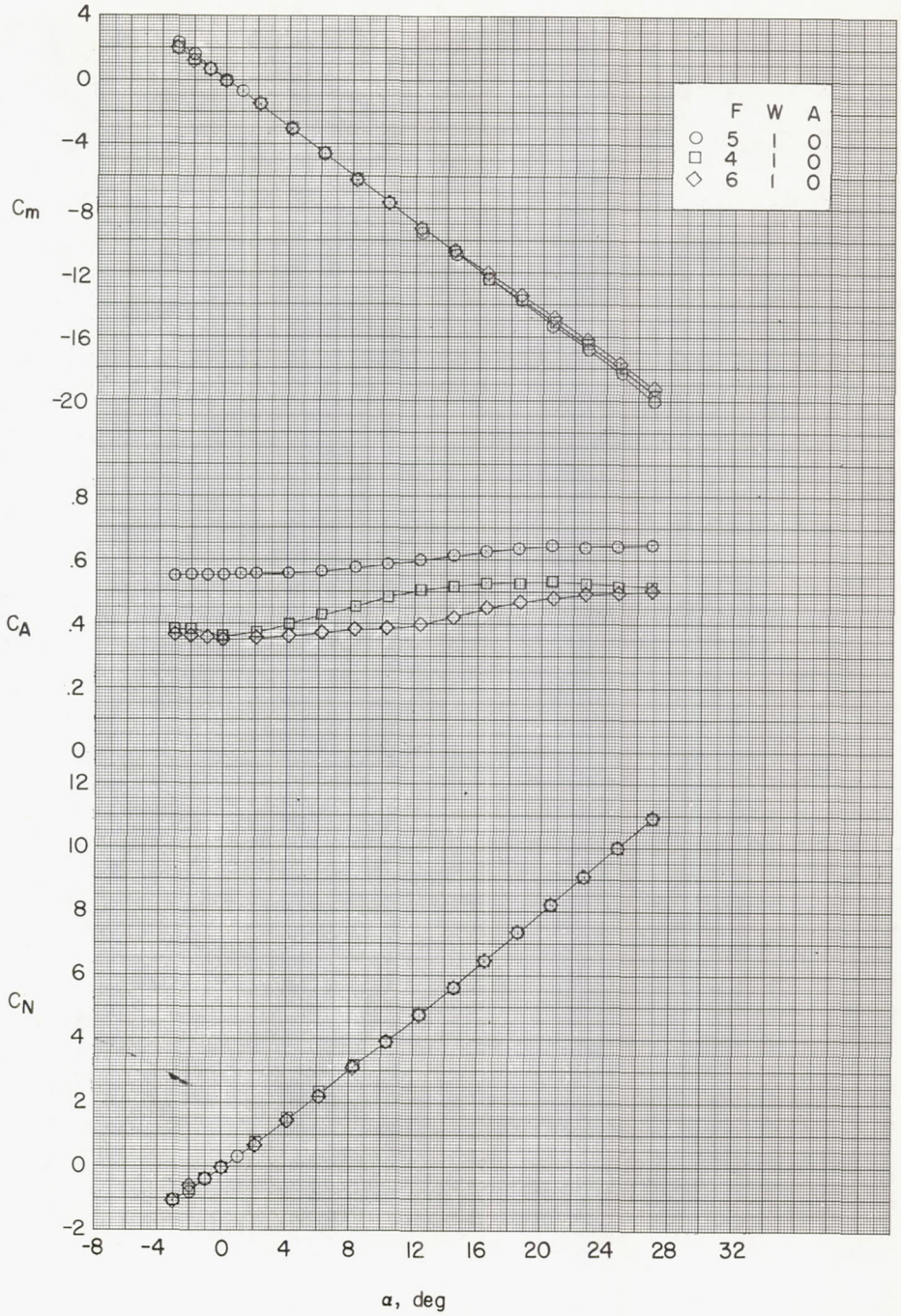
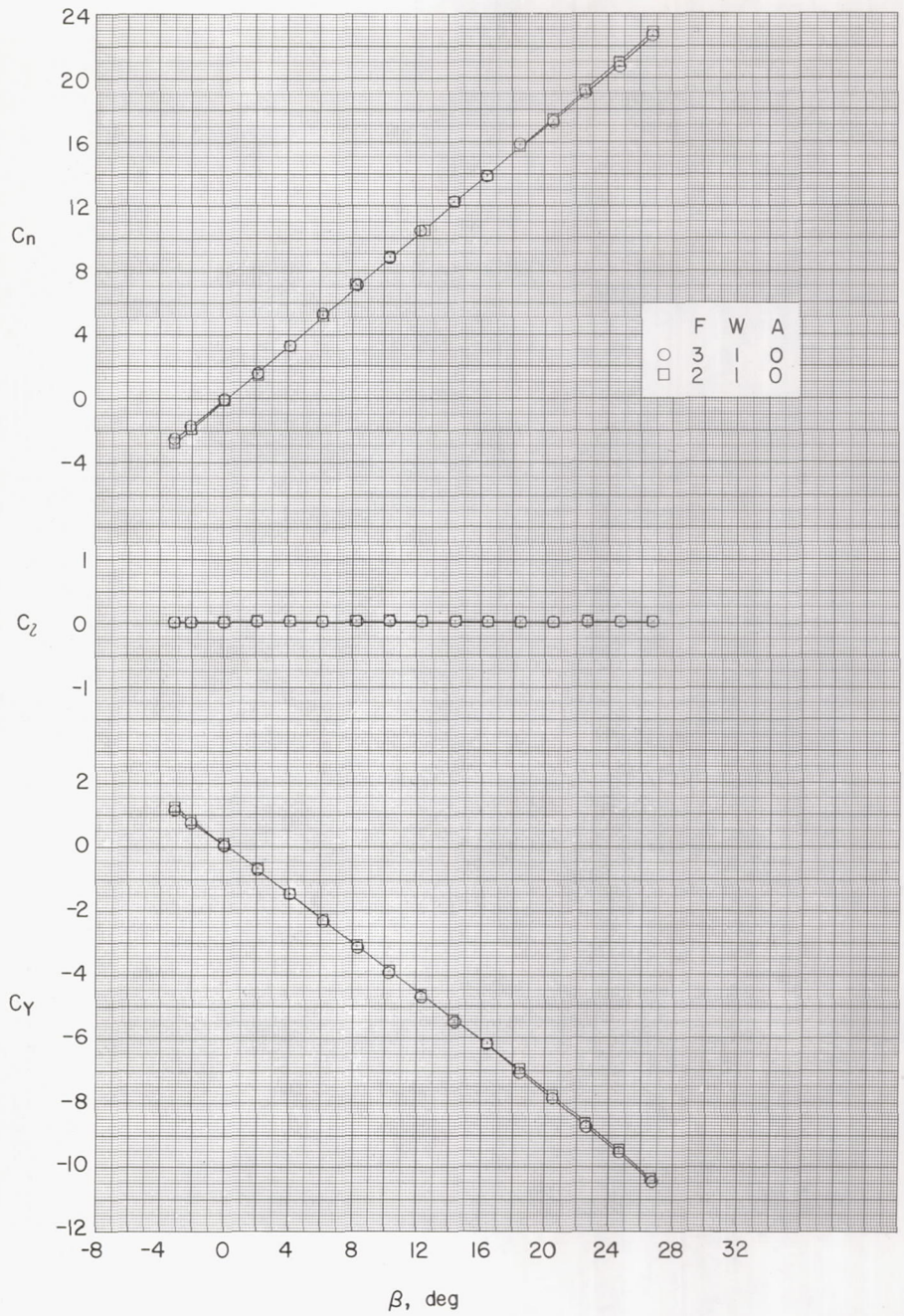
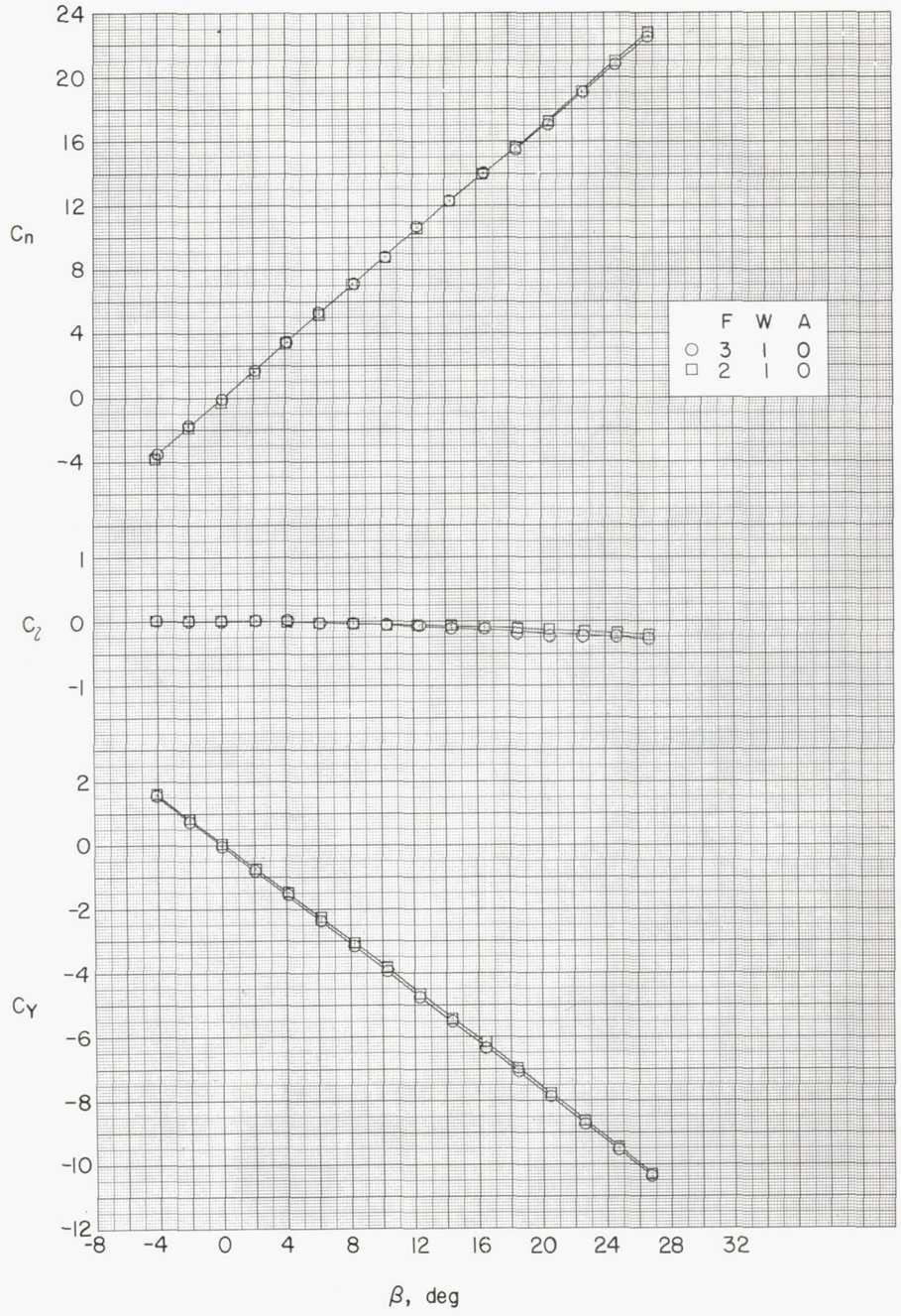


Figure 41.- Aerodynamic characteristics in pitch of rounded nose configuration (F_5) with spike (F_4) and with slotted-cone (F_6). No afterbody; large delta wings.



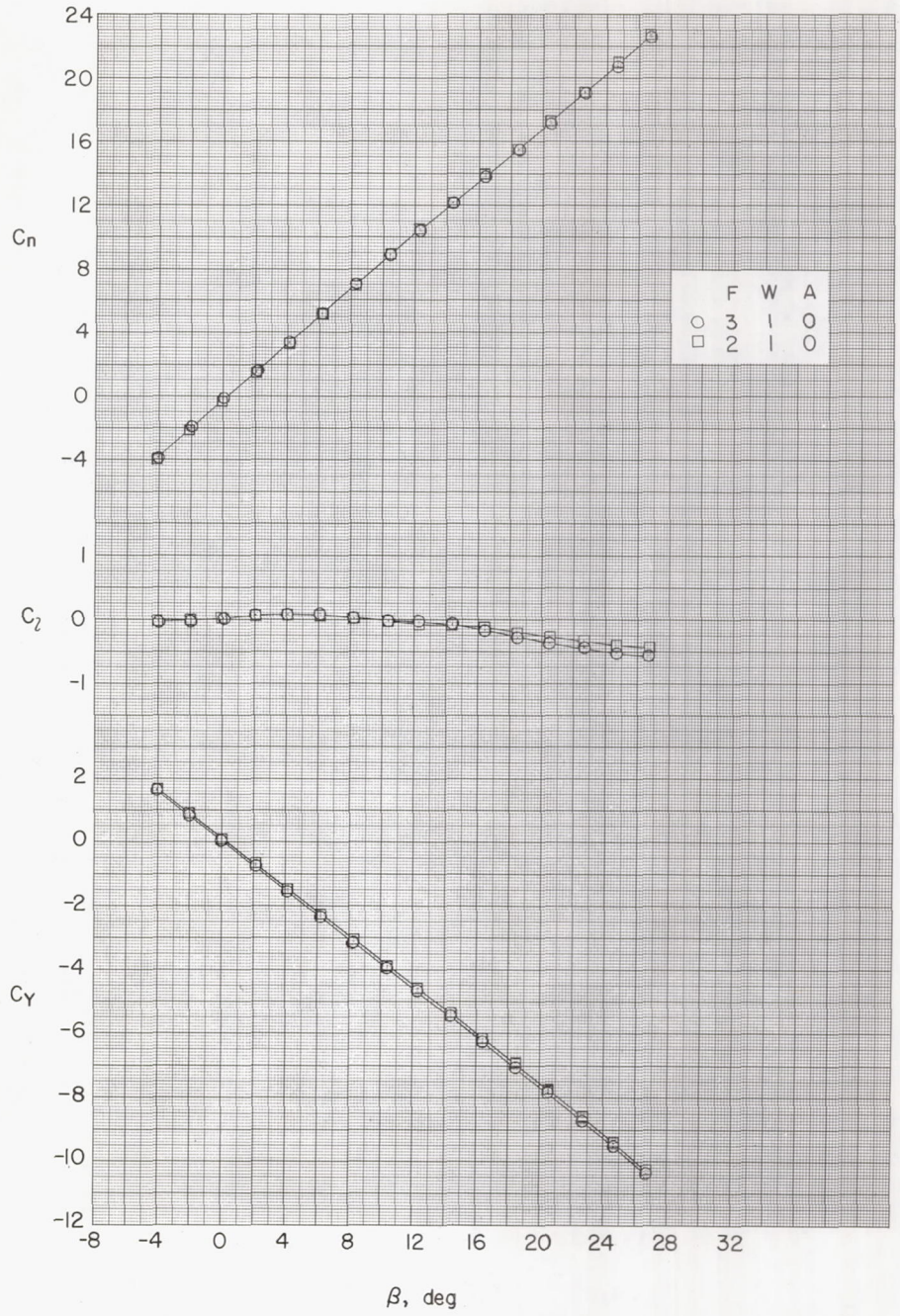
(a) $\alpha \approx 0^\circ$.

Figure 42.- Aerodynamic characteristics in sideslip of tripod nose configuration with screen (F_3) and without screen (F_2). No afterbody; large delta wings.



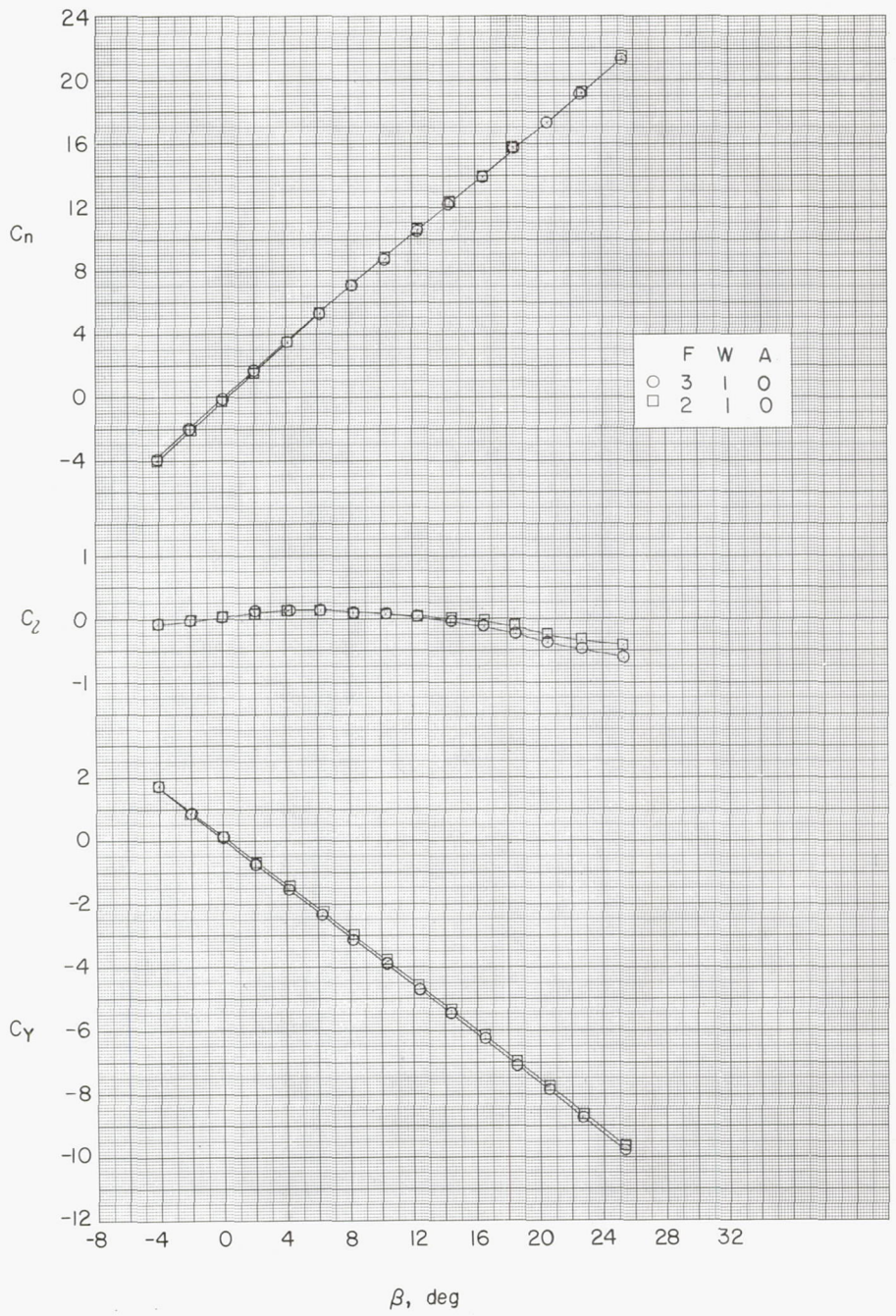
(b) $\alpha \approx 4.1^\circ$.

Figure 42.- Continued.



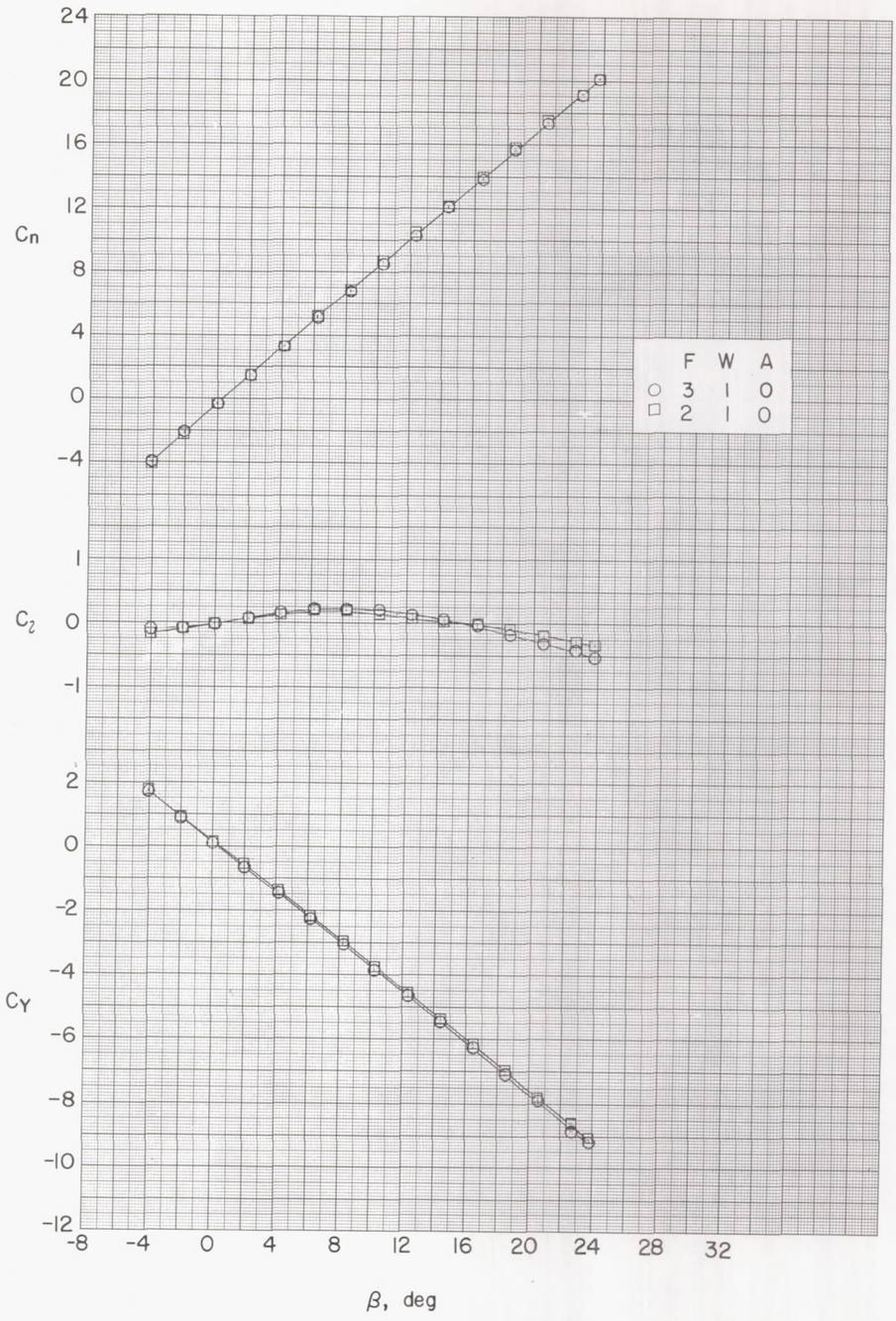
(c) $\alpha \approx 8.2^\circ$.

Figure 42.- Continued.



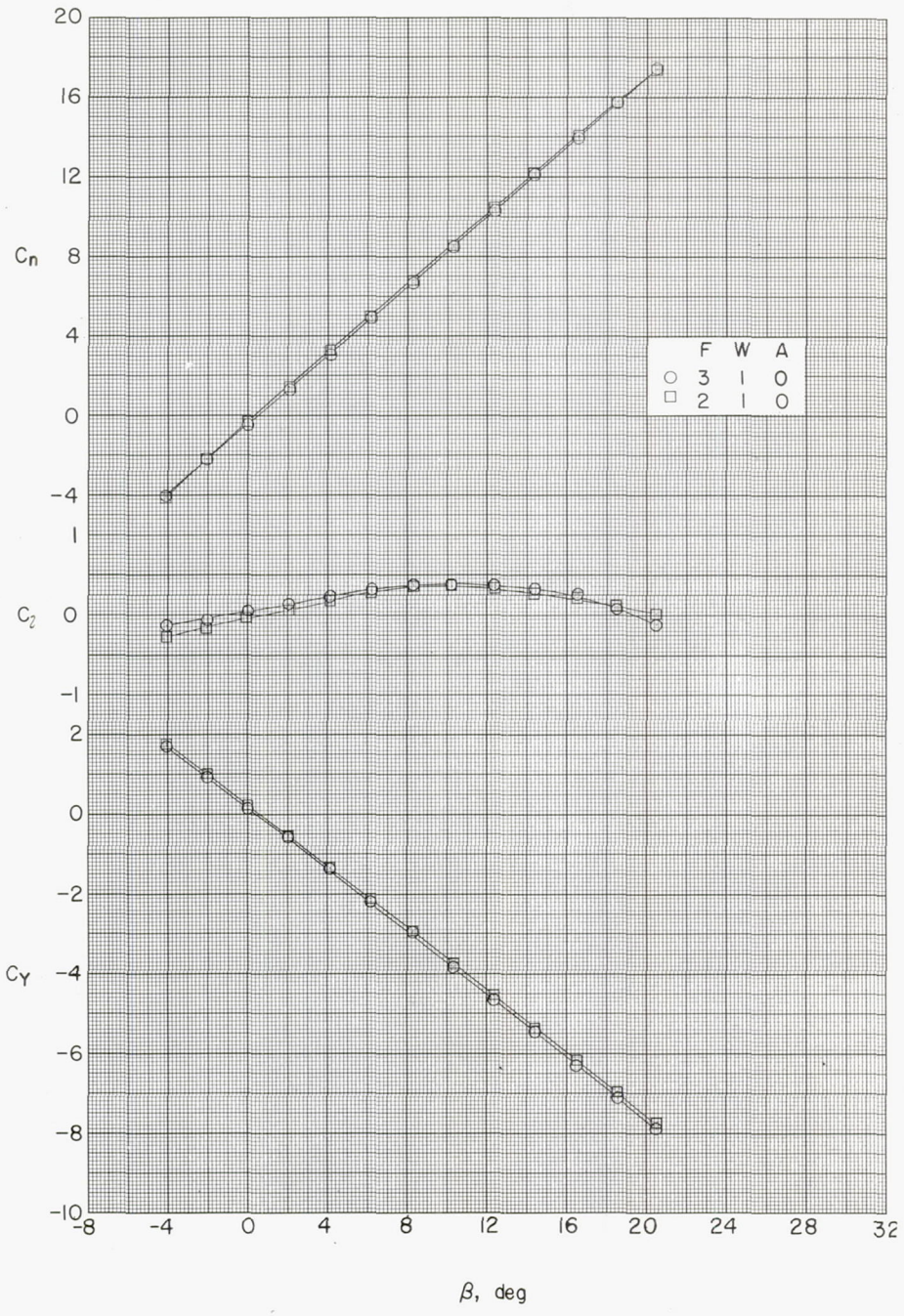
(d) $\alpha \approx 12.3^{\circ}$.

Figure 42.- Continued.



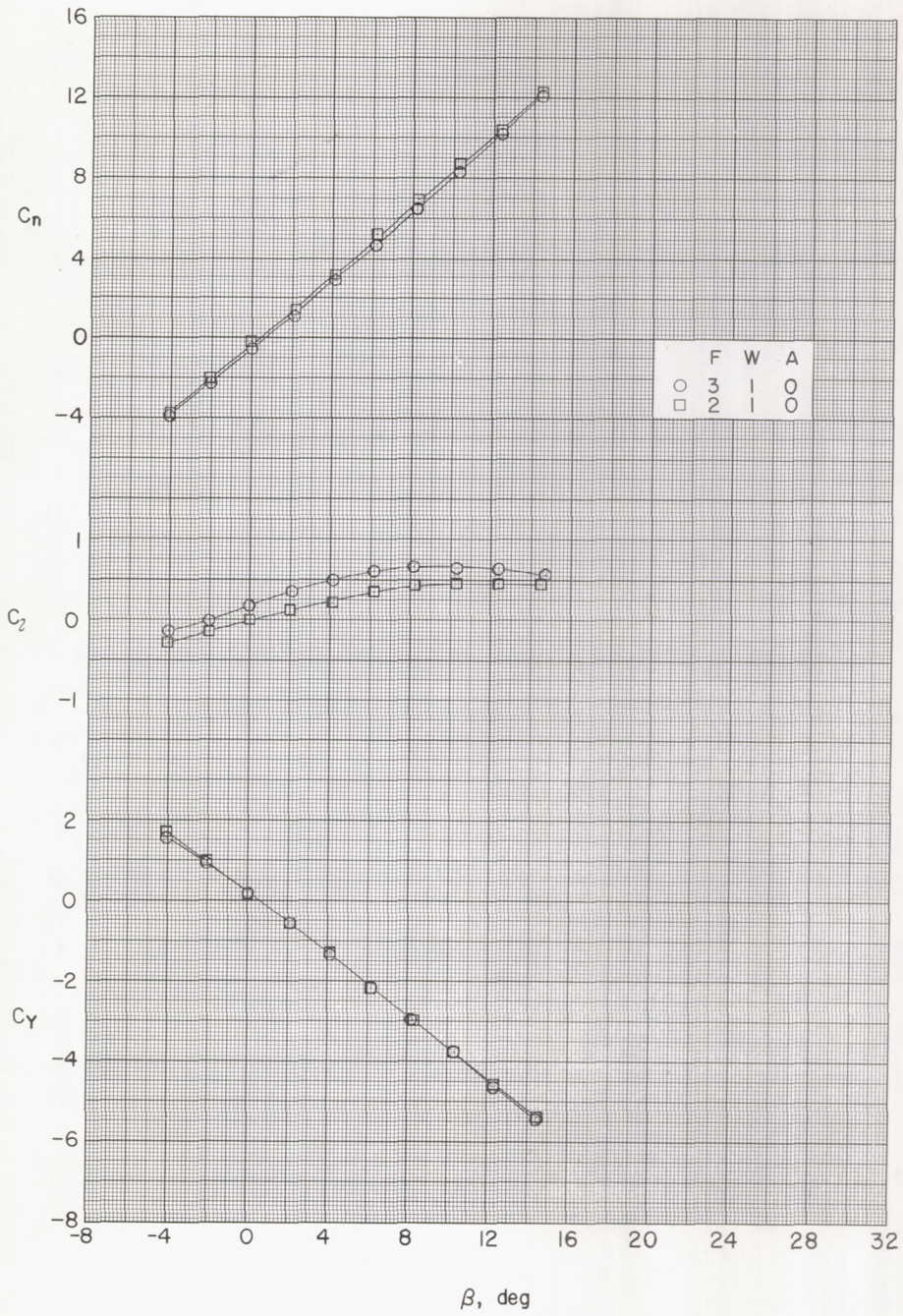
(e) $\alpha \approx 16.4^{\circ}$.

Figure 42.- Continued.



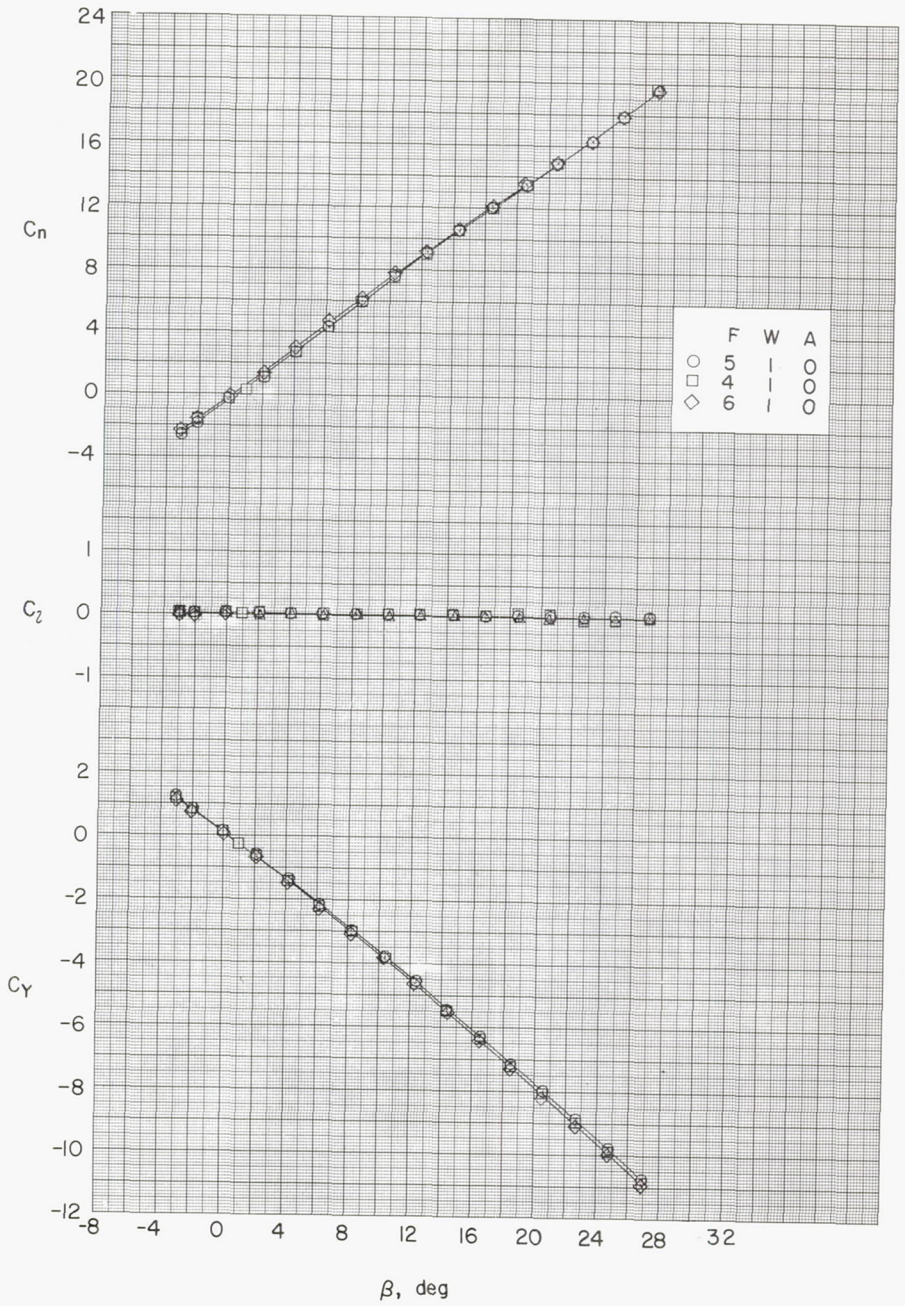
(f) $\alpha \approx 20.5^{\circ}$.

Figure 42.- Continued.



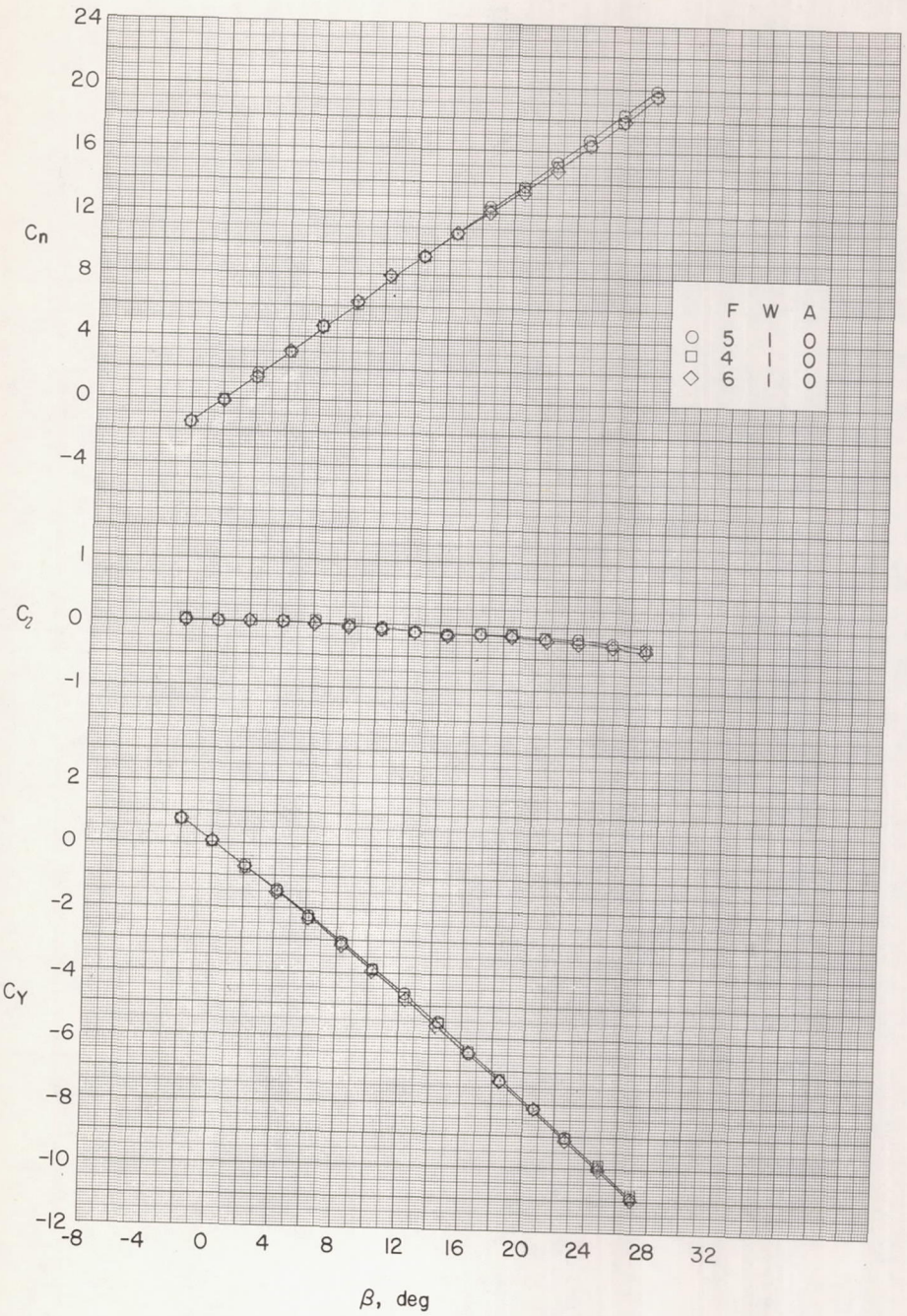
(g) $\alpha \approx 24.7^{\circ}$.

Figure 42.- Concluded.



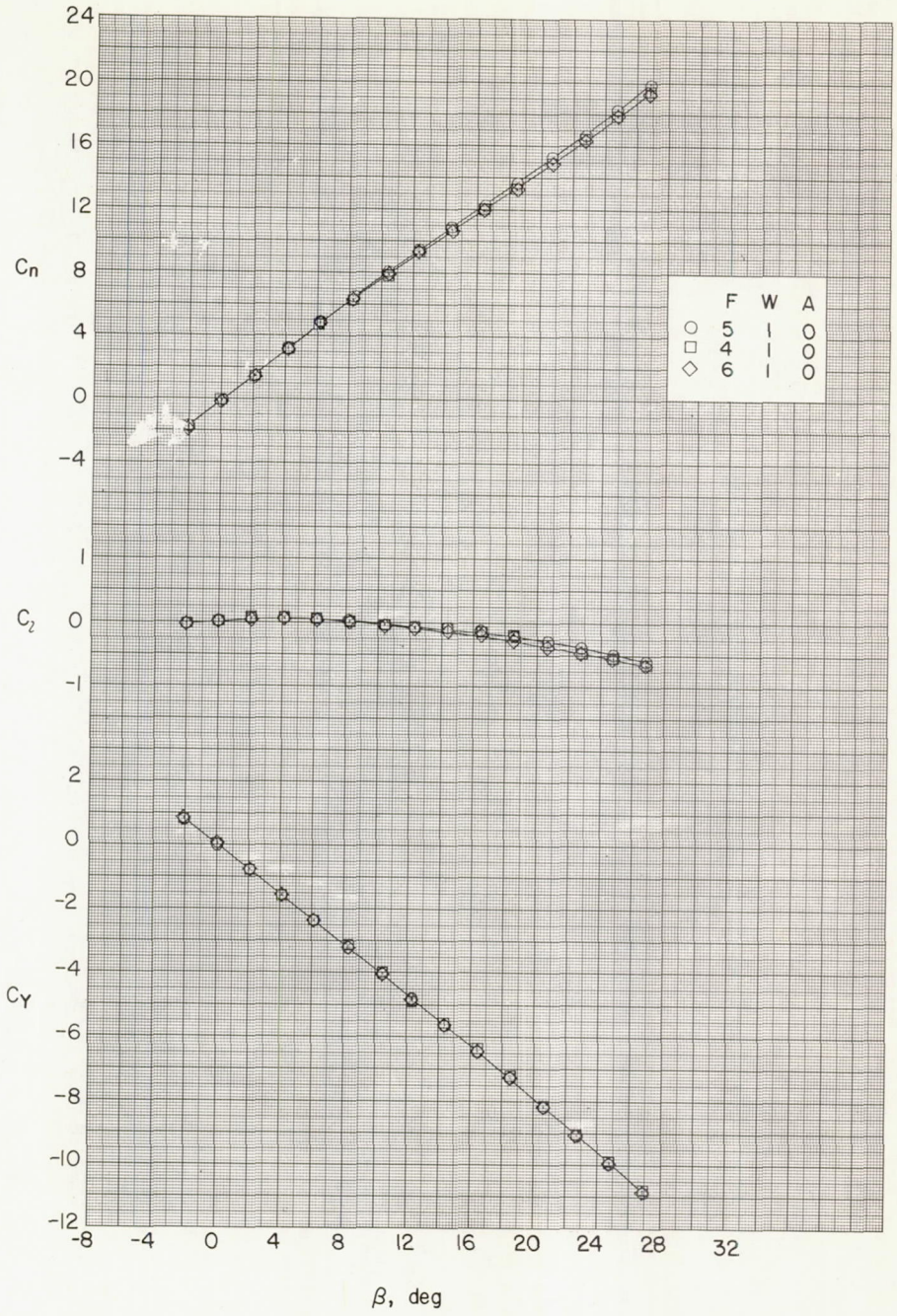
(a) $\alpha \approx 0^\circ$.

Figure 43.- Aerodynamic characteristics in sideslip of rounded-nose configuration (F_5) with spike (F_4) and with slotted cone (F_6). No afterbody; large delta wings.



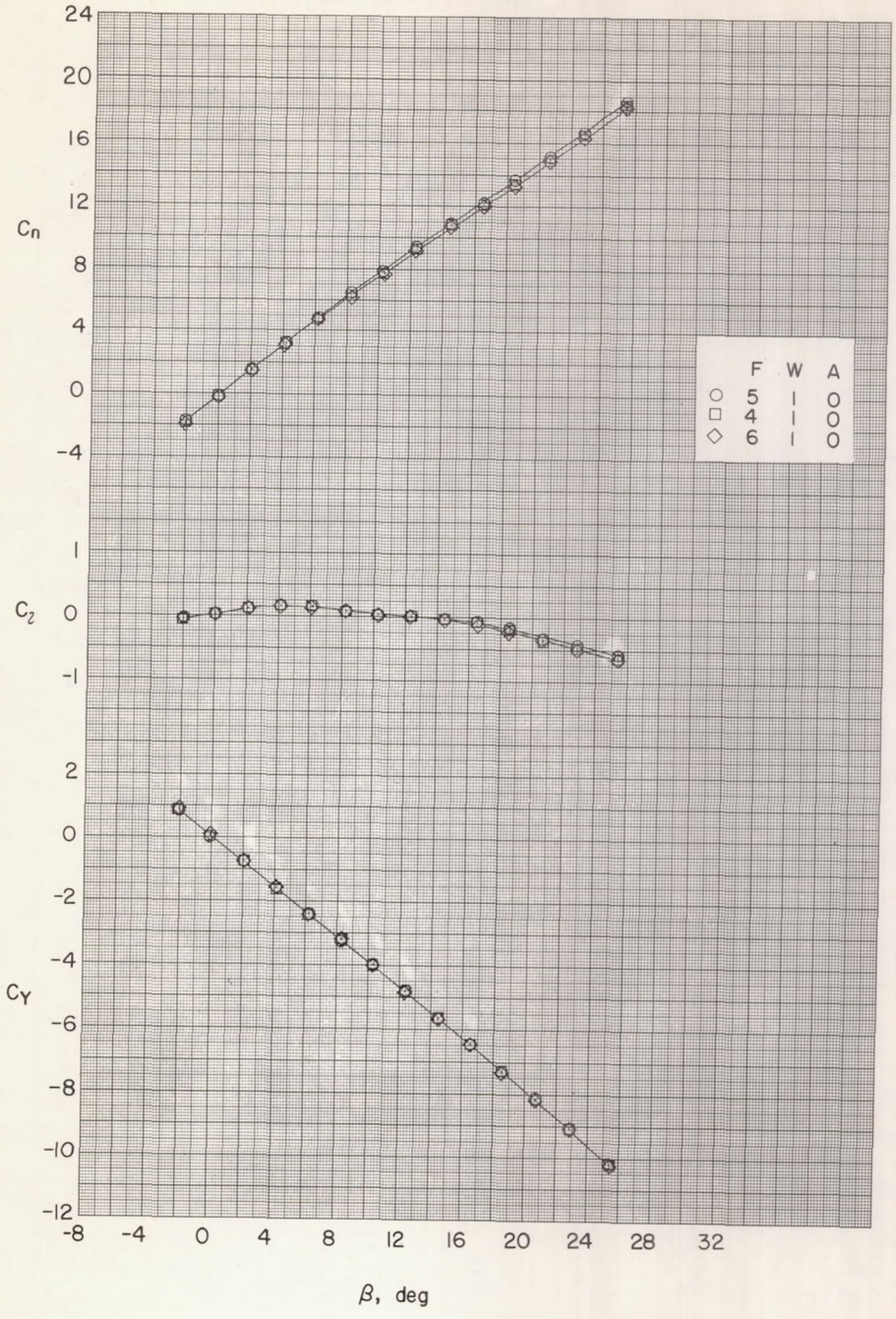
(b) $\alpha \approx 4.1^\circ$.

Figure 43.- Continued.



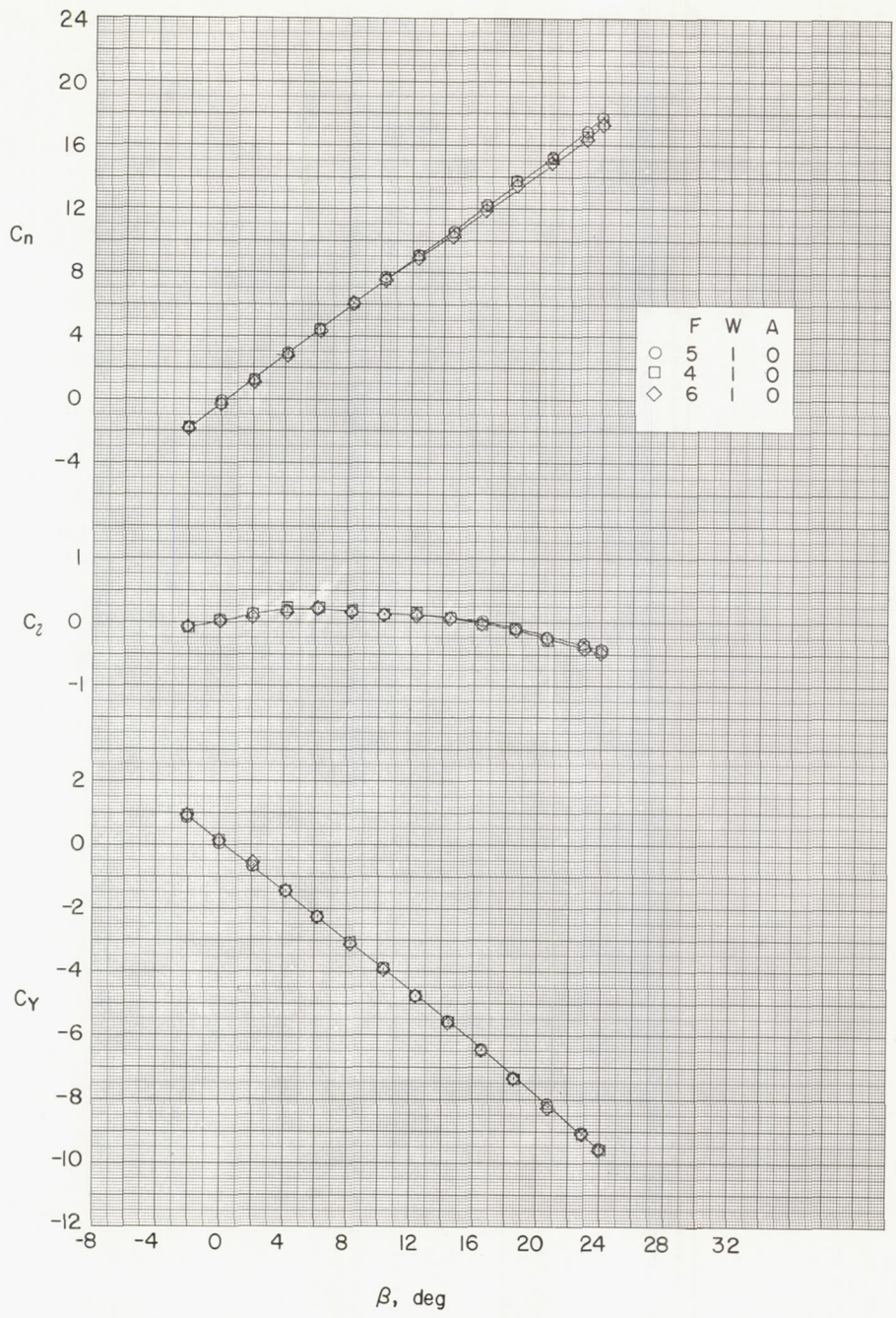
(c) $\alpha \approx 8.2^\circ$.

Figure 43.- Continued.



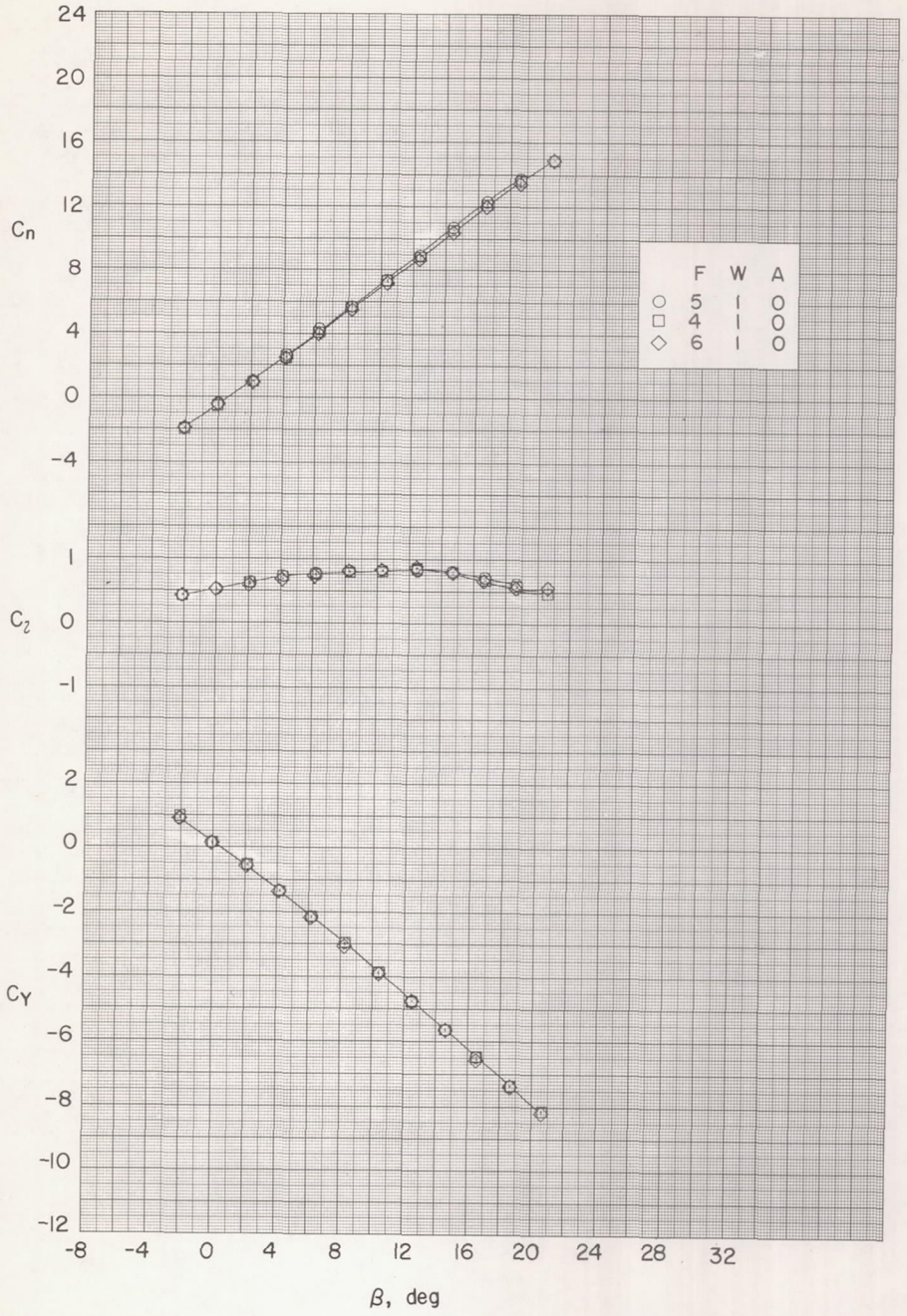
(d) $\alpha \approx 12.3^{\circ}$.

Figure 43.- Continued.



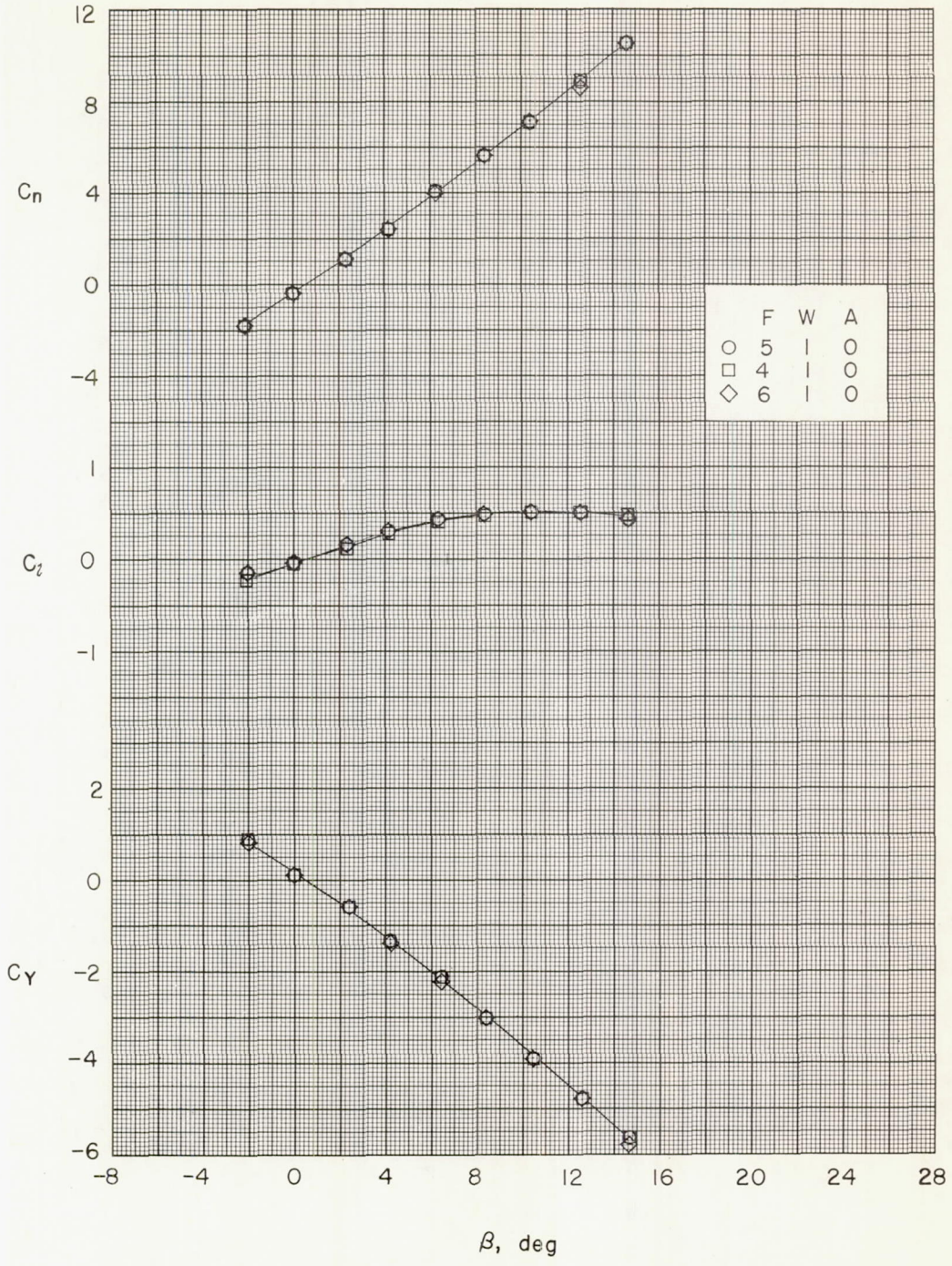
(e) $\alpha \approx 16.4^\circ$.

Figure 43.- Continued.



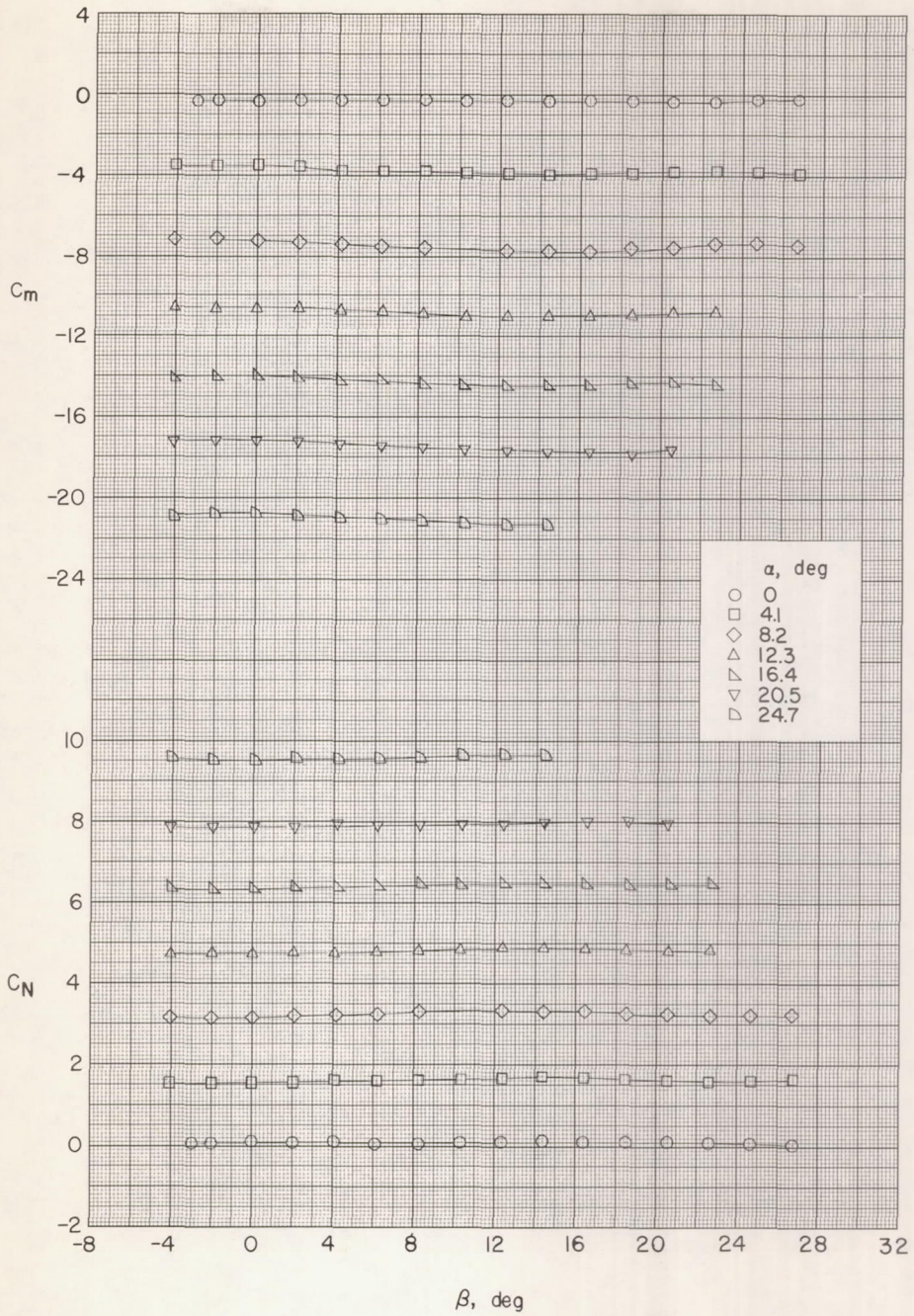
(f) $\alpha \approx 20.5°$.

Figure 43.- Continued.



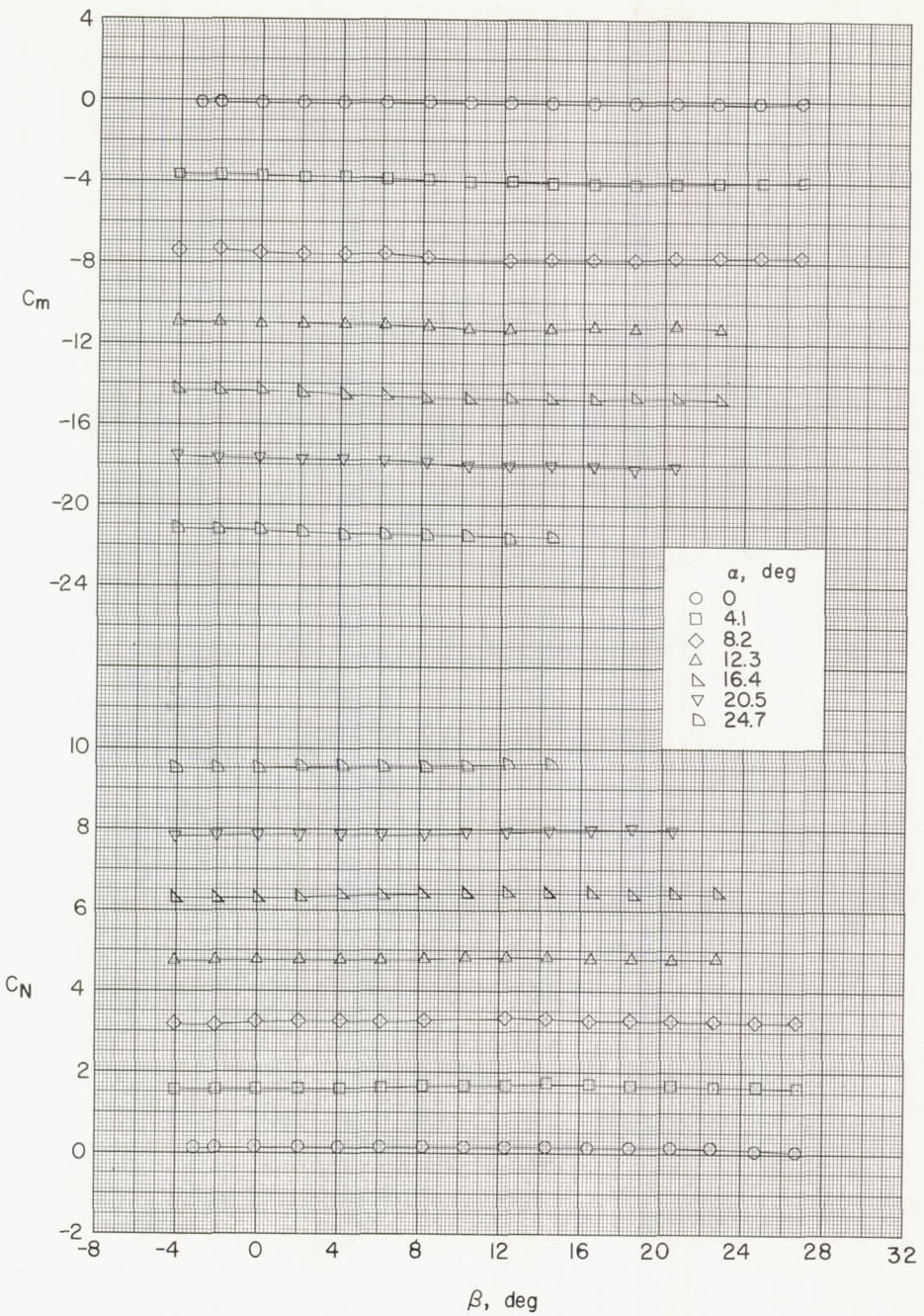
(g) $\alpha \approx 24.7^{\circ}$.

Figure 43.- Concluded.



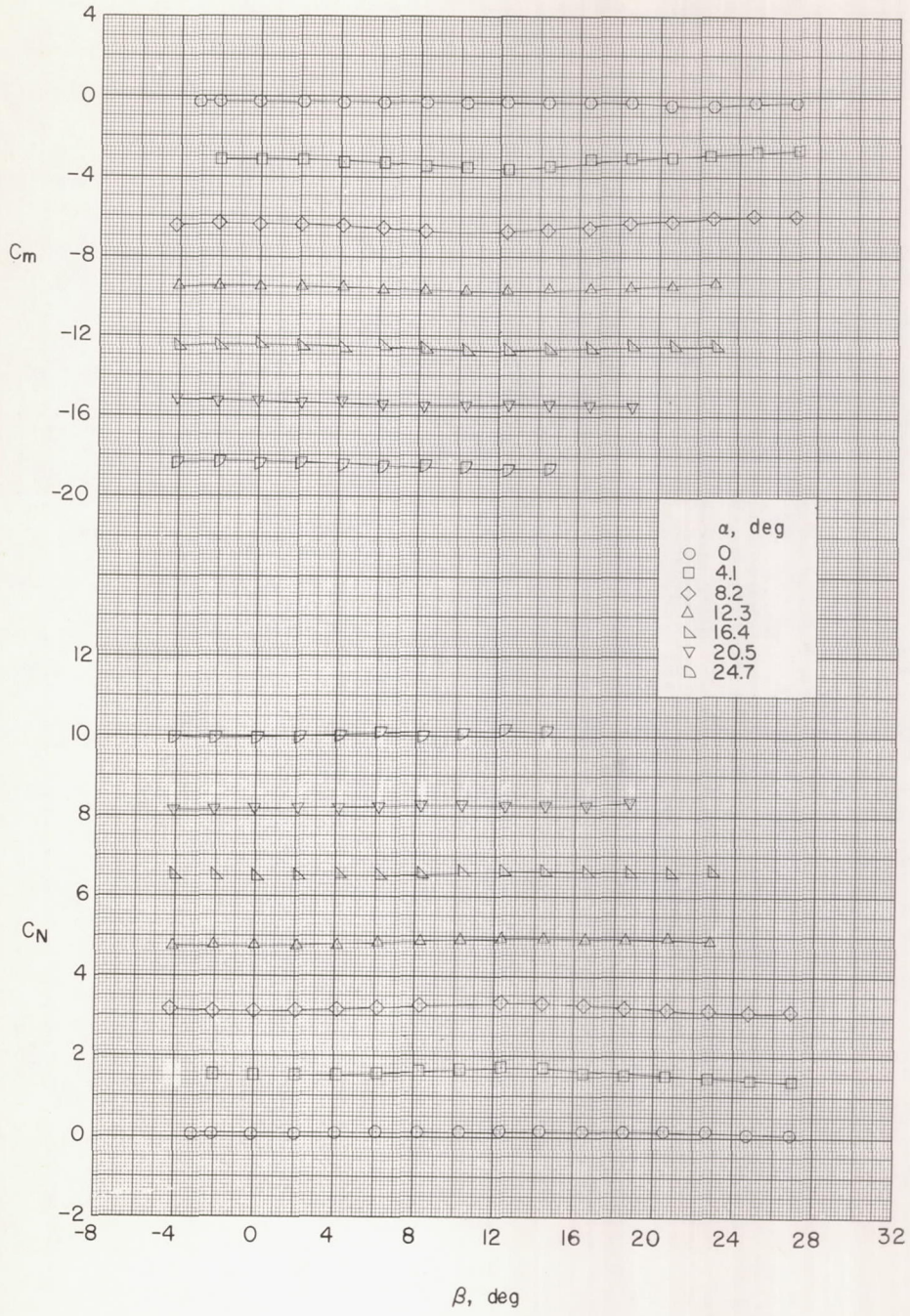
(a) Screen on, $F_3W_1A_0$.

Figure 44.- Variation of C_m and C_N with β for various angles of attack. Tripod-nose configurations; no afterbodies; large delta wings.



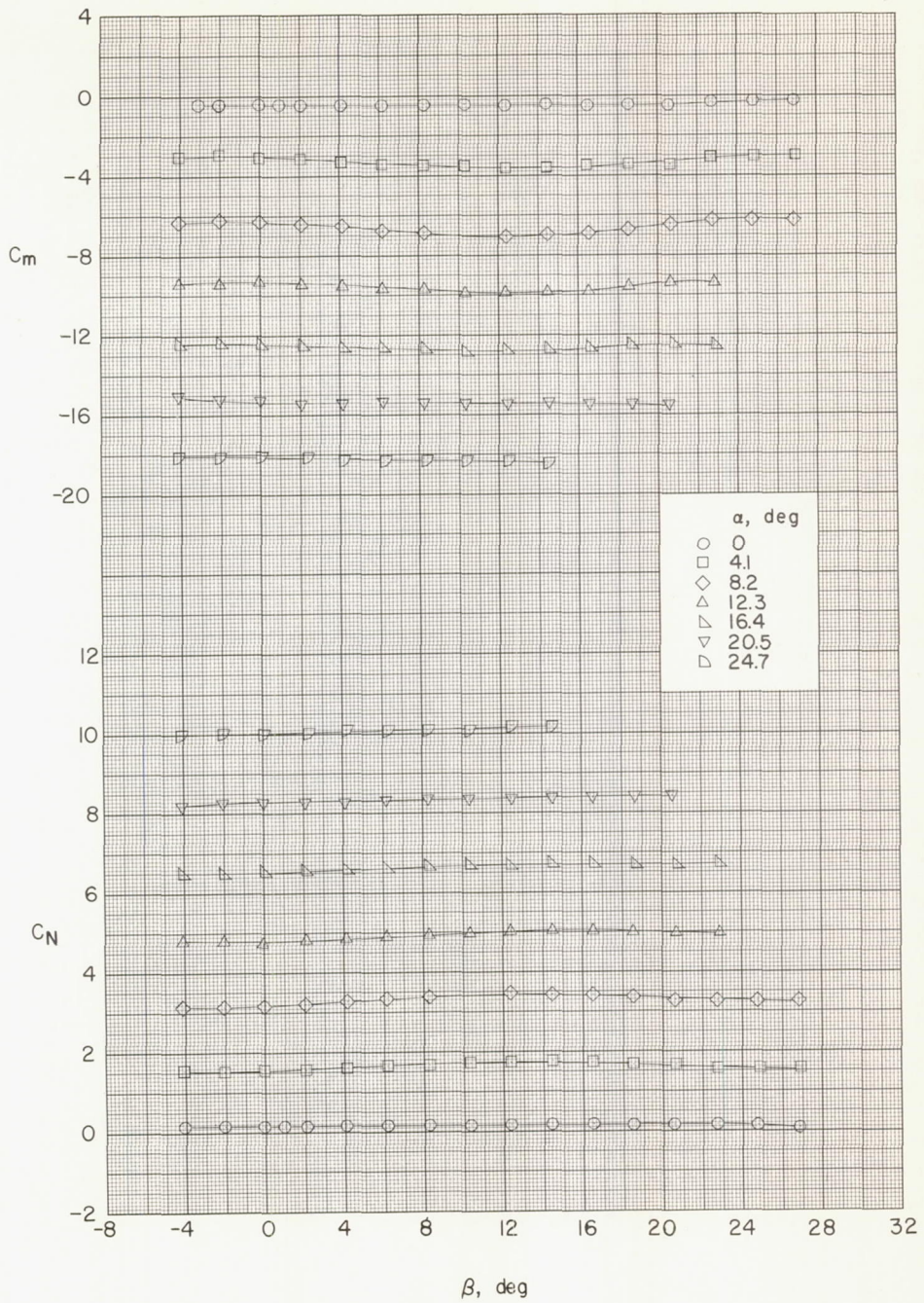
(b) Screen off, $F_2W_1A_0$.

Figure 44.- Concluded.



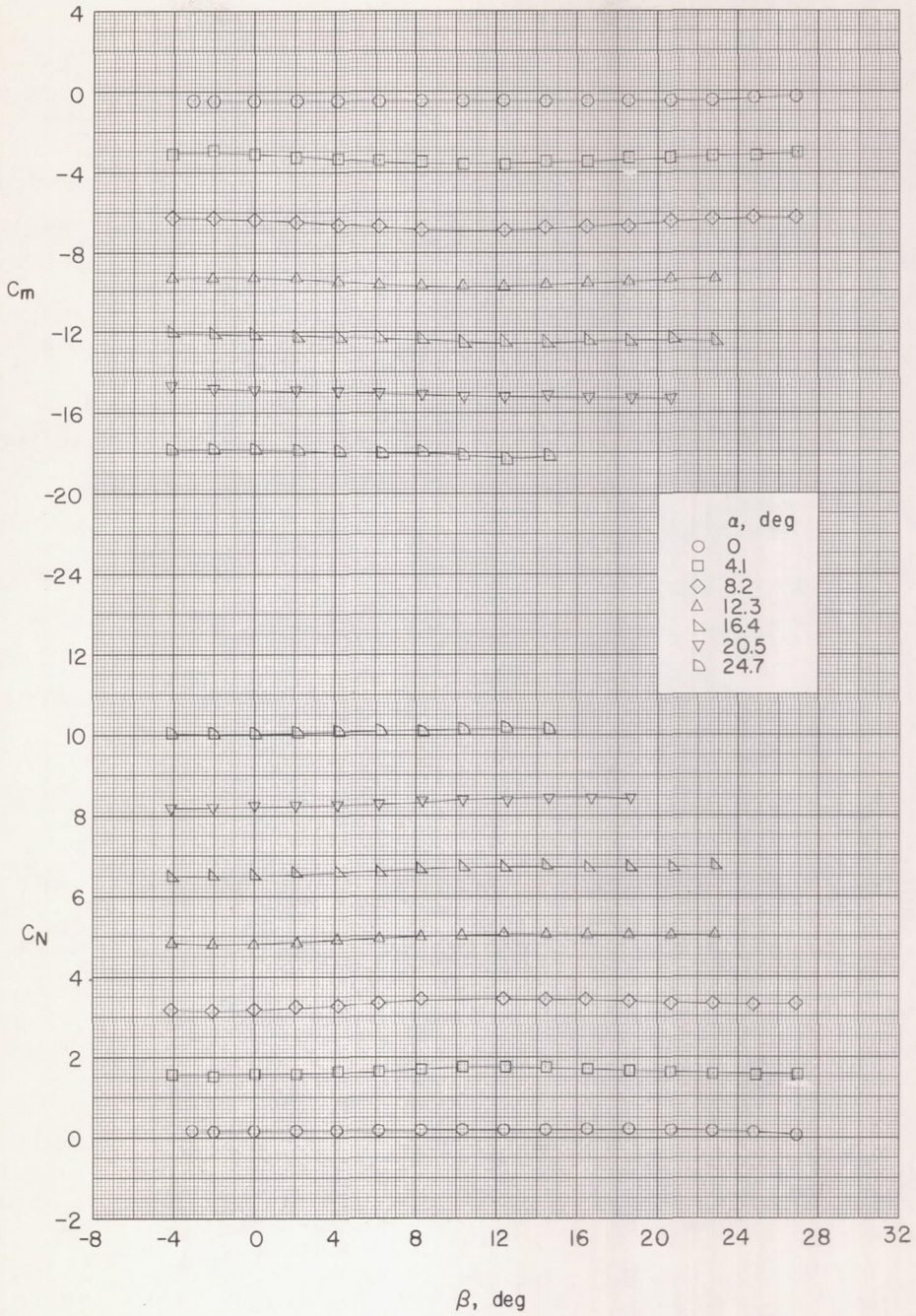
(a) Rounded-ogive nose, $F_5W_1A_0$.

Figure 45.- Variation of C_m and C_N with β for various angles of attack. Rounded-ogive nose; no afterbody; large delta wings.



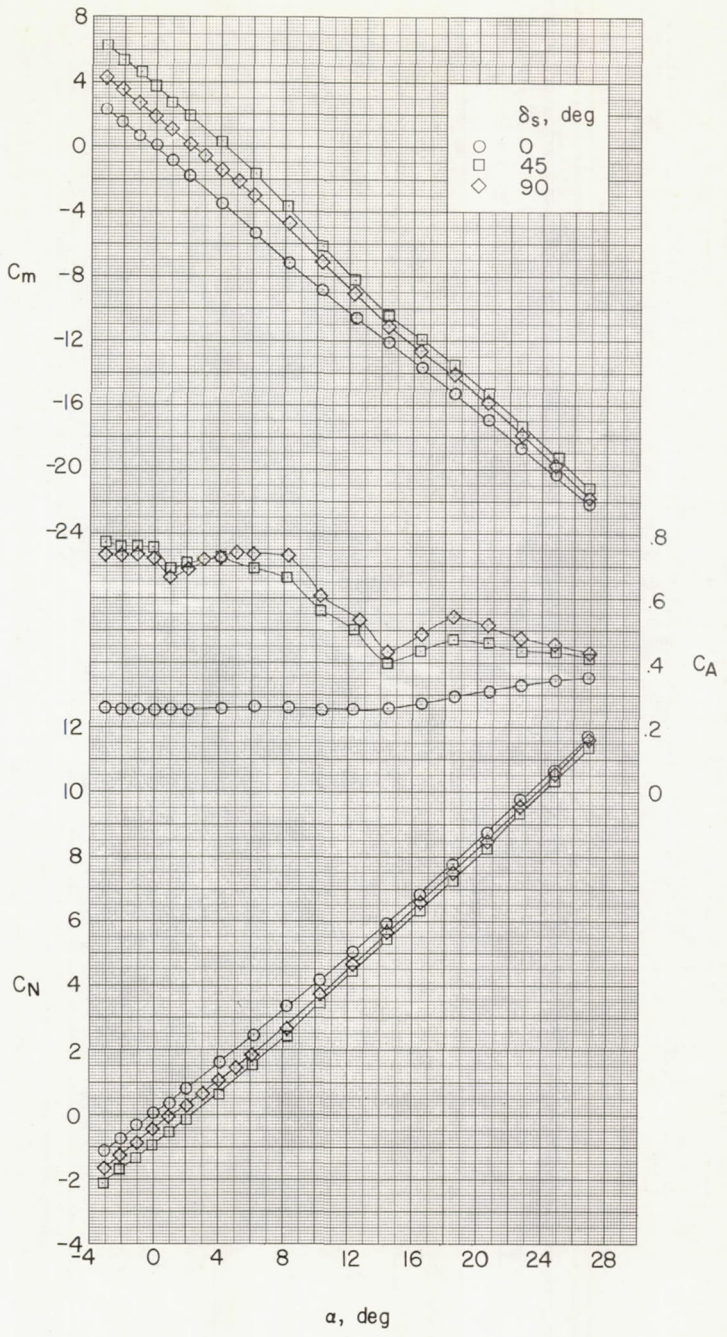
(b) Rounded-ogive nose with spike, $F_4W_1A_0$.

Figure 45.- Continued.



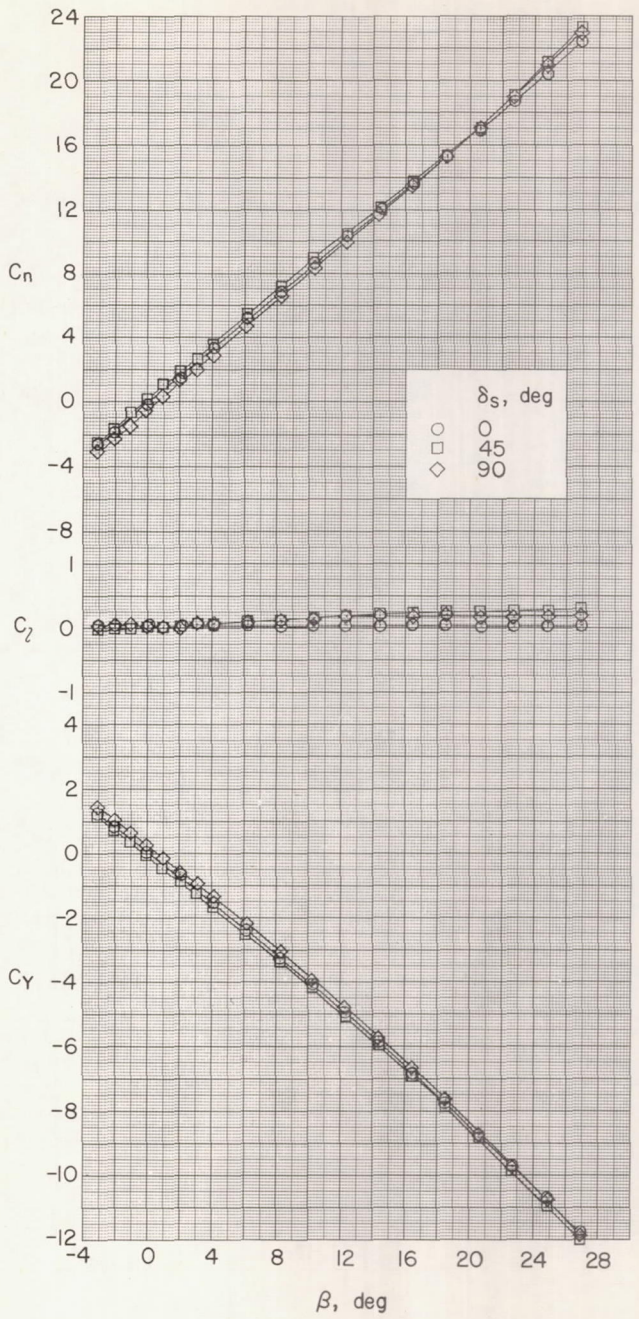
(c) Rounded-ogive nose with slotted cone, $F_6W_1A_0$.

Figure 45.- Concluded.



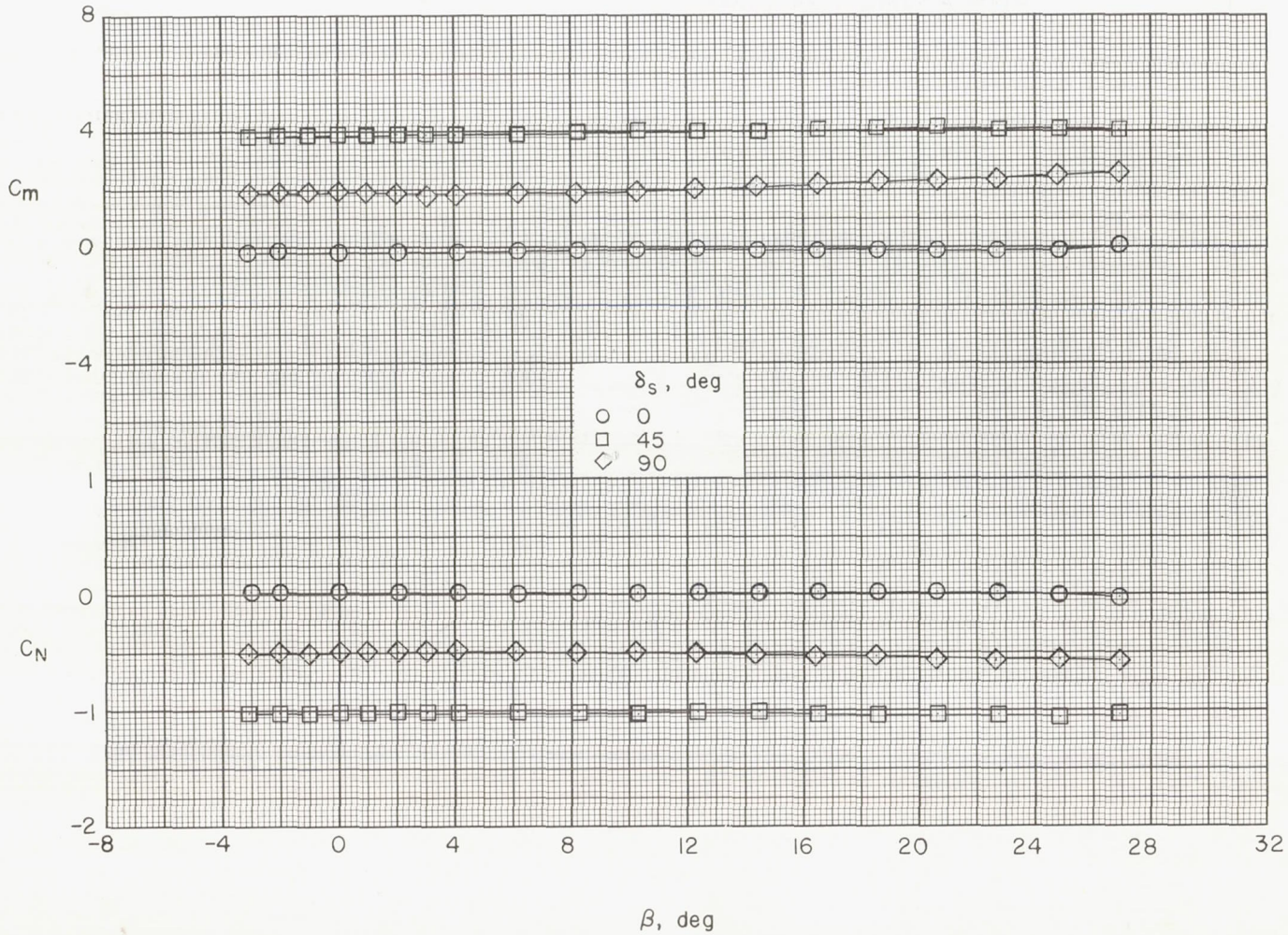
(a) The variation of C_m, C_A, and C_N with α. $\beta = 0^\circ$.

Figure 46.- Effects of spoiler deflection on aerodynamic characteristics $(F_7W_1A_1)$. One-caliber afterbody; large delta wings; $l/d = 10$.



(b) The variation of C_n, C_l, and C_Y with β. $\alpha = 0^\circ$.

Figure 46.- Continued.



(c) The variation of C_m and C_N with β. $\alpha = 0^\circ$.

Figure 46.- Concluded.